www.rsc.org/greenchem

Highlights

Markus Hölscher reviews some of the recent literature in green chemistry

DOI:10.1039/b409817j

Green and ultra-deep desulfurization of diesel

Environmental regulations to be applied by 2006 in Europe, the US and other countries limit the sulfur levels in diesel to less than 15 ppm. To meet these stringent conditions novel desulfurization processes are needed to ensure sustainable and economically acceptable technology. It is a challenging goal to reduce the amount of sulfur in diesel from its several hundred ppm to only a few ppm, which was recently accomplished by Li and coworkers from the State Key Laboratory of Catalysis, Dalian (*Chem. Eur. J.*, 2004, **10**, 2277–2280). They chose an oxidation–extraction approach basing on heteropolytungstate oxidation catalysts operating efficiently with aqueous H_2O_2. The strategy is based on the fact that the sulfides contained in the diesel fuel are not easily extractable due to their relative similarity to the diesel. However, an oxidation yields sulfones, which can be more easily extracted due to their higher polarity. The progress they made therefore is a highly efficient and selective oxidation catalyst, which can be easily recycled and which utilizes the oxidant efficiently.

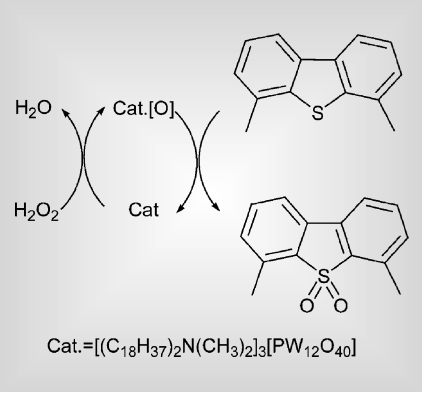

The H_2O–H_2O_2 mixture forms metastable emulsion droplets with $[(C_{18}H_{37})_2N(CH_3)_2]3[PW_{12}O_{40}]$ in diesel, and the droplets can easily be demulsified by centrifugation, allowing for simple catalyst recycling. Test experiments employing 4,6-dimethyldibenzothiophene (4,6-DMDBT) showed the oxidation to proceed fast with complete conversion after 80, 30 and 8 min at reaction temperatures of 30, 60 and 90 °C, respectively. The sulfones can be extracted with a polar extractant such as 1-methyl-2-pyrrolidinone. When this catalyst system was applied to real diesel all sulfur containing compounds were successfully oxidized/extracted yielding diesel with a sulfur content of less than 0.1 ppm. In recycling experiments the catalyst's activity was retained completely, which in summary characterizes this process as green, since only stoichiometric amounts of H_2O_2 are consumed, the only by-product is water and the reaction is run under mild conditions.

Application of sonochemistry to asymmetric heterogeneous catalysis

Highly selective heterogeneous catalyzed processes are still not very abundant for enantioselective hydrogenations of C–C double bonds. The introduction of sonochemistry to proline modified Pd/Al_2O_3 catalysts by Török *et al*. from the Michigan Technological University therefore is an encouraging progress in this regard. They showed that isophorone can be hydrogenated to dihydroisophorone with very high ee values when Pd/Al_2O_3 catalysts are modified with (*S*)-proline and presonicated prior to use (*Chem. Commun.*, 2004, 984–985).

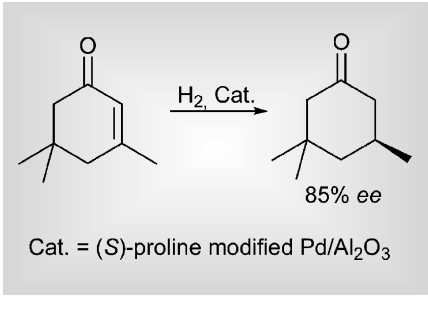

In optimizing the reaction conditions they found that (i) the modifier is necessary for appreciable enantioselective performance, (ii) that different presonication times influence the ee value with optimum times of around 20 min., (iii) that the hydrogen pressure has a significant influence on the enantioselectivity with 40 bar and above being superior to low H_2 pressures. Also the catalyst/substrate ratio is of importance. Optimized conditions yielded 85% ee for the (*S*)-product. According to electron micrographs the presonication reduced the mean particle size significantly. As it was shown that modifier-free presonications reduced the ee value the authors propose the proline molecule to adsorb more strongly to the catalyst surface due to surface cleaning by sonication. Interesting new methods for hydrogenation of C–C double bonds in other α,β-unsaturated compounds may soon open up.

Electroorganic solid phase synthesis

Although organic solid phase synthesis is a well established tool for the syntheses of large libraries, electroorganic reactions using common polymers as solid support are not yet developed. Achieving this would allow electrochemical reactions to be included in the reactions used for library syntheses. Breinbauer and Nad succeeded in developing such an approach (*Angew. Chem.*, 2004, **116**, 2347–2349). As a model reaction they chose the 2,5-dimethoxylation of furans, which is a Br^- mediated process well established in organic syntheses and also operated by industry. After linking the corresponding furyl alcohol to the Tentagel and polystyrene resins in separate experiments the electrochemical transformation was conducted in the presence of methanol and NH_4Br.

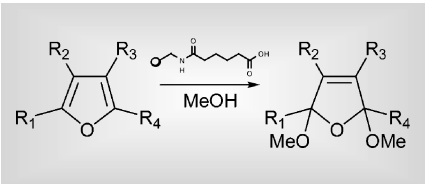

Subsequent ester cleavage yielded 2,5-dimethoxydihydrofuran as a *cis*/*trans*-mixture in 95 and 97% purity and with 57% yield using polystyrene beads. Different substituents present on the furan ring do not affect the reaction significantly in most cases (yields up to 63% with purities up to 97%), one of the exceptions

being 5-(dimethylaminomethyl)furfuryl alcohol. Replacing methanol by ethanol in the syntheses yields diethoxylated products. Also the α-hydroxylated 2,5-dialkoxydihydrofuran **2** was available *via* this route by using diol **1** as reactant.

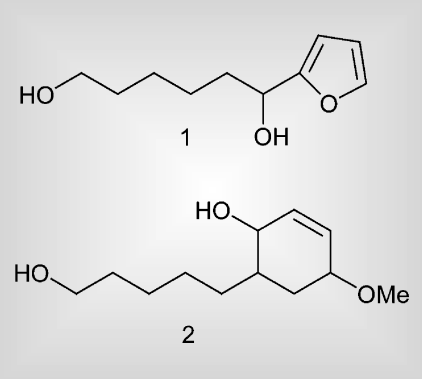

www.rsc.org/greenchem

Focus on education in Green Chemistry

As the principles of Green Chemistry and the concepts of sustainability in chemical manufacturing are becoming part of the explicit corporate policy and aims in the chemical industry, there is a rapidly growing need for the education of chemists in this field (for example see ref. 1). Special events such as the ACS-PRF Summer School[2] or the European Green Chemistry Summer School in Venice[3] and similar workshops all around the world are excellent examples of how a first introduction to the area can be provided by bringing graduate students from various universities together in a unique environment. At the level of individual teaching institutions, an even more detailed and continuing influence is possible. This can be achieved by specialized Green Chemistry curricula or by incorporating the principles and examples into regular courses at the appropriate level. Conveying the theoretical concepts and presenting exciting real world examples to the students is getting easier for the teacher as textbooks and teaching materials are becoming more widely available (visit the Green Chemistry Institute homepage[4] for an excellent overview of selected activities).

Green Chemistry is, however, to a great extent an experimental science. Most schoolchildren and students remember an experiment much better than a lecture, and the fascination of molecular sciences is often directly linked to and based on phenomenological impressions. One approach to address the practical side of education can be to include important aspects into classical laboratory classes on organic synthesis (for example see ref. 5). But how do we exemplify Green Chemistry in simple and reliable experiments that can be carried out at an undergraduate or even high school level? How can Green Chemistry be communicated in demonstration lectures to a large audience? The answer is probably to concentrate on specific issues in detail, rather than to try to cover too many aspects at one time. The two educational papers in this issue provide excellent examples of this strategy for the use of compressed gases as alternative solvents, using complementary approaches.

The transportable kit presented by Pete Licence from Nottingham allows a fascinating demonstration of the phenomenon of the critical point without the need for any additional supply of gases, heat or pressure. Once the real-time experiment has caught the attention of the audience (and I can assure you it does!), they will be open to more information on the unique properties and the potential applications of the impressive transition they just witnessed. The design of the experiment and the equipment are ideally suited for display on open days, fairs or in demonstration courses. It is at least as impressive as throwing bits of sodium into water, but generates a remarkably different image of chemistry and chemists among the audience.

The approach described by Jim Hutchison and his team at Oregon is designed more as a hands-on experiment for laboratory classes. The beauty of this teaching experiment lies in the simplicity of the set up and the direct connection to the practical application. The aspect of solvent replacement becomes immediately apparent and the fact that one isolates a natural product in appreciable amounts adds to the "effect" of the performance. At the same time, the transition of a solid to a liquid and finally a gas gives a nice introduction to phase diagrams and their principles.

These two recent examples may only be the tip of an iceberg of activities going on in many labs at present. Hopefully, they will help to further stimulate the design and development of similarly simple and yet dramatic experiments to communicate Green Chemistry and its principles. This remains a continuing challenge, not only for alternative solvents but also for other concepts such as catalysis, atom efficiency, renewable raw materials or energy saving. After all, in addition to seeding the interest for more information, such experiments transport another important message: *Green Chemistry is great fun!*

For other articles on green chemistry education published in *Green Chemistry* see refs. 6–10.

Professor Walter Leitner
Scientific Editor, *Green Chemistry*

References

1 M. M. Kirchhoff, *J. Chem. Educ.*, 2001, **78**, 1577.
2 http://www.chemistry.org/portal/a/c/s/1/acsdisplay.html?DOC=greenchemistryinstitute%5Csummer_school%5C2004gcsummer.html.
3 http://venus.unive.it/inca/summer_school.htm.
4 http://www.chemistry.org/portal/a/c/s/1/acsdisplay.html?DOC=education\greenchem\index.html.
5 http://www.oc-praktikum.de.
6 A. Matlack, *Green Chem.*, 1999, **1**, G19.
7 M. G. Warner, G. L. Succaw and J. E. Hutchison, *Green Chem.*, 2001, **3**, 267.
8 D. Lennon, A. A. Freer, J. M. Winfield, P. Landon and N. Reid, *Green Chem.*, 2002, **4**, 181.
9 S. Tavener, J. Hardy, N. Hart and A. Goddard, *Green Chem.*, 2003, **5**, G46.
10 A. F. Houri and H. Wehbe, *Green Chem.*, 2003, **5**, G49.

DOI: 10.1039/b412202j

www.rsc.org/greenchem

"Supercriticality"; a dramatic but safe demonstration of the critical point

Peter Licence,* David Litchfield, Martin P. Dellar and Martyn Poliakoff
School of Chemistry, The University of Nottingham, Nottingham, UK NG7 2RD. E-mail: peter.licence@nottingham.ac.uk

The image of a fluid passing up through its critical point and back down again is one of the most beautiful and fascinating physical transformations that can be demonstrated to an audience. Unfortunately this image is not often seen; safety issues often restrict educators from carrying out such demonstrations in the public arena. In this article we describe a self contained demonstration apparatus that may be used to illustrate this transition in a very safe and controlled way. The demonstration apparatus may be used as a hands-on teaching instrument in the classroom, or alternatively, with the aid of an LCD projector and screen, be used as an interactive demonstration during larger lectures or exhibitions.

DOI:10.1039/b407764b

Introduction

A good scientific demonstration should show science in a clear and comprehensible manner, but retain an element of surprise or drama. The image of a fluid passing up through its critical point and back down again is one of the most beautiful and fascinating physical transformations that can be demonstrated to an audience. However, there are three substantial barriers to demonstrating this transition in practice, (1) making a high pressure demonstration visible to a large audience; (2) making the demonstration quick enough to retain the audience's attention; and (3) addressing the safety issues that surround high pressure experimentation. Some years ago, we described such a demonstration using a modified overhead projector,[1] this satisfied all of these criteria as a lecture demonstration. However, it was too complicated and vulnerable for use at public exhibitions where any exhibit must be essentially "tamper proof". The innovations of the approach presented here are (a) to use a robust, small volume, high pressure cell; (b) to sandwich the cell between two Peltier coolers so by reversing the applied voltage, the cell can be alternately heated or cooled; and (c) to view the cell through a borescope[2] with CCD video camera so that an enlarged image can be displayed on a TV monitor. For a wider audience, an LCD video projector may be used instead.

Scientific background

A supercritical fluid (SCF) is a gas that has been compressed until its density is close to that of a liquid. More formally, it may be defined as any substance that is held above its critical temperature (T_c) and critical pressure (p_c), and having a density close to, or higher than, its critical density. This definition can be understood with a phase diagram such as Fig. 1. The unique physical properties associated of SCFs,

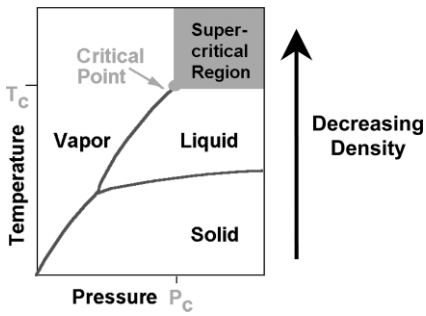

Fig. 1 Phase diagram for a pure substance. Conventionally such diagrams are shown with the *p* and *T* axes interchanged. However the format shown here is convenient for teaching purposes because the solid, liquid and SCF phases are arranged in order of decreasing density.

most notably their "tunable solvation abilities", render them excellent replacements for many environmentally damaging volatile organic solvents and poly-halogenated hydrocarbons including CFCs. Indeed SCFs are used in a variety of day to day processes including the decaffeination of coffee,[3] the production of fine chemicals,[4] and even the dry-cleaning of clothes.[5]

Unfortunately, the *critical parameters*, T_c and p_c (which must be exceeded for a pure substance to become supercritical), are often too high (see Table 1) for such scientific demonstrations to be deemed "safe" for use within a public environment. Fortunately, by careful selection of the fluid, it is possible to minimise such risks. Furthermore, the design of the optical cell and surrounding casing can be engineered with a large margin of safety and extra containment so that even in the worst case scenario, all components of the demonstration (including the expanded gaseous material) are efficiently contained within the demonstration itself.

Table 1 Critical parameters of commonly employed fluids[6]

Fluid	T_c/K	p_c/MPa
Water (H_2O)	647.3	22.06
Carbon dioxide (CO_2)	304.4	7.38
Propane (C_3H_8)	369.8	4.25
Sulfur hexafluoride (SF_6)	318.7	3.76

For our demonstration, we selected a fluid (SF_6) that possesses both low critical parameters (T_c 318.7 K, p_c 3.76 MPa) and equally importantly poses minimal toxicological risk[7] in the event of any unforeseen leakage of the contents of the optical cell.

Brief description of the demonstration

The apparatus is centred on an "over-engineered" (safety factor >3), minimal volume optical cell[8] (1 mL) which contains a small amount of liquefied SF_6 (0.5 mL). The cell is mounted between two Peltier devices that allow the cell to be rapidly heated or cooled depending on the polarity of the applied voltage. The cell and coolers are sandwiched between two channelled copper heat exchangers that are maintained at a constant temperature (313 K) by a conventional laboratory recirculating thermostated water bath, see Fig. 2. This minimises the time and amount of additional energy that is required to heat the cell through the critical point (318.7 K) inducing the liquid-vapour/SCF phase transition.

Additional energy in the form of heat is rapidly pumped either into; or out of, the cell by varying the polarity of the voltage applied across to the Peltier devices. This is efficiently controlled by a dual set point controller unit (Eurotherm 2108i) and a toggle switch labelled "Heat" and "Cool"

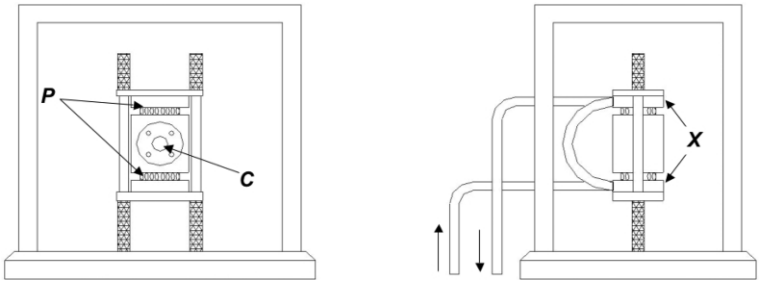

Fig. 2 Diagrammatic views of the SCF laboratory demonstration; C – optical cell containing SF_6 mounted in a copper block; P – Peltier cooler; X – channelled copper heat exchanger, supported by laboratory recirculation bath (not shown). The display is mounted within an aluminium framed, Lexan™ safety case, electrical control wires and heat pump services are introduced *via* suitable access glands in the casing. The optical cell is lit from behind by a white light LED fitted with a Teflon diffuser to give uniform illumination (not illustrated).

which can be safely operated by an unskilled viewer. The recirculation pump effectively acts as a heat sink that allows rapid cooling of the system re-establishing the original two-phase liquid–vapour system. In fact, the time that is required for the demonstration to cycle through both phase transitions can be reduced to just 2 minutes!

The demonstration

Fig. 3 shows the equipment in action. It provides a near perfect view of the phase transition that occurs when a liquid–vapour mixture is heated through the critical point in a sealed cell.

Most people are surprised that cooling the cell does not follow the same process in reverse. Indeed a much more dramatic phase transition occurs when the contents of the cell are cooled. As the temperature approaches T_c, there is great turbulence in the cell as condensed droplets of liquid and bubbles of gas separate within the cell, see Fig. 4.

Conclusion

This demonstration has been highly successful. For example, it operated literally thousands of times over a three day period when the apparatus formed the centrepiece of an exhibit entitled "Putting the Fizz into Chemistry" at The Royal Society – Summer Science Exhibition held in London in July 2002 (Fig. 5). During that period, the demonstration intrigued visitors from all backgrounds, quite literally from young school children to Nobel Prize winners!

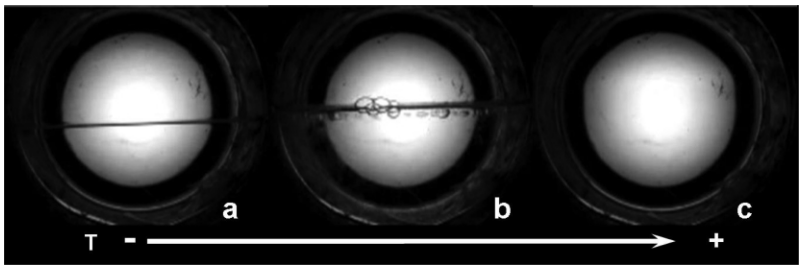

Fig. 3 Still photographs illustrating the phase transition observed as SF_6 is heated through its critical temperature (318.7 K); (a) initial 2 phases [liquid + gas]; (b) boiling liquid, and rise in the meniscus as a result of volumetric expansion indicating a drop in the density of the liquid phase; (c) the single phase, SCF, after the temperature has exceeded T_c.

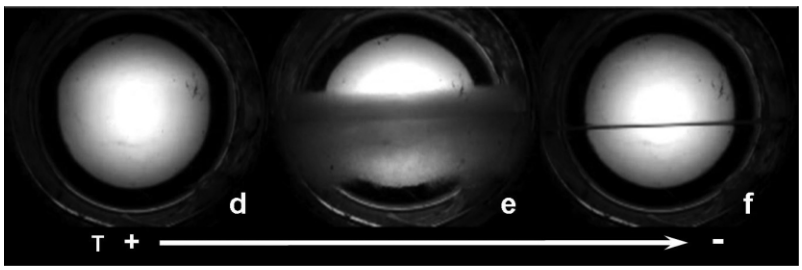

Fig. 4 One of the great surprises for any audience is that cooling of the SCF is not the reverse of heating up a liquid. The reason is that as the temperature (T) of the fluid drops below T_c droplets of liquid form uniformly in the fluid. Gravity then causes the droplets to fall and gas to rise creating the "storm" shown in (e) before separation back into two distinct phases (f).

Fig. 5 Interactive critical point demonstration. *N.B.* the supporting laboratory recirculation bath is positioned under the surface of the table.

An obvious criticism of the demonstration is that the pictures are displayed on a TV monitor and, nowadays, nobody believes anything on a TV because of image manipulation. However, this criticism is unfounded because (a) in a small scale exhibition, the viewers can look directly into the cell itself (through the safety screen incorporated into the display unit) to check that there is no sleight of hand, and (b) for a larger audience the demonstrator can shake the table so that everyone can see the resulting waves on the liquid inside the cell, proving to all that the image is real.

Important safety note

Each piece of equipment must be subjected to its own individual safety assessment. Neither the authors nor The University of Nottingham accepts liability for the safety of any equipment or apparatus built upon the basis of this article.

Acknowledgements

The development of this demonstration involved major contributions from the technical support staff within The School of Chemistry at The University of Nottingham. Considerable thanks are due to Messrs J. Whalley, M. Beasley, P. Fields, J. Warren and R. Wilson. The optical cell that was incorporated in the display was donated by François Cansell of L'Institut de Chemie de la Matière Condensée de Bordeaux. We thank the EPSRC, The Royal Society and The CRYSTAL Faraday Partnership for financial support.

References

1 J. A. Banister and M. Poliakoff, *J. Supercrit. Fluids*, 1993, **6**, 233–235.
2 Borescope: a prismatic optical device used to inspect otherwise inaccessible places,

commonly employed in engineering.
3 For an excellent introduction to the application of SCFs in the extraction industry please see: M. A. McHugh and V. J. Krukonis, *Supercritical fluid extraction: principles and practice*, 2nd edn., Butterworth-Heinemann, Boston, 1994.
4 P. Licence, J. Ke, M. Sokolova, S. K. Ross and M. Poliakoff, *Green Chem.*, 2003, **5**, 99–104.
5 For further information please see http://www.hangersdrycleaners.com/.
6 For a list of the properties of many fluids, please see http://webbook.nist.gov/chemistry/.
7 The toxicological effects associated with SF_6 are very low.However, as pointed out by a referee, SF_6 is a persistent greenhouse gas and has a global warming potential 23 900 times that of CO_2, but the amounts used in this experiment are minimal. For further information, please refer to the material safety data sheet for SF_6; an example is available from the BOC safety database: http://www1.boc.com/uk/sds/.
8 The optical cell is constructed with sapphire windows (Ø = 12 mm, d = 5 mm).The maximum working pressure (P_{max}) of the cell is 70 MPa, the security factor (wrt P_{max}) = 3.4.

www.rsc.org/greenchem

Green chemical processing in the teaching laboratory: a convenient liquid CO_2 extraction of natural products†

Lallie C. McKenzie,[a] John E. Thompson,[b] Randy Sullivan[c] and James E. Hutchison*[a]
[a]*Department of Chemistry and the Material Science Institute, University of Oregon, OR 97403, USA. E-mail: hutch@uoregon.edu*
[b]*Department of Chemistry, Lane Community College, OR 97405, USA*
[c]*Department of Chemistry, University of Oregon, OR 97403, USA*

A unique liquid CO_2 extraction laboratory developed for a greener organic teaching lab curriculum provides an effective, inexpensive, and convenient procedure for teaching natural products extraction concepts and techniques using modern green extraction technology. The procedure is appropriate for the teaching lab, does not require any special equipment, and allows the students to see the phase change and extraction as they occur. Students learn extraction and spectroscopic analysis skills, are exposed to a dramatic visual example of phase change, and are introduced to commercially successful green chemical processing with CO_2.

DOI:10.1039/b405810k

Introduction

Although there have been many advances in green chemistry in the industrial and research fields, integration of these concepts into the teaching environment is still in its infancy. This may be due to the limited availability of educational materials that illustrate the methods, techniques, and principles of green chemistry. To address this problem, we developed a new green organic laboratory curriculum to teach fundamental chemical concepts and techniques along with the tools and strategies of green chemistry.[2–6] Integration of these goals into the laboratory curriculum required the development of a broad collection of experiments that work well in the laboratory, improve the safety of the laboratory environment, and modernize the curriculum through the introduction of state-of-the-art methods. A green organic chemistry laboratory textbook[2] and several manuscripts describe the criteria and process for greening experiments.[3,4,6]

Here we describe a new laboratory exercise that uses liquid CO_2 to extract D-limonene from citrus rind. This safe and convenient procedure successfully addresses the diverse goals of green chemistry experiment development by simultaneously teaching practical techniques, fundamental chemical concepts, and green chemistry applications. In this experiment, the commonly taught concepts of natural product extraction and phase transitions are demonstrated through a novel procedure employing liquid CO_2 as a green solvent. The experiment introduces modern green chemical approaches through discussions of industrial use of liquid CO_2 as a green replacement solvent (*e.g.*, dry cleaning) and supercritical fluid extraction (SFE) as an example of a successful commercial green process (*e.g.*, decaffeination of coffee). Replacement of traditional natural product extraction experiments through incorporation of this green chemistry research and technology promotes an understanding of the current practice of green chemical methods. This exciting, convenient, and straightforward procedure offers an opportunity to teach core organic chemistry concepts and skills in the context of applicable green chemistry.

In this report, a short review of the background and current industrial uses of CO_2 and the relevance of this technology to the teaching laboratory are described. The new laboratory procedure is summarized in the Experimental section.[7] In the Results and discussion section, both the chemical and green lessons of this process are discussed and extensions are proposed.

Supercritical and liquid CO_2

At pressures above ambient, carbon dioxide can exist in forms usable as a solvent (*i.e.* as a liquid or supercritical fluid). As shown in the phase diagram in Fig. 1, CO_2 is a liquid under relatively mild temperatures and pressures, in the ranges of −56.6 to 31.0 °C and 5.2 to 73.8 bar. Supercritical carbon dioxide ($scCO_2$) is produced at temperatures higher than the critical temperature (31.0 °C) and between the critical pressure (73.8 bar) and extremely high pressures (approximately 10^4 bar). Supercritical fluids have no distinct liquid or vapor phase but retain properties of each. $ScCO_2$ is especially beneficial when used as a solvent in selective extraction processes. The gas-like properties, such as very low surface tension and viscosity, allow the solvent to penetrate into the substrate, while the liquid-like properties solubilize compounds and remove them from the substrate. Small changes in pressure or temperature alter the bulk density of the fluid leading to increased or decreased solubility of various compounds. In this way, the use of supercritical fluids can allow for control of separations of materials. Through manipulation of temperature and pressure conditions within accessible ranges, both the phase and properties of CO_2 can be easily controlled.

During the past two decades, technical advances have been made in the industrial use of supercritical and liquid carbon dioxide in place of organic solvents.[8–10] CO_2 is useful as a green alternative solvent because it provides environmental and safety advantages: it is nonflammable, relatively nontoxic, readily available, and environmentally benign. Processing with CO_2 also poses minimal hazard in the event of unintentional release or residual solvent in the product. Although CO_2 is a greenhouse gas, when used as a solvent it is captured and employed, not generated, resulting in no net environmental harm. Additionally, a closed loop system can be used to compress the gas in order to use the supercritical fluid or liquid in processing, depressurize the solvent for separation of dissolved compounds, and recompress the CO_2 to begin the cycle again. CO_2 extraction processes can also be run at relatively constant pressure when liquid–liquid extraction against water is used for product recovery. These loop systems allow for easy recovery and recycling of the pure solvent.

†Electronic supplementary information (ESI) available: experimental procedure (including instructors' notes, student handout, and demonstration procedure) and movie clip of extraction process. See http://www.rsc.org/suppdata/gc/b4/b405810k/

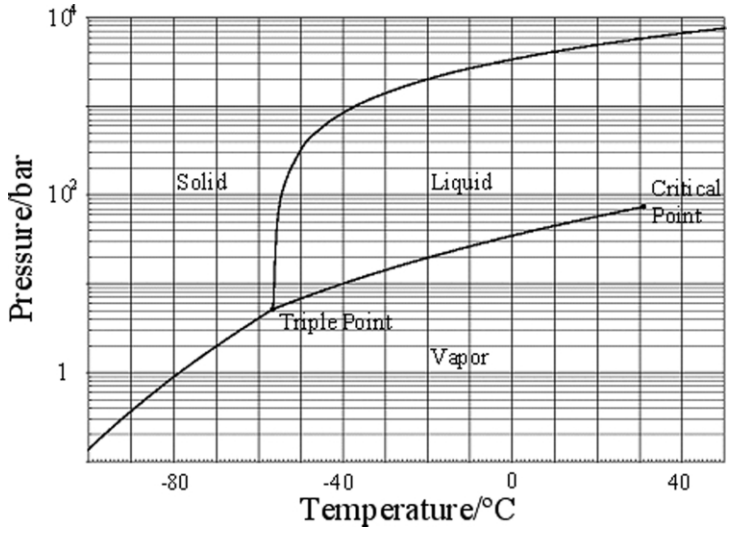

Fig. 1 The temperature–pressure diagram for carbon dioxide clearly indicates the pressures and temperatures for the phase transformations, triple point, and critical point. Adapted and used with permission from ChemicaLogic Corporation.[1]

Applications of CO_2 as an alternative solvent

Large-scale CO_2 processing has had commercial success in many separation and extraction processes.[8,9] The tunable solubility properties, low toxicity, and ease of removal of CO_2 have led to well established $scCO_2$ technology for the extraction of various food products, including essential oils and hops, and for the decaffeination of coffee and tea. The mild conditions necessary for extraction and absence of residual solvent result in superior products and have motivated an industrial shift to CO_2 from hazardous solvent extractions or steam distillations. The oil products from $scCO_2$ extraction processes are of higher purity and contain no thermal degradation products. The ability to influence solubility of compounds through variations in temperature and pressure has resulted in enhanced extraction of desired compounds from natural products and in the ability to enrich oils during post-extraction treatment with CO_2.[11,12] $ScCO_2$ has also been used in other processes including analytical extractions and chromatography, metal degreasing, and textile dyeing.

A commitment to replacing hazardous solvents and improving environmental footprints has led to many new green methods of materials synthesis and processing with CO_2.[8,9,13] Carbon dioxide is relatively inert, is resistant to oxidation, cannot serve as a chain transfer agent, and provides for tunable miscibility. These chemical advantages have led to an increasing number of industrial-scale reactions which use CO_2. Carbon dioxide has been employed in the synthesis of polymers such as DuPont™ Teflon® fluoropolymer resins and for commercial-scale hydrogenation and oxidation reactions.[8] The UNICARB® VOC Reduction Process uses $scCO_2$ as the carrier and atomizing agent for spraying paints and coatings.[9] The variable solubility permits the use of CO_2 in the formation of micron-sized particles, technology which has been employed in the synthesis of inhalable medications.[14] In addition to these demonstrated uses for CO_2, current research is also investigating its applicability in the microelectronics industry, in catalysis reactions, and as a simultaneous reaction medium and raw material.[13]

Although most industrial applications use supercritical CO_2, *liquid phase* carbon dioxide has also proven effective. The wide range of lower temperatures and pressures offers flexibility in the design of processes using liquid CO_2. The mild conditions prevent degradation of products. As with $scCO_2$, ideal density, viscosity, and surface tension can be obtained through manipulation of pressure and temperature. Liquid CO_2 has been employed extensively as an industrial solvent for the extraction of essential oils[15] and in new greener methods of dry cleaning.[8,9]

To date, a convenient liquid CO_2 extraction method using standard laboratory materials has not been reported. The laboratory experience described here brings the liquid CO_2 extraction process into the teaching or research laboratory in an inexpensive, effective, and accessible manner. It offers an opportunity for students to learn extraction techniques, observe striking phase changes, and appreciate the benefits of using greener chemical methods. This carbon dioxide extraction procedure provides a convenient drop-in replacement for currently used natural product steam distillation or solvent extraction laboratories.

Experimental

Dry ice sublimes at atmospheric pressure and temperatures above −78 °C. If the CO_2 is sealed in a vessel during sublimation, the internal pressure in the vessel increases. After the temperature and pressure have increased sufficiently, liquid carbon dioxide forms. Due to this accessible phase change, carbon dioxide can be used for bench top extraction processes. In this experiment (see Fig. 2 and ESI†), approximately two and a half grams of grated orange peel and a wire and filter paper or metal screen solid trap are placed in a 15 mL polypropylene centrifuge tube with plug seal cap (Corning catalog #430052).[16] The centrifuge tube is completely filled with crushed dry ice, capped tightly, and dropped (tapered end down) into a plastic cylinder or polycarbonate bottle which is half-filled with warm (40–50 °C) tap water.

As pressure builds in the tube, gas escapes slowly through the threading of the cap.[17] After approximately fifteen seconds, the solid begins to melt, and liquid CO_2 appears in the tube. Solid, liquid, and gas phases are visible in the tube for a short period of time.[18] The liquid boils, and gas escapes for almost three minutes. During this time, the liquid CO_2 moves through the solid, extracts the oil from the orange rind, and collects in the bottom of the tube. The solid trap successfully prevents the orange rind from moving into the tip of the tube during extraction because the wire coils are supported by the sides of the centrifuge tube at the point where it narrows. After the extraction solvent completely evaporates, isolated product remains in the tip of the tube. Once the liquid has stopped bubbling and gas is no longer escaping, the centrifuge tube is removed from the cylinder with tweezers, and the extraction process is repeated by refilling the tube containing the orange rind and solid trap with dry ice, recapping it, and replacing it in the cylinder. Two or three extraction cycles result in isolation of approximately 0.1 mL of pale yellow oil. Typical yields are comparable to organic solvent extraction or cold pressing (1–2% recovery, based upon initial mass of rind used during extraction).[19] The extracted product is predominantly D-limonene by ^{1}H NMR and IR analysis and 97% D-limonene as indicated by GC-MS.

Results and discussion

The inspiration for this laboratory came from a desire to develop a reliable, convenient, inexpensive, and safe approach to CO_2 extraction that could be performed easily in any teaching laboratory. A secondary goal was to allow students to visually observe the phase changes of CO_2. Several liquid and supercritical CO_2

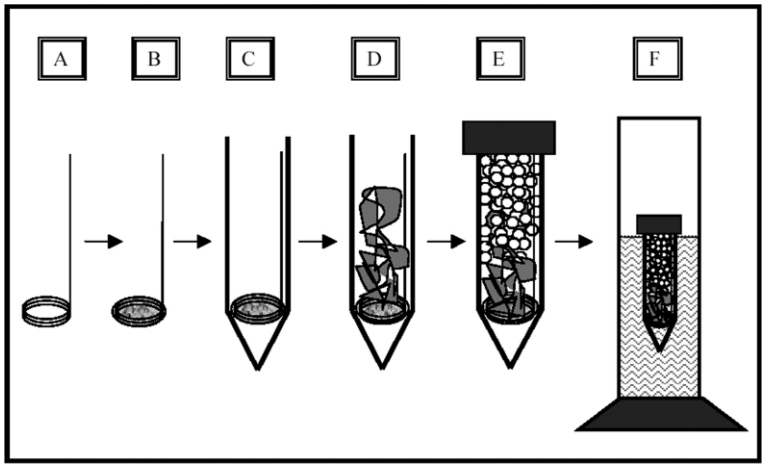

Fig. 2 Illustration of the liquid CO_2 extraction procedure. A solid trap is constructed by (A) bending copper wire into coils and a handle, (B) placing filter paper or metal screen between the wire coils, and (C) placing the solid trap in a centrifuge tube. For extraction, (D) grated orange peel is placed in the tube, and (E) the tube is filled with crushed dry ice and sealed with a cap. (F) The prepared centrifuge tube is placed in the water in the graduated cylinder, and the liquefaction and extraction occur over the following three minutes.

procedures have been developed previously, but these methods show the phase change for a brief time and do not allow for extraction, limit visualization of the phase transitions, or require expensive extraction equipment.[20–22] We sought to make carbon dioxide extraction of natural products widely accessible and lengthen the observation period of phase changes, while maintaining a high degree of safety. The following sections detail the core organic laboratory concepts and skills as well as the green lessons taught through this new approach. Although the scope of this report is limited to a summary of the laboratory experience, more specific information and detailed instructions are included in the ESI.†

Natural products extraction and spectroscopy

Organic laboratory courses often include a natural product extraction in order to introduce solid/liquid extraction methods and the chemistry of the terpene compounds. The most commonly used methods are those of steam distillation and organic solvent extraction. In the procedure described herein, the techniques of liquid/solid extraction are taught through repeated extractions of orange peel with carbon dioxide (see Scheme 1). The introduction of CO_2 extraction into the curriculum allows students to use a green solvent and to compare and contrast separation techniques. The practical and reliable procedure provides reproducible results and isolable yields of pure product which are comparable to those of other extraction methods. The volume of product collected is large enough for analysis by spectroscopic methods, and the use of ^1H NMR and IR spectroscopy provides opportunities for detailed analysis of complex spectra. Gas chromatography-mass spectroscopy can be used to compare the purity of samples generated by different extraction methods or to evaluate the composition of oils from different citrus fruits.

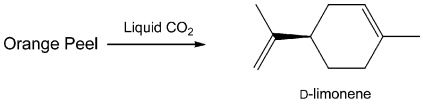

Scheme 1 Extraction of D-limonene from grated orange rind using liquid CO_2 as a green extraction solvent. The product is 97% D-limonene and has no solvent residue.

Phase transitions

Changes in physical states of compounds, the effects of temperature and pressure on these states, and their representation with phase diagrams are discussed often in chemistry courses. The opportunity to introduce these concepts in an easy and visual manner is a challenge addressed by few laboratory materials.[20,21] Students are familiar with the sublimation of CO_2 and with the use of CO_2 in fire extinguishers and fountain drinks. Carbon dioxide provides accessible phase changes requiring low temperatures and relatively low pressures. In particular, the liquid state is accessible through slight increases in pressure. During this laboratory experiment, the solid dry ice melts quickly when appropriate pressure and temperature conditions are reached. For at least one minute, solid, liquid and gas phases are visible. The transparent plastic extraction vessels and containment cylinders used in this procedure allow the students to observe these phase changes safely and easily.

Green messages

In this laboratory, there are opportunities for discussions of many green chemistry principles.[23] Primarily, the focus is on prevention of waste and using safer solvents. Students are encouraged to consider the effects of solvent choice and extraction method on the extraction process and product. Using CO_2 as a solvent presents no risk to human health or the environment, and the extraction is as effective as extraction with other commonly used solvents. Both solvent extraction and steam distillation procedures produce significant amounts of solvent waste for very little product, but there is no solvent waste when carbon dioxide is used. The product of this extraction exhibits higher purity due to the absence of solvent residue. Students also are exposed to a green chemical process which has been widely incorporated into industrial practice. This view of green chemistry as an active and applicable set of principles improves the students' perception of chemistry and provides beneficial preparation for students who may become chemists in industrial or academic settings.

Extensions

Due to the pressure limitations of the simple equipment used in this experiment, extractions with this procedure are limited to those that can be performed in liquid CO_2. Specially-designed equipment is required to extend to supercritical fluid extractions (SFE). Teaching laboratory instructors must balance the need for an inexpensive and convenient procedure with the opportunity to demonstrate the versatility of CO_2 extraction. While lab-scale supercritical fluid extractors are available, they are expensive. If financially feasible, introducing SFE technology into the teaching laboratory through the use of supercritical fluid equipment would provide opportunities for extraction of a wide variety of compounds and improved quantitative analysis.

Extensions of this laboratory exercise include further exploration of the principles and practice of green chemistry. This procedure can be used to help students improve their understanding of the concepts of cleaner processing through the evaluation of yields, purity, waste generated, and energy costs of different extraction methods.[2] Through reading scientific literature, students can explore the current trends of industrial processing with CO_2. Discussion of the benefits and difficulties of using CO_2 as a green solvent can provide students with an awareness of the challenges involved in solvent replacement.

Although supercritical and liquid CO_2 have been used to extract natural products from coffee, hops, and many fruits,

flowers, and spices,[15] this laboratory procedure has only successfully extracted natural products from citrus rinds. Modification of the extraction conditions to include a larger amount of substrate are required to allow for extraction of materials of lower density, and grinding or other processing may be necessary when introducing large solid matrices.

This lab is readily adapted as a classroom demonstration. Visibility is improved, and safety is enhanced by placing the centrifuge tube in water in a large polycarbonate cylinder. Using this apparatus, students may view the demonstration at closer range. The demonstration also may be projected using a video camera and projector.[24]

Conclusions

The liquid CO_2 extraction laboratory described herein incorporates modern green chemistry into the organic teaching environment in a visible and exciting manner. Equally important, this procedure fits the constraints of the teaching laboratory, including those of time, safety, effectiveness, affordability, and convenience. The one to two hour procedure, including all preparation, extraction, and analysis, can be performed on its own or conducted concurrently with another experiment. In this laboratory exercise, all chemical hazards of traditional extraction procedures have been removed, and laboratory conditions provide for safe viewing of the phase changes and extraction. All required materials are readily available and inexpensive. Unlike steam distillation or organic solvent extraction procedures, there is no waste disposal cost with CO_2 extraction.[25] Comparisons of product recovery and purity, generation of waste, and risk to students and the environment indicate that this procedure provides the greenest natural product extraction laboratory currently available.[26] The convenient, rapid liquid CO_2 natural product extraction is based on the foundation of commercially successful green chemical processing. Through the application of principles and strategies of green chemistry and instruction in practical techniques and concepts, this drop-in replacement natural product extraction laboratory exercise easily teaches fundamental chemical lessons and successfully incorporates green chemistry into the teaching laboratory.

Acknowledgements

This work was supported by the University of Oregon, the National Science Foundation (CHE-9702726 and DUE-0088986), and the American Chemical Society. We thank Gary Nolan for his assistance with GC/MS data collection, and the students enrolled in Organic Laboratory at Lane Community College for their assistance in optimizing and testing this experiment. J.E.H. is an Alfred P. Sloan Research Fellow and a Camille Dreyfus Teacher-Scholar.

References

1 ChemicaLogic Corporation. http://www.chemicalogic.com/download/co2_phase_diagram.pdf (accessed Feb 2004).
2 K. M. Doxsee and J. E. Hutchison, *Green Organic Chemistry: Strategies, Tools, and Laboratory Experiments*, Brooks/Cole, Pacific Grove, CA, 2004.
3 S. M. Reed and J. E. Hutchison, *J. Chem. Educ.*, 2000, **77**, 1627–1629.
4 M. G. Warner, G. L. Succaw and J. E. Hutchison, *Green Chem.*, 2001, **3**, 267–270.
5 L. C. McKenzie, L. M. Huffman, K. E. Parent, J. E. Hutchison and J. E. Thompson, *J. Chem. Educ.*, 2004, **81**, 545–548.
6 L. C. McKenzie, L. M. Huffman and J. E. Hutchison, The Evolution of a Green Chemistry Laboratory Experiment: Greener Brominations of Stilbene, *J. Chem. Educ.*, in press.
7 Detailed notes for instructors, spectral data, student handout, and demonstration procedure are available in the electronic supplementary information (ESI) of this journal. See http://www.rsc.org/suppdata/gc/b4/b405810k/.
8 E. J. Beckman, *Environ. Sci. Technol.*, 2002, **36**, 347A–353A.
9 E. J. Beckman, *Ind. Eng. Chem. Res.*, 2003, **42**, 1598–1602.
10 The two reviews cited here provide detailed background information on current sustainable materials processing with CO_2. A list of websites which provide information about specific CO_2 technologies is included in the instructors' notes in the ESI.
11 F. Benvenuti and F. Gironi, *J. Chem. Eng. Data*, 2001, **46**, 795–799.
12 A. Chafer, A. Berna, J. B. Monton and A. Mulet, *J. Chem. Eng. Data*, 2001, **46**, 1145–1148.
13 N. Tanchoux and W. Leitner, in *Handbook of Green Chemistry and Technology*, eds. J. Clark and D. Macquarrie, Blackwell Science, Oxford, 2002, pp. 482–501.
14 Thar Technologies, Supercritical Fluid Particle Formation Home Page. http://www.thartech.com/systems/particle/ (accessed Feb 2004).
15 M. Mukhopadhyay, *Natural Extracts Using Supercritical Carbon Dioxide*; CRC Press, Washington, DC, 2000.
16 This procedure has only been successfully tested with centrifuge tubes of this brand and part number. The caps of larger Corning tubes (50 mL) did not withstand the pressure. The tubes must withstand temperatures from −78 to 50 °C and pressures from 1 to at least 6 atm. For safety reasons, the ability to withstand higher pressures is desired.
17 Under experimental conditions, carbon dioxide gas leaks from the centrifuge tube at an average rate of 2.5 g min^{-1}.
18 The simple apparatus used in this experiment does not allow for accurate determination of temperature and pressure conditions under which the extraction is occurring. Although the system is not at equilibrium, the phase diagram and physical observations can be used to estimate the conditions in the tube. Observation of both the gas/liquid and solid/liquid interfaces indicates that locally the temperature is between the temperature at the triple point (−56.6 °C) and the critical temperature (31.1 °C). Formation of ice on the surface of the tube further brackets the temperature to between −56.6 and 0 °C. The pressure is passively regulated by the leaking from the tube and, due to the liquefaction, is assumed to be above the pressure at the triple point (5.2 bar) but below the pressure that would induce tube rupture. These observations indicate that conditions approach those of the triple point.
19 D. C. Smith, S. Forland, E. Bachanos, M. Matejka and V. Barrett, *Chem. Educ.*, 2001, **6**, 28–31.
20 V. T. Lieu, *J. Chem. Educ.*, 1996, **73**, 837.
21 *Introduction to Green Chemistry: Instructional Activities for Introductory Chemistry*, eds. M. A. Ryan and M. Tinnesand, American Chemical Society, Washington, DC, 2002.
22 N. H. Snow, M. Dunn and S. Patel, *J. Chem. Educ.*, 1997, **74**, 1108–1111.
23 P. T. Anastas and J. C. Warner, *Green Chemistry: Theory and Practice*, Oxford University Press, New York, 1998.
24 Detailed demonstration procedures are included in the ESI.
25 Cost per student is approximately $1.00 for laboratory materials including centrifuge tubes, dry ice, and citrus fruit. Plastic containment cylinders can be purchased or constructed for $2–3 each. One cylinder per student per lab period will be required. Further details are provided in the ESI.
26 Product recovery ranges from 1–2% based on initial mass of rind used. GC-MS data of student-performed steam distillation, pentane extraction, and carbon dioxide extraction are available in the ESI.

COMMUNICATION

www.rsc.org/greenchem

Glycerol hydrogenolysis on heterogeneous catalysts

Julien Chaminand,[a] L.aurent Djakovitch,*[a] Pierre Gallezot,[a] Philippe Marion,[b] Catherine Pinel*[a] and Cécile Rosier[b]

[a] *Institut de Recherches sur la Catalyse, 2 avenue Albert Einstein, 69626 Villeurbanne Cedex, France. E-mail: laurent.djakovitch@catalyse.cnrs.fr. E-mail: pinel@catalyse.cnrs.fr; Fax: +33(0)4 7244 5399*

[b] *Rhodia, 85 avenue des Frères Perret, BP 62, 69192 Saint-Fons Cedex, France*

Received 17th May 2004, Accepted 6th July 2004
First published as an Advance Article on the web 6th August 2004

Aqueous solutions of glycerol were hydrogenolysed at 180 °C under 80 bar H_2-pressure in the presence of supported metal catalysts in an attempt to selectively produce 1,2- and 1,3-propanediol. Catalysts (Cu, Pd, Rh), supports (ZnO, C, Al_2O_3), solvents (H_2O, sulfolane, dioxane) and additives (H_2WO_4) were tested to improve reaction rate and selectivity to the target molecules. The best selectivity (100%) to 1,2-propanediol was obtained by hydrogenolysis of water solution of glycerol in the presence of CuO/ZnO catalysts. To improve the selectivity to 1,3-propanediol the reaction was conducted with rhodium catalysts with tungstic acid added to the reaction medium. The best result in terms of conversion and selectivity to 1,3-propanediol (1,3-PDO/1,2-PDO = 2) was obtained by operating in sulfolane. The presence of iron dissolved in the reaction medium was also beneficial for the selectivity to 1,3-PDO. A mechanism was proposed to account for the effect of these different parameters.

Introduction

This study is part of the global challenge aiming at the production of marketable chemicals *via* the catalytic transformation of bio-sustainable resources employed as substitutes for fossil fuels. Polyfunctionalised compounds such as polysaccharides and fatty oils are available at low cost in large supply from renewable raw materials. Because of the development of biodiesel production by transesterification of vegetable oils, large amounts of glycerol are available as a reaction by-product. Finding new outlets for glycerol consisting of high value-added products would improve the economy of the whole process.

Previously, we developed the selective oxidation with air of glycerol in the presence of carbon-supported metal catalysts to obtain valuable oxygenated derivatives.[1] Thus, an 80% yield of glyceric acid was obtained in the presence of a Pd/C catalyst at basic pH, while dihydroxyacetone, a useful product in the cosmetic industry, was the main product obtained using a Pt–Bi/C catalyst at acidic pH. Another investigation devoted to the selective hydrogenolysis of starch-derived polyols in the presence of CuO–ZnO catalysts yielded mainly deoxyhexitols suitable for polymer applications.[2]

Our current objective is to study the hydrogenolysis of glycerol in the presence of heterogeneous catalysts to produce 1,2-propanediol (1,2-PDO) and 1,3-propanediol (1,3-PDO). 1,3-Propanediol is copolymerised with terephthalic acid to produce the polyester SORONA® from DuPont, or CORTERRA® from Shell, which are used in the manufacture of carpet and textile fibres exhibiting unique properties in terms of chemical resistance, light stability, elastic recovery, and dyeability.[3,4] 1,3-PDO is currently produced from petroleum derivatives such as ethylene oxide (Shell route) or acrolein (Degussa-DuPont route) by chemical catalytic routes.[5,6] 1,2-Propanediol is an important commodity chemical derived from propylene oxide.[7] These diols can be produced by an alternative route involving selective dehydroxylation of glycerol. In 1985, Celanese patented the hydrogenolysis of glycerol water solution under 300 bar of syngas at 200 °C in the presence of a homogeneous rhodium complex ($Rh(CO)_2(acac)$) and tungstic acid. 1,3-PDO and 1,2-PDO were produced with 20 and 23% yield, respectively.[8] Shell developed the use of homogenous palladium complex in a water–sulfolane mixture in the presence of methane sulfonic acid. After 10 h reaction, 1-propanol, 1,2-propanediol and 1,3-propanediol were detected in a 47 : 22 : 31 ratio.[9] More recently, Bullock *et al*. described the dehydroxylation of glycerol in sulfolan catalyzed by a homogeneous complex of ruthenium. The reaction proceeded under milder conditions (52 bar, 110 °C) but very low yields of 1,2-PDO and 1,3-PDO were achieved (< 5%).[10] Performing this transformation over solid catalysts was also attempted. The treatment of glycerol under hydrogen in the presence of copper–chromium-based catalysts yielded only 1,2-PDO.[11] Montassier *et al*. reported that the hydrogenolysis of glycerol under 300 bar H_2 at 260 °C in the presence of Raney nickel, Ru, Rh and Ir catalysts yielded mainly methane, but in the presence of Raney copper 1,2-PDO was the main reaction product.[12,13] Recently, Werpy patented the hydrogenolysis of glycerol and other polyols over Ni/Re catalyst. After 4 h at 230 °C under 82 bar H_2, 44% of 1,2-PDO and 5% of 1,3-PDO were obtained together with 13% of ethylene glycol.[14]

In the present paper, the catalytic hydrogenolysis of glycerol was conducted over heterogeneous catalysts as a function of various reaction parameters to minimize carbon–carbon bond rupture and improve the rate and selectivity of the reaction towards 1,2-PDO and 1,3-PDO (Scheme 1). As the latter has a much higher commercial value, we will focus on increasing its formation

Results and discussion

Several catalysts were tested for the selective hydrogenolysis of glycerol (Tables 1 and 2). Initially, our choice was directed to a CuO–ZnO catalyst because of its efficiency in the hydrogenolysis of sorbitol to deoxyhexitols.[2] Its activity in glycerol hydrogenolysis was low since with 5 mol% catalyst, after 90 h reaction under 80 bar H_2 at 180 °C only 19% conversion was achieved. However this copper-based catalyst was quite selective to 1,2-PDO in agreement with the earlier report by Montassier *et al*. using Raney copper catalyst.[12] The addition of tungstic acid to the reaction medium did

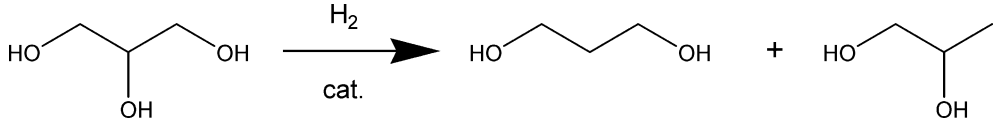

Scheme 1

DOI: 10.1039/b407378a

Table 1 Influence of the catalyst on the hydrogenolysis of glycerol in water[a]

Catalyst	Additive	Conversion (%) (90 h)	Yield 1,3-PDO (%)[b]	Yield 1,2-PDO (%)
CuO/ZnO	—	19	n.d.	19
CuO/ZnO	H_2WO_4	21	n.d.	17
Pd/C	—	< 1	n.d.	0.4
Pd/C	H_2WO_4	3	n.d.	2
Rh/C	—	2.5	n.d.	2
Rh/C	H_2WO_4	10	2.6	5.2

[a] Reaction conditions: 15 g glycerol, 65 mL H_2O, 180 °C, 80 bar H_2, 0.5 mmol Rh or Pd (0.3%), 0.08 mol Cu (50%), 5 mmol H_2WO_4, without Teflon lining. [b] n.d. = not detected.

Table 2 Influence of the support on the hydrogenolysis of glycerol[a]

Catalyst	Conversion (%)	Yield 1,3-PDO (%)[b]	Yield 1,2-PDO (%)[b]	1,3-PDO/ 1,2-PDO
Rh/C (5%)	21	1.3 (6)	15 (70)	0.1
Rh/Al_2O_3 (5%)	27	3.1 (12)	12.4 (45)	0.3
Rh/Nafion (1%)	8	1.5 (19)	4.3 (54)	0.35
Rh/HY (3.5%)	3	0	0	—

[a] Reaction conditions: 15 g glycerol, 65 mL H_2O, 180 °C, 80 bar, 168 h, 0.5 mmol Rh (0.3%), 5 mmol H_2WO_4, with Teflon lining. [b] Selectivity in brackets.

not significantly affect the activity and selectivity, except small amounts of products produced from C–C cleavage were detected.

Carbon-supported metallic catalysts (Pd and Rh) were then tested for this transformation. In the presence of 0.3 wt% (metal-based) of Pd/C or Rh/C catalysts a small conversion was achieved after 90 h (< 2.5%). The addition of tungstic acid enabled us to obtain an increase of conversion, particularly with rhodium catalyst (2.5 and 10% without and with tungstic acid, respectively). In the presence of palladium catalyst, the 1,2-PDO was the only diol detected while the use of rhodium catalyst yielded 1,3-PDO and 1,2-PDO with 26 and 52% selectivity, respectively. Under identical conditions, the homogeneous rhodium complex described by Celanese[8] was inactive. The relative amounts of the different products were constant within the experimental error up to 25% conversion. Further studies were then performed to improve the activity of the rhodium catalyst and to determine the impact on the selectivity of the reaction.

The nature of the solvent had a dramatic effect on the rate and selectivity of the reaction (Table 3). In sulfolane, higher conversion

Table 3 Influence of the solvent on the hydrogenolysis of glycerol over 5% Rh/C catalyst[a]

Solvent	Conversion (%)	Yield 1,3-PDO (%)[b]	Yield 1,2-PDO (%)[b]	1,3-PDO/ 1,2-PDO
H_2O	21	1.3 (6)	15 (70)	0.1
Sulfolane	32	4 (12)	2 (6)	2
Dioxane[c]	15	2 (13)	2 (13)	1

[a] Reaction conditions: 15 g glycerol, 65 mL solvent, 180 °C, 80 bar, 168 h, 0.5 mmol Rh (0.3%), 5 mmol H_2WO_4, with Teflon lining. [b] Selectivity in brackets. [c] Reaction time: 48 h

was observed, the main product was 1-propanol and the yield of 1,3-PDO was twice that of 1,2-PDO. Dioxane favoured the breakage of C–C bonds and significant amounts of glycol, ethanol and methanol were detected. As far as 1,3-PDO and 1,2-PDO were concerned, similar selectivities were achieved. We also performed the reaction in the absence of any solvent but, in that case, the results were not reproducible.

The influence of the temperature was also studied. As expected, when the temperature increased, the reaction rate was higher and the activation energy was calculated to be 98 kJ in the range of 180–240 °C. However when high temperature was used, the selectivity to diols was poor (< 2%). Volatile hydrocarbons were formed because the carbon balance determined by GC in the final solution was very low (17% at 240 °C).

The influence of the nature of the support was studied with rhodium-based catalysts in a Teflon protected autoclave (Table 2). Nafion-supported rhodium catalyst was prepared according to the work of Laufer and Hoelderich.[15] This support was chosen because the presence of acid in the medium has a significant influence on the conversion as well as on the ratio 1,3-PDO/1,2-PDO, as reported in homogeneous catalysis[10] and in Table 1. The Rh/Nafion catalyst yielded 8% conversion after 168 h with 19 and 54% selectivity to 1,3-PDO and 1,2-PDO, respectively. Despite the very low activity of this catalyst, it exhibited interesting performances thanks to high diol selectivity (72%) and a significant 1,3-PDO/1,2-PDO ratio. Zeolite-based catalyst yielded only 1-propanol and a low glycerol conversion (3% after 168 h) which could be attributed to diffusion limitation of polyols in the zeolite pores. In contrast carbon and alumina-supported rhodium catalysts gave higher conversion (21 and 27%, respectively, after 168 h). The carbon-supported rhodium exhibited higher selectivity towards 1,2-PDO compared to alumina-supported catalyst.

It was shown that rate and selectivity data depended upon whether the reaction vessel was lined with Teflon or not. After 120 h, the conversion of glycerol reached 19% in the lined autoclave compared to only 9% in the absence of a lining. In both cases 1,2-PDO was the main product, but the formation of 1,3-PDO was favoured in the naked-wall autoclave. Thus, at 10% conversion, the selectivity to 1,3-PDO attained 7 and 27% with and without Teflon lining, respectively. These values corresponded to a ratio 1,3-PDO/1,2-PDO of 0.1 and 0.5 respectively. To interpret these data the partial dissolution of metals from the inox walls of the reactor was suspected and this hypothesis was verified by chemical analysis after reaction of the solution and catalyst where Fe, Ni, and Mn were detected. These metals could interact with the catalyst and/or with the substrate thus improving the selectivity of the reaction in favor of 1,3-PDO at the expense of the activity. To confirm this hypothesis, a reaction was performed in a protected autoclave in the presence of an iron salt. The conversion decreased after addition of 0.2% of $FeCl_2$ in the medium and the 1,3-PDO/1,2-PDO ratio increased up to 0.5 (*versus* 0.1 in the absence of iron salt, Table 3). A similar phenomenon was observed after addition of other iron salts such as $Fe(acac)_2$, $FeSO_4$; that is to say, increasing the selectivity in favour of 1,3-PDO to 0.7 and 0.45, respectively. Further work must be performed with defined Rh–Fe catalyst to establish the influence of the iron. Addition of copper salts ($Cu(NO_3)_2$, $CuCO_3$) dramatically reduced the conversion (< 10%) and the 1,3-PDO/1,2-PDO ratio was increased to *ca.* 0.6.

In view of these results, a general mechanism can be proposed to explain the influence of the different parameters on the activity and selectivity of the reaction (Scheme 2). The diols can be formed *via* several routes. It was shown that the presence of tungstic acid increased the reaction rate. The acid can favour the dehydration route (route A) *via* protonation of the hydroxyl groups and loss of water.[10] The keto group formed as intermediate can be easily reduced under the reaction conditions. However, the use of alternative acid (HCl) yielded low conversion suggesting that the acidity of H_2WO_4 was not its dominant property for the considered reaction. Furthermore, the formation of a Rh–W catalyst can not be excluded and can affect the selectivity and the activity of the hydrogenolysis. The addition of a second metal (Fe or Cu) in the reaction medium reduced the activity as if it poisoned the rhodium catalyst. Moreover, iron can be chelated by a diol and thus modifies the selectivity of the hydrogenolysis (route C).

In conclusion, it was shown that heterogeneous catalytic hydrogenolysis of glycerol was possible in the presence of tungstic acid. Many parameters influenced the activity and the selectivity of the reaction. Thus in sulfolane, which may have favoured the dehydration *via* an E1-like mechanism (route A), the selectivity to

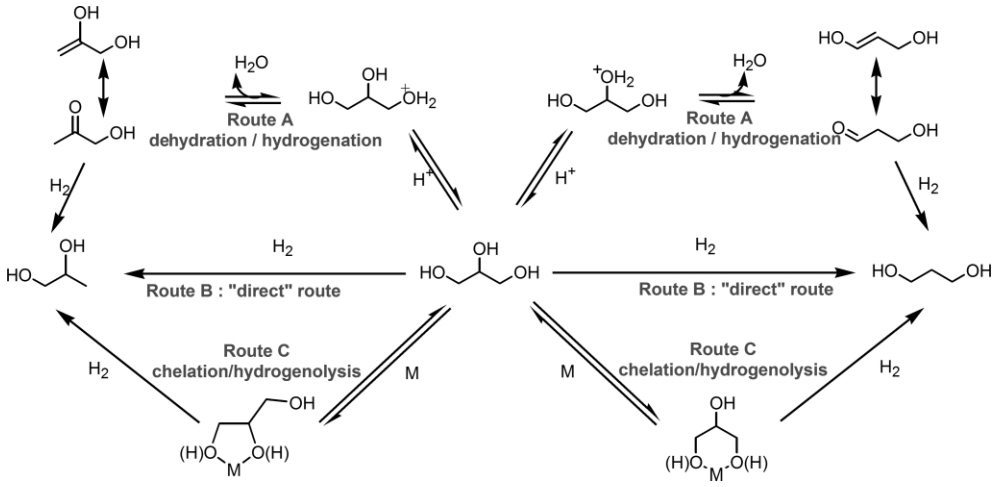

Scheme 2

1,3-PDO was two times larger than that to 1,2-PDO. In water, 1,2-PDO was formed predominantly but the presence of a second metal improved the selectivity towards 1,3-PDO. Further work is under progress to establish the mechanism and to optimize this reaction.

Experimental

Hydrogenolysis was carried out in a 150 mL stainless steel stirred autoclave protected with graphite-stabilized Teflon vessel when mentioned. Glycerol (15 g) dissolved in water (65 mL), supported metal catalyst (0.4% with respect to glycerol), and optionally tungstic acid (4%), were introduced into the autoclave which was pressurized with hydrogen. The temperature was increased to 180 °C and the pressure was maintained at 80 bar. Samples of the reaction medium were taken out regularly and analyzed by GC on a Chrompack Parabond Q (10 m × 0.32 μm) column. tBuOH was added as external standard. 1,3-PDO, 1,2-PDO, ethylene glycol, 1-propanol, 2-propanol, ethanol and methanol were analyzed.

Acknowledgements

We are indebted to AGRICE (programme 02.01.006) for financial support. We thank referees for constructive comments.

References

1 R. Garcia, M. Besson and P. Gallezot, *Appl. Catal.*, 1995, **127**, 165.
2 B. Blanc, A. Bourrel, P. Gallezot, T. Haas and P. Taylor, *Green Chem.*, 2000, 89.
3 P. N. Caley and R. C. Everett, Patent US 3 350 871, 1967, (DuPont).
4 D. Zimmerman and R. B. Isaacson, Patent US 3 814 725, 1974, (Celanese Corp).
5 D. Arntz, T. Haas, A. Müller and N. Wiegand, *Chem. Ing. Tech.*, 1991, **63**, 733.
6 K. T. Lam, J. P. Powell and P. R. Wieder, Patent WO 97 16250, 1997, (Shell).
7 R. Perrin and J. P. Scharff, *Chimie industrielle*, 1993, Masson Ed.
8 T. M. Che, Patent US 4 642 394, 1987, (Celanese Corp).
9 E. Drent and W. W. Jager, Patent US 6 080 898, 2000, (Shell Oil Co).
10 M. Schlaf, P. Ghosh, P. J. Fagan, E. Hauptman and R. M. Bullock, *Angew. Chem., Int. Ed.*, 2001, **40**, 3887.
11 T. Fleckenstein, G. Goebel and F.-J. Carduck, Patent DE 4 302 464, 1994.
12 C. Montassier, D. Giraud and J. Barbier, in *Stud. Surf. Sci. Catal.*, ed. M. Guisnet, J. Barrault, C. Bouchoule, D. Dupres, C. Montassier and G. Pérot, Elsevier, Amserdam, 1988, p. 165.
13 C. Montassier, D. Giraud, J. Barbier and J.-P. Boitiaux, *Bull. Soc. Chim. Fr.*, 1989, 148.
14 T. Werpy, J. Frye, A. Zacher and D. Miller, Patent WO 03 035 582, 2002, (Michigan State University).
15 W. Laufer and W. F. Hoelderich, *Chem. Commun.*, 2002, 1684.

www.rsc.org/greenchem

Green Engineering

What is the difference between Green Engineering and Green Chemistry? The US Environmental Protection Agency website yields a very interesting analysis. Green Engineering is defined as "the design, commercialization, and use of processes and products, which are feasible and economical while minimizing 1) generation of pollution at the source and 2) risk to human health and the environment,"[1] whereas Green Chemistry is defined as "the design of chemical products and processes that reduce or eliminate the use and generation of hazardous substances."[2] From this, one would conclude that Green Engineering is concerned with the *design*, *commercialization* and *use* of *all types* of processes and products, whereas Green Chemistry covers just a very small subset of this—the *design* of *chemical* processes and products. So Green Chemistry is a subset of Green Engineering!

Green Engineering is, in fact, a very broad field, encompassing everything from improving energy efficiency in manufacturing processes to developing plastics from renewable resources. What we focus on in this issue is several aspects of Green Chemical Engineering. One important aspect of this is the development of mathematically-based tools that aid in decision-making when faced with alternatives. A number of the papers in this issue address this area. Another is the discovery and development of new technology that makes the design, commercialization and use of processes and products that reduce or eliminate pollution possible. In particular, one major focus of both Green Chemistry and Green Chemical Engineering is developing alternatives to the volatile organic solvents used so pervasively in chemical and manufacturing processes. In a representative year (1997) in the United States solvents comprised 66% of all industrial emissions.[3] Efforts to address this pressing need of developing alternative solvents for synthesis, separation and processing are covered in four of the articles in this special issue. O'Neil and Watkins[4] describe how supercritical carbon dioxide can be used not just to replace the copious amounts of organic and aqueous solvents used in the microelectronic industries, but also how CO_2 presents unique technical advantages in device fabrication. Subramaniam *et al.*[5] demonstrate advantages in the rate of an oxidation reaction, by performing it in a liquid where part of the organic solvent has been replaced by CO_2 (a CO_2-expanded liquid). Eckert *et al.*[6] show how strong mineral acids can be eliminated by choosing a solvent (either hot water or a CO_2-expanded liquid) where the acid catalyst can be produced reversibly *in situ*. In all these cases, the new solvent system presents some real technological advantage over conventional systems; *i.e.*, it's not just solvent substitution. Rebelo and coworkers[7] present a wealth of phase behavior and thermophysical property data on a system containing a completely non-volatile solvent—an ionic liquid. These are exactly the kind of data that are needed to evaluate the potential of ionic liquids for reaction and separation processes.

Hopefully, the articles in this special issue demonstrate that Green Chemistry and Green Engineering represent slightly different shades of a seamless continuum that ranges from discovery through design and decision-making all the way to commercialization and use of products and processes that prevent pollution.

Joan F. Brennecke
Keating-Crawford Professor
Department of Chemical and Biomolecular Engineering
University of Notre Dame
Notre Dame, IN 46556
jfb@nd.edu

References

1 http://www.epa.gov/opptintr/greenengineering/whats_ge.html.
2 http://www.epa.gov/greenchemistry/whats_gc.html.
3 D. T. Allen and D. R. Shonnard, *Green Engineering*, 2002, Prentice-Hall, Englewood Cliffs, NJ.
4 A. O'Neil and J. Watkins, *Green Chem.*, 2004, **6**, DOI: 10.1039/b403729d, this issue.
5 M. Wei, G. T. Musie, D. H. Busch and B. Subramaniam, *Green Chem.*, 2004, **6**, DOI: 10.1039/b310523g, this issue.
6 T. S. Chamblee, R. R. Weikel, S. A. Nolen, C. L. Liotta and C. A. Eckert, *Green Chem.*, 2004, **6**, DOI: 10.1039/b400393d, this issue.
7 L. P. N. Rebelo, V. Najdanovic-Visak, Z. P. Visak, M. Nunes da Ponte, J. Szydlowski, C. A. Cerdeiriña, J. Troncoso, L. Romaní, J. M. S. S. Esperança, H. J. R. Guedes and H. C. de Sousa, *Green Chem.*, 2004, **6**, DOI: 10.1039/b400374h, this issue.

DOI: 10.1039/b411954c

CRITICAL REVIEW

Green chemistry in the microelectronics industry

Adam O'Neil and James J. Watkins*
Department of Chemical Engineering, University of Massachusetts, Amherst MA 01003

Received 12th March 2004, Accepted 28th April 2004
First published as an Advance Article on the web 6th August 2004

Microelectronic devices and materials now represent one of the largest manufacturing sectors in the world. Like many large industries, growth has been accompanied by increasing concerns regarding environmental emissions and impact. One challenge for the high end of the market is the identification of alternative process technologies that are not just "greener" but provide compelling technical advantages that could foster adaptation. This review examines a few opportunities where this is possible, including the use of supercritical fluids such as carbon dioxide in advanced device fabrication. The implementation of more acceptable materials in commodity markets, including lead free solder for printed wiring boards, is also discussed.

Introduction

The microelectronics industry has advanced rapidly over the last 20 years resulting in massive increases in processor performance and reductions in the cost of computing. As a whole, it is currently the single largest industry in the world and is expected to maintain growth for the foreseeable future.[1] The desire to move towards green processing is present in all sectors of the industry, however, differences in technical constraints and manufacturing naturally lead to differences in how new technology will be integrated. For the purposes of this article we will divide the industry into two segments: the fabrication of advanced devices, such as integrated circuits using a silicon wafer platform, and the production of high volume commodity materials, such as printed wiring board and casings.

Advancement in leading-edge semiconductor components is often measured against Moore's Law, which predicts that the number of devices per unit area on a chip will double every 18 months.[2] This can occur by innovative component design, but has more commonly been achieved by consistent reduction in component size. The economic and technological incentive to maintain or even surpass Moore's law is enormous and compels innovation. The fabrication of advanced devices relies on the damascene process. The process involves a sequence of successive steps, including deposition of a dielectric material, photolithography, etching of device features, cleaning, deposition of metal, metal planarization and capping that is repeated numerous times to leave a highly integrated structure. Continued reduction in feature size requires advances at each stage. However, given the complexity of wafer fabrication, evolutionary change is always preferred. New technology must therefore not only provide a clear technical advantage, but also compete on cost of ownership and overcome the perceived risk of a new process. While the same considerations apply for implementation of "greener" alternatives, there is incentive for change. The damascene process generates a large amount of waste per chip. Williams *et al.* point out that a 2 g microchip requires 1.6 kg of secondary fossil fuels, 72 g of chemicals, 32 kg of water and 0.7 kg of elemental gases.[3] For high volume commodity items such as printed wiring board, the technical constraints are fewer, but cost and performance remain critical issues.

This review will discuss several examples for the microelectronics industry where 'green chemistry' is possible. The use of supercritical fluids (SCF) as process solvents, for example, offers both enhanced capability and environmental advantages and have been shown to be effective in almost every stage of device fabrication, including materials deposition and cleaning.

The implementation of 'green processing' is also evident in

Adam O'Neil was born in the UK in 1977. He received his PhD in Chemistry from the University of Nottingham, England in 2003. He is currently pursuing postdoctoral studies at the University of Massachusetts at Amherst, USA. His research interests include metal deposition in supercritical solutions and supercritical fluid mediated crystallization.

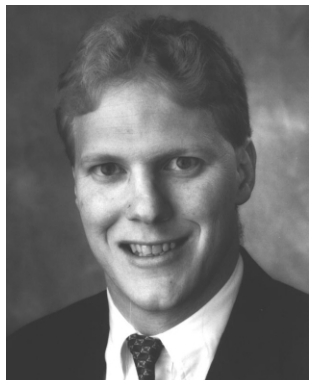

Jim Watkins was born in the United States in 1965. He received his PhD in Polymer Science and Engineering in 1997 from the University of Massachusetts at Amherst, USA. He remained at Amherst and is currently an Associate Professor of Chemical Engineering. He also holds an Adjunct Professorship in Polymer Science and Engineering department and is co-director of the multidisciplinary MassNanoTech center. His current research interests include deposition of metals and low k dielectrics using supercritical fluids. He also is conducting fundamental studies of the phase behavior of multi-component polymer systems in the presence of supercritical fluids.

DOI: 10.1039/b403729d

fabrication of commodity items such as printed circuit boards (PCB). Significant advances have been made in elimination of lead from solders and in the reduction of toxicity of IC packaging.[4] These changes, which center around the removal of lead, antimony and bromine, have had a beneficial environmental impact without compromising performance. SCFs can be used as a plating medium for wiring boards and could provide a potential substitute for traditional aqueous plating baths, a major source of heavy metal waste. Finally, the industry has also given consideration to the fabrication materials and components, and the possibility of their recycling.[5–7]

Supercritical fluids in microelectronics

A supercritical fluid is a material that is heated and compressed beyond its critical temperature and pressure, see Fig. 1.[8] In the

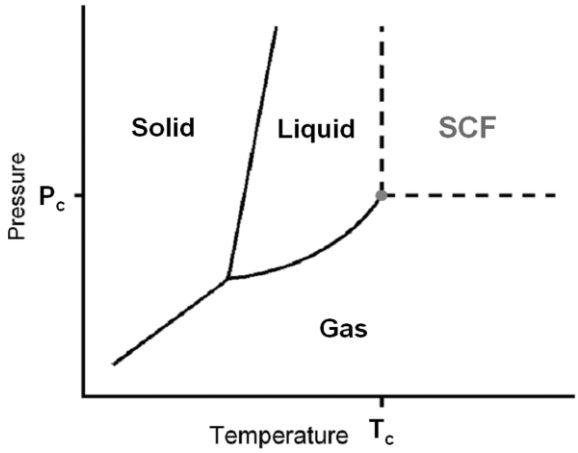

Fig. 1 Phase diagram of a pure substance. A material becomes supercritical when the critical temperature, T_c, and pressure, P_c, are exceeded. The critical point is marked with a dot.

microelectronics industry, the most studied fluid is carbon dioxide, which has the advantages of being inert, non-flammable, non-toxic, cheaply available and possessing easily accessible critical parameters (CO_2 – P_c = 73.77 bar, T_c = 30.98 °C).[9] The real benefits of SCF processing become apparent as device dimensions fall far below 100 nm. Most traditional cleaning, resist processing and some depositions are conveniently carried out in solution. However, at length scales relevant to the smallest features, and especially for the introduction of next generation dielectric materials containing sub-5 nm pores, surface tension and transport become significant issues. In these respects, vacuum and vapor based processes offer significant advantages, but the benefits of solution based processing are lost. The use of SCFs makes it possible to retain the former without surrender of the latter. Fig. 2

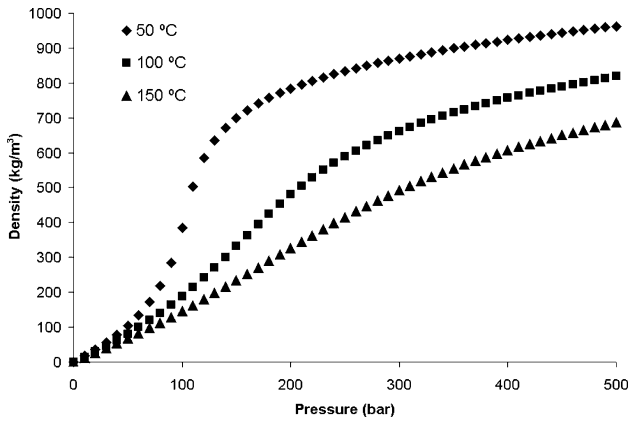

Fig. 2 Isotherms of supercritical CO_2 show tunable liquid-like densities.

shows the density of CO_2 as a function of pressure for several isotherms, 50, 100 and 150 °C.[9] Note that at modest temperatures and pressures, the density of supercritical CO_2 can approach that of liquids, enabling the dissolution of many organic and organometallic species.[12] Fig. 3 shows the surface tension of liquid CO_2,

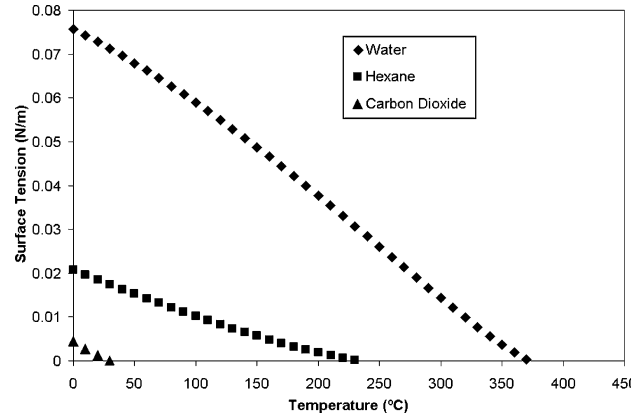

Fig. 3 Surface tension change with increasing temperature of three solvent systems. Surface tension drops to zero as the material exceeds T_c under saturated conditions. Water offers a very small window on potential operation, irrespective of corrosion concerns. Hexane possibly has some, higher temperature opportunities, while CO_2 offers zero surface tension over the whole range, making it the most attractive option.

water and hexane as a function of temperature at saturation.[9] At temperatures above the critical point, the surface tension vanishes. The absence of surface tension combined with liquid-like densities offer the possibility of solution based processes in the highly confined geometries of microelectronic structures.

Supercritical fluid deposition

Controlled metal deposition is a vital part of the generation of IC components. Systems are built in many steps in which metal and insulator layers are added sequentially to a semiconductor substrate, interspersed with etching, to generate a 3D lattice of components on a very small scale, Fig. 4. Metal deposition is also

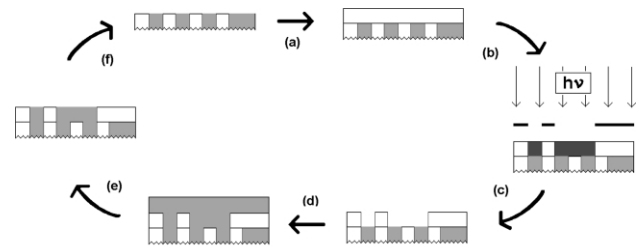

Fig. 4 Creating a metal interconnect structure is carried out in layers. Deposition of each layer requires a number of separate stages. (a) An interconnect structure is coated with a photoresist. (b) The sample is exposed to UV light through a mask. In the diagram the mask is 1 : 1, however in an industrial arrangement a 4× larger mask is used and the light passing through it is focused by lenses underneath. The UV light initiates a chemical reaction in selective regions of the photoresist. (c) In this example of a positive resist system the exposure to UV light has made regions of the photoresist more soluble and these are removed with cleaning solutions to leave the desired resist structure. (d) The wafer is then coated in copper to create the electrical contact. (e) Excess copper is removed by chemical mechanical planarization (CMP). (f) The cycle is complete and the process can begin again one layer higher.

required for many other products, including printed wiring boards. These depositions are traditionally carried out by chemical vapor deposition (CVD), aqueous electrolytic or electroless plating techniques or sputtering.[10] Each of these techniques has its own distinct advantages and disadvantages.

Electroless methods involve the plating of surfaces using electrochemical baths containing the desired metals. This process can occur at low temperatures and be carried out using inexpensive precursors, however it is limited by slow mass transport and capillary forces that can damage finely etched structures. Also, due

to the insolubility of gas reductants in water, more toxic liquid systems must be used, such as sodium hypophosphite and formaldehyde. Electroless deposition also requires the use of several plating and rinsing baths and as such generates large volumes of waste water, which then require remediation.

Cu interconnect structures, in advanced integrated circuits, are presently fabricated using electrolytic plating. The process involves the sequential deposition of a continuous Cu seed layer by sputtering followed by aqueous plating. The seed layer serves as the cathode for the plating process and thus must be continuous. Plating in narrow features is enabled through a combination of additives that promote bottom-up filling and the use of surfactants to reduce surface tension. While limitations to plating from solution will exist at successively smaller dimensions, the first limitation involves the preparation of conformal seed layers in high aspect ratio features. SCFs offer the possibility of eliminating both constraints by void-free filling in < 100 nm topographies and by the ability to deposit continuous seed layers. These features could be applied simultaneously, followed by a simple electroplating step which would fill very small structures and prepare other larger structures for electroplating, see Fig. 5.

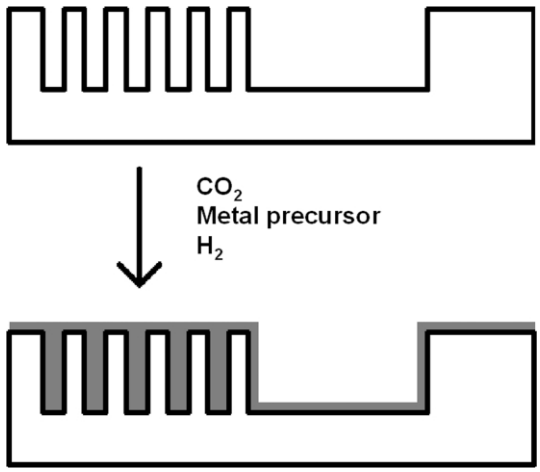

Fig. 5 SCF deposition allows the possibility of completely filling small structures, while simultaneously adding a seed layer to larger topographies for later conventional aqueous electrolytic plating.

CVD relies on the deposition of metals from the vapor of a suitable metal precursor compound.[11–13] The process can yield high purity metal films, however it is limited by a number of factors. The metal precursors often do not exhibit sufficient vapor pressure to yield high concentrations in the CVD atmosphere. Low precursor concentration can lead to mass transfer limitations, which prevent conformal coverage in narrow features.[14] CVD can also require high temperatures due to precursor volatility constraints, reduction chemistry and/or desorption of ligand fragments from the nascent film surface. For IC fabrication, the deposition temperatures must be kept below 400 °C to avoid thermal damage. Significant advances have been made using metal–organic precursors (MOCVD) to increase vapor pressure and allow deposition at lower temperatures. This commonly means the use of fluorinated ligands or toxic carbonyl compounds which generate their own contamination, performance and emission issues. In particular, the presence of fluorine adversely impacts adhesion.

The use of supercritical fluids as a deposition medium circumvents many of the problems mentioned above by allowing an amalgamation of liquid and vapor phase techniques. $scCO_2$ provides an inert solvent for the dissolution of metal precursors. This allows orders of magnitude greater concentrations of precursor to be present in the deposition system. At the same time the overall deposition temperature can be lowered to the temperature required to reduce or oxidize the precursor species (typically 200–300 °C). Moreover, precursor vapor pressure is no longer an issue, therefore the fluorination of precursors is not needed, and hydrocarbon based ligand systems can often be used. Low surface tension of the SCF allows facile transport within finely etched surfaces and can lead to very good filling in high aspect ratios. $scCO_2$ is miscible with H_2 and O_2, so these simple species are able to provide clean deposition agents. For high volume plating operations in particular, the potential elimination of aqueous waste streams represents a significant advantage.[15–17] Finally, plating in CO_2 involves a less severe deposition step and does not necessarily destroy the precursor ligand, instead merely liberating it, allowing it to dissolve into the CO_2. Therefore it may be possible to recycle ligands when the deposition is complete.

The first use of supercritical fluids connected with CVD was carried out by Sievers *et al.*, where CO_2 was used to dissolve a mixture of precursor and a deposition promoting agent [18,19] This mixture was then sprayed onto a surface by the rapid expansion of a supercritical solvent (RESS), which allowed mixing on a very small scale. The process generated a very fine precursor aerosol. The sprayed surface could then be annealed (500–800 °C) under atmospheric pressure to generate an even film. The process was given the name supercritical fluid transport and chemical deposition (SFT-CD). Films of Al, Ag, Cr, Cu, In, Ni, Pd, Y and Zr have been successfully grown using this technique. The process has been modified to generate metal oxide films by expansion from solutions in N_2O into high energy plasma. Under these circumstances, N_2O was the oxidizing agent and surface temperatures of only around 100 °C were required. This technique has allowed the generation of Al_2O_3, Cr_2O_3, CuO, SiO_2 and B and P doped SiO_2. Sievers research enabled the synthesis of YBa_2Cu_3O by spraying quantities of components in supercritical propane, followed by annealing.[19] Novel fluid systems were also used by Popov *et al.* who synthesized films of InP by a similar method, though the previous name was abbreviated to supercritical fluid chemical deposition (SFCD).[20] This was carried out by the expansion of a CO_2, C_2F_6 or Xe solution of triphenyl phosphine and tris(*o*-dimethylaminomethyl-phenyl) indium(III). InP was then generated by heating in a vacuum after deposition. This technique improved consistency of mixed components and was able to support IC architecture of the time, however as size decreased the spraying of solids has become less useful. It is important to note that, in each of these processes, the actual deposition does not occur in a SCF medium and likely will not yield conformal coverage in confined geometries.

More recently SCFs have successfully been used to allow direct chemical deposition onto a surface by chemical fluid deposition (CFD). This has allowed generation of high quality, conformal films of metal using CO_2 as solvent.[21–30] A typical experiment involves the placement of a substrate wafer on a heated stage in a cold wall, high pressure reactor. The vessel is loaded with a quantity of precursor and the system is purged with N_2. The vessel is then pressurized with SCF and a quantity of reducing agent (H_2 or alcohol). The substrate wafer is brought to temperature by heating the pedestal stage it is mounted on. The deposition is believed to occur rapidly and a film generated. A number of precursor systems have been investigated using this technique including 2,2,6,6-tetramethyl-3,5-dionate, 1,5-cyclooctadienyl, cyclopentadienyl, 2-butyne, vinyltrimethylsilane, 2-methyl-1-hexene-3-yne, methyl allyl and allyl ligands. Using these systems films of Au, Co, Cu, Ni and Pd have been grown. This system circumvents some of the problems associated with CVD and aqueous plating and permits access to a sub 100 nm chip architecture in a cold-wall reactor. Use of the cold-wall reactor confines deposition to the heated substrate. Mixed precursor systems can be used to produce alloys or to catalyze the deposition of metals such as Ni and Cu by the presence of easily reduced precursors such as Pd, Pt and other metals.[21]

A new adaptation of this technique was applied by Ye *et al.* who used HF as a reacting agent to facilitate deposition on Si and Ge surfaces by the fluorination of semiconductor surfaces initiating reduction of the precursor.[31] This has allowed growth of films of Ag, Cu and Pd.

Supercritical drying

For sub-50 nm structures, removal of liquid solvents by evaporation can be problematic as the liquid–vapor interface can exert damaging capillary forces on a surface. This is particularly important in next generation ICs where high aspect ratio resist patterns are used and simple evaporation of a solvent can lead to the collapse of etched structures.[32–34] Feature collapse becomes increasingly important as porosity is introduced into advanced dielectrics. Supercritical drying avoids these difficulties by eliminating the liquid vapor interface. Fluids above the mixture critical point do not exhibit surface tension, so removal of solvents in this state does not lead to feature collapse. In one approach, aqueous solutions are exchanged for solvents such as alcohols that are miscible with CO_2. In other approaches miscible solvents are removed directly by dissolution in CO_2. Co-solvents can also be added to CO_2 without initiating phase changes and act to promote water solubility in the fluid.[35] Alternatively, the addition of surfactants can be used to remove water more effectively.[32]

In one study, Goldfarb *et al*. demonstrated the use of a CO_2–hexane–surfactant system.[36–38] Structural integrity was maintained during the drying of resist lines 140 nm thick, with a spacing of 370 nm, aspect ratio of 6.8 and length of 8 μm.[38] To emphasize the point these samples were then rewetted with water and hexane and allowed to dry conventionally. The resist structures all collapsed under these conditions. Namatsu was later able to show that it is possible to dry features as small as 7 nm in width with an aspect ratio of 10.[39]

Photolithography

Photolithography is the selective exposure of specific regions of a photoresist with radiation of a defined wavelength to initiate a chemical change in the resist structure. This change is often promoted by chemical amplification, usually through the presence of a photoacid generator (PAG) that catalyzes the desired transformation. Exposure can lead to cleavage of a chemical bond to deprotect a functional group, induce chain scission to reduce the molecular weight of the resist, or crosslink the resist. These structural transformations alter the solubility of the exposed regions through polarity and/or molecular weight changes. For example, reduction of the molecular weight of a polymer to make it soluble in a rinsing solution creates a positive resist pattern. Alternatively, cleavage of a protecting group on the polymer chain that renders the exposed region insoluble in the rinsing solution yields a negative resist pattern. In either case the soluble region would be traditionally removed by conventional solvent, which in turn could be dried by CO_2 as above. Ober *et al.* showed the possibility of eliminating solvents from the rinsing step by using silicon and fluorinated resist systems that could be developed directly in supecritical CO_2.[40,41] Hoggan *et al.* produced similar results also using a fluorinated polymer system.[42] The North Carolina group also developed a technique analogous to conventional spin coating using $scCO_2$ as solvent.[43]

Supercritical cleaning

Cleaning of IC systems using CO_2 is a process that has received much attention.[44,45] The ability to remove solid waste material from lithographic processes effectively, yet gently enough not to damage device structures, offers significant advantages over existing techniques that rely on chemical washes. The most common wash systems are H_2SO_4–H_2O_2, HF–H_2O, NH_4OH–H_2O_2–H_2O and HCl–H_2O_2–H_2O. All systems are then rinsed with ultra-pure H_2O.[46] The key reason behind the harsh solvent use is the ability to remove tenaciously deposited residues of metals, photoresists and anti-reflection coatings. However, this becomes increasingly difficult as the trench dimensions are reduced due to surface tension and damage. Moreover, continuous reduction in device dimensions requires the introduction of dielectric materials containing sub-5 nm pore structures. It is imperative that contamination or damage to the dielectric structure be avoided during lithography, etching and cleaning. The use of carbon dioxide to clean these structures eliminates concerns over residual solvent and pore collapse due to capillary forces and has been shown to be highly effective.[47,48]

In some processes, CO_2 is used in its solid form sprayed through a nozzle as fine solid particles. These particles physically remove material from the surface while not leaving any residue behind. The concept has been improved recently in the SCORR system developed at the National Laboratories in Los Alamos, in conjunction with SC Fluids Inc.[49] Here CO_2 bombardment is carried out under a CO_2 atmosphere containing modifier molecules. The pressure of the system is pulsed from 7.5–11 MPa to remove debris then rinsed with a purge of CO_2. The waste materials are not believed to be solubilized by the fluid system, yet sufficient mobility is afforded to the surface debris to remove it from the wafer.[50] This has allowed highly efficient cleaning of narrow wafer patterns. The commercialization of this process won a 2002 Presidential Green Chemistry Challenge award.[51]

Synthesis

SCF has long been used as a solvent for synthesis of various materials.[52] In this review two classes are of interest, porous low *k* dielectrics and nanoparticles and wires.

Low *k* dielectrics are currently a major issue for the microelectronics industry as current techniques are unlikely to be extended below a dielectric constant around 2.5. It is necessary to continue the reduction in *k*, however the only perceived way to do this requires a porous material. As porosity is introduced into a structure, however, the system is physically weakened, making it less able to survive chemical mechanical planarization (CMP), to remove excess material, or the final IC packaging process. Synthesis of mesoporous silicas in $scCO_2$ offers an elegant solution to both problems. Block co-polymer surfactants have been shown to successfully self assemble, producing highly ordered arrays over a large area.[53] This structure can be rapidly penetrated by silica precursors, such as tetraethoxysilane (TEOS), dissolved in $scCO_2$, which condense to form a silicates network.[54] A key to the process is the containment of the precursor reaction to one phase domain of the template by partitioning a catalyst to a specific region. Moreover, while CO_2 facilitates transport of the precursor into the template, the presence of the solvent does not disrupt order. Removal of the template then yields a robust, highly ordered mesoporous film that survives CMP. The process occurs rapidly relative to conventional sol–gel synthesis and per wafer process times in the order of minutes are accessible.

Supercritical fluids have also been useful in the generation of nanoparticles and nanowires of conducting and semiconducting materials. These materials are believed to be increasingly important in the future of microelectronics.[55] The topic has been recently reviewed by Ye and Wai[15] and Holmes *et al*.[56] Several routes have been suggested to generate nano-systems including RESS, antisolvent precipitation and direct synthesis in a SCF. Each of these systems have produced interesting results, however they also have their own inherent difficulties: RESS relies on solubility in the SCF, antisolvent precipitation is only viable for high value added products and direct synthesis has tended to require a SCF with high Tc and Pc, such as water or hexane.[57] Recent research in the field has been conducted on water in CO_2 microemulsions, which use surfactants to yield ultra-fine suspensions of water in $scCO_2$.[58] These regions of water are then capable of dissolving ionic species, allowing a reaction to occur and precipitating nanoparticulate materials when the CO_2 pressure is released. Using this system nanoparticles of several materials have been generated, including Ag, CdS, Cu, TiO_2, ZnS.[59–63]

Other non-SCF based synthetic routes have been suggested for the generation of nanomaterials. For example Peng uses the principles of green chemistry to examine more environmentally friendly methods to generate CdSe and CdTe.[64] Similarly a

synthetic route to CdS has been suggested by Bayer *et al.* for generation of thin films for photovoltaic cells.[65]

Toxic chemical reduction

The second aspect of this review, dealing with the replacement of toxic chemicals in device manufacture.

Lead free soldering

Lead exists as finish on printed circuit boards and the component leads as well as solder for establishing electrical contacts. Europe and Japan have put forth much effort in the pursuit of lead free solders for manufacturing. By 2003 70–80% of the Japanese electronics industry had established lead free technologies.[66] By 2005 all are expected to have made the transition to lead free alternatives; a legislative deadline currently exists for lead removal by 2006. An overview of the Japanese approach to lead free manufacture is given by Fukuda *et al.*[66] A similar approach to the issue is taken in Europe with the Waste Electrical and Electronic Equipment directive from the EU set to mandate the removal of Pb, Cd, Hg, hexavalent chromium, polybrominated biphenyls (PBBs) and polybrominated diphenyl ethers from electronic equipment by 1st July 2006.[67] The efforts have produced new soldering systems that provide safer alternatives without compromise on conventional Sn–Pb mixtures.[68] In Japan the release of products labeled 'lead free' were greeted by a 20% market share increase of sales by Sony and 4.7–15% by Matsushita.[66]

The solder itself must physically and electrically link materials with very different thermal expansion coefficients. Mechanical stress will rise as the connection points decrease in line with miniaturization. The materials challenges are significant. The solder must have adequate wetting properties to connect components when fluid and enough mechanical strength to hold the contact in place when solid. Melting also must occur at temperatures close to that of Pb–Sn solder (183–230 °C) to allow use of current soldering manufacturing. The system is also complicated by the fact that two types of soldering joint exist: Level 1, which connects a microchip to a substrate, with many precise linkages; and Level 2, which connects conventional components, such as resistors and capacitors, to a printed circuit board (PCB).[4] Traditionally Pb–Sn solder has been used in a near eutectic mixture for both applications. Investigation of replacement materials permits tailoring of the novel compound to one process or the other.[68] The review by Abtew *et al.* details the precise features and compositions of the many possible lead free solders available in 2000, with a detailed description of the physical properties and how they are measured.[4] Properties of traditional and novel solders have also been studied by Plumbridge, who compared Pb–Sn with two lead free systems.[69]

Specific companies are developing their own replacement technology, however most center around Sn blended with one or two of the following: Al, Ag, Bi, Cu, In, Pd or Zn.[66] The presence of Ag, In or Pd in the solder will increase the raw materials costs. This has led to Pb free solders typically costing 2–3 times that of traditional solder. Sn–Cu solders only cost 1.3 times that of the conventional material and have therefore found favor in some applications.[70] Since European and Japanese legislation mandates the change there is little room to maneuver. The small quantities used in each device, coupled with the high value of IC products, suggest that the cost change has not had a large impact on production. A cursory search reveals more than 50 US patents in this area.

Lower toxicity IC packaging

Following a similar trend in the elimination of lead from manufacture, the examination of 'green' casings attempts to remove Sb and Br from the compounds used to seal microchips. This follows from safety concerns over toxicity of waste products in a similar manner to the removal of lead. As mentioned above, the removal of the Br based compounds is scheduled for mid 2006 in Europe.[67] These compounds are used as flame retardants and alternative materials must be found to replace them. These compounds must be able to seal the chip from contamination, particularly moisture, yet be resistant to thermal damage during soldering. Lin *et al.* describe possible alternatives to the conventional system and point out that incorporating a lead free soldering environment means that the casing system must exhibit stability to a greater temperature than for leaded solder. This is due to the higher melting point of the most commonly used lead free alternatives to conventional Sn–Pb solder.[71,72] As with Pb free solder, there are too many patented systems to list here. Unfortunately, relatively few papers on the subject exist in the open literature.

Conclusion

Technologies that offer distinct technical advantages and also minimize reactant toxicity and waste inherent in conventional syntheses are the most likely to be adapted in demanding fabrication schemes for integrated device manufacturing. Supercritical fluids may provide both of these advantages. Changes in packaging materials and commodity items such as printed wiring board are more accessible and are currently under way. Environmental concerns and increasing legislation will likely hasten development in all areas.

References

1 S. Luryi, J. Xu and A. Zaslavsky, *Future Trends in Microelectronics*, IEEE, 2002.
2 *International Technology Roadmap for Semiconductors (ITRS)*, 2003, http://public.itrs.net/Files/2003ITRS/Home2003.htm.
3 E. D. Williams, R. U. Ayres and M. Heller, *Environ. Sci. Technol.*, 2002, **36**, 5504.
4 M. Abtew and G. Selvaduray, *Mater. Sci. Eng. R-Rep.*, 2000, **27**, 95.
5 L. K. Moyer and S. M. Gupta, *J. Electron. Manuf.*, 1997, **7**, 1.
6 P. L. Timms, *J. Chem. Soc., Dalton Trans.*, 1999, 815.
7 W. T. Tsai, H. P. Chen and W. Y. Hsien, *J. Loss Prev. Process Ind.*, 2002, **15**, 65.
8 M. A. McHugh and V. J. Krukonis, *Supercritical Fluid Extraction: Principles and Practice*, Butterworths, Boston, 1986.
9 E. W. Lemmon, M. O. McLinden and D. G. Friend, in *Thermophysical Properties of Fluid Systems*, ed. L. P. J. and M. W. G., NIST Chemistry WebBook, NIST Standard Reference Database Number 69, Gaithersburg, MD, 2003, 20899 (http://webbook.nist.gov).
10 J. Li, Y. Shachamdiamand and J. W. Mayer, *Mater. Sci. Rep.*, 1992, **9**, 1.
11 P. Serp, P. Kalck and R. Feurer, *Chem. Rev.*, 2002, **102**, 3085.
12 K. L. Choy, *Prog. Mater. Sci.*, 2003, **48**, 57.
13 T. Kodas and M. Hampden-Smith, *The Chemistry of Metal CVD*, VCH Publishers Inc., New York, 1994.
14 M. J. Hampden-Smith and T. T. Kodas, *Chem. Vap. Deposition*, 1995, **1**, 8.
15 X. G. Ye and C. M. Wai, *J. Chem. Educ.*, 2003, **80**, 198.
16 G. L. Weibel and C. K. Ober, *Microelectron. Eng.*, 2003, **65**, 145.
17 J. M. DeSimone, *Science*, 2002, **297**, 799.
18 R. E. Sievers and B. N. Hansen, 1990, US patent, 4,970,093.
19 B. N. Hansen, B. M. Hybertson, R. M. Barkley and R. E. Sievers, *Chem. Mater.*, 1992, **4**, 749.
20 V. K. Popov, V. N. Bagratashvili, E. N. Antonov and D. A. Lemenovski, *Thin Solid Films*, 1996, **279**, 66.
21 J. M. Blackburn, D. P. Long, A. Cabanas and J. J. Watkins, *Science*, 2001, **294**, 141.
22 J. J. Watkins and T. J. McCarthy, 1998, US patent, 5,789,027.
23 J. J. Watkins, J. M. Blackburn and T. J. McCarthy, *Chem. Mater.*, 1999, **11**, 213.
24 J. M. Blackburn, D. P. Long and J. J. Watkins, *Chem. Mater.*, 2000, **12**, 2625.
25 D. P. Long, J. M. Blackburn and J. J. Watkins, *Adv. Mater.*, 2000, **12**, 913.
26 A. Cabanas, J. M. Blackburn and J. J. Watkins, *Microelectron. Eng.*, 2002, **64**, 53.
27 A. Cabanas, X. Y. Shan and J. J. Watkins, *Chem. Mater.*, 2003, **15**, 2910.

28 C. M. Wai, H. Ohde and S. Kramer, 2003, US patent, 6,653,236.
29 E. Kondoh and H. Kato, *Microelectron. Eng.*, 2002, **64**, 495.
30 E. T. Hunde and J. J. Watkins, *Chem. Mater.*, 2004, in press.
31 X. R. Ye, C. M. Wai, D. Q. Zhang, Y. Kranov, D. N. McIlroy, Y. H. Lin and M. Engelhard, *Chem. Mater.*, 2003, **15**, 83.
32 H. Namatsu, *J. Vac. Sci. Technol., B*, 2000, **18**, 3308.
33 H. Namatsu, K. Yamazaki and K. Kurihara, *Microelectron. Eng.*, 1999, **46**, 129.
34 H. Namatsu, K. Kurihara, M. Nagase, K. Iwadate and K. Murase, *Appl. Phys. Lett.*, 1995, **66**, 2655.
35 C. Millet, A. Danel, M. Ndour and F. Tardif, *Ultra Clean Process. Silicon Surf. V*, 2003, **92**, 113.
36 J. M. Cotte, D. L. Goldfarb, K. J. McCullough, W. M. Moreau, K. R. Pope, J. P. Simons and C. J. Taft, 2002, US patent, 6,398,875.
37 J. M. Cotte, D. L. Goldfarb, K. J. McCullough, W. M. Moreau, K. R. Pope, J. P. Simons and C. J. Taft, 2002, US patent, 6,454,869.
38 D. L. Goldfarb, J. J. de Pablo, P. F. Nealey, J. P. Simons, W. M. Moreau and M. Angelopoulos, *J. Vac. Sci., Technol. B*, 2000, **18**, 3313.
39 H. Namatsu, *J. Vac. Sci. Technol., B*, 2001, **19**, 2709.
40 C. K. Ober, A. H. Gabor, P. GallagherWetmore and R. D. Allen, *Adv. Mater.*, 1997, **9**, 1039.
41 N. Sundararajan, S. Yang, K. Ogino, S. Valiyaveettil, J. G. Wang, X. Y. Zhou, C. K. Ober, S. K. Obendorf and R. D. Allen, *Chem. Mater.*, 2000, **12**, 41.
42 E. N. Hoggan, J. L. Kendall, D. Flowers, R. G. Carbonell and J. M. DeSimone, *Abstr. Pap. Am. Chem. Soc.*, 1999, **218**, PMSE 0052.
43 J. M. DeSimone and R. G. Carbonell, 1999, US patent, 6,001,418.
44 Anon, *Chem. Eng. News*, 2003, **81**, 10.
45 Anon, *Chem. Eng. Prog.*, 1998, **94**, 18.
46 M. Heyns, P. W. Mertens, J. Ruzyllo and M. Y. M. Lee, *Solid State Technol.*, 1999, **42**, 37.
47 T. Rajagopalan, B. Lahlouh, J. A. Lubguban, N. Biswas, S. Gangopadhyay, J. Sun, D. H. Huang, S. L. Simon, A. Mallikarjunan, H. C. Kim, W. Volksen, M. F. Toney, E. Huang, P. M. Rice, E. Delenia and R. D. Miller, *Appl. Phys. Lett.*, 2003, **82**, 4328.
48 J. A. Lubguban, J. Sun, T. Rajagopalan, B. Lahlouh, S. L. Simon and S. Gangopadhyay, *Appl. Phys. Lett.*, 2002, **81**, 4407.
49 L. B. Davenhall and J. B. Rubin, 2002, US patent, 6,403,544.
50 Anon, *MRS Bull.*, 2001, **26**, 602.
51 http://www.epa.gov/greenchemistry/past.html#2002.
52 P. G. Jessop and W. Leitner, *Chemical Synthesis Using Supercritical Fluids*, Wiley-VCH, New York, 1999.
53 Z. Q. Lin, D. H. Kim, X. D. Wu, L. Boosahda, D. Stone, L. LaRose and T. P. Russell, *Adv. Mater.*, 2002, **14**, 1373.
54 R. A. Pai, R. Humayun, M. T. Schulberg, A. Sengupta, J. N. Sun and J. J. Watkins, *Science*, 2004, **303**, 507.
55 M. Jose-Yacaman and R. F. Mehl, *Metall. Mater. Trans. A-Phys. Metall. Mater. Sci.*, 1998, **29**, 713.
56 J. D. Holmes, D. M. Lyons and K. J. Ziegler, *Chem.-Eur. J.*, 2003, **9**, 2144.
57 T. Hanrath and B. A. Korgel, *Adv. Mater.*, 2003, **15**, 437.
58 J. C. Liu, Y. Ikushima and Z. Shervani, *Curr. Opin. Solid State Mater. Sci.*, 2003, **7**, 255.
59 K. T. Lim, H. S. Hwang, M. S. Lee, G. D. Lee, S. S. Hong and K. P. Johnston, *Chem. Commun.*, 2002, **14**, 1528.
60 H. Ohde, F. Hunt and C. M. Wai, *Chem. Mater.*, 2001, **13**, 4130.
61 J. L. Zhang, B. X. Han, M. H. Liu, D. X. Liu, Z. X. Dong, J. Liu, D. Li, J. Wang, B. Z. Dong, H. Zhao and L. X. Rong, *J. Phys. Chem. B*, 2003, **107**, 3679.
62 J. L. Zhang, B. X. Han, J. C. Liu, X. G. Zhang, Z. M. Liu and J. He, *Chem. Commun.*, 2001, 2724.
63 H. Ohde, M. Ohde, F. Bailey, H. Kim and C. M. Wai, *Nano Lett.*, 2002, **2**, 721.
64 X. G. Peng, *Chem.-Eur. J.*, 2002, **8**, 335.
65 A. Bayer, D. S. Boyle, M. R. Heinrich, P. O'Brien, D. J. Otway and O. Robbe, *Green Chem.*, 2000, **2**, 79.
66 Y. Fukuda, M. G. Pecht, K. Fukuda and S. Fukuda, *IEEE Trans. Compon. Packag. Technol.*, 2003, **26**, 616.
67 *Waste electrical and electronic equipment*, 2002, European Parliament, 2002/95/EC.
68 J. Mueller, H. Griese, H. Reichl and K. H. Zuber, *Inf. Midem-J. Microelectron. Electron. Compon. Mater.*, 2002, **32**, 262.
69 W. J. Plumbridge and C. R. Gagg, *Proc. Inst. Mech. Eng. Pt. L-J. Mater.-Design Appl.*, 2000, **214**, 153.
70 K. Suganuma, *Curr. Opin. Solid State Mater. Sci.*, 2001, **5**, 55.
71 T. Y. Lin, *IEEE Trans. Compon. Packag. Technol.*, 2003, **26**, 492.
72 T. Y. Lin, C. M. Fang, Y. F. Yao and K. H. Chua, *Microelectron. Reliab.*, 2003, **43**, 811.

PAPER

www.rsc.org/greenchem

A detailed thermodynamic analysis of $[C_4mim][BF_4]$ + water as a case study to model ionic liquid aqueous solutions

L. P. N. Rebelo,*[a] V. Najdanovic-Visak,[a] Z. P. Visak,[a] M. Nunes da Ponte,[ac] J. Szydlowski,[ae] C. A. Cerdeiriña,[b] J. Troncoso,[b] L. Romaní,[b] J. M. S. S. Esperança,[c] H. J. R. Guedes[c] and H. C. de Sousa[d]

[a] *Instituto de Tecnologia Química e Biológica, Universidade Nova de Lisboa, Apartado 127, 2780-901 Oeiras, Portugal. E-mail: luis.rebelo@itqb.unl.pt; Fax: +351 21 4411 277; Tel: +351 21 4469 441*

[b] *Departmento de Física Aplicada, Universidad de Vigo, Facultad de Ciencias del Campus de Ourense, E 32004 Ourense, Spain*

[c] *REQUIMTE, Departamento de Química, FCT, Universidade Nova de Lisboa, 2829-516 Caparica, Portugal*

[d] *Departamento de Engenharia Química, FCT, Universidade de Coimbra, Polo II – Pinhal de Marrocos, 3030-290 Coimbra, Portugal*

[e] *Chemistry Department, Warsaw University, Zwirki I Wigury 101, 02-089 Warsaw, Poland*

Received 12th January 2004, Accepted 16th June 2004
First published as an Advance Article on the web 11th August 2004

Since determining experimentally a wide variety of thermophysical properties—even for a very small portion of the already known room temperature ionic liquids (and their mixtures and solutions)—is an impossible goal, it is imperative that reliable predictive methods be developed. In turn, these methods might offer us clues to understanding the underlying ion–ion and ion–molecule interactions. 1-Butyl-3-methylimidazolium tetrafluoroborate, one of the most thoroughly investigated ionic liquids, together with water, the greenest of the solvents, have been chosen in this work in order to use their mixtures as a case study to model other, greener, ionic liquid aqueous solutions. We focus our attention both on very simple methodologies that permit one to calculate accurately the mixture's molar volumes and heat capacities as well as more sophisticated theories to predict excess properties, pressure and isotope effects in the phase diagrams, and anomalies in some response functions to criticality, with a minimum of information. In regard to experimental work, we have determined: (a) densities as a function of temperature ($278.15 < T/K < 333.15$), pressure ($1 < p/bar < 600$), and composition ($0 < x_{IL} < 1$), thus also excess molar volumes; (b) heat capacities and excess molar enthalpies as a function of temperature ($278.15 < T/K < 333.15$) and composition ($0 < x_{IL} < 1$); and (c) liquid–liquid phase diagrams and their pressure ($1 < p/bar < 700$) and isotopic (H_2O/D_2O) dependences. The evolution of some of the aforementioned properties in their approach to the critical region has deserved particular attention.

Introduction

In spite of the recent rise in the rate of research on ionic liquids (IL) as alternative, "green" solvents, resulting in a marked increase in the number of publications per year in the field,[1] comparatively little is still known as far as their properties and those of their mixtures and solutions are concerned.[2] As for the latter, a detailed knowledge of the behavior of mixtures of IL + water is certainly paramount both from industrial and fundamental perspectives; in particular very interesting features emerge from a purely thermodynamic point of view. Furthermore, accurate thermophysical data are required for the optimization of the design of any industrial process.

Water is certainly the most common and important substance. In addition, it is the "greenest" of the solvents. In respect to ILs, when all their ternary mixtures are accounted for, up to a potential trillion cases can be identified.[3] Since it is impossible to determine experimentally a wide variety of properties even for a very small portion of that figure, reliable predictive methods have to be established. In this context, the application and development of predictive methods of thermophysical behavior constitute a useful tool for applied purposes while they also lead to a deepening awareness of the underlying microscopic behavior (at the ion–ion and ion–molecule level of interactions) of these new liquids.

To this end, a few ILs have been selected for study. Historically, mainly hexafluorophosphate, $[PF_6]^-$, but also tetrafluoroborate, $[BF_4]^-$, based ILs combined with 1-alkyl-3-methylimidazolium ($[R_n mim]^+$) cations have deserved special attention. As they have proven to potentially be harmful,[4,5] more recently, the scientific community has refocused its attention on fluorine-free ILs.[6] Nonetheless, at present, a large body of information is still only available for those fluorine-containing ILs, and, thus, within this family of ILs theoretical correlations are facilitated. Although possibly improper and unappealing for industry, they nevertheless constitute one of the best model systems for developing predictive methods, which can then be used for the other lesser known, "greener", or more environmentally friendly, ionic liquids. In the current work, we focus our attention on $[C_4mim][BF_4]$, or $[bmim][BF_4]$, and its aqueous solutions including the use of heavy water. This IL has an advantage over its partner $[bmim][PF_6]$, for any proportion of its solutions with water can be investigated both in the totally homogeneous region and in the partially miscible one, at convenient temperatures. Preliminary studies of this system containing H_2O showed that liquid–liquid phase separation (commonly encountered for this kind of solution) occurs at just below near-room-temperature.[7–9] Anthony *et al.*[10] presented a solution thermodynamic study of imidazolium-based ionic liquids where the solubilty of water in $[C_8mim][BF_4]$ can be found. Ternary phase diagrams of IL + water + alkanol have proven the existence of a strong co-solvent effect between water and alkanols in their mixtures with ILs.[2,5,7,11] Letcher *et al.*[12] determined activity coefficients at infinite dilution of several solutes in $[C_6mim][BF_4]$. Holbrey and Seddon[13] mapped the phase diagrams of pure BF_4^--based ILs. Huddleston *et al.* as well as Fredlake *et al.*[14] presented several physical characteristics of pure imidazolium-based ILs, including those that incorporate the BF_4^- anion. Seddon *et al.*[15,16]

DOI: 10.1039/b400374h

and Wang *et al.*[17] measured both viscosities and densities of pure [bmim][BF_4] and its mixtures with water and with organic solvents, respectively.

Our attention is focused on (i) very simple methodologies that permit one to calculate accurately the molar volumes of a broad range of pure ILs as well as some of their solution thermodynamic properties, including heat capacities, with a minimum of information; (ii) more elaborated models that, in turn, relate solution thermodynamic properties (such as excess volumes, v^E, and excess enthalpies, h^E) with increasing or decreasing solvent quality as pressure is applied (pressure derivative of the critical temperature loci of the phase diagram); (iii) theoretical models which rationalize liquid–liquid equilibrium data and enable us to extract estimates of the enthalpy of mixing; (iv) specific quantum-mechanical models, allowing for the prediction of changes in the critical temperature of liquid–liquid phase separation upon isotopic substitution; and (v) special features of the temperature–pressure–composition phase diagram, which permit us to anticipate certain characteristics of critical anomalies. As for (i) we show that simple estimates of the effective "core-sizes" of the anions and cations[7] lead to very reliable predictions of IL molar volumes and that both molar volumes and heat capacities of solutions of IL + solvent are, from a practical and applied perspective, simply determined by linear relationships anchored at the pure components' values. Both densities (as a function of temperature, pressure, and composition) as well as heat capacities (as a function of temperature and composition), including the critical region, have been experimentally determined for [bmim][BF_4]. In the case of (ii), we invoke the "recently rediscovered" Prigogine and Defay equation[18,19] where the critical behavior of second-order derivatives as related to excess properties is intimately linked to the pressure derivative of the critical temperature, dT_c/dp. Phase diagrams and their pressure dependence have been experimentally determined for [bmim][BF_4] + water. As for (iii), a compressible, phenomenological g^E-model[2a,18,20] based on Flory–Huggins type models is used. In (iv), the Theory of Isotope Effects[21] (TIE), which makes use of the observed (or calculated) vibrational mode frequency shifts upon isotopic substitution (H_2O/D_2O) and phase change (of pure liquid water to its infinite dilution in the IL), is applied to solution thermodynamics.[2a,22] The phase diagram shift upon deuterium substitution on water has been experimentally determined. Finally, in (v) Griffiths and Wheeler's geometrical picture[23] is used to relate dT_c/dp to the critical behavior of volumetric properties. Experimental runs showing the evolution of the critical mixture's volume in its approach to the immediate vicinity of the critical temperature have been realized.

The experimental part of this work was performed in two laboratories, Oeiras-Portugal and Ourense-Spain, using samples of IL taken from the same source. In the case of some properties, the study was duplicated (Oeiras and Ourense) in order to assess how distinct purifications, methodologies, and experimental setups can affect the property's value. The current study provides useful information about some intriguing thermodynamic behavior of aqueous solutions of this type of complex liquid.

Experimental

Chemicals and preparation of solutions

1-Butyl-3-methyl-imidazolium tetrafluoroborate was purchased from Solvent Innovation (stated purity > 98%), Germany. In order to reduce the water content and volatile compounds to negligible values, vacuum (0.1 Pa) and moderate temperature (60 °C) were applied to several samples of [bmim][BF_4] for several days always immediately prior to their use. Untreated, original samples reveal 3900–4300 ppm of water while those undergoing drying show less then 75 ppm ("Crison" Karl–Fischer titration) and 70 ± 10 ppm (coulometric "Aquapal" Karl–Fischer). The Cl^- content is in the range of 80–130 ppm (Dionex HPLC anion exchange chromatography = 121 ± 7 ppm; photometric detection of the unreacted excess of iron thyocyanate(III) after the addition of mercury thiocyanate(II) and an iron salt = 84 ppm; Cl^- specific electrode using the standard addition method = 100 ± 20 ppm). MS in the positive and negative modes solely revealed the expected complexes of the general form $\{[bmim]_x[BF_4]_y\}^{x-y}$, thus no impurities within the limit of detection of *ca.* 0.3 %mol. Water was distilled and deionized using a Milli-Q water filtration system from Millipore. Deuteriated water, D_2O (99.84% atom D), was a donation from the KFKI, Hungary. All liquid solutions were gravimetrically prepared to an estimated uncertainty of 0.02% for a typical non-diluted mass percentage.

Equipment and methodology

Accurate phase diagrams were obtained by a laser light scattering technique using two apparatus. One of them, which operates up to pressures of 50 bar, has a thick-walled Pyrex glass tube cell (internal volume ~ 1.0 cm^3, optical length ~ 2.6 mm) connected to a pressurization line and separated from it by a mercury plug. The apparatus, as well as the methodology used for the determination of phase transitions, have recently been described in detail.[24] Here, only a brief description is provided. Scattered light intensity is captured at a very low angle ($2 < 2\theta/° < 4$) in the outer part of a bifurcated optical cable,[25] while transmitted light is captured in the inner portion of this cable. The cloud-point is the point on the $(I_{sc,corr})^{-1}$ against pressure (p) or temperature (T) least-squares fits where the slope changes abruptly. Temperature accuracy is typically ±0.01 K in the range $240 < T/K < 400$. As for pressure, accuracy is ±0.1 bar up to 50 bar. The other apparatus uses a stainless steel cylindrical cell[18b] closed on both sides with thick sapphire windows. It was used for experiments where pressure was raised up to 700 bar. In this case, the hydraulic fluid is the pure solvent (water) in contact with a sufficiently long (1/16)″ SS tube filled with the solution (buffer volume), in order to avoid contamination during compression/expansion cycles. The total volume (buffer + optical) of injected solution is typically 1.6 cm^3, although the optical volume roughly corresponds to a mere 0.5 cm^3. In the case of isothermal runs, temperature accuracy is maintained (±0.01 K) but it worsens a bit for isobaric runs. As for pressure, the uncertainty is ±1 bar in this higher-pressure range. Either cell can be operated in the isobaric or isothermal mode. Abrupt changes in either the transmitted or scattered light upon phase transition sharpen as the thermodynamic path approaches a perpendicular angle to the one-phase/two-phase surface. Pressure can be changed much more quickly than temperature, but, nonetheless, experimental runs had to be performed in the isobaric mode due to the low critical T–p slope presented by the current binary mixture (see Results and discussion). If the T–p slope is low, isothermal runs correspond to almost parallel paths to the transition line.

Densities were determined using either an Anton Paar DMA512P (up to 600 bar) or an Anton–Paar DSA-48 (at 1 bar) density and sound analyser. Descriptions of both the apparatus as well as the experimental procedures can be found elsewhere.[26,27] For the former, the overall density precision is typically 0.002%, while its estimated accuracy is 0.02%.[26] In the case of the second apparatus, 0.002% and 0.01% are the estimated values for the precision and accuracy,[27] respectively. The temperature control is made through a solid-block thermostat *via* the Peltier effect.

A Calvet isothermal flow calorimeter from Setaram was used for the determination of the excess enthalpies. This apparatus and the experimental technique have been previously described.[28] The enthalpies were obtained at a high single temperature, 333.15 K. This temperature (usually, h^E is determined at 298.15 K) was selected due to the high viscosity of [C_4mim][BF_4] at room temperature, a fact that produced a very long mixing process with a nearly vanishing calorimetric signal. The uncertainty in h^E is estimated to be ±1%. The procedure for obtaining h^E as a function of temperature involves the determination of excess molar isobaric heat capacities (T). This is accomplished by combining C_p/V with

density measurements. As for the first, a Micro DSC II differential scanning calorimeter from Setaram was employed[29] at a scanning rate of 0.25 K min^{-1}. Uncertainties (accuracies) associated with $C_p(T)$ and $C_p^E(T)$ determinations are, respectively, of about ± 2 J mol^{-1} K^{-1} and ± 0.2 J mol^{-1} K^{-1}.

Results and discussion

Experimental phase diagrams including pressure and isotope effects. Cloud-points for [bmim][BF_4] + H_2O and [bmim][BF_4] + D_2O

Fig. 1 illustrates the atmospheric pressure phase diagrams of ([bmim][BF_4] + H_2O) and ([bmim][BF_4] + D_2O) using two

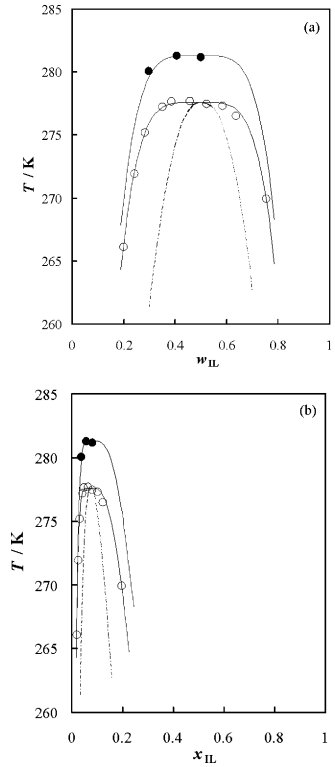

Fig. 1 Atmospheric pressure phase diagrams of ([bmim][BF_4] + H_2O) (○) and ([bmim][BF_4] + D_2O) (●) mixtures using two different field variables, (a) mass, w_{IL}, and (b) mole, x_{IL}, fractions of [bmim][BF_4]. The two-phase region is located inside the envelopes. The solid lines represent least-squares fits to experimental data using the scaling-type eqn. (1). Its parameters are reported in Table 2. In the case of H_2O as solvent, the solid lines also represent the results of the g^E-model calculation (see Table 3); the dashed lines correspond to the spinodal curve using the same g^E-model (see Results and discussion).

different field variables, mass and mole fractions. These systems present upper critical solution temperature (USCT) behavior. This is in accordance with previous findings where, whenever a critical point is found in IL + solvent, only UCST-type of phase diagrams is observed. Moreover, judging from the literature,[2,5,7,9–11,30] so far only water or alkanols have been able to produce critical L–L demixing in ILs. As can be seen in Fig. 1 the phase diagrams lose their symmetry as the field variable is altered from mass to mole fraction. In the latter case, criticality (maximum of the T–x envelope defining the binodal curve) is observed for very low fractions of IL. Therefore, there are analogies between the phase diagrams of ionic liquid solutions and polymeric ones. The coordinates (including pressure) of all cloud-points experimentally observed for these two systems, ([bmim][BF_4] + H_2O) and ([bmim][BF_4] + D_2O) are reported in Table 1. Our results for ([bmim][BF_4] + H_2O) are compatible (difference of about +1 K) with the single datum point reported by Wagner *et al.*,[9a] T_c ~ 276.8 K and with (difference of about −0.5 K) the phase diagram reported by Dullius *et al.*,[9b] who employed less accurate and precise

Table 1 Cloud-point data and their pressure dependence for [bmim][BF_4] + water (H_2O and D_2O). w_{IL} and x_{IL} represent mass and mole fractions of IL, respectively

p/bar	T/K	$10^2\ w_{IL}$	$10^2\ x_{IL}$	[dT/dp] × 10^3/K bar^{-1}
[bmim][BF_4] + H_2O				
2.27	266.09	19.92	1.94	−7.4
11.00	266.05			
19.94	265.97			
30.28	265.89			
40.30	265.82			
2.04	271.94	24.15	2.47	−2.1
10.69	271.92			
20.01	271.90			
30.15	271.87			
40.27	271.86			
2.00	275.20	28.19	3.03	−1.8
9.87	275.19			
20.02	275.16			
30.08	275.15			
41.90	275.13			
2.04	277.23	35.02	4.12	+0.40 ± 0.2
10.06	277.26			
20.58	277.25			
30.92	277.26			
40.41	277.25			
2.22	277.65	38.54	4.76	+0.40 ± 0.2
10.67	277.66			
21.23	277.66			
31.20	277.66			
40.34	277.66			
2.24	277.71	45.68	6.28	+0.40 ± 0.2
10.23	277.71			
20.13	277.71			
30.06	277.71			
40.46	277.72			
2.08	277.46	52.17	7.99	+0.40 ± 0.2
10.79	277.42			
20.51	277.42			
42.62	277.44			
2.10	277.34	58.40	10.06	+0.40 ± 0.2
10.82	277.35			
20.17	277.35			
29.52	277.35			
41.65	277.35			
2.05	276.52	63.51	12.17	+0.40 ± 0.2
6.69	276.54			
11.34	276.54			
22.30	276.54			
27.55	276.55			
30.91	276.55			
41.40	276.57			
2.11	269.96	75.31	19.55	−2.4
10.04	269.94			
19.06	269.92			
29.65	269.89			
39.71	269.87			
28.40	277.42	47.45	8.11	+1.5 ± 0.5
102.5	277.50			
205.2	277.63			
300.5	277.91			+3.1 ± 0.5
400.4	278.31			
507.1	278.74			
600.0	279.27			+5.7 ± 0.5
700.0	279.84			
[bmim][BF_4] + D_2O				
1.87	280.07	29.70	3.6	−1.5
21.82	280.05			
42.14	280.01			
1.23	281.31	40.52	5.69	−1.9
10.48	281.29			
20.21	281.27			
30.04	281.25			
44.14	281.23			
1.73	281.18	49.91	8.10	−1.3
10.94	281.17			
19.91	281.16			
29.63	281.14			
42.18	281.13			

techniques. It is also worth noting that although our temperature precision is 0.01 K, sample impurities are certainly responsible for greater uncertainties, and, consequently, we do not claim a cloud-point temperature accuracy better than ±0.5 K.

Deuteriation of water decreases the miscibility of [bmim][BF_4], provoking an upward shift on the critical temperature of demixing of about 3.7 K. Pressure effects are very subtle (taken at atmospheric pressure) and more complicated. In the case of H_2O as solvent, data show that, while for off-critical concentrations pressurization helps miscibility ($dT/dp < 0$), the opposite is true for near-critical concentrations ($dT/dp > 0$).

This also implies that the shape of the phase diagram is flatter at low pressures becoming more acute as pressure increases. The pressure effect of near-critical concentrations of ([bmim][BF_4] + H_2O) has been studied in more detail by using the high-pressure stainless steel cell allowing for measurements up to 700 bar (see Fig. 2).

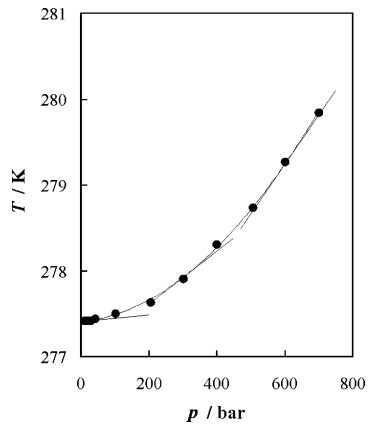

Fig. 2 Experimental pressure effects in the liquid–liquid demixing of [bmim][BF_4] + H_2O at a near-critical concentration, $x_{IL} \sim 0.08$. The segments illustrate the slope (0.4, 3.1, and 5.7 mKbar^{-1}) of the curve at three nominal pressures (1, 300, and 600 bar, respectively).

The *T*–*p* slope of the critical transition, which is very mild when measured at atmospheric pressure, increases as pressure increases. Interestingly, when D_2O is used instead of H_2O, the transition temperatures of near-critical concentrations suffer a downward shift ($dT/dp < 0$) – see Table 1. Both these isotope and pressure effects are theoretically interpreted in subsequent sections.

In order to represent concisely the atmospheric pressure data, the following scaling-type equation has been applied to fit the experimental cloud-points:

$$|w - w_c| = A\left(\frac{T_c - T}{T_c}\right)^{\beta} \qquad (1)$$

It estimates the critical parameters, T_c and w_c. A and β are the critical amplitude and exponent, respectively. Parameters of the scaling-type equation at atmospheric pressure are given in Table 2.

Table 2 Parameters of the scaling-type eqn. (1) for a nominal pressure of 1 bar. w_c and x_c are the mass and mole fractions of IL, respectively

	[bmim][BF_4] + H_2O	[bmim][BF_4] + D_2O
A	0.580	0.580
β	0.218	0.218
T_c/K	277.6	281.3
w_c	0.49	0.46
x_c	0.07	0.07

A lack of sufficient data points for fitting in the case of the ([bmim][BF_4] + D_2O) system combined with a well-known inability to detect experimentally the isotope effect on the critical *mole* fraction[22,31] led us to use for this system the previous (H_2O) parameters with the exception of those of the critical temperature (see Table 2) and, obviously (by molecular mass effect), the critical *mass* fraction.

Interpretation of phase diagrams and critical lines

The aforementioned similarity between phase diagrams of polymer solutions and those of ionic liquid solutions† prompted us to use a "polymer-like", compressible g^E-model[18,20] to rationalize, in a phenomenological fashion, the phase splitting observed for these mixtures as temperature decreases. The model has already been successfully applied to other IL solutions,[2a] those of ILs + alkanols. The asymmetry in the phase diagram is due to a mixing entropic effect originated by the large difference between the volumes (in the language of lattice models, volumes translate as segments) occupied by the mixture's components. In the case of an IL + solvent system, the resulting solution is assumed to constitute a pseudo-binary mixture, as the IL is treated as a molecular entity (or anion–cation pair). A very brief description follows. The model relies on the following change of the molar Gibbs energy of the binary system upon mixing,

$$\Delta G_m/\text{J mol}^{-1} = RT\left[x_1 \ln \varphi_1 + x_2 \ln \varphi_2 + \chi(T,p) x_2 \varphi_1\right] \qquad (2)$$

where the subscripts 1 and 2 refer to the larger and smaller components, respectively, x_i to mole fractions, φ_i to segment fractions, and $\chi(T)$ is the segment–segment temperature- and pressure-dependent interaction parameter between unlike molecules, a measure of the excess Gibbs energy of the mixture (last term of eqn. 2). Segment fractions are easily related to mole fractions through eqns. 3(a,b),

$$\varphi_1 = \frac{rx_1}{rx_1 + x_2} \qquad \varphi_2 = \frac{x_2}{rx_1 + x_2} \qquad (3)$$

where r is the ratio between the number of segments occupied by species 1 in respect to the number of segments occupied by a molecule of component 2 (the latter assumed as unity). Usually, r should not differ greatly from the ratio of molar volumes of the pure components, $r \sim V_1/V_2$. The simplest functional form of the energy interaction parameter that is capable of generating all known types of L–L phase diagrams[18] in the T, p, x space is the following

$$\chi(T,p) = d_0(p) + \frac{d_1(p)}{T} - d_2 \ln T \qquad (4)$$

where d_i are parameters with physical meaning and are generally pressure dependent. Phase separation is dictated by the attainability of a certain critical value for χ (in other words, for the excess molar Gibbs energy of the mixture), which is dependent on the ratio, r, between the segment-number of solute (1) to solvent (2). Parameters of eqn. (4) and r (which determines the temperature independent segment fraction, φ) are obtained by a least-squares fitting to sets of experimental cloud-point data. Once they are set, many other thermodynamic properties of the mixture are as well. For instance, one should recall that the excess molar enthalpy is intimately related to the temperature derivative of the mixture's Gibbs energy. In particular, the following properties can easily be obtained,[2a,18,20]

$$h^E/\text{J mol}^{-1} = RT\left(\frac{d_1}{T} + d_2\right)\frac{rx_1x_2}{rx_1 + x_2} \qquad (5)$$

$$C_p{}^E/\text{J mol}^{-1}\,\text{K}^{-1} = Rd_2\frac{rx_1x_2}{rx_1 + x_2} \qquad (6)$$

† Independently from us and using perspectives distinct from ours, some authors (*e.g.* (a) J. Dupont *et al.*[49]; (b) S. G. Kazarian *et al.*[50]) have pointed out that 1,3-dialkylimidazolium ionic liquids behave similarly to polymers and can be considered as three-dimensional networks of anions and cations linked by weak interactions. This is revealed in the solid and liquid states and even in solution as well.

$$\ln(\gamma_2^{\infty}) = -\ln(r) + (1 - 1/r) + \chi(T,p) \quad (7)$$

for the excess molar enthalpy, excess molar isobaric heat capacity, and activity coefficient of component 2 at infinite dilution in component 1. As for the excess molar volume, it is determined, as dictated by thermodynamics, as the pressure derivative of the excess molar Gibbs energy. Alternatively, v^E can be estimated indirectly by using the so-called Prigogine and Defay equation. We have recently brought to the attention of the scientific community[18,19] the importance and accuracy of this almost forgotten equation in relating excess properties with critical demixing lines, as merely a handful of researchers have sporadically been using it. Under some restrictive assumptions,[18,19] the Prigogine–Defay equation establishes a Clapeyron-type relationship between, on the one hand, the pressure dependence of the critical temperature and, on the other, the ratio between the excess volume and enthalpy,

$$\left(\frac{dT}{dp}\right)_c \cong T_c(p)\frac{v^E(T_c(p),x)}{h^E(T_c(p),x)} \quad (8)$$

The current compressible, phenomenological model conforms inherently to the above-mentioned constraints, and generates eqn. (8) as a true equality.[18] A system that phase separates on cooling must present a positive excess enthalpy, $h^E > 0$ (endothermic process of mixing). Therefore, for a positive T–p slope of a critical demixing line (see Fig. 2), one can anticipate a positive excess volume, $v^E > 0$ (expansion upon mixing).

We have used the current model (in a simplified version where the interaction parameter defined by eqns. (4–6) was set to $d_2 = 0$) in order to find the best values of d_0 and d_1 to reproduce the experimental phase diagrams. Fig. 1 also depicts the model results for the binodal (full lines) and spinodal (dashed–dotted lines) of ([bmim][BF_4] + H_2O) at a nominal pressure of 1 bar in comparison with the experimental cloud-point data and Table 3 the correspond-

Table 3 Parameters of the simplified version of the g^E-model where $d_2 = 0$ (see text)

Rd_1/J mol^{-1}	Rd_0/J mol^{-1} K^{-1}	r	T_c/K	$\varphi_{1,c}$	$x_{1,max}$[a]	H^E_{max}/J mol^{-1}	(γ_2^{∞})[b]	$V^E_{max} \times 10^6$/m^3 mol^{-1}
6263	−13.87	5.284	279.1	0.303	0.303	+3033	1.18	+0.22

[a] $x_{1,max}$ represents the mole fraction of IL at the extremum of the excess properties. [b] At 280 K.

ing parameters. Taking into consideration the crudeness of the model, its performance is highly rewarding. It should be kept in mind, though, that this is a phenomenological model, not a molecular theory, and, therefore, that the complex molecular interactions that take place in solutions containing ILs cannot be fully understood in detail in light of this model. It should also be noted that C_p^E was considered null ($d_2 = 0$, see eqn. 6). As we shall see later, although from a practical perspective this approximation is acceptable, C_p^E's do not vanish (to the best of our knowledge the values reported in the current article are the first for excess heat capacities of IL solutions). The approximation also implies that h^E is temperature independent. Its maximum value (in respect to concentration) extracted from the model (~3000 J mol^{-1}) compares reasonably well with that found experimentally (between ~2400 and 2100 J mol^{-1} in the 280–330 K temperature range). As for v^E the model's result at its maximum (~0.22×10^{-6} m^3 mol^{-1}) should be compared with the corresponding experimental one at near the critical temperature (~0.29×10^{-6} m^3 mol^{-1}). Taking into account that only phase equilibria information was used as input data, the agreement between predicted and experimental excess properties is good. Detailed experimental information on the excess properties can be found in subsequent sections.

It is also possible to estimate the activity coefficient of water at infinite dilution in [bmim][BF_4], γ_2^{∞}, (see Table 3 and eqns. 4 and 7). The calculated values shift from 1.18 to 0.79 as temperature is raised from 280 to 330 K. This is a very important parameter, often used to assess the separation ability of a given solvent towards different solutes (selectivity is the ratio of γ_i^{∞} values).[12] Unfortunately, there are no known experimental data to compare with. It is just experimentally known[10] that in the case of [R_8mim][BF_4] the activity coefficients vary from 2.65 to 1.76 in the 283–308 K interval. Qualitatively, this experimental information and that theoretical estimation are compatible because [R_8mim][BF_4] and water are only totally miscible above[9] ~333 K. In any case, in a previous paper[2a] we demonstrated the acceptable agreement between model's γ^{∞} and experimental ones in IL + alkanol systems.

In contrast to the situation in these IL + alkanol systems, where the optimised r value was found to be close to the ratio of volumes of the mixture's constituents, in [bmim][BF_4] + water r is about two times smaller than that predictable *a priori* by the mere analysis of volumes ratio. This suggests that water molecules tend to be associated in clusters, which, on average, are well represented by dimers.

Interpretation of the observed H_2O/D_2O isotopic effect: a quantum statistical-mechanical treatment

Water has 3 internal OH vibrations—the symmetric stretching vibration, ν_1, the antisymmetric stretching vibration, ν_3, and the bending vibration, ν_2. Besides, in the liquid state, one has to add the so-called external modes: 3 hindered translations and 3 hindered rotations, called librational modes. The vibrational spectra of liquid water are very complicated—they reflect both the intramolecular and the intermolecular vibrations.[32–36] The stretching vibrations ν_1 and ν_3 in the liquid almost merge, giving rise to a broad band. This broadening is mostly due to the effect of strong hydrogen bonding, Fermi resonance between ν_1 and $2\cdot\nu_2$, and strong interaction with the lattice vibrations. Unfortunately, librations also produce broad and unresolved bands which makes the assignment extremely difficult. Because of this complexity, the maximum of the librational band is often considered as a good mean value and is used for each of the three librations[37]—the most frequently used value is around 700 cm^{-1}. In each case the accuracy of the assignment is rather poor and bands are given with uncertainties up to ±20 cm^{-1}. An interesting paper on the vibrational properties of water in ILs has recently been published.[38] Table 4 presents the most recent vibrational data of neat liquid water and that in [bmim][BF_4]. The magnitudes of the frequency shifts on transferring a water molecule from its pure liquid state, "o", to infinite dilution in the IL, "±", suggests that water forms relatively weak hydrogen bonding with the anion BF_4^-. These shifts are comparable with those observed when the solvent is CH_2Cl_2 or CH_3CN[39] (see Table 4). Probably, a symmetrical aggregate is formed—one H_2O molecule with two BF_4^- anions. No data on the frequency shift of the hindered translational and librational modes have been reported.

Table 4 Frequency assignment from the observed spectra of water (in cm^{-1}). Values in parentheses are calculated (see text)

Vibrational mode	H_2O/ Walrafen[33]	H_2O/ Carey and Korenowski[36]	H_2O in [bmim][BF_4][38]	H_2O in CH_3CN[39]
ν_1	3247	3233	3560	3520
ν_2	1645	1640	1625	1633
ν_3	3435	3393	3640	3696
ν_{L1}	722	795	(536)	510
ν_{L2}	550	650	(439)	472
ν_{L3}	450	430	(290)	420

Within the framework of the statistical–mechanical theory of isotope effects[21] (TIE) and following our previous representation[2a,22] of isotope effects on miscibility, we obtain, in first

approximation, the following expression relating the measured isotope shift in the UCST with the frequency shift upon transfer of water from its pure liquid state to a solution at infinite dilution:

$$-\Delta T_c = \left(\frac{1}{\chi_c - d_o}\right)\frac{1}{2}\left(\frac{hc}{k}\right)\left\{\left[\left(\nu_i' - \nu_i\right)^o - \left(\nu_i' - \nu_i\right)^\infty\right]_{sym} + \left[\left(\nu_i' - \nu_i\right)^o - \left(\nu_i' - \nu_i\right)^\infty\right]_b + \left[\left(\nu_i' - \nu_i\right)^o - \left(\nu_i' - \nu_i\right)^\infty\right]_{asym} + LIB\right\} \quad (9)$$

where *sym*, *asym* and *b* refer to the symmetric, antisymmetric, and bending modes, respectively; *LIB* is the contribution from all librational modes. ν_i's are the mode frequencies for H_2O and D_2O (the primes label the lighter isotopologue, H_2O). χ_c is the critical value of the interaction parameter of our g^E-model that triggers phase separation and d_0 is one of the parameters of the χ function (eqn. 4). It should be noted that for the sake of simplicity all mode frequencies are treated in the zero-point energy approximation, even those representing librations (~ 600 cm^{-1}). The error in doing this amounts to about 5% in the vibrational contribution in eqn. (9). The contribution of the translations to the above equation is very small (the greatest frequency lies at 160 cm^{-1}) and can be neglected. Using available frequency shifts of the intramolecular vibrations as well as the experimentally determined isotope shift of the UCST, one can estimate the frequency shift of the librational modes upon the transfer from pure liquid water to the IL solution at infinite dilution. For this purpose we assume a harmonic model for all vibrational modes. Isotopic shifts of the intramolecular vibrations are presented in terms of the reduced mass dependence while those for the librational modes are governed by the ratio of moments of inertia. According to Wolff,[37] the isotopic ratio of the averaged librational frequency of water calculated from the inertia moments of water (I_A, I_B, I_C) is equal to ν_{D_2O}/ν_{H_2O} = 0.724. Basically, the same value is obtained for the square root of the ratio of the reduced masses $\left(\frac{m'_{r,OH}}{m_{r,OH}}\right)^{1/2} = 0.728$ hence, eqn. (9) simplifies to:

$$\Delta T_c = \left(\frac{1}{\chi_c - d_o}\right)\frac{1}{2}\left(\frac{hc}{k}\right)\left(1 - \left(\frac{m'_{r,OH}}{m_{r,OD}}\right)^{1/2}\right) \left[\left(\nu^\infty - \nu^o\right)_{sym} + \left(\nu^\infty - \nu^o\right)_b + \left(\nu^\infty - \nu^o\right)_{asym} + 3\left(\nu^\infty - \nu^o\right)_{lib}\right]_{H_2O} \quad (10a)$$

where now all frequencies are those of H_2O. The factor represented by the square brackets (sum of four terms) can be considered as a total, net frequency shift, $\Delta\nu_{net}$, when the water molecule is transferred from the neat liquid water to the infinitely diluted solution in the IL. $\Delta\nu_{net}$ can be now easily calculated using the following data (see text and Table 3): ΔT_c = −3.7 K, χ_c = 1.0296, d_0 = −1.6695, and r = 5.284.

The calculation gives $\Delta\nu_{net}$ = −51 cm^{-1}. The fact that it is negative means that the frequency shift of the librational vibrations (always red shift) is greater than that resulting from the blue shift of both stretching frequencies. From Table 4 (Carey's values[36]) the latter is estimated as a total 574 cm^{-1} blue shift. Taking into account the small red shift of the bending frequency (−15 cm^{-1}) one gets the value of 559 cm^{-1} characterizing the overall blue shift of all internal frequencies upon transfer from pure liquid to infinite dilution in the IL. Hence, taking into account the calculated $\Delta\nu_{net}$ = −51 cm^{-1}, one gets −610 cm^{-1} characterizing the red shift of all librational modes on transfer from pure liquid to the solution. It means that the average shift of the single librational mode is equal to *ca.* −203 cm^{-1}. Accepting the average value for librational modes at 710 cm^{-1} in pure liquid water,[37] we can assign this mode in the IL solution at infinite dilution at 507 cm^{-1} (case *a*). Alternatively, assuming that all three librational modes given in Table 4 change in the same proportion upon the transfer to solution, we can tentatively assign them in the IL solution at 536 cm^{-1}, 439 cm^{-1} and 290 cm^{-1} (case *b*). These values can be compared with the results of another study of a weak hydrogen bonded system; that of water in acetonitrile[39] (see Table 4) and, as can be judged, the agreement between both results is reasonable. Finally, using the average value of 625 cm^{-1} in pure liquid water (Carey's results[36] for the librational modes) one gets 422 cm^{-1} (case *c*) as the corresponding mean value in the IL solution (to be compared with 467 cm^{-1} in acetonitrile).

The above-mentioned approximate calculations have the merit of providing us with a molecular picture with simple, straightforward physical insight although at the expense of some inaccuracy. The major uncertainty arises from the lack of a self-consistent force constant field for the vibrational modes of water as pure liquid and diluted in the IL (the treatment of isotope effects in the light of the FG matrix[21d]); the other uncertainty is related to the assumption of a zero-point energy approximation, thus neglecting excitation. It is possible to account for these excited sates maintaining the formalism of eqn. (10a). It is out of the scope of this work to offer the details of such a development. Here, we merely mention that excited states for the low-frequency librations (LIB_{exc}) can be accounted for to a very good approximation[21e] as a fifth term in the summation inside the square brackets of eqn. (10a). Namely,

$$LIB_{exc} = 3\times 2\left(\frac{\nu^o + \partial\nu}{\exp\left(\frac{hc}{kT}\left(\nu^o + \partial\nu\right)\right) - 1} - \frac{\nu^o}{\exp\left(\frac{hc}{kT}\left(\nu^o\right)\right) - 1}\right) \quad (10b)$$

where $\partial\nu = \nu^\infty - \nu^o$. At 279 K and for ν^o = 710 cm^{-1} one obtains $\partial\nu$ = −266 cm^{-1}, while for ν^o = 625 cm^{-1}, $\partial\nu$ = −302 cm^{-1}. Alternatively, one can perform the reversed exercise predicting isotope effects on the phase diagram by using mode frequency assignments of the isotopically substituted molecule in systems where it behaves similarly to that under investigation.

Solution thermodynamics. Experimental data and additional predictive tools

Density and heat capacity of [bmim][BF_4]. Table 5 reports measured densities, ρ, at nominal pressures and Table 6 presents isobaric molar heat capacities $C_{p,m}$ for the pure [C_4mim][BF_4] in the 278.15 to 333.15 K temperature range. As a rule, deviations between density data of this work (Oeiras's and Ourense's laboratories) are small (see Fig. 3) as compared with those where literature data are involved. For instance, at 298.15 K and atmospheric pressure, while Huddleston *et al.*[14] report 1.12 g cm^{-3} and 1.17 g cm^{-3} (their ref. 36), values found in the articles of Wang *et al.*,[17] Seddon *et al.*,[15] and Fredlake *et al.*[14b] are quoted as 1.21105 g cm^{-3}, 1.2048 g cm^{-3}, and 1.2037 g cm^{-3}, respectively (in the latter two cases a least-squares fit to their data was applied in order to make comparisons at the same nominal temperature of 298.15 K). A more detailed comparison between our results (H_2O = 72 ppm; Cl^- = 80 to 130 ppm) and those of both Seddon (H_2O = 307 ppm; Cl^- = 40 ppm) and Fredlake (H_2O = 1900 ppm; Cl^- = 10 ppm) reveals that on average our results agree with theirs within ±5 × 10^{-4} g cm^{-3} in the 298.15–333.15 K range. This is an excellent agreement. A comment is pertinent at this point. Based on the conclusions of the study of Seddon *et al.*,[16] the presence of 1 wt% of Cl^- in this IL reduces its density by 0.016 g cm^{-3}. Therefore, *e.g.* 300 ppm of Cl^- reduces the density by 5 × 10^{-4} g cm^{-3}. On the other hand, the water effect is much milder. Our very precise measurements for the mixtures (*vide infra*) show that a 2 mol% (or, equivalently, 1600 ppm) contamination with water merely reduces the density by 4 × 10^{-4} g cm^{-3} (the same conclusion is obtained by assuming ideal volumetric behaviour for this IL + water mixture).

In respect to heat capacities, to the best of our knowledge, these were the first reported $C_{p,m}$ values for [C_4mim][BF_4]. During the refereeing process of this article we have become aware of other,

Table 5 Experimental densities of pure [bmim][BF_4] from two laboratories, Oeiras-Portugal and Ourense-Spain, at several temperatures and some selected rounded pressures

	ρ/g cm^{-3}	
T/K	Oeiras lab.	Ourense lab.
p = 1 bar		
278.15	—	1.219351
283.15	—	1.215571
288.15	—	1.211756
293.15	—	1.208055
298.15	1.20518	1.204362
303.15	1.20139	1.200752
313.15	1.19423	—
323.15	1.18763	—
333.15	1.18073	—
p = 100 bar		
298.15	1.20974	—
303.15	1.20593	—
313.15	1.19868	—
323.15	1.19223	—
333.15	1.18542	—
p = 300 bar		
298.15	1.21845	—
303.15	1.21470	—
313.15	1.20745	—
323.15	1.20122	—
333.15	1.19453	—
p = 600 bar		
298.15	1.23048	—
303.15	1.22698	—
313.15	1.22011	—
323.15	1.21402	—
333.15	1.20739	—

Table 6 Experimental isobaric molar heat capacities for the pure [bmim][BF_4] in the 278.15 to 333.15 K temperature range[a]

T/K	$C_{p,m}$/J mol^{-1} K^{-1}
278.15	355.69
283.15	357.72
288.15	359.93
293.15	362.31
298.15	364.71
303.15	367.37
308.15	369.94
313.15	372.84
318.15	375.71
323.15	379.03
328.15	382.23
333.15	385.86

[a] Regression polynomial: $C_{p,m} = 464.88 - 1.1755T + 0.002815T^2$.

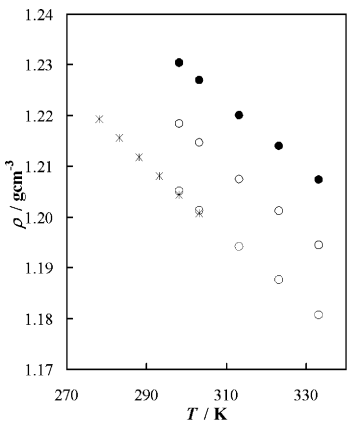

Fig. 3 Experimental densities of [bmim][BF4] *vs.* temperature; circles (Oeiras lab.): white (1 bar), grey (300 bar), black (600 bar); stars (Ourense lab.).

very recent measurements (Fredlake *et al.*[14b]). Our results lie some 3.7 to 5.5% higher than those of this reference. Fredlake *et al.* mention an uncertainty of ±3.7%, so the agreement between both sets of data is satisfactory. Our measurements were performed using an extremely precise instrumentation (see above) working at a very small scanning rate. This is why it was possible to detect deviations from ideality of the IL + water mixtures (*vide infra*) as small as 1 J mol^{-1} K^{-1} with an extremely high internal consistency (0.05 J mol^{-1} K^{-1}). Although the precision of our measurements is very high, we are aware of the fact that even small traces of impurities do affect the accuracy of the absolute values of $C_{p,m}$. Assuming ideal behaviour for the heat capacity (*vide infra*), 0.1 mol% (~70 ppm) of water reduces the heat capacity by 0.3 J mol^{-1} K^{-1}, while contamination at a level of 2 mol% (~1600 ppm) of water decreases it by 6 J mol^{-1} K^{-1}, and so forth. Our level of water contamination is very close to the first case. The influence of the presence of Cl^- is more difficult to assess. Nonetheless, an estimation is possible. The influence of the presence of Cl^- is probably mild in the case of heat capacities. Neglecting its counterion, note that a ternary mixture $[C_4mim]^+ + [BF_4]^- + [Cl]^-$ can be obtained by hypothetical mixing of [C_4mim][BF_4] with [C_4mim][Cl]. Assuming, in first approximation, "ideal behaviour" for such an equivalent binary mixture, and considering that *e.g.* 350 ppm of Cl^- (~three times the actual level of this impurity) in [C_4mim][BF_4] is equivalent to the presence of 0.23 mol% of [C_4mim][Cl], one obtains a very small decrease of 0.1 J mol^{-1} K^{-1}. In this calculation we have used the values of heat capacity presented by Fredlake *et al.*[14b] According to the authors, values for [C_4mim][Cl] are lower than those of [C_4mim][BF_4] by about 30 J mol^{-1} K^{-1}. It is interesting to note that this same concept of an ideal, hypothetical binary mixture of [C_4mim][BF_4] and [C_4mim][Cl] leads to very similar conclusions about the influence on the density resulting from the presence of Cl^- as before (see above). To perform this estimation we have used the estimated molar volume[7] of supercooled [C_4mim][Cl] at 298.15 K, V° = 159.44 cm^3 mol^{-1}.

Considering all the aforementioned discussion on the influence of impurities (water and chloride), we trust that an estimated uncertainty (accuracy) of ±2 J mol^{-1} K^{-1} for our values of heat capacity is a generous number.

A regular (quasi-linear) temperature dependence of the $C_{p,m}$ of [C_4mim][BF_4] is observed as previously found for other ILs.[14b,40] In the particular case of [C_4mim][PF_6], isobaric heat capacities in the ideal gas state $C^\circ_{p,m}$ are also available from the literature.[41] The residual heat capacities for this liquid, *i.e.* the quantity $C_{p,m} - C^\circ_{p,m}$, were found to be very small (about 4% of $C_{p,m}$) as compared with those of normal liquids.[42] The well-known fact that $C^{res}_{p,m}$ comes mainly from the destruction of liquid structure—as in the case of alcohols, where hydrogen bond rupture contributes significantly to $C^{res}_{p,m}$, depending strongly on temperature producing complex $C_{p,m}(T)$ curves[42]—is consistent with the very strong structure of ionic liquids arising from Coulombic interactions. Thus, it can be concluded that the C_p behavior of ILs will be governed by $C^\circ_{p,m}$.

Knowing $\rho(T,p)$ enables one to calculate both the isobaric thermal expansivity, $\alpha_p = -(\partial\ln\rho/\partial T)_p$, and the isothermal compressibility, $k_T = (\partial\ln\rho/\partial p)_T$ as a function of T and p. Discussing these quantities is out of the scope of the present work but it is still pertinent to include a few comments. Generally, one can state that both these quantities are *ca.* 2–3 times smaller than in conventional, organic solvents,[7] meaning that both the temperature and the pressure dependence of the density are subtle. Therefore, the uncertainties associated with their determination increase. This seems to be particularly important when one wishes to determine the temperature dependence of α_p. Note that this involves the correct assignment for the second derivative of the volumetric properties, or, in other words, the curvature of density–temperature (or volume–temperature) plots. In a previous, preliminary study[7] we showed that, although it appears that α_p of the studied ILs increases with T (as is generally expected for any liquid), the slope

of this rise decreases significantly as the size of the IL's anion decreases. In other words, if the size of the anion becomes sufficiently small, we speculate that it may be possible to find an IL where α_p does not change with T and even others where α_p *decreases* as T increases. This is a very rare situation, apparently limited to a very few, small chain alkanols at very low temperature.[43] Note that even water, which presents a α_p anomaly (change of sign at the locus of its maximum density), always presents α_p increasing as T rises. Nonetheless, the possibility of finding α_p decreasing with T is supported by some simulation studies.[44] It implies that at some higher temperature α_p presents a minimum (as occurs with those aforementioned alkanols) because it is a thermodynamic requirement that expansivity diverges to $+\infty$ at the highest liquid temperature, the critical one.

In contrast to the situation encountered with ILs containing larger anions, the above discussion is particularly pertinent in the case of [bmim][BF_4] (small anion) because the $\rho(T,p)$ data, despite their high precision, reveal that it is extremely difficult, if not impossible, to define whether the density–temperature plot has any curvature—positive or negative—or not. The latter two cases (negative or no curvature) would lead to a "normal" behavior, while the first would provoke an (interesting) anomaly; and would expose another one: $C_{p,m}$ would increase with increasing pressure (see eqn. 11 below). We speculate here that these potential anomalies are an indication of unusually high order—solid like—in the liquid state. It is thus important to perform high-precision measurements with ILs containing anions such as NO_3^- or Cl^-. We intend to do this in due course. Within the frames of any of the scenarios, α_p for [bmim][BF_4] is basically temperature independent at near room temperature. For the present moment, we simply report that α_p = $(5.95 \pm 0.15) \times 10^{-4}$ K^{-1} and that k_T = $(3.65 \pm 0.05) \times 10^{-5}$ bar^{-1}, at 298.15 K and atmospheric pressure.

Following the argumentation above and taking into account the thermodynamic relation,

$$\left(\frac{\partial C_p}{\partial p}\right)_T = -T\left(\frac{\partial^2 V}{\partial T^2}\right)_p = -TM_w\left[\frac{2(\alpha_p)^2}{\rho} - \frac{1}{\rho^2}\left(\frac{\partial^2 \rho}{\partial T^2}\right)_p\right] \quad (11)$$

it is expected that [bmim][BF_4] will show a very small variation of C_p with pressure ($\sim 10^{-3}$ J mol^{-1} K^{-1} bar^{-1}).

Volumetric and calorimetric properties of the ([bmim][BF_4] + water) system. Fig. 4 shows both molar volumes, V_m, and isobaric molar heat capacities, $C_{p,m}$, for the

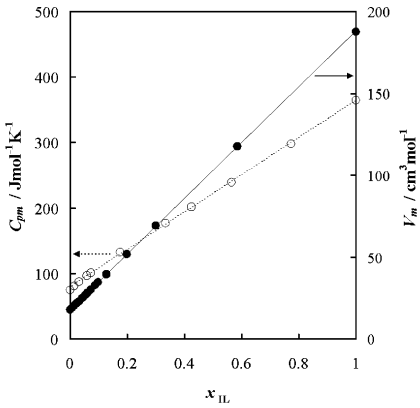

Fig. 4 Isobaric molar heat capacities (○) and molar volumes (●) of the ([bmim][BF_4] + H_2O) system *versus* the mole fraction of IL at 298.15 K and 1 bar. Note the high linearity of both plots.

[C_4mim][BF_4] + H_2O system at 298.15 K over the whole composition range. Both V_m and $C_{p,m}$ for the mixtures were obtained from data contained in this work together with $C^E_{p,m}$ data.[8] Linear behavior with respect to the ionic liquid mole fraction x is observed to an excellent approximation—deviations from linearity (excess quantities, see Figs. 5 and 6) do not seem to be relevant at

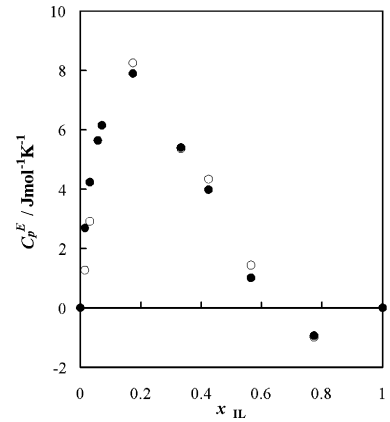

Fig. 5 Experimental excess molar isobaric heat capacities of [bmim][BF_4] + H_2O *versus* the mole fraction of IL at 278.15 K (○) and 333.15 K (●), and 1 bar.

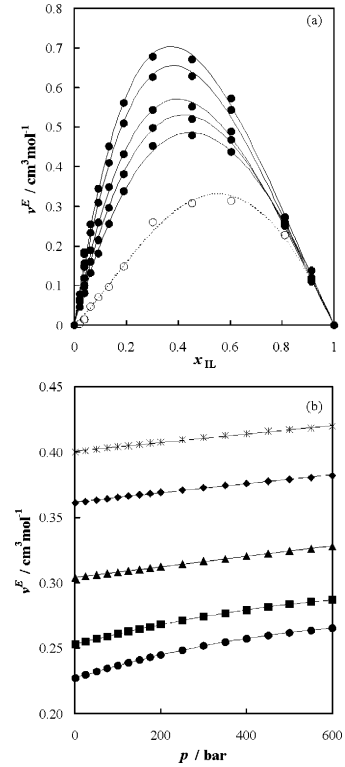

Fig. 6 Experimental excess molar volumes of [bmim][BF_4] + H_2O. (a) *versus* composition at 1 bar of nominal pressure. v^E's decrease as temperature decreases (333.15, 323.15, , 333.15, 303.15, 298.15, and 278.15 K). At the latter temperature, values (○) were obtained as an extrapolation to $\sim T_c$ and, at the scale of the figure, are indistinguishable from the direct measurements performed in Ourense up to x_{IL} = 0.3 (see Table 7). Lines represent Redlich–Kister fittings whose parameters are given in Table 9. (b) *versus* pressure at x_{IL} = 0.01003. v^E's decrease as temperature decreases (333.15, 323.15, 313.15, 303.15, and 298.15 K).

a solution-thermodynamic-property level. It is evident that this linearity of V_m and $C_{p,m}$ constitutes a useful tool for predicting the values of these quantities from those of the pure liquids.

Specifically, the molar volume of 1-alkyl-3-methylimidazolium [$R_n$mim]$^+$ based ILs has been found to vary linearly with n, irrespective of the anion, showing a common slope (of 34.4 ± 0.5 cm^3 mol^{-1} per each pair of additional carbons).[7] The difference in the y-intercepts owes to the difference in the size of the anions. This fact suggests that some type of *group contribution method* can account for the *effective* molar sizes, V_{eff}, of cations and anions once the core size of one of them is known.[7] Using spectroscopic data,[9] we anchored the size of PF_6^- as that of an equivalent hard sphere of radius equal to 3.08 Å (effective volume of 73.71 cm^3 mol^{-1}). The difference between the molar volumes of the series of PF_6^--based ILs and those of the series containing BF_4^- establishes

the effective size of the latter, and so forth. For instance, it was found[7] that $V_{eff,[BF_4]^-}$ = 53.42 cm^3 mol^{-1} and $V_{eff,[C_4mim]^+}$ = 133.58 cm^3 mol^{-1}. The procedure gives V_m = 187.00 cm^3 mol^{-1} for [C_4mim][BF_4] at atmospheric pressure and 298.15 K, which is in good agreement with experimental data: 187.55 cm^3 mol^{-1} (this work, Oeiras), 187.67 cm^3 mol^{-1} (this work, Ourense) and 187.62 cm^3 mol^{-1}.[15]

Thus, starting from effective core sizes of ions, one can predict by summation the V_m values of a large number of ionic liquids and ionic liquid mixtures (IL_1 + IL_2) and, then, also of ionic solutions if the molar volume of the non-ionic solvent is known (linear plots). More detailed information about this core size methodology can be found elsewhere.[7]

Experimental excess molar volumes v^E (T,p,x) obtained in both laboratories are reported in Table 7 and plotted in Figs. 6a,b

Table 7 Experimental excess molar volumes of [bmim][BF_4] + H_2O from Oeiras (only a small sample at some nominal pressures) and Ourense

v^E/cm^3 mol^{-1}

Oeiras laboratories

x_{IL}	T = 298.15 K	T = 303.15 K	T = 313.15 K	T = 323.15 K	T = 333.15 K
p = 1 bar					
0.0209	0.045	0.059	0.066	0.078	0.078
0.0385	0.081	0.100	0.119	0.147	0.156
0.0627	0.132	0.160	0.189	0.233	0.255
0.0924	0.181	0.214	0.258	0.309	0.344
0.1337	0.255	0.296	0.349	0.409	0.451
0.1896	0.338	0.382	0.431	0.510	0.561
0.3014	0.453	0.498	0.543	0.626	0.678
0.4533	0.480	0.521	0.551	0.628	0.671
0.6031	0.437	0.468	0.488	0.543	0.573
0.8104	0.251	0.255	—	0.259	0.273
0.9128	0.137	0.110	0.111	0.109	0.120
p = 100 bar					
0.1003	0.237	0.261	0.308	0.365	0.404
0.3477	0.699	0.719	0.774	0.864	0.926
0.5905	0.441	0.432	0.445	0.536	0.589
p = 300 bar					
0.1003	0.252	0.274	0.316	0.373	0.411
0.3477	0.714	0.729	0.770	0.860	0.919
0.5905	0.452	0.441	0.438	0.533	0.582
p = 600 bar					
0.1003	0.265	0.287	0.328	0.382	0.420
0.3477	0.730	0.745	0.779	0.865	0.919
0.5905	0.462	0.455	0.451	0.542	0.583

Ourense laboratories

x_{IL}	T = 278.15 K	T = 283.15 K	T = 288.15 K	T = 293.15 K	T = 298.15 K	T = 303.15 K
p = 1 bar						
0.0040	−0.0360	−0.0335	−0.0307	−0.0283	−0.0258	−0.0237
0.0073	−0.0414	−0.0363	−0.0313	−0.0270	−0.0228	−0.0188
0.0132	−0.0405	−0.0317	−0.0234	−0.0162	−0.0087	−0.0022
0.0210	−0.0332	−0.0206	−0.0088	0.0017	0.0121	0.0223
0.0246	−0.0322	−0.0181	−0.0049	0.0071	0.0188	0.0300
0.0302	−0.0236	−0.0082	0.0067	0.0205	0.0341	0.0477
0.0420	−0.0099	0.0094	0.0279	0.0450	0.0625	0.0829
0.0530	—	0.0255	0.0464	0.0668	0.0864	0.1125
0.0596	—	0.0336	0.0563	0.0779	0.0992	0.1197
0.0719	—	0.0507	0.0760	0.1004	0.1238	0.1449
0.0865	—	0.0719	0.1003	0.1271	0.1530	0.1781
0.0974	0.0553	0.0867	0.1157	0.1436	0.1721	0.2000
0.1260	0.0928	0.1299	0.1633	0.1950	0.2266	0.2588
0.1979	0.1777	0.2182	0.2567	0.2937	0.3305	0.3661
0.2994	0.2811	0.3213	0.3578	0.3942	0.4296	0.4665

(Oeiras' results). As for the data for the same property obtained in the Ourense's labs, we focused our attention on temperatures and concentrations closer to the critical ones. The good agreement between both sets of data can be judged by analyzing the values at the two overlapping temperatures (Table 7) and the plot at one of them (see Fig. 7). We have deliberately represented v^E's *versus*

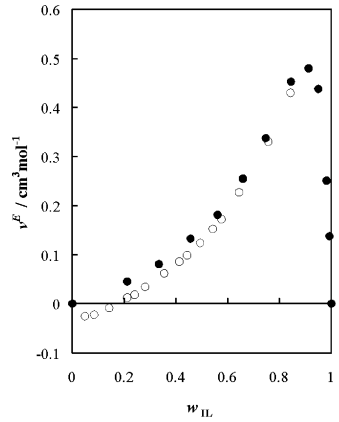

Fig. 7 Comparison of experimental v^E's *vs.* mass fraction of ([bmim][BF_4] + water). Data at 298.15 K; (●) Oeiras lab., (○) Ourense lab.

mass fraction in order to enhance the near-critical region. In turn, these two sets of data agree semi-quantitatively with results reported previously by Seddon *et al.*[16] In contrast with Seddon *et al.*, we have found more symmetrical, well-behaved shapes, and our results indicate lesser non-ideality at the maximum.

Experimental excess molar enthalpies h^E at atmospheric pressure (Ourense's labs) can be found in Table 8, and Fig. 8 depicts their shape. There are no other experimental results to compare with; merely simulations performed by Hanke and Lynden-Bell[45] suggesting that for a similar system, [C_1mim][PF_6] + water, equimolar mixing is accompanied by an endothermic excess energy of *ca.* 1 kJ mol^{-1}. Parameters of Redlich–Kister fits to the Oeira's data on v^E values as well as to those of Ourense on h^E values, at atmospheric pressure, are reported in Table 9. The large positive h^E values at all temperatures reflect energetically unfavorable mixing as expected at least near the UCST. These values suggest that water reduces the strong electrostatic attractions between the ions[16] and/or that the hydrogen bonding water-anion is energetically weak (see discussion above about isotope effects) and does not superimpose some loss of water–water and anion–cation hydrogen bonds upon mixing. The power of water to significantly reduce the Coulombic attractions is expected since these are inversely proportional to the dielectric constant, ε, of the media and water presents an unusually high value of ε. It should also be noted that h^E values are almost temperature insensitive. As shown previously, this system exhibits, at atmospheric pressure, a liquid–liquid phase transition, the critical coordinates of which are T_c = 277.6 K and w_c = 0.49 (x_c = 0.07). Excess volumes are always positive at the highest measuring temperatures but decrease as temperature is lowered becoming S-shaped. From Figs. 6a and Fig. 7, it can be observed that the excess volumes at near-critical compositions and low temperatures, $v^E(x_c,T)$, take a quasi-null value. This result is in very good agreement with that previously obtained from the extrapolation of Oeiras' data within the 298.15–333.15 K temperature interval to the critical temperature.[8]

In general, hydrogen bonding is certainly more T-dependent (becoming negligible at high temperatures) than Coulombic interactions. The always-positive v^E's at high temperatures probably accounted for the above-mentioned fall of the anion–cation electrostatic attraction upon insertion of water molecules. As temperature is lowered, a negative *contribution* to v^E starts to appear, mainly in the low-concentration of IL region, which is certainly not independent of some enhancement of hydrogen bonds (the loss of water–water and ion–ion H-bonds upon their transfer from the pure components to the solution is superimposing the gain of water–ion H-bonds).

Both v^E and h^E data at near-critical conditions are useful for predicting the slope of the critical line by means of the restricted Prigogine and Defay equation (eqn. 8). In spite of its simplicity, the

Table 8 Excess molar enthalpies and excess molar isobaric heat capacities of [bmim][BF_4] + H_2O at several temperatures and at 1 bar nominal pressure

h^E/J mol^{-1}									
x_{IL} T/K	278.15	283.15	288.15	293.15	298.15	303.15	313.15	323.15	333.15
0.0143	183	190	198	206	216	225	247	271	296
0.0311	398	412	428	443	459	476	512	549	590
0.0587	—	722	748	773	797	822	872	924	979
0.0713	—	857	886	914	941	968	1022	1079	1139
0.1746	1552	1593	1631	1669	1706	1743	1818	1895	1974
0.3327	2052	2079	2106	2133	2160	2187	2241	2295	2350
0.4232	2049	2070	2092	2113	2134	2155	2196	2237	2277
0.5642	1654	1660	1666	1672	1677	1682	1692	1702	1711
0.7736	1040	1034	1028	1021	1015	1008	995	983	973
C_p^E/J mol^{-1} K^{-1}									
x_{IL} T/K	278.15	283.15	288.15	293.15	298.15	303.15	313.15	323.15	333.15
0.0143	1.27	1.48	1.64	1.89	1.84	2.03	2.29	2.47	2.69
0.0311	2.91	2.96	3.08	3.26	3.32	3.40	3.65	3.88	4.24
0.0587	—	5.42	5.07	4.99	4.83	4.92	5.11	5.32	5.64
0.0713	—	6.09	5.64	5.52	5.41	5.40	5.62	5.82	6.16
0.1746	8.26	7.80	7.52	7.50	7.38	7.39	7.49	7.68	7.90
0.3327	5.38	5.37	5.34	5.40	5.42	5.42	5.48	5.44	5.40
0.4232	4.34	4.31	4.27	4.19	4.17	4.18	4.17	4.04	3.99
0.5642	1.44	1.20	1.16	1.13	1.07	0.98	0.99	0.91	1.02
0.7736	−0.99	−1.28	−1.35	−1.32	−1.32	−1.28	−1.20	−1.17	−0.93

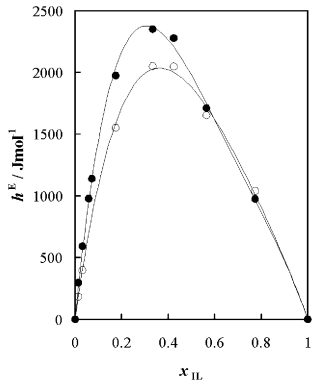

Fig. 8 Experimental excess molar enthalpies of [bmim][BF_4] + water mixture at 1 bar nominal pressure; (●) −333.15 K, (○) −278.15 K. Lines represent Redlich–Kister fittings whose parameters are given in Table 9.

Table 9 Parameters of Redlich–Kister fittings, $X^E = x_{IL}(1 - x_{IL})(A + B(2x_{IL} - 1) + C(x_{IL} - 1)^2)$, for the excess molar volumes ($X^E = v^E$) and excess molar enthalpies ($X^E = h^E$) of [bmim][BF_4] + H_2O mixture at several temperatures and at 1 bar nominal pressure

T/K	A	B	C
Parameters for v^E/cm^3 mol^{-1}			
298.15	1.92214	−0.41467	−0.00007
303.15	2.07417	−0.68784	−0.03731
313.15	2.17704	−0.95624	0.16677
323.15	2.45430	−1.31484	0.18361
333.15	2.61068	−1.48976	0.31202
Parameters for h^E/J mol^{-1}			
278.15	7515.87	−4183.84	1841.75
283.15	7555.05	−4419.48	2064.46
288.15	7593.20	−4654.20	2284.76
293.15	7631.88	−4885.94	2489.97
298.15	7670.16	−5116.88	2691.85
303.15	7707.67	−5348.09	2896.47
313.15	7779.69	−5813.33	3329.34
323.15	7847.28	−6282.95	3808.83
333.15	7910.51	−6754.80	4344.80

equation has proven to provide reliable predictions. Extrapolation of experimental h^E and v^E contained in Table 7 and 8 to T_c was made for three near-critical compositions taken from the Ourense results (see Table 10) owing to the uncertainty in the determination

Table 10 Calculated (see eqn. 8) and experimental T–p slopes of the critical locus of [bmim][BF_4] + H_2O. Excess molar volumes and enthalpies were obtained from the low temperature results of Ourense's laboratories by a small extrapolation to T_c

x_{IL}	v^E/cm^3 mol^{-1}	h^E/J mol^{-1}	$T_c \frac{v^E(T_c)}{h^E(T_c)} 10^3$ /K bar^{-1}	$\left(\frac{dT}{dp}\right)_{exp} 10^3$ /K bar^{-1}
p = 1 bar				
0.0530	0.0058	636	0.3	
0.0596	0.0125	702	0.5	0.4 ± 0.2
0.0719	0.0260	819	0.9	
p = 300 bar				
0.1003	0.133	990	3.7	3.1 ± 0.5
p = 600 bar				
0.1003	0.165	950	4.9	5.7 ± 0.5

of the critical composition from phase equilibria measurements. This results in a $(dT/dp)_c$ ranging from 0.3 to 0.9 mK bar^{-1}, which is in quite good agreement with the directly measured value (0.4 ± 0.2) mK bar^{-1}. For the first time, Prigogine and Defay's equation has been applied to ionic solutions. Similar calculations at high pressure demonstrate that the equation is also capable of relating excess properties with solvent quality as pressure varies. As one can note from data reported in Table 1 as well as the plot illustrated in Fig. 2, the slope of the critical line increases with increasing pressure. Direct measurements of the influence of pressure on v^E were performed (Table 7) but not on h^E.

Nevertheless, thermodynamics dictates that,

$$\left(\frac{\partial H^E}{\partial p}\right)_T = -T\left(\frac{\partial V^E}{\partial T}\right)_p + V^E \qquad (12)$$

Therefore, excess enthalpies can be calculated at pressures different from the atmospheric one by correcting for the pressure dependence of h^E, which amounts to about −0.20 J mol^{-1} bar^{-1} at low pressure

decreasing to −0.15 J mol^{-1} bar^{-1} at 600 bar, for near critical concentrations and temperatures. Table 10 reports the values of v^E and h^E at high pressures.

Since v^E increases (see Fig. 6) and h^E decreases as pressure rises, the P&D equation correctly predicts an increase in dT_c/dp, with an agreement that is quasi-quantitative. Another test of the predictive capabilities of eqn. 8 can be performed by analyzing the deuterium substitution on water. As previously discussed (see text and Table 1), in contrast to using H_2O as solvent, in the case of D_2O, applying pressure provokes better miscibility (T_c shifts downwards). Fig. 9

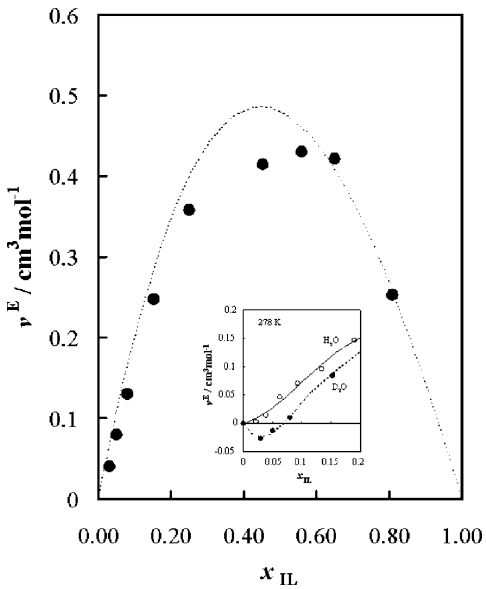

Fig. 9 Effect of isotopic substitution (H_2O/D_2O) on the excess molar volumes of [bmim][BF_4] + water at 298.15 K and 1 bar. For the sake of clarity, in the case of H_2O the results are represented by the Redlich–Kister fitting to the data (Table 9). (●) D_2O. The insert shows a magnification of the near-critical mole fraction region at a near critical temperature of 278 K.

illustrates the effect of isotopic substitution on the excess volumes of the system by comparing this property in the two cases (water and heavy water) at 298.15 K and 1 bar.

Table 11 reports all measured values of v^E for D_2O as solvent for several temperatures. Deuteration slightly decreases (by about

Table 11 Experimental excess molar volumes of the ([bmim][BF_4] + D_2O) system at several temperatures and atmospheric pressure

v^E/cm^3 mol^{-1}			
x_{IL}	T = 288.15 K	T = 293.15 K	T = 298.15 K
0.0301	0.007	0.025	0.041
0.0501	0.034	0.058	0.080
0.0800	0.071	0.102	0.131
0.1524	0.167	0.209	0.248
0.2501	0.270	0.315	0.358
0.4519	0.346	0.382	0.415
0.5593	0.376	0.404	0.430
0.6503	0.377	0.400	0.422
0.8078	0.239	0.247	0.253

10%) the v^E values at the maximum of the v^E–x curve, but more importantly, the v^E values have now a *negative* sign at near-critical conditions. The insert to Fig. 9 shows values of v^E (H_2O) in comparison with those when D_2O was used, magnifying the near-critical concentrations, the latter of which were determined by a small extrapolation of the existing data (Table 11) to T_c. It is clear that this change in the sign of $v^E{}_c$ is responsible for the distinct response of the system as pressure is applied upon isotopic substitution.

Critical behavior of second-order derivatives. Universality is one of the most fascinating features of critical phenomena since it implies that systems of different physical nature show the same pattern of behavior near the critical point—it is said that all of them belong to the same universality class. Gas–liquid critical points of pure substances, Curie points of uniaxial magnets, and liquid–liquid critical points of binary liquid mixtures belong to the three dimensional Ising model (Ising-3D) universality class. From a microscopic point of view, the structure of these systems near the critical point is characterized by long-range fluctuations of the order parameter—a macroscopic physical quantity—so that microscopic details of interparticle interactions become unimportant. In other words, near the critical point, systems lose their physical identity at the expense of universality.

One of the most important steps in the study of critical phenomena of a given system consists of identifying the order parameter. In liquid–liquid critical points, concentration is the order parameter; consequently, the structure of binary mixtures in the critical region is characterized by long-range concentration fluctuations. Although universal, the critical behavior in binary mixtures varies richly in respect to the type of crossover behavior they exhibit. In mixtures containing simple liquids, the system *crosses over* from an Ising-like regime to states further from criticality where fluctuations are unimportant and classical mean-field apply; this occurs in a natural fashion, implying that the crossover is never completed in the critical region (a few Kelvin around the critical temperature). Complex mixtures, such as polymer or micellar solutions exhibit a more singular behavior in the critical domain. In particular, complex systems verify Ising-like behavior, however, the crossover to mean-field behavior can occur in the critical region resulting in an intermediate non-universal critical behavior that depends on the physical nature of the system. The extreme case comprises very strong interparticle interactions so that Ising-like behavior cannot be observed in the experimentally accessible region. In addition, another interesting type of crossover criticality can be found in polymer mixtures when the increase of the polymer molecular weight drives criticality from Ising-like to theta-point tricritical behavior.

Although complete understanding of ionic solution criticality is still a controversial issue,[9,46] it is now recognized that, as for other complex systems, Ising-like behavior must be observed in the immediate neighborhood of the critical point. The main problem lies in the characterization of the crossover criticality. Most researchers speculate that crossover from Ising-like to some type (not well understood) of tricritical behavior must be fulfilled, however, more accurate experimental data than that currently available is necessary. Room temperature ionic liquids may play an important role at this level since they seem to overcome experimental difficulties inherent to classical organic salts.

Here, we focus on the critical behavior of second-order derivatives as related to the slope of the critical line. It is well-known[47] that, near the critical point, C_p/V, α_p, and κ_T follow α-power-law behavior (divergence to infinity):

$$Y = \frac{Y_0^{\pm}}{\alpha}\left|\frac{T - T_c}{T_c}\right|^{-\alpha} \qquad (13)$$

where Y can be C_p/V, α_p, and κ_T. The quantities Y_0 (+ and − denote the homogeneous and heterogeneous regions, respectively) and α are the critical amplitude (measure of the size of the critical anomaly) and the critical exponent (its universal value is 0.110), respectively. Griffiths and Wheeler's geometrical analysis[23] establishes the following limiting relations between second-order derivatives at the critical point:

$$\left(\frac{dT}{dp}\right)_c = T_c\frac{\alpha_p}{C_p/V} \qquad \left(\frac{dT}{dp}\right)_c^2 = T_c\frac{\kappa_T}{C_p/V} \qquad (14)$$

Introduction of eqn. (13) in eqns. (14) gives

$$\left(\frac{dT}{dp}\right)_c = T_c\frac{B}{A} \qquad \left(\frac{dT}{dp}\right)_c^2 = T_c\frac{C}{A} \tag{15}$$

where A, B, and C denote the critical amplitudes of C_p/V, α_p, and κ_T, respectively. Therefore, knowledge of A and $(dT/dp)_c$ allows for prediction of the size of the anomalies in α_p and κ_T. In a previous work,[8] Ising-like behavior of the isobaric heat capacity per unit volume C_p/V for a $[C_4mim][BF_4]$ + H_2O critical mixture at atmospheric pressure was experimentally encountered with A^+ = 0.017 J K^{-1} cm^{-3}. This value lies within the typical range, whereas, as shown previously, $(dT/dp)_c$ is very small. Consequently, eqns. 15 predict negligible values for B and C. Current experimental methods do not permit us to detect κ_T anomalies, even in the most favorable cases. In contrast, ρ *vs.* T measurements near the critical point can provide reasonably reliable B values.[48] Fig. 10 shows density data for a critical mixture 1 K above the critical temperature, which demonstrate linear behavior within the precision level of measurements.

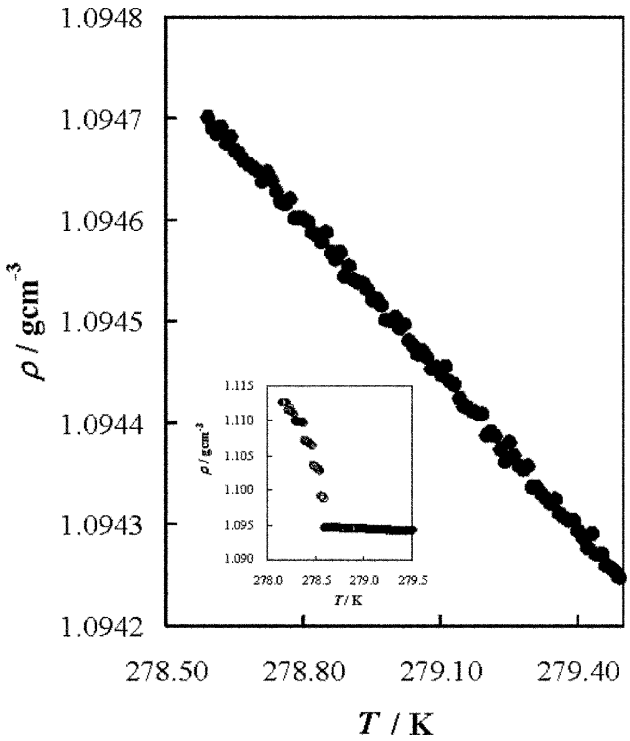

Fig. 10 Experimental run of density (x_{IL} ~ 0.07) *versus* temperature, starting 1 K above the critical temperature, in its approach to the mixture's critical point. The insert shows the extension of the run's temperature interval to a few extra tenths of Kelvin below T_c.

For this critical mixture, α_p also varies in an almost linear fashion from 4.5 × 10^{-4} K^{-1} (279.15 K) to 5.4 × 10^{-4} K^{-1} (298.15 K). From a theoretical perspective, a deviation from $\rho(T)$ linearity was expected in the near-critical temperature region (α_p diverging behavior). However, it is experimentally undetectable at the precision level of our measurements owing to the smallness of the α_p anomaly.

When seen *via* Prigogine and Defay's equation, the small anomalies of α_p and κ_T are ascribed to the quasi-null v^E value at the critical point since the $h^E(w_c,T_c)$ value cannot account for them. It must be remembered that the experimental v^E data of this work confirm this point. Taking into account the small negative $(dT/dp)_c$ value for the ($[C_4mim][BF_4]$ + D_2O) system, a negative α_p anomaly, probably undetectable, is expected. This is inferred from the previously found extrapolated small and negative $v_c^E(w_c,T_c)$ value for this system.

Acknowledgements

Work at the *Universidade Nova de Lisboa* was financially supported by *FC&T*, Portugal, under contract POCTI/EQU/35437/00, and at the University of Vigo at Ourense, Spain, by *Secretaría de Estado de Política Científica y Tecnológica* and *Dirección Xeral de I + D da Xunta de Galicia* (Spain), under contracts #BFM2003–09295 and #PGIDIT-03-DPI-38301-PR, respectively. V. N.-V., Z. P. V. and J. M. S. S. E. are grateful to *FC&T* for doctoral fellowships. We are also grateful to Dr. Susana Barreiros for Karl–Fischer titrations, Dr. Ascensão Reis for anion exchange chromatograms, and Dr José Canongia Lopes for determinations of the chloride content using a specific Cl^- electrode and the standard addition method. We wish to acknowledge Elisabete Pires and Dr. Ana Coelho for providing data from the Mass Spectrometry Service at the ITQB-UNL, Oeiras, Portugal.

References and notes

1 (*a*) K. R. Seddon, *Green Chem.*, 2002, **4**, G25; (*b*) K. R. Seddon, *Nat. Mater.*, 2003, **2**, 363.
2 (*a*) V. Najdanovic-Visak, J. M. S. S. Esperança, L. P. N. Rebelo, M. Nunes da Ponte, H. J. R. Guedes, K. R. Seddon, H. C. de Sousa and J. Szydlowski, *J. Phys. Chem. B*, 2003, **107**, 12797 and references therein (*b*) K. N. Marsh, J. A. Boxall and R. Lichtenthaler, *Fluid Phase Equilib.*, 2004, **219**, 93 and references therein (*c*) J. M. Crosthwaite, S. N. V. K. Aki, E. J. Maginn and J. F. Brennecke, *J. Phys. Chem. B*, 2004, **108**, 5113.
3 J. D. Holbrey and K. R. Seddon, *Clean Prod. Process.*, 1999, **1**, 223.
4 (*a*) R. P. Swatloski, J. D. Holbrey and R. D. Rogers, *Green Chem.*, 2003, **5**, 361; (*b*) A. E. Visser, R. P. Swatloski, W. M. Reichert, S. T. Griffin and R. D. Rogers, *Ind. Eng. Chem. Res.*, 2000, **39**, 3596.
5 V. Najdanovic-Visak, J. M. S. S. Esperança, L. P. N. Rebelo, M. Nunes da Ponte, H. J. R. Guedes, K. R. Seddon and J. Szydlowski, *Phys. Chem. Chem. Phys.*, 2002, **4**, 1701.
6 J. Brennecke, *Chem. Eng. News*, 2001, **79**, 86.
7 L. P. N. Rebelo, V. Najdanovic-Visak, R. Gomes de Azevedo, J. M. S. S. Esperança, M. Nunes da Ponte, H. J. R. Guedes, Z. P. Visak, H. C. de Sousa, J. Szydlowski, J. N. Canongia Lopes and T. C. Cordeiro, Phase Behavior and Thermodynamic Properties of Ionic Liquids, Ionic Liquid Mixtures, and Ionic Liquid Solutions in *Ionic Liquids III: Fundamentals, Progress, Challenges, and Opportunities*, ed. R. Rogers and K. R. Seddon, *ACS Symp. Ser. 857*, American Chemical Society, Washington, DC, 2004, in press.
8 C. A. Cerdeirina, J. Troncoso, C. Paz Ramos, L. Romani, V. Najdanovic-Visak, J. M. S. S. Esperança, M. Nunes da Ponte, H. J. R. Guedes, Z. P. Visak and L. P. N. Rebelo, Criticality of The $[C_4mim][BF_4]$ + Water System in *Ionic Liquids III: Fundamentals, Progress, Challenges, and Opportunities*, ed. R. Rogers and K. R. Seddon, *ACS Symp. Ser. 857*, American Chemical Society, Washington, DC, 2004, in press.
9 (*a*) M. Wagner, O. Stanga and W. Schröer, *Phys. Chem. Chem. Phys.*, 2003, **5**, 3943; (*b*) J. E. L. Dullius, P. A. Z. Suarez, S. Einloft, R. F. de Souza, J. Dupont, J. Fisher and A. D. Cian, *Organometallics*, 1998, **17**, 815.
10 J. L. Anthony, E. J. Maginn and J. F. Brennecke, *J. Phys. Chem. B*, 2001, **105**, 10942.
11 (*a*) R. P. Swatloski, A. E. Visser, W. M. Reichhert, G. A. Broker, L. M. Farina, J. D. Holbrey and R. D. Rogers, *Chem. Commun.*, 2001, 2070; (*b*) R. P. Swatloski, A. E. Visser, W. M. Reichhert, G. A. Broker, L. M. Farina, J. D. Holbrey and R. D. Rogers, *Green Chem.*, 2002, **4**, 81.
12 T. M. Letcher, B. Soko, P. Reddy and N. Deenadayalu, *J. Chem. Eng. Data*, 2003, **48**, 1587.
13 J. D. Holbrey and K. R. Seddon, *J. Chem. Soc. Dalton Trans.*, 1999, 2133.
14 (*a*) J. G. Huddleston, A. E. Visser, W. M. Reichert, H. D. Willauer, G. A. Broker and R. D. Rogers, *Green Chem.*, 2001, **3**, 156; (*b*) Joan Brennecke (private information): C. P. Fredlake, J. M. Crosthwaite, D. G. Hert, S. N. V. K. Aki and J. F. Brennecke, *J. Chem. Eng. Data*, 2004, **49**, 954.
15 K. R. Seddon, A. Stark and M.-J. Torres, in *Clean Solvents: Alternative Media for Chemical Reactions and Processing*, ed. M. Abraham and L. Moens, *ACS Symp. Ser., 819*, American Chemical Society, Washington, DC, 2002, p. 34.
16 K. R. Seddon, A. Stark and M.-J. Torres, *Pure Appl. Chem.*, 2000, **72**, 2275.
17 J. Wang, Y. Tian, Y. Zhao and K. Zhuo, *Green Chem.*, 2003, **5**, 618.

18 (*a*) L. P. N. Rebelo, *Phys. Chem. Chem. Phys.*, 1999, **1**, 4277; (*b*) L. P. N. Rebelo, Z. P. Visak, H. C. de Sousa, J. Szydlowski, R. Gomes de Azevedo, A. M. Ramos, V. Najdanovic-Visak, M. Nunes da Ponte and J. Klein, *Macromolecules*, 2002, **35**, 1887.

19 L. P. N. Rebelo, V. Najdanovic-Visak, Z. P. Visak, M. Nunes da Ponte, J. Troncoso, C. A. Cerdeiriña and L. Romani, *Phys. Chem. Chem. Phys.*, 2002, **4**, 2251.

20 (*a*) Z. P. Visak, L. P. N. Rebelo and J. Szydlowski, *J. Phys. Chem. B*, 2003, **107**, 9837; (*b*) H. C. de Sousa and L. P. N. Rebelo, *J. Polym. Sci. B: Polym. Phys.*, 2000, **38**, 632.

21 (*a*) J. Bigeleisen, *J. Chem. Phys.*, 1961, **34**, 1485; (*b*) G. Jancsó, L. P. N. Rebelo and W. A. Van Hook, *Chem. Rev.*, 1993, **93**, 2645; (*c*) G. Jancsó, L. P. N. Rebelo and W. A. Van Hook, *Chem. Soc. Rev.*, 1994, **23**, 257; (*d*) M. Stern, M. Wolfsberg and W. A. Van Hook, *J. Chem. Phys.*, 1963, **39**, 3179; (*e*) J. Bigeleisen and M. G. Mayer, *J. Chem. Phys.*, 1947, **15**, 261.

22 A. Siporska, J. Szydlowski and L. P. N. Rebelo, *Phys. Chem. Chem. Phys.*, 2003, **5**, 2996.

23 R. B. Griffiths and J. C. Wheeler, *Phys. Rev. A*, 1970, **2**, 1047.

24 H. C. de Sousa and L. P. N. Rebelo, *J. Chem. Thermodyn.*, 2000, **32**, 355.

25 J. Szydlowski, L. P. N. Rebelo and W. A. Van Hook, *Rev. Sci. Instrum.*, 1992, **63**, 1717.

26 R. Gomes de Azevedo, J. Szydlowski, P. F. Pires, J. M. S. S. Esperança, H. J. R. Guedes and L. P. N. Rebelo, *J. Chem. Thermodyn.*, 2004, **36**, 211.

27 J. Troncoso, E. Carballo, C. A. Cerdeiriña, D. González and L. Romaní, *J. Chem. Eng. Data*, 2000, **45**, 594.

28 (*a*) E. Calvet and H. Prat, *Microcalorimetrie. Aplications Physico–Chimiques et Biologiques*, Masson et Cie, Paris, 1956; (*b*) M. I. Paz Andrade, *Les Developpements Recents de la Microcalorimetrie et de la Thermogenese*, ed. du CRNS, Paris, 1967.

29 (*a*) C. A. Cerdeiriña, J. A. Miguez, E. Carballo, C. A. Tovar, E. de la Puente and L. Romaní, *Thermochim. Acta*, 2000, **347**, 37; (*b*) C. A. Cerdeiriña, J. Troncoso, E. Carballo and L. Romaní, *Phys. Rev. E*, 2002, **66**, 31507.

30 (*a*) K. N. Marsh, A. Deev, A. C.-T. Wu, E. Tran and A. Klamt, *Korean J. Chem. Eng.*, 2002, **19**, 357; (*b*) C.-T. Wu, K. N. Marsh, A. V. Deev and J. A. Boxall, *J. Chem. Eng. Data*, 2003, **48**, 486; (*c*) A. Heintz, J. K. Lehmann and C. Wertz, *J. Chem. Eng. Data*, 2003, **48**, 472; (*d*) D. S. H. Wong, J. P. Chen, J. M. Chang and C. H. Chou, *Fluid Phase Equilib.*, 2002, **194–197**, 1089; (*e*) U. Domanska and A. Marciniak, *J. Chem. Eng. Data*, 2003, **48**, 451; (*f*) U. Domanska and A. Marciniak, *J. Phys. Chem. B*, 2004, **108**, 2376.

31 R. R. Singh and W. A. Van Hook, *J. Chem. Phys.*, 1987, **87**, 6097.

32 J. R. Scherer, The vibrational spectroscopy of water, in *Advances in Infrared Raman Spectroscopy*, ed. R. J. H. Clark and R. E. Hester, Heyden, London, 1978, **5**, p. 149.

33 (*a*) G. E. Walrafen, *J. Chem. Phys.*, 1968, **48**, 244; (*b*) G. E. Walrafen, Raman and Infrared Spectral Investigations of Water Structure, in *Water*, ed. F. Franks, Plenum Press, New York, 1972, vol. 1, p. 151.

34 R. A. More O'Ferall, G. W. Koeppl and A. J. Kresge, *J. Am. Chem. Soc.*, 1971, **93**, 1.

35 R. Ludwig, *Angew. Chem., Int. Ed.*, 2001, **40**, 1808.

36 D. M. Carey and G. M. Korenowski, *J. Chem. Phys.*, 1998, **108**, 2669.

37 (*a*) H. Wolff and E. Wolff, *Ber. Bunsenges, Phys. Chem.*, 1969, **71**, 393; (*b*) H. Wolff, in *Physics of Ice*, ed. N. Riehl, B. Bullemer, and H. Engelhardt, Plenum Press, New York, 1969, p. 305.

38 L. Cammarata, S. G. Kazarian, P. A. Salter and T. Welton, *Phys. Chem. Chem. Phys.*, 2001, **3**, 5192.

39 A. Burneau, L. Schriver, L. Manceron and J. P. Perchard, *J. Chim. Phys. Phys. Chim. Biol.*, 1985, **82**, 19.

40 (*a*) J. W. Magee, in *Book of Abstracts 17th IUPAC Conf. Chem. Thermodyn.*, Rostock, Germany, 2002, p. 306; (*b*) J. D. Holbrey, W. M. Reichert, R. G. Ramana and R. D. Rogers, in *Ionic Liquids as Green Solvents, ACS Symp. Ser. 856*, American Chemical Society, Washington, DC, 2003, p. 121.

41 Y. U. Paulechka, G. J. Kabo, A. V. Blokhin, O. A. Vydrov, J. W. Magee and M. Frenkel, *J. Chem. Eng. Data*, 2003, **18**, 457.

42 C. A. Cerdeiriña, D. González-Salgado, L. Romani, M. C. Delgado, L. A. Torres and M. Costas, *J. Chem. Phys.*, 2004, **120**, 6648.

43 I. Cibulka, *Fluid Phase Equilib.*, 1993, **89**, 1.

44 (*a*) T. I. Morrow and E. J. Maginn, *J. Phys. Chem. B*, 2002, **106**, 12807; (*b*) J. K. Shah, J. F. Brennecke and E. J. Maginn, *Green Chem.*, 2002, **4**, 112.

45 C. G. Hanke and R. M. Lynden-Bell, *J. Phys. Chem. B*, 2003, **107**, 10873.

46 (*a*) J. V. Sengers, R. F. Kayser, C. J. Peters and H. J. White Jr, *Equations of State of Fluids and Fluid Mixtures (Chapter 17)*, Elsevier, Amsterdam, 2000; (*b*) K. Gutkowski, M. A. Anisimov and J. V. Sengers, *J. Chem. Phys.*, 2001, **114**, 3133; (*c*) P. C. Albright, Z. Y. Chen and J. V. Sengers, *Phys. Rev. B (Rapid Commun.)*, 1987, **36**, 877; (*d*) M. A. Anisimov, A. A. Povodyrev, V. D. Kulikov and J. V. Sengers, *Phys. Rev. Lett.*, 1995, **75**, 3146; (*e*) Y. B. Melnichenko, M. A. Anisimov, A. A. Povodyrev, G. D. Wignall, J. V. Sengers and W. A. Van Hook, *Phys. Rev. Lett.*, 1997, **79**, 5266.

47 A. Kumar, H. R. Krishnamurthy and E. S. R. Gopal, *Phys. Rep.*, 1983, **98**, 57.

48 J. Troncoso, PhD Thesis, University of Vigo, Spain, 2003.

49 J. Dupont, R. F. de Souza and P. A. Z. Suarez, *Chem. Rev.*, 2002, **102**, 3667.

50 S. G. Kazarian, B. J. Briscoe and T. Welton, *Chem. Commun*, 2000, 2047.

PAPER

Reversible *in situ* acid formation for β-pinene hydrolysis using CO_2 expanded liquid and hot water

Theresa S. Chamblee, Ross R. Weikel, Shane A. Nolen, Charles L. Liotta and Charles A. Eckert*

Schools of Chemical and Biomolecular Engineering and Chemistry and Biochemistry and the Specialty Separations Center, Georgia Institute of Technology, Atlanta, Georgia 30332–0100

Received 13th January 2004, Accepted 5th April 2004
First published as an Advance Article on the web 26th April 2004

Large amounts of waste may result from the neutralization of homogeneous acid catalysts following reaction. Here we present examples of *in situ* acid formation and self-neutralization, thus eliminating waste and offering advantages for product recovery. The formation of α-terpineol (**2**) from β-pinene (**1**) is a reaction of commercial significance that is typically run with strong acid. We demonstrate that the reaction can be performed under more environmentally benign conditions using the *in situ* acid formation capabilities of two different green technologies: CO_2 expanded liquids and reactions in hot water (200 °C). This work presents an example of the application of these methods to a reaction that has commercial significance and adds to our knowledge about the benefits and effects of co-solvents. The relative rates and product distributions achieved in each system are presented and discussed.

Introduction

Development of environmentally benign alternatives for acid catalysts and organic solvents is an active area of investigation because both enjoy widespread use in the production of commercial chemicals. The use of supercritical carbon dioxide ($scCO_2$) as an effective replacement for hazardous organic solvents has been well documented.[1] However, even though $scCO_2$ has been shown to be an effective and environmentally benign alternative, it has some disadvantages. For example, relatively high pressures are required (typically hundreds of bars) and the solvation power, though superior to gases, is relatively low for high molecular weight compounds.[2] The use of gas-expanded liquids (GXL's) at CO_2 pressures of only a few tens of bars can overcome these limitations.

A gas-expanded liquid here refers to the dissolution of CO_2 into an organic liquid solvent. The resulting expanded liquid will have somewhat enhanced transport properties due to the addition of the gas and tunable solvent properties. The use of gas-expanded liquids to improve transport properties and adjust solvent properties has been well demonstrated. For example, gas-expanded liquid mobile phases in liquid chromatography (often called "enhanced fluidity") have achieved faster separations because of enhanced mass transfer and increased optimum linear velocities.[3] The enhanced solvating power of GXL's relative to supercritical fluids has been utilized for extraction of high molecular weight solutes and extractions from difficult matrices such as sediment.[4] GXL's have also been used in antisolvent processes. By increasing or "tuning" the composition of the gas in a GXL mixture, precipitation of individual compounds can be achieved. This property can be used for catalyst recovery, reaction work-up, crystallization or compound purification.[5]

GXL's have also found use as a reaction solvent. Blanchard and Brennecke achieved improved yields for the esterification of acetic acid with ethanol under equilibrium conditions by incorporating 30 mol% CO_2 (333 K, 58.6 bar).[6] Subramaniam and co-workers demonstrated the unique and "green" benefits of CO_2 expanded solvents for performing homogeneous catalytic oxidations.[2,7] By using up to 80% CO_2 in acetonitrile, they achieved greater turnover frequencies due to increased solubility of oxygen and the catalysts in the system. Another unique and potentially useful property of CO_2–aqueous GXL's is the generation of *in situ* acid. When CO_2 and water are combined, carbonic acid is formed (Scheme 1).

The acidity of carbonic acid has been investigated in CO_2–aqueous systems. Towes *et al.* measured pH values of 2.8–2.95 in supercritical CO_2–water systems.[8] A decrease in pH also occurs in CO_2 GXL's. Wen and Olesik determined the pH in CO_2–water–MeOH gas-expanded liquids.[9] They report pH values of around 4.5 in MeOH–water systems containing from 1–20% CO_2. The pH actually decreases to 4.22 at 5.6 mol% CO_2, but increases as more CO_2 is added. This is explained as the result of a competing effect of dielectric constant. Dielectric constant decreases with addition of CO_2 and thus dissociation of the weak acid is inhibited as CO_2 is added above ~6 mol%. West *et al.* reported that the *in situ* formation of acid found in water–CO_2 systems (carbonic acid) extends to alcohol–CO_2 systems as well (Scheme 1).[10] They found enhanced rates for the disappearance of diazodiphenylmethane in an acetone–CO_2–alcohol GXL with methanol and ethanol *vs.* water. The presence of methyl carbonic acid in MeOH–CO_2 mixtures was further demonstrated by Xie *et al.* in studies of acetal formation with cyclohexanone in CO_2–MeOH GXL's (10–40 bar).[11]

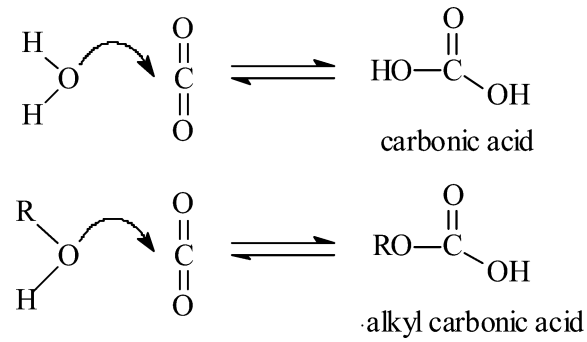

Scheme 1 Formation of carbonic acid and alkyl carbonic acid.

Supercritical water (400 °C, 200 bar) and nearcritical water (275 °C, 60 bar) are other systems that have received attention as environmentally benign alternative solvent/reaction media.[12] Near-critical water is a useful medium for organic reactions due to the physical and chemical changes that occur to water at elevated temperature. For example, both density (1 to 0.7 g cm^{-3}) and dielectric constant (ε = 80 to 20) decrease as water approaches 275 °C. Thus water at nearcritical conditions has solvent properties similar to a polar organic solvent such as acetone. Other properties of the water are affected as well. The hydrogen bond donating ability (Kamlet–Taft α) of water decreases from ~1.2 to ~0.8 as water is heated from sub-ambient to 275 °C.[13] Additionally, the ionization constant of water (K_w) increases by three orders of

DOI: 10.1039/b400393d

magnitude from 10^{-14} at 25 °C to a maximum just below 10^{-11} at 250–275 °C.[14] K_w represents the ability of water to dissociate into H^+ and OH^- ions. Thus, water at elevated temperatures has the ability to perform acid and base catalyzed reactions.[12,15] Hot water at 200 °C (well below the critical point) also has modified solvent properties sufficient enough to make it a useful reaction media.

We present further evidence for the *in situ* acid formation capabilities of both GXL's and hot water (200 °C) with the hydrolysis reaction of β-pinene. This reaction requires the addition of strong acid and later separation of the products from the acid.[16] It can be successfully performed utilizing the *in situ* acid formation capability of a CO_2 expanded MeOH–water solution. We also demonstrate that the *in situ* acid effect of hot water (200 °C) is sufficient to affect pinene hydrolysis. The use of co-solvents with hot water provides some benefits for product selectivity. The self-neutralizing ability of the CO_2 GXL and hot water systems result in complete elimination of acid waste and simplified product recovery. For example, when the pressure is released (GXL) or heat is removed (hot water), the *in situ* acid of the system disappears.

The reaction of pinene to form α-terpineol has been known since the late nineteenth century.[17] Pinene is relatively abundant in nature, with the major source being pine trees (wood pulp, turpentine and other wood products). α- and β-Pinene (**1**) will hydrolyze in aqueous acid to form a tertiary carbocation as shown in Scheme 2.[18] The major product of the reaction is α-terpineol (**2**);

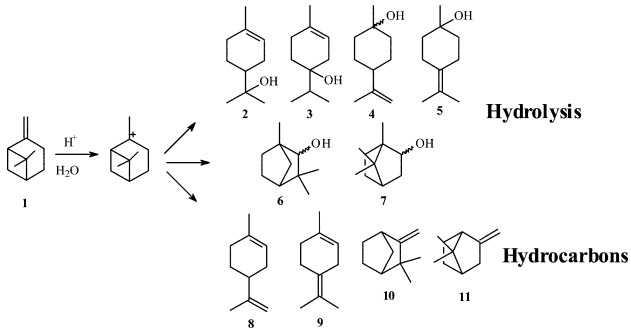

Scheme 2 β-Pinene acid catalyzed hydrolysis.

however, rearrangement of the carbocation also occurs to give isomers such as terpinen-4-ol (**3**) β- and γ-terpineol (**4**, **5**). Together these monocyclic alcohols are known as "terpineol." Smaller amounts of the bicyclic alcohols fenchol (**6**) and borneol (**7**) are formed through Wagner–Meerwein rearrangement. Ethers will also form when the reaction is performed in alcohol. Undesirable side reactions producing hydrocarbons (through elimination and dehydration) are also possible and difficult to eliminate completely.[19] Terpineol and the other alcohols are used in the flavor and fragrance industry in perfumes, toiletries, cleaning solutions and beverages.

Terpineol was one of the first fragrance chemicals to be commercially produced and many methods for its production have been reported.[17] Some improvements in the process have occurred, such as the use of emulsifiers[20] and addition of co-solvents.[21] However, the conventional processes can still involve relatively long reaction times (up to 24 h) and addition of strong acids (*i.e.* 0.05 N or greater H_2SO_4, $HClO_4$, *etc.*). We were able to achieve a similar and in some cases more favorable product distribution for the hydrolysis reaction of β-pinene in both a CO_2–MeOH–water GXL and hot water with co-solvent system compared to the conventional methods.

Results and discussion

CO_2 gas-expanded liquid (GXL)

The most successful CO_2-GXL for hydrolysis of β-pinene from a yield and product distribution standpoint was a 1 : 1 mixture (by volume) of MeOH–water containing ~3 mol% CO_2. This system achieved 71% conversion of β-pinene in 24 h and produced a favorable product distribution. In order to confirm the *in situ* acid formation ability of the GXL, several control reactions were performed with either no CO_2 or no heat. When the reactor was run for 24 h at room temperature (25 °C) with MeOH–water (1 : 1), β-pinene and no CO_2 there was no reaction, as expected. Recovery of unreacted pinene was 98%. At 75 °C, MeOH–water (1 : 1), β-pinene and no CO_2 (24 h) the GC analysis showed only 84% recovery of starting material but still no detection of hydrolysis products.

These results suggest that polymerization or other loss of pinene (such as condensation in the stirring mechanism) occurs at the higher temperature. This phenomenon has been described in the literature for bicyclic unsaturated terpenes. For example, oxidation reactions of 3-carene and α-pinene were conducted at room temperature to avoid polymerization.[22] Pinene is a relatively volatile compound. In fact, it is considered to be a flammable liquid in neat form with a flash point of 35 °C. In addition, it is insoluble in water at room temperature and only slightly soluble in 1 : 1 MeOH–water at room temperature and 75 °C. Therefore, the pinene MeOH–water GXL is not homogeneous.

In summary, the control reactions showed that loss of pinene at elevated temperatures can be expected due to possible polymerization or loss of material in the reactor apparatus. Also, hydrolysis reactions of β-pinene do not occur in MeOH–water mixtures held at 75 °C for 24 h.

When the reactor was charged with CO_2 and run at 25 °C with MeOH–water (1 : 1 volume) and β-pinene, there was still virtually no reaction with 99% of the pinene recovered and less than 1% reaction products detected after 24 h. This demonstrated that some heat is required for the reaction to proceed at a reasonable rate. At 75 °C for 24 h and the same reaction loading, hydrolysis products are detected and the conversion of β-pinene is 71% (± 1% for duplicate experiments) (Table 1). An average mass recovery of 92% (± 4%) was achieved. The product distribution was: 14% hydrocarbons, 58% terpineol, 7% bicyclic alcohols, 19% methyl ether and 2% unknown GC volatile material. This product distribution is quite favorable compared to the literature which

Table 1 Summary of GXL composition and results

Volume/mL (solvent : water volume ratio)	Mole fraction (%)	% Conversion of β-pinene after 24 h	Product distribution (%)		% Mass recovery
			Hydrolysis	Hydrocarbons	
MeOH/water/CO_2	**MeOH/water/CO_2**				
50/0.5/3 (100 : 1)	94/2/4	2.1	59.2	40.8	101.2
37/13/4 (3 : 1)	53/42/4	18.9	68.1	31.9	84.6
25/25/3 (1 : 1)	30/67/3	70.9	84.0	14.0	94.2
13/37/4 (1 : 3)	13/84/3	49.3	84.0	16.0	68.9
0/50/5 (100% H_2O)	0/97/3	47.6	80.9	19.1	65.8
EtOH/water/CO_2	**EtOH/water/CO_2**				
25/25/3 (1 : 1)	23/74/3	48.6	78.2	21.8	62.3
Acetone/water/CO_2	**Acetone/water/CO_2**				
25/25/4 (1 : 1)	19/77/4	10.4	75.6	24.4	94.9

reports product distributions of 30–50% for hydrocarbons, 30–50% for terpineol and 6–20% for bicyclic alcohols.[20,21]

In addition to the favorable product distribution, there are other advantages to the GXL system. The self-neutralization capability of the system (the acid disappears when the CO_2 pressure is released) results in complete elimination of waste salt or acid separation steps. Additionally, product recovery is simplified because upon depressurization, the products are present in a simple aqueous mixture (water and co-solvent) which can be used as is or concentrated as needed.

The fastest conversion of pinene occurred at a 1 : 1 volume ratio of methanol to water. A range of other mixtures was studied from almost pure methanol to pure water (Table 1). As the water content increased the pinene conversion decreased from 70% to less than 50%. This was expected since carbonic acid (pK_a = 6.37[23]) is a weaker acid than methyl carbonic acid (pK_a = 5.61[24]). The product distribution was similar except for progressively less ether product being formed as the alcohol co-solvent was decreased. An increase in water was also accompanied by lower recovery of starting material from the reactor. Since pinene is virtually insoluble in water, recovery from the heated, pressurized reaction vessel was difficult when the water content was high. Therefore, the calculated conversion of pinene was at most 50% and likely lower due to expected pinene loss.

Interestingly, as the methanol to water ratio was increased, the conversion dropped precipitously to 2% for a 100 : 1 methanol to water ratio. This is likely due to the decrease in dielectric constant of the mixed solvent. Previous studies have shown an inverse linear relationship between pK_a of a weak acid and dielectric constant of various water–organic mixed solvents.[25] The lower the dielectric constant, the more difficult it is for the acidic proton to dissociate from the acid. Thus, as the mixed solvent becomes mostly methanol (ε = 32), the acid strength drops, which in turn slows conversion of pinene. When the mixed solvent is mostly water (ε = 80), one might expect increased acid strength. However, the acid is changing from methyl carbonic to carbonic acid, a weaker acid. The decrease in dielectric constant is competing with acid strength which explains a maximum conversion with varying solvent ratio. Both acetone and ethanol were also tested with water as co-solvents for the reaction. Since the dielectric constants of acetone (ε = 21) and ethanol (ε = 24) are both below that of methanol, one would expect lower conversion for these GXLs than methanol GXLs at any solvent ratio, which was observed. Ethanol, with only a slightly higher dielectric constant than acetone, gave much higher conversion (49%) *versus* acetone (10%), which also agrees with the concept of alkylcarbonic acid playing an important role in GXL catalysis.

Hot water (200 °C)

The reaction of β-pinene in hot water (200 °C) is relatively fast with 90% conversion of β-pinene achieved in 20 min. However, the yield of terpineol is small (~10%) *vs.* the formation of hydrocarbons, which are the major products formed under these conditions. Reactions run at 250 °C showed even greater hydrocarbon formation. The elevated heat and apparent acid strength of the 100% water system favors dehydration/elimination. Sampling of the reaction over time indicates that some pinene converts directly to hydrocarbon and some hydrolyzes to form terpineol. The α-terpineol, however is subsequently dehydrated to produce hydrocarbons upon continued exposure to the heat and acidity of the hot water system.

The addition of co-solvents slows the reaction and resulted in improved hydrolysis product recovery (see Table 2). For example, with 50/50 isopropanol/water (Table 2), 80% conversion of β-pinene was achieved after 2.2 h and the distribution of hydrocarbons/hydrolysis products is ~1 : 1 with ~40% overall yield of each. In fact, by sampling the reactions over several time intervals it was possible to see that a ratio of ~1 : 1 is achieved with each of the co-solvents at the 80% pinene conversion point. Allowing the reaction to continue to 90% conversion resulted in dehydration of terpineol and an increase of hydrocarbon products as shown in Table 2. Therefore, the maximum yield of terpineol was 40%. Greater yields could potentially be achieved if it was possible to remove the alcohol product from the system as it is formed.

One explanation for the relative rate results is the simple effect of less water (the source of the acid catalyst) being present in the co-solvent systems, therefore, less acid strength (or higher pH). While the results in the EtOH–water systems agree with this, the other co-solvent mixtures do not (Table 2). For example, the acetone, THF and IPA systems each contain the same level of water on a molar basis, yet the time to achieve 90% conversion of pinene ranges from 30 min to 150 min. Again, it is thought that several competing solvent properties are involved which are apparently affecting the acid strength and reaction intermediate and product stability in the system.

Several control reactions were analyzed to confirm the *in situ* acid effect of the hot water. β-Pinene plus (1) 100% hexane; (2) 100% acetone and (3) 100% ethanol, were heated in sealed reactor tubes at 200 °C for 2 h. All the pinene was recovered unreacted with hexane and ethanol. Ten percent loss of pinene was observed with 100% acetone. Analysis of the GC/MS plot for this reaction showed a late eluting peak which is tentatively identified as the reaction product of β-pinene with acetone. Only trace amounts of hydrolysis product were found. These results confirm that the water is required to achieve the *in situ* acid effect; and the protic solvent ethanol does not contribute appreciably to the *in situ* acid effect.

Although the product distribution for the hot water reaction is not as favorable as the GXL systems with respect to hydrocarbon production, the results are still comparable to conventional acid systems.[20,21] The hot water system gives faster reaction times compared to the GXL's and also provides the benefits of simplified product recovery over conventional systems due to elimination of acid separation steps. This system further offers a greater variety of co-solvent choices that show promising results.

Conclusion

CO_2 gas-expanded liquids and hot water (200 °C) are demonstrated as green substitutes for strong acid in the hydrolysis of β-pinene. Relatively mild CO_2 pressures (well below the critical pressure) can be used to create a GXL and provide the *in situ* catalysis. Additionally the ratio of desired hydrolysis products to hydrocarbon products was improved in the GXL over most conventional

Table 2 Hot water/co-solvent compositions

Volume ratios	mmol water	Time for 90% conversion/min	Dielectric constant of co-solvent	Product distribution (%)	
				Hydrolysis	Hydrocarbons
100 water	89	20	80	16	84
75/25 water/EtOH	67	20	24	24	76
50/50 water/acetone	44	30	21	38	62
50/50 water/EtOH	44	40	24	43	57
50/50 water/THF	44	90	7	44	56
50/50 water/isopropanol	44	150	18	49	51

acid catalyzed systems. Hot water, well below the critical point at 200 °C, is also a successful reaction media for β-pinene hydrolysis. The reaction rate and product distribution can be tuned to achieve greater hydrolysis over dehydration by the use of various organic co-solvents. Both reaction systems require no added acid and allow for simple neutralization by either depressurization and/or cooling, thus simplifying product recovery and waste disposal.

Experimental

Materials

(1S)-(−)-β-Pinene (99% by GC) from Aldrich Chemical Company was used. HPLC grade solvents were obtained from Aldrich: water; methanol (anhydrous 99.8%); ethanol (reagent grade, anhydrous); acetone (Aldrich, 99.9+%); tetrahydrofuran; isopropanol. Methylene chloride was from Fisher. Tetradecane internal standard (99% by GC) was obtained from Fluka. Carbon dioxide (SFC/SFE grade) was obtained from AirGas. All materials were used as purchased.

CO_2 gas-expanded liquids

The reactions were performed in a Model 4560, inconel, 100 mL Parr reactor fitted with an overhead magnetic stirrer controlled by a Model 4842 stirrer and heater controller. The temperature of the reactor was maintained within 1 °C of the setpoint and stirring was maintained at 725 rpm. The CO_2 was added to the reactor using an Isco 500 D syringe pump with a Series D controller. The pressure of the Parr reactor was monitored using an Ashcroft pressure gauge. The pressure of the reactor was typically 200–300 psi (14–21 bar). At the end of the reaction period the reactor was allowed to cool to room temperature (~1–1.5 h) and the pressure was released into a 250 mL degassing flask fitted with a glass frit filter and ~200 mL of acetone. The degassing process continued for ~5 min.

Reaction work-up consisted of extracting the Parr contents with methylene chloride after addition of internal standard and subsequent concentration of the organic layer using a Kuderna–Danish evaporator. The acetone degassing solution was also concentrated and analyzed separately. The degas solution typically contained 5% or less of the starting material. This material was included in the mass balance. The concentrated samples were analyzed by GC-FID and GC-MSD.

Phase equilibria studies were conducted with a 300 mL Parr vessel equipped with an observation window. The same temperature and stirring controller as previously described were used. The reaction mixture (total volume = 100 mL in this case) and CO_2 were added to the Parr as previously described and the phase behavior of the system was observed at the window as the reactor temperature was increased. All GXL solvent mixtures used in this study were found to be monophasic at reaction conditions. Once pinene was added, the mixture was biphasic since pinene was not fully soluble at these concentrations.

Hot water, 200 °C

Reactions were conducted in 3 mL sealed titanium reactor tubes. Titanium was used due to its low level of impurities which can catalyze undesirable reactions and its resistance to corrosion *vs.* other metals. The reactors were heated using a thermostated aluminium block with temperature control of ±1 °C. See reference 15 for a diagram of the reaction set-up. The temperature block was capable of heating to the reaction setpoint (200 °C) in 5 min or less. Rapid cooling was achieved using a cold water bath. Solvents and β-pinene were added to the reactor tubes using an Eppendorf pipette, 1000 μl. The concentration of pinene in the reactors was ~2% (0.16 M). Mass balance recovery was excellent at 95% or greater for all systems tried. Experiments performed with a windowed cell indicate that the hot water–EtOH–pinene solutions are homogeneous at the reaction conditions. Hot water–pinene reactions were not completely homogeneous at reaction conditions. Reaction work-up consisted of transferring the contents of the reactor tube after cooling with a glass pipette to a 10 mL volumetric flask. Tetradecane was added as an internal standard. The reactor tube was rinsed with acetone and the rinse solvent was added to the volumetric flask up to 10 mL. Samples were analyzed by GC-FID and GC-MS.

GC and GC-MS

An HP 5890 GC equipped with a 6890 series autosampler was used for GC-FID analysis with a DB-5 capillary column. An Agilent GC Chemstation was used for peak integration and data analysis. Response factors were calculated for all of the major compounds based on the internal standard tetradecane and the results were reported as absolute concentration values (mg mL^{-1}). These were converted to percent of reaction products. GC-MS analysis was conducted on an HP 5972 MSD coupled with an HP 5890 GC, using a DB-5 capillary column. Peak identifications were made using an in house library, the Wiley 6th edition MS library and retention time data found in the literature.[26]

Acknowledgements

The authors thank the National Science Foundation Grant #CTS-0328019 and the J. Erskine Love, Jr. Institute Chair for their financial support. The authors also thank Kyle Ross and Kristen Kitagawa for their laboratory assistance.

References

1 C. A. Eckert, B. L. Knutson and P. G. Debenedietti, *Nature*, 1996, **383**, 313–318; C. A. Eckert and K. Chandler, *J. Supercrit. Fluids*, 1998, **13**, 187–195.
2 G. Musie, M. Wei, B. Subramaniam and D. H. Busch, *Coord. Chem. Rev.*, 2001, **219–221**, 789–820.
3 Y. Ciu and S. V. Olesik, *Anal. Chem*, 1991, **63**, 1812–1819; S. T. Lee and S. V. Olesik, *Anal. Chem.*, 1994, **66**, 4498–4506; S. T. Lee and S. V. Olesik, *J. Chromatogr., A*, 1995, **707**, 217–224; H. Yuan, I. Souvignet and S. V. Olesik, *J. Chromtogr. Sci*, 1997, **35**, 409–416; H. Yuan and S. V. Olesik, *Anal. Chem.*, 1998, **70**, 1595–1603.
4 H. Yuan and S. V. Olesik, *J. Chromatogr.*, 1997, **764**, 265–277; M. Monserrate and S. V. Olesik, *J. Chromatogr. Sci.*, 1997, **35**, 82–90; T. S. Reighard and S. V. Olesik, *Anal. Chem.*, 1996, **68**, 3612–3621.
5 C. J. Chang and A. D. Randolph, *AIChE J.*, 1990, **36**(6), 939–942.; C. A. Eckert, D. Bush, J. S. Brown and C. L. Liotta, *Ind. Eng. Chem. Res.*, 2000, **39**, 4615–4621; C. Lin, G. Muhrer, M. Mazzotti and B. Subramaniam, *Ind. Eng. Chem. Res.*, 2003, **42**(10), 2171–2182.
6 L. A. Blanchard and J. F. Brennecke, *Green Chem.*, 2001, **3**, 17–19.
7 B. Subramaniam, C. J. Lyon and V. Aurunajatesar, *Appl. Catal., B.*, 2002, **37**, 279–292; M. Wei, G. T. Ghezai, D. H. Buschand and B. Subramaniam, *J. Am. Chem., Soc.*, 2002, **124**(11), 2513.
8 K. L. Towes, R. Shroll, C. M. Wai and N. G. Smart, *Anal. Chem.*, 1995, **67**, 4040–4043.
9 D. Wen and S. V. Olesik, *Anal. Chem.*, 2000, **72**, 475–480.
10 K. N. West, C. Wheeler, J. P. McCarney, K. N. Griffith, D. Bush, C. L. Liotta and C. A. Eckert, *J. Phys. Chem. A.*, 2001, **105**, 3947–3948.
11 X. Xie, C. Liotta and C.A. Eckert, submitted.
12 A. R. Katritzky, S. M. Allin and M. Siskin, *Acc. Chem. Res.*, 1996, **29**, 399–406; P. E. Savage, *Chem. Rev.*, 1999, **99**, 603–621; M. Siskin and A. R. Katritzky, *Chem. Rev.*, 2001, **101**, 825–835; A. R. Katritzky, D. A. Nichols, M. Siskin, R. Murugan and M. Balasubramanian, *Chem. Rev.*, 2001, **101**, 837–892.
13 J. Lu, J. S. Brown, C. L. Liotta and C. A. Eckert, *Chem. Commun.*, 2001, 665–666; Y. Marcus, *Chem. Soc. Rev.*, 1993, **22**, 409–416.
14 W. L. Marshall and E. U. Franck, *J. Phys. Chem. Ref. Data*, 1981, **10**, 295–304.
15 K. Chandler, F. Deng, A. K. Dillow, C. L. Liotta and C. A. Eckert, *Ind. Eng. Chem. Res.*, 1997, **36**, 5175–5179; C. A. Eckert and K. Chandler, *J. Supercrit. Fluids*, 1998, **13**, 187–195; K. Chandler, C. L. Liotta and C. A. Eckert, *AIChE J.*, 1998, **44**, 2080–2087; H. P. Lesutis, R. Gläser, C. L. Liotta and C. A. Eckert, *Chem. Commun.*, 1999, 2063–2064; C. A. Eckert, C. L. Liotta and J. S. Brown, *Chem. Ind.*, 2000, **3**, 94–97; J. S. Brown, R. Gläser, C. L. Liotta and C. A. Eckert, *Chem. Commun.*, 2000, 1295–1296; C. A. Eckert, D. Bush, J. S. Brown and C. L. Liotta, *Ind. Eng. Chem. Res.*, 2000, **39**, 4615–4621; H. P. Lesutis, R. Gläser, K. Griffith, C. L. Liotta and C. A. Eckert, *Ind. Eng. Chem. Res.*, 2001, **40**, 6063–6067; S. A. Nolen, C. L. Liotta, C. A. Eckert and R. Glaser, *Green Chem.*, 2003, **5**, 663–669.

16 W. C. Mculy, (Dupont), US patent 2,088,030, Feb. 1, 1936; A. Weissenborn, US Patent 2,2295,705, August 24, 1938; R. Herrilnger, (American Cyanamid), US Patent 2,898,380, Aug. 4, 1959.
17 P. Z. Bedoukian, "Terpineol," in *Perfumery and Flavoring Synthetics*, Elsevier Publishing Company, Amsterdam, 1967, pp. 328–343.
18 B. C. Clark, Jr. and T. S. Chamblee, "Acid-Catalyzed Reactions of Citrus Oils and Other Terpene Containing Flavors," in *Off-Flavors in Foods and Beverages*, ed. G. Charalambous, Elsevier Science Publishers B.V., Amsterdam, 1992, pp. 229–285 and references therein.
19 G. W. Gladden and G. Watson, *Perfum. Essent. Oil Rec.*, 1964, 793–803.
20 M. Charwath (Krems-Chemie, G.m.b.H.) Eur. Pat. Appl. EP 35, 703 (Cl. C07C33/14), 16 Sep. 1981, AT Appl. 80/1309, 10 March 1980.
21 C. M. Williams and D. Whitaker, *J. Chem. Soc. B*, 1971, 668–672; G. Valkanas and N. Iconomou, *Helv. Chim. Acta*, 1963, **46**, 1089–1096; H. Indyk and D. Whittaker, *Chem. Soc. Perkin Trans. 2*, 1974, **3**, 313–317; H. J. Chaves das Neves and J. S. Marques Vital, *Rev. Port. Quim.*, 1984, **26**(3–4), 183–196.
22 G. Rothenburg, Y. Yatziv and Y. Sarson, *Tetrahedron*, 1998, **54**, 593–598.
23 *CRC Handbook of Chemistry and Physics*, 52nd edn., The Chemical Rubber Company, Cleveland, OH, 1971.
24 G. Gattow and W. Behrendt, *Angew. Chem.*, 1972, **84**, 549–550.
25 Y. Xue and S. J. Traina, *Environ. Sci. Technol.*, 1996, **30**, 3177–3183; U. Muinasmaa, C. Rafols, E. Bosch and M. Roses, *Anal. Chim. Acta*, 1997, **340**, 133–141; K. Sarmini and E. Kenndler, *J. Biochem. Biophys. Methods*, 1999, **38**, 123–137.
26 R. P. Adams, *Identification of Essential Oil Components by Gas Chromatography/Mass Spectroscopy*, Allured Publishing, Carol Stream, IL, 1995.

PAPER

www.rsc.org/greenchem

Autoxidation of 2,6-di-*tert*-butylphenol with cobalt Schiff base catalysts by oxygen in CO_2-expanded liquids

Ming Wei,[a] Ghezai T. Musie,[b] Daryle H. Busch*[bc] and Bala Subramaniam[ac]

[a] *Department of Chemical and Petroleum Engineering, The University of Kansas, Lawrence, KS 66045-2223, USA*

[b] *Department of Chemistry, The University of Kansas, Lawrence, KS 66045-2223, USA*

[c] *Center for Environmentally Beneficial Catalysis, The University of Kansas, Lawrence, KS, USA*

Received 1st September 2003, Accepted 19th January 2004
First published as an Advance Article on the web 4th February 2004

CO_2-expanded acetonitrile and methylene chloride have been used in this first detailed study of catalytic O_2 oxidations in these remarkably effective reaction media. The autoxidation of 2,6-di-*tert*-butylphenol (DTBP) with the cobalt Schiff-base (Co(salen*) in these so-called CO_2-expanded liquids (CXLs) has been extensively studied using precisely controlled and monitored batch reactions. The dependence of conversion, selectivity and turn-over-frequency on various reaction parameters, including temperature, [O_2], [catalyst], and solvent composition has been evaluated. The rates of O_2-oxidation in CXLs are typically 1–2 orders of magnitude greater than those obtained with either the neat organic solvent or supercritical CO_2 as reaction media. In keeping with the proposed mechanism, the dependence of both the selectivity and conversion on O_2 concentration and catalyst concentration indicates that the O_2 adduct, and not free O_2, serves as oxidant in two critical steps in these systems. The increase in conversion with increasing temperature supports formation of the phenoxy radical as the rate determining step. In contrast, the temperature independence of selectivity is as expected for two competing radical coupling reactions. The balance between O_2 solubility and mixed-solvent dielectric constant determines some of the benefits of the CXLs. Because of the greatly increased solubility of O_2 in CXLs, the conversion in those media is substantially greater than that in either *sc*CO_2 or the neat organic solvent. However, conversion eventually decreases with increasing CO_2 content of the solvent because of the decreasing dielectric constant of the medium. The solubilities of O_2 and Co(salen*) have been determined in CXLs based on methylene chloride.

Introduction

This work exploits the beneficial chemical and physical properties of mixed solvents containing liquid CO_2 (abbreviated CXLs) to perform homogeneous catalytic oxidations. CXLs are produced by condensing relatively large amounts of sub-critical CO_2 into fixed amounts of an organic solvent. Each CO_2-expanded solvent may, in principle, generate a continuum of media ranging from the neat organic solvent to neat CO_2. Thus, the solvent properties may be varied to accommodate contrasting solubilities simultaneously, like those of permanent gases (O_2, H_2 and CO) and homogeneous catalysts based on metallic elements. A large amount of CO_2 favors oxygen solubility and polar organic solvents favor metal catalyst solubility. CXLs have been exploited for performing homogenous catalysis, including hydrogenations,[1a–c] oxidations,[1d–f] and hydroformylations.[1g] In the referenced applications, dense phase CO_2 is partnered with a variety of solvents such as methanol,[1a] acetonitrile,[1d,e] and ionic liquids.[1c,f,g]

Reactions in CXLs benefit both in terms of improved behavior of the fundamental chemical processes and potential benefits to the environment as shown elsewhere.[1d,e]

Reaction advantages of CXLs:

• higher oxygen miscibility (as much as two orders of magnitude) compared to organic solvents

• adequate solubility of transition metal catalysts without such ligand modifications as the use of environmentally deleterious fluorination

• enhanced turnover frequencies

• comparable or better product selectivities than in neat organic solvent or *sc*CO_2

• facile catalyst separation following the reaction cycle, by adding more CO_2 and adjusting the temperature

Environmental and economic advantages:

• substantial (up to ~80 vol%) replacement of organic solvents with dense-phase CO_2

• milder process pressure (tens of bars) compared to *sc*CO_2 (hundreds of bars)

• operation with CO_2-based media in the near-critical region (where the specific heat increases with isothermal pressure increases) lessens the risk of reaction runaway and explosions[2]

• enhanced reaction rates and low process pressures yield process economics that are favorable over those for *sc*CO_2

As reviewed elsewhere,[1d,3] homogeneous "green" oxidation in *sc*CO_2 as the solvent, has been the focus of many investigations. Carbon dioxide is non-toxic, not subject to oxidation, non-flammable, inexpensive, recyclable and has a relatively low critical temperature (31.1 °C) and moderate critical pressure (73.8 bar). The application of CO_2 in catalytic chemistry and reaction engineering satisfies several of the green chemistry and engineering principles.[4] For instance, dense phases of CO_2 are considered benign alternatives to traditional organic solvents. Further, since traditional organic solvents will always emit their vapors, replacement with CO_2 represents pollution prevention. Further, the toxicity of CO_2 is lower than those of many organic solvents and CO_2 is abundantly available.

During the last decade, many of the advantages of *sc*CO_2 have been demonstrated for chemical reactions on a laboratory scale. While it is recognized that performing catalytic reactions in *sc*CO_2 offers maximum environmental benefit, there exist major barriers impeding the application of CO_2 in industrial chemical processes. In many cases, *sc*CO_2-based homogeneous catalytic reactions are limited by inadequate solubilities of preferred homogeneous catalysts. In addition, CO_2 is non-polar with a non-tunable dielectric constant, which usually results in lower reaction rates compared to those attained with conventional organic solvents. Furthermore, high process pressures (hundreds of bars) are required in most reported applications. This combination of high pressures and low reaction rates clearly does not favor process economics.

We report here a systematic study of homogeneous catalytic oxidation of 2,6-di-*tert*-butylphenol (DTBP) by molecular oxygen

DOI: 10.1039/b310523g

in CO_2-expanded solvent media, CXLs, using cobalt(II) Schiff base complexes as catalysts. This reaction has been studied well in both heterogeneous[5] and homogeneous[6] systems, as well as in *sc*CO_2.[7] DTBP is converted to a mixture of 2,6-di-*tert*-butyl-1,4-benzoquinone (DTBQ) and the related product of radical coupling, 3,5,3′,5′-tetra-*tert*-butyl-4,4′-diphenoquinone (TTDBQ).

Scheme 1 shows the mechanism proposed for this reaction in most media. The first step is rate determining and involves

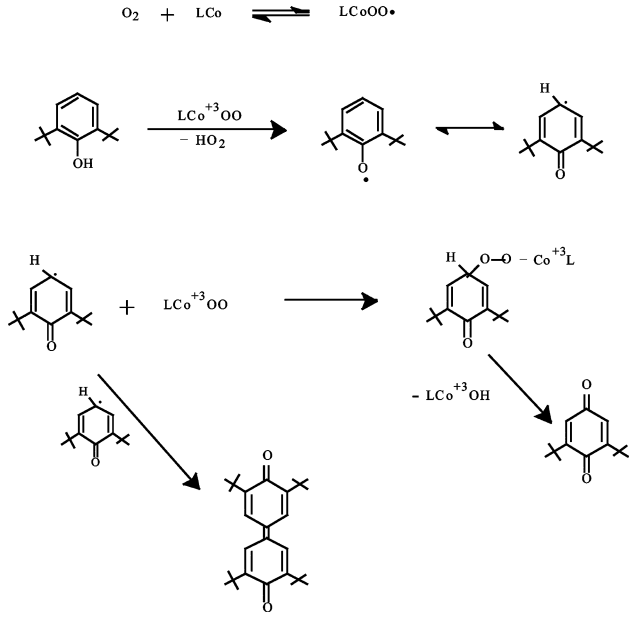

Scheme 1 The broadly accepted mechanism for the oxidation of 2,6-di-*tert*-butyl phenol by Schiff base cobalt catalysts: Co(salen*) and Co(salen).

conversion of phenol to the phenoxy radical by the oxygen adduct of the catalyst [Co(salen*)O_2]. Subsequently, two parallel reactions compete: capture of the phenoxy radical by a second mole of the oxygen adduct leads to DTBQ, the desired product; the coupling of two phenoxy radicals ultimately yields TTDBQ. In the work that follows, we specifically address the following questions:

1. How do the efficacies of the reactions in CXLs compare with those in *sc*CO_2 or neat organic solvent?

2. How do the operating variables (pressure, temperature, and extent of solvent replacement by CO_2) affect the turnover frequency and product selectivity?

3. How does the mechanism of the O_2 oxidation reaction change in going from *sc*CO_2 or neat organic solvent to CXLs?

4. How does the replacement of an organic solvent by CXLs affect catalyst and oxygen solubilities?

Methylene chloride and acetonitrile are employed as solvents that are expanded by carbon dioxide to provide the new reaction media, CXLs. Our previous studies of this reaction system in CO_2-expanded acetonitrile[1e] and in *sc*CO_2[7] provide the bases for comparison.

Experimental section

Apparatus

The experimental units and procedures for measuring the solubilities of oxygen and of the catalyst complexes in CO_2-expanded solvents, including safety features and analytical methods for measuring O_2 concentrations, are described in detail elsewhere.[1d,e,7] The catalytic oxidation studies, including conversion and selectivity measurements, were performed in specially constructed batch view cells as described elsewhere.[7]

Materials

HPLC grade CH_3CN and CH_2Cl_2, and the catalysts, [{*N*,*N*′-Bis(3,5-di-*tert*-butylsalicylidene)1,2-cyclohexanediaminato-(2−)}cobalt(II)], {*i.e.*, Co(salen*)}, and, [{*N*,*N*′-Bis(salicylidene)1,2-cyclohexanediaminato(2−)}cobalt(II)], {*i.e.*, Co(salen)}, were purchased from Aldrich Chemical Co., Inc., and used without further treatment. The substrate 2,6-di-*tert*-butylphenol (DTBP) was purchased from Aldrich Chemical Co., Inc., and recrystallized from hexane. Methylimidazole and toluene were purchased from Fisher Scientific and used as received. Coolant grade liquid CO_2, in cylinders with dip tubes, and cylinders of ultra high purity oxygen were purchased from Air Products and Chemicals, Inc.

Results and discussion

Oxidation of substituted phenols by transition metal complexes

Previous studies in these laboratories provided strong support for the mechanism given in Scheme 1 for the O_2 oxidation of DTBP in *sc*CO_2 as the solvent and using Co(salen*) for the catalyst.[7] The same reaction has now been studied in two families of CXLs using precisely controlled and monitored batch reactions. The influences of reaction parameters (oxygen concentration, catalyst concentration, reaction temperature, and expansion ratio) on DTBP conversion and DTBQ selectivity during the oxidation reaction were determined. The fixed values of the operating parameters are as follows: catalyst concentration, 0.416 mM; reaction temperature, 60 °C; reaction time, 2 h; catalyst : substrate : O_2 mole ratio, 1 : 80 : 800; expansion fold (V/V_0),2; mole ratio of methyl imidazole to catalyst 1.28; solvent ,CH_3CN; effective reaction volume, 10 mL. In a given set of experiments, any of these parameters may be chosen as a reaction variable.

Fig. 1 shows that the DTBP conversion and DTBQ selectivity remain virtually constant when the [O_2] increases from 33.3 mM to

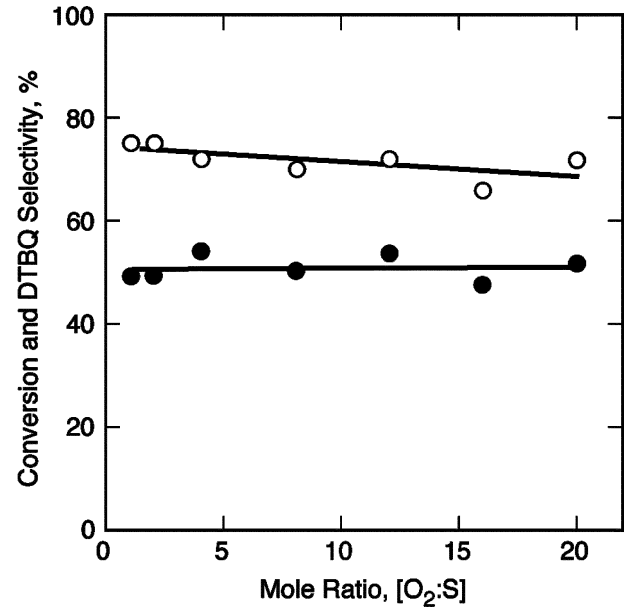

Fig. 1 Effect of O_2 concentration on DTBP (●) conversion and DTBQ selectivity (○) in CO_2-expanded CH_3CN. Reaction conditions: catalyst [Co(salen*)] concentration = 0.416 mM; reaction time = 2 h; reaction temperature = 60 °C; DTBP: catalyst mole ratio = 1:80; expansion ratio (V/V_0) = 2; volume of methyl imidazole = 2 μL.

667 mM. A different behavior is observed in *sc*CO_2[7] where the DTBP conversion and DTBQ selectivity increase linearly with the oxygen concentration for [O_2]/[DTBP] ratios less than 100, and only reach saturation for greater values of this ratio. The obvious conclusion in both cases is that free oxygen does not contribute to the reactions that determine the conversion and selectivity of these systems. It follows that the cobalt oxygen complex, [Co(salen*)O_2], and not O_2, is the reagent responsible for the initial oxidation, producing the phenoxy radical, and that the only pathway leading to DTBQ formation is the radical coupling

between the phenoxy radical and [Co(salen*)O_2].[7] Because O_2 is totally miscible in *sc*CO_2, the observed saturation behavior in CXLs at much lower [O_2]/[DTBP] ratios cannot be attributed to O_2 solubility considerations. However, it seems plausible that the higher dielectric constant in this CXL (due to the presence of acetonitrile) may stabilize [Co(salen*)O_2] at lower O_2 concentrations compared to *sc*CO_2, which has a very low dielectric constant. The binding of O_2 to cobalt(II) formally constitutes a redox process producing cobalt(III) and the bound superoxide ion, a highly polar grouping.[8] Because it is the oxygen adduct, [Co(salen*)O_2], that oxidizes DTBP to the phenoxy radical and, subsequently, oxidizes that radical to DTBQ, its abundance determines two of the three important reaction rates. (The third reaction is radical–radical coupling between phenoxy radicals.) Therefore, the presence of excess free O_2 is not expected to significantly influence conversion rates and product distribution.

In Fig. 2, the DTBP conversion and DTBQ selectivity are shown as functions of reaction temperature in fixed-time, batch studies.

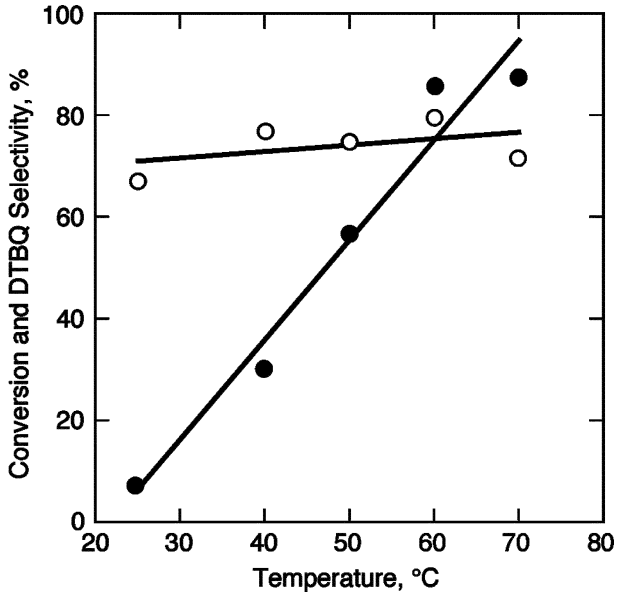

Fig. 2 Effect of temperature on DTBP conversion (●) and DTBQ selectivity (○)in CO_2-expanded CH_3CN. Reaction conditions: catalyst [Co(salen*)] concentration = 0.25 mg mL^{-1}; reaction time = 2 h; catalyst : substrate : O_2 mole ratio = 1 : 80 : 800; expansion fold (V/V_0) = 2; volume of methyl imidizole = 2 μL.

The DTBP conversion increased monotonically from 10% to approximately 90% when the temperature was increased from 25 °C to 70 °C, while the DTBQ selectivity remained virtually constant at ~75%. The constant DTBQ selectivity with increasing temperature is similar to that reported previously for this reaction system in *sc*CO_2 medium. The mechanism commonly attributed to this reaction in other media[6] (Scheme 1) is entirely consistent with the behavior just described for the reaction conducted in a CXL. The pathways to both products begin with the formation of a common radical, the phenoxy radical, which appears to be the rate determining event. Selectivity is determined by competition between oxygenation of the first-formed radical and its dimerization. Because the activation energy is very low for radical reactions, one would not expect the product distribution to change with temperature. Thus, the mechanism given in Scheme 1 is appropriate for this reaction in both *sc*CO_2 and CXLs.

The influence of catalyst concentration on the DTBP conversion and DTBQ selectivity is shown in Fig. 3. As expected, the DTBP conversion increases with increasing catalyst concentration and reaches its highest value of 85% at a catalyst concentration of 1.3 mM, above which the catalyst precipitates and the reaction no longer occurs in a homogeneous phase. Similarly, the DTBQ selectivity increases with increasing catalyst concentration. In both

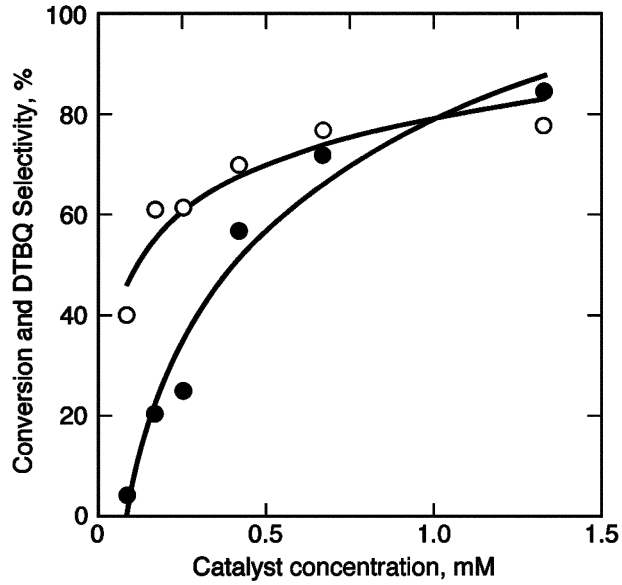

Fig. 3 Effect of catalyst [Co(salen*)] concentration on DTBP conversion (●) and DTBQ selectivity (○) in CO_2-expanded CH_3CN. Reaction conditions: reaction time = 2 h; reaction temperature = 60 °C; substrate : O_2 mole ratio = 1 : 10; expansion ratio (V/V_0) = 2; volume of methyl imidizole = 2 μL.

cases, the concentration dependence resembles that commonly observed for saturation processes. This behavior is different than the reported observation for the same reaction system in *sc*CO_2, where the selectivity was independent of catalyst concentration. This may be attributed to the lower concentration of O_2 in CXLs, compared to *sc*CO_2, in which the oxygen is completely miscible with the solvent. Under the conditions of the previously reported experiments in *sc*CO_2, the catalyst is converted entirely to the oxygen adduct at all catalyst concentrations studied; *i.e.*, the adduct formation equilibrium is always saturated. In contrast, because of the lower O_2 concentration in CXLs, the concentration of the oxygen complex, [Co(salen*)O_2], increases with catalyst concentration. Because the product distribution is determined by competition between the oxidation of the phenoxy radical and its dimerization, higher concentrations of [Co(salen*)O_2] favor the formation of DTBQ.

The O_2 concentration, the transport properties (diffusivity and viscosity) and the dielectric constant may be tuned in CXLs by simply manipulating the CO_2 fraction. With increasing CO_2 content, the O_2 solubility increases.[1e] We speculate that the mobility of the radicals increases with CO_2 content in CXLs while the dielectric constant decreases, all relative to the neat organic solvent. Decreased dielectric constant may decrease the stability of the O_2 adduct, [Co(salen*)O_2], and increased mobility (and collisions) may cause more rapid coupling between pairs of phenoxy radicals. Thus several complicating factors add complexity to conversion and product selectivity. Fig. 4 depicts the DTBP conversion and DTBQ selectivity in CXLs at various levels of expansion. The DTBP conversion decreases with increasing levels of expansion. The reduced dielectric constant at greater levels of expansion with CO_2 hinders DTBP conversion because of the highly polar transition state for the rate determining step. The opposite trend in the case of DTBQ selectivity, which increases moderately with increasing levels of expansion, can be attributed to two factors. The increased CO_2 content increases the oxygen concentration in the liquid phase, thereby converting more of the catalyst into the O_2 adduct, and as discussed above, that favors DTBQ formation. Further, the retarded rate of conversion is, in fact, a decrease in the rate of production of phenoxy radicals, and that works against the undesirable phenoxy radical coupling reaction. The expected enhancement of transport rates with increased CO_2 content does not enter into these explanations. Fundamental studies of the variations of dielectric constant and transport properties of

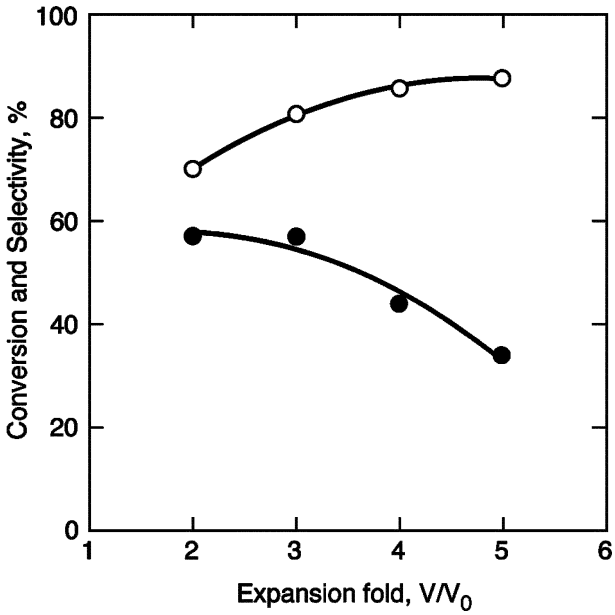

Fig. 4 Effect of solvent expansion by CO_2 on DTBP conversion (●) and DTBQ selectivity (○) in CO_2-expanded CH_3CN. Reaction conditions: catalyst [Co(salen*)] concentration = 0.25 mg mL^{-1}; reaction time = 2 h; reaction temperature = 60 °C; catalyst : substrate : O_2 mole ratio = 1 : 80 : 800; volume of methyl imidizole = 2 μL.

CXLs, and their effects on the concentrations of various species are needed to develop a better understanding of the observed effects.

Comparison of turnover frequencies in different reaction media

The physicochemical properties of CXLs may be tuned, not only by varying the proportion of the CO_2 relative to the chosen organic solvent (as explained above), but also by varying the organic solvent itself. To better understand solvent effects, we compared the DTBP oxidation in different reaction media as follows: neat CH_3CN, *sc*CO_2, CO_2-expanded CH_3CN, and CO_2-expanded CH_2Cl_2. The reaction conditions are as follows: catalyst concentration, 0.415 mM; reaction time, 2 h; catalyst : substrate : O_2 mole ratio, 1 : 80 : 800; expansion (V/V_0), 2; mole ratio of methyl imidizole to catalyst, 1.28; effective reaction volume, 10 mL.

Fig. 5 compares the turnover frequency (TOF) (defined as the moles of DTBP converted per mole of catalyst per hour) as a function of reaction temperature in the different reaction media. The TOFs in CO_2-expanded solvent media (V/V_0 = 2; p = 60–90 bars) are between one and two orders of magnitude greater than in *sc*CO_2 (p = 207 bar) or neat CH_3CN. Among the CXLs, higher TOF numbers are obtained for the DTBP oxidation in CO_2-expanded CH_3CN than for those in $CHCl_2$. As shown in Fig. 6, although the TOFs in CXLs are one to two orders of magnitude higher than that in *sc*CO_2, the DTBQ selectivity is more or less similar for all dense CO_2 phases, increasing moderately with reaction temperature. In comparison to DTBQ selectivity obtained in various organic solvents,[1d] higher DTBQ selectivity is observed in *sc*CO_2 and CXLs. It is not uncommon to observe "ignition" or step-type temperature dependence during oxidation reactions as we do in the case of the CO_2-expanded CH_2Cl_2. The reasons for the differing temperature dependence in the various CXLs are not fully understood as yet. Ongoing mechanistic investigations should provide a better understanding in this regard.

The common inexpensive Co(salen) catalyst is insoluble in *sc*CO_2 and shows no detectable activity as a DTBP oxidation catalyst in that medium. In sharp contrast, Co(salen) shows remarkable activity in CO_2-expanded CH_3CN. As shown in Fig. 7, the DTBP conversion increased from less than 5% to around 40% as the temperature increased from 25 °C to 70 °C, while the DTBQ selectivity increased from 60% to 70% over the same temperature range. This example demonstrates an important advantage of

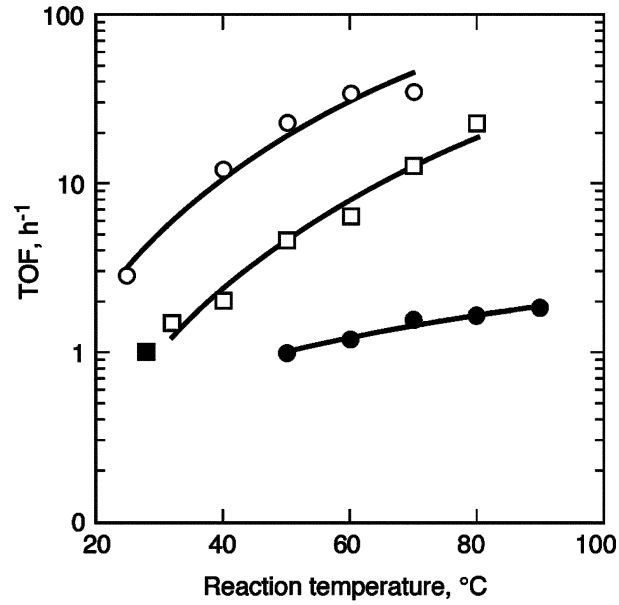

Fig. 5 Effect of temperature on turnover frequencies (TOFs) for 2,6-di-*tert*-butyl phenol oxidation with Co(Salen*) catalysts in supercritical CO_2 (●), neat CH_3CN (■), CO_2-expanded CH_3CN (○), and CO_2-expanded CH_2Cl_2 (□). Reaction conditions: total pressure = 1 bar (in neat solvent); 207 bar (in *sc*CO_2) and 50–90 bar (in CO_2-expanded solvent depending on reaction temperature); Catalyst concentration = 0.25 mg mL^{-1}; catalyst : substrate : O_2 mole ratio = 1 : 80 : 800; volume of methyl imidizole = 2 μL; V/V_0 = 2 (in the case of CO_2-expanded solvent media); reaction volume = 10 mL.

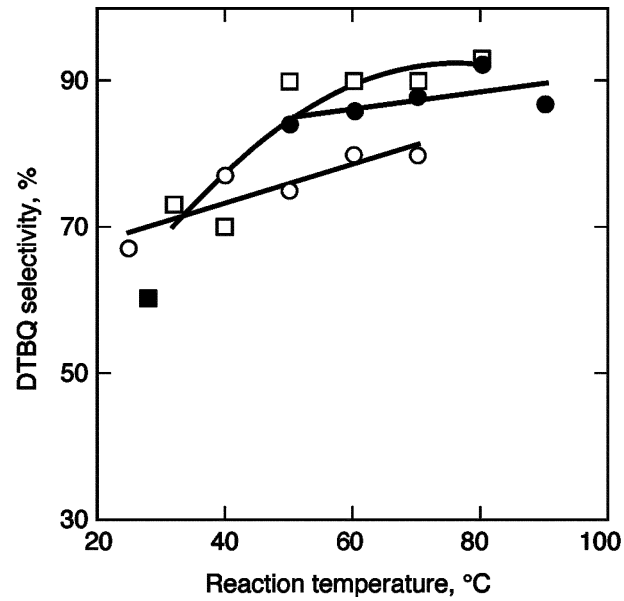

Fig. 6 Influence of reaction temperature on DTBQ selectivity during 2,6-di-*tert*-butyl phenol oxidation with Co(salen*) catalyst in supercritical CO_2 (●), neat CH_3CN (■), CO_2-expanded CH_3CN (○), and CO_2-expanded CH_2Cl_2 (□). Reaction conditions: total pressure = 1 bar (in neat solvent); 207 bar (in *sc*CO_2) and 50–90 bar (in CO_2-expanded solvent depending on reaction temperature); Catalyst concentration = 0.25 mg mL^{-1}; catalyst : substrate : O_2 mole ratio = 1 : 80 : 800; volume of methyl imidizole = 2 μL; V/V_0 = 2 (in the case of CO_2-expanded solvent media); reaction volume = 10 mL.

CXLs. Because most conventional solvents are expanded by CO_2, it is possible to dissolve most homogeneous transition metal catalysts in CXLs containing an appropriate solvent. In contrast, most unmodified transition metal complexes have inadequate solubilities in *sc*CO_2. These results clearly show that CO_2-expanded solvents complement *sc*CO_2 as reaction media by broadening the range of conventional catalyst + solvent combinations with which homogeneous O_2-based oxidations can be performed.

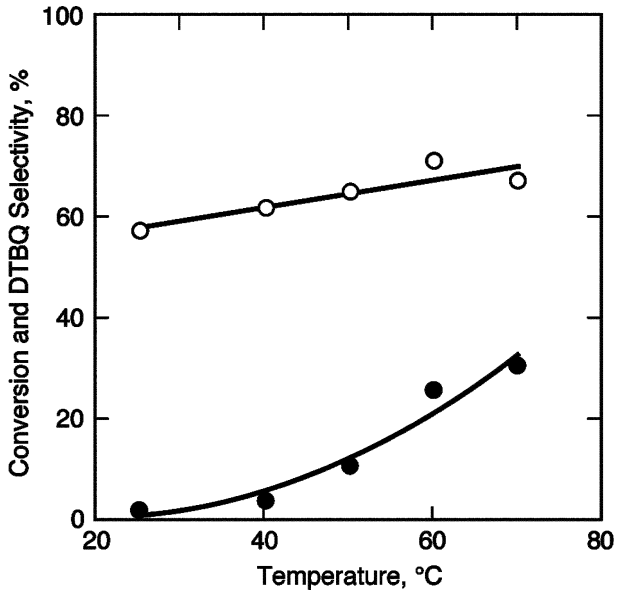

Fig. 7 Effect of reaction temperature on DTBP conversion (●) and DTBQ selectivity (○) during DTBP oxidation by O_2 in CO_2-expanded CH_3CN. Reaction conditions: catalyst [Co(salen)] concentration = 0.25 mg mL^{-1}; reaction time = 2 h; catalyst : substrate : O_2 mole ratio = 1 : 80 : 800; expansion fold (V/V_0) = 2; volume of methyl imidizole = 2 μL.

Influence of CO_2-addition on solubility of Co(salen*) in CXLs

Adding CO_2 to CO_2-miscible solvents "expands" the solvent volume as the CO_2 pressure is increased. However, the solubilities of polar solutes in CXLs decrease upon CO_2 addition. We investigated the effect of isothermal CO_2 addition on solutions of catalyst in organic solvents. Fig. 8 shows isothermal volumetric

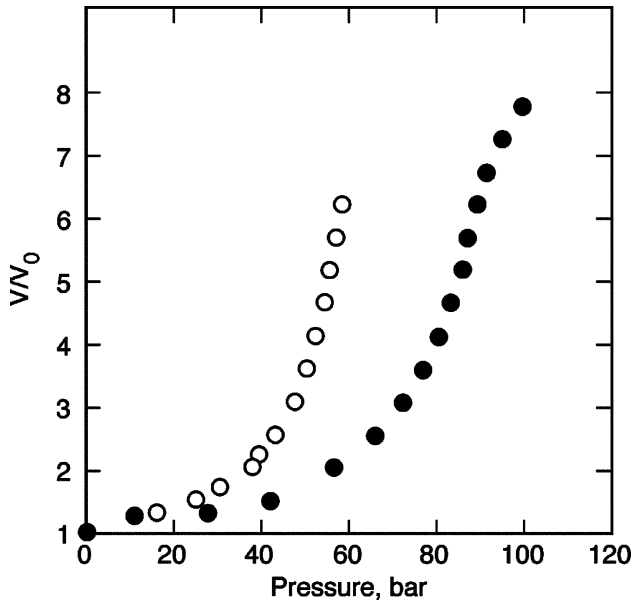

Fig. 8 Volumetric expansion of Co(Salen*) + CH_2Cl_2 solution (0.419 mM) by CO_2 at 25 °C (○) and 50 °C (●).

expansion profiles at 25 °C and 50 °C for the catalyst [*N*,*N*′-Bis(3,5-di-*tert*-butylsalicylidene)1,2-cyclohexanediaminato(2-)]cobalt(II) (abbreviated Co(salen*)) in CH_2Cl_2 (0.415 mM). As expected, higher pressures are required at higher temperatures to reach the same expansion level. At both temperatures the catalyst solubility in the expanded solvent decreases with CO_2 addition and catalyst precipitation eventually occurs at a certain expansion level, termed the "maximum homogeneous expansion limit", MHEL. Fig. 9 shows isothermal MHEL curves for the Co(salen*)/CH_2Cl_2 system. The region below the curves represents the homogenous expanded

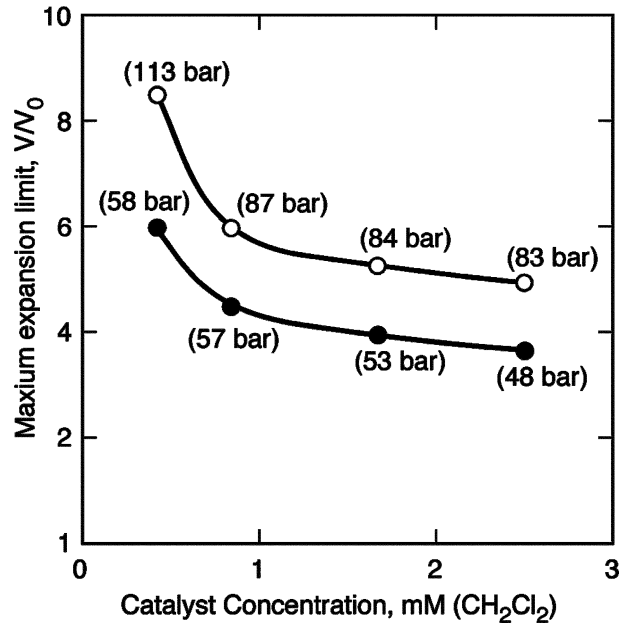

Fig. 9 Maximum limits for homogeneous expansion (MHEL) of CH_2Cl_2 + catalyst solutions by CO_2 at 25 °C (●) and 50 °C (○).

phase available for performing reactions while the region above the curves is suitable for catalyst separation, post reaction. For a given catalyst/solvent combination, the MHEL increases with temperature but decreases with increasing initial catalyst concentration. As shown in Fig. 9, the MHEL at 25 °C is roughly 5 for the 0.4 mM CH_2Cl_2 solution of the Co(Salen*) catalyst and 2.5 for the corresponding 2.5 mM solution. At 50 °C, the MHEL is roughly 4 for the 2.5 mM solution, implying that up to 80 vol.% of the organic solvent may be replaced by CO_2 in the CXL while retaining catalyst solubility. It is noteworthy that the total pressures at the MHEL are tens of bars, as compared to hundreds of bars for *sc*CO_2. MHEL data are clearly essential to define operating conditions both for homogeneous oxidations and for catalyst separation, post reaction.

Enhancement of oxygen solubilities in CXLs

It has been a matter of contention whether O_2 is much more soluble in CXLs than in organic solvents. This issue is important because the concentration, and, therefore, the reactivity of O_2 may be critical to the rates and selectivities of catalytic reactions. We previously reported a method for measuring equilibrium O_2 concentrations in CXLs.[1b] This method is based on directly sampling the expanded phase and the vapor phase, and employing GC/TCD analysis for measuring the O_2 concentrations in the two phases. We employed the same technique to measure O_2 concentration in liquid CO_2. As shown in Fig. 10, the measured oxygen concentrations in liquid CO_2 are in excellent agreement with the data from literature,[9] thus confirming the reliability of our method for measuring O_2 concentration in CXLs.

As shown in Fig. 11, the measured O_2 mole fraction in the CO_2-expanded CH_2Cl_2 liquid phase (at V/V_0 = 2) increases approximately linearly with the total oxygen content of the system, the values being on the order of hundredths of a mole fraction. These values are about an order of magnitude greater than the O_2 solubility in neat CH_2Cl_2 (mole fraction = 1×10^{-3} at 25 °C and 1 bar[10]) and are of the same order of magnitude observed for liquid CO_2.[9] In contrast, the O_2 solubility in CO_2-expanded CH_3CN is about two orders of magnitude greater than that in neat CH_3CN.[1c] As shown in Fig. 12, the O_2 concentrations also increase linearly upon CO_2 addition, reaching ~7–8 mol % at expansion levels (V/V_0) of 7 to 8. However, such high expansions are not suitable for homogeneous reactions since the catalyst would precipitate from solution. These new results confirm the significant enhancement of

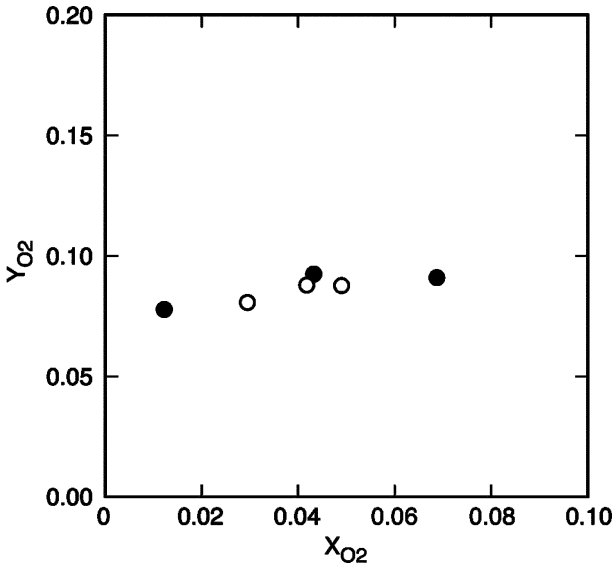

Fig. 10 Comparison of measured solubilities of oxygen in dense CO_2 at 25 °C; This study (●); Data from Battino *et al.*[9](○).

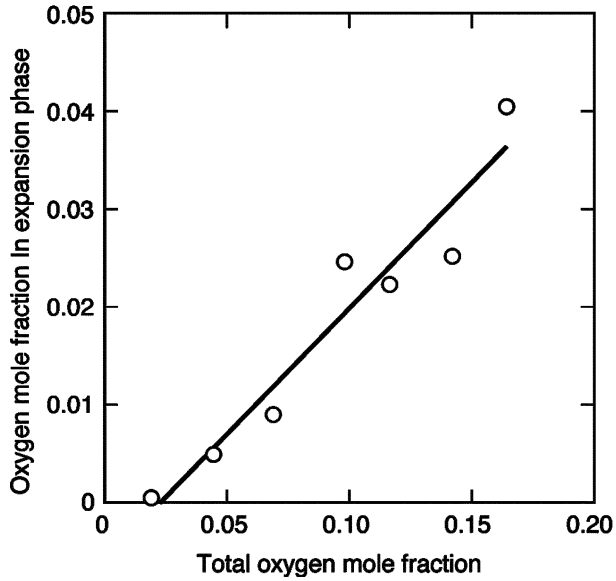

Fig. 11 Variation of O_2 mole fraction in CO_2-expanded CH_2Cl_2 (V/V_0 = 2) as a function of total O_2 content in the system (T = 30 °C).

O_2 solubilities in CXLs compared to the corresponding neat solvents, albeit the enhancement varies depending on the solvent.

Conclusion

This report demonstrates that continua of CO_2-expanded solvents (CXLs), formed by combining organic solvents and *sc*CO_2, are excellent media for catalytic oxidation reactions. The O_2 oxidation of DTBP to DTBQ with Co(salen*) as the catalyst has been investigated in CO_2-expanded solvent media based on CH_3CN and CH_2Cl_2 and the results have been compared with those obtained in *sc*CO_2, and in the neat organic solvents. Reaction rates, as estimated from turnover-frequencies, are increased by as much as two orders of magnitude over that of the reaction in *sc*CO_2 or neat organic solvents, and with comparable selectivity toward the desired oxidation product DTBQ. Thorough evaluation has been made of the effects on reaction rates and product distribution of reaction parameters (oxygen concentration, catalyst concentration, reaction temperature, extent of expansion, choice of solvent). Dependence on these parameters confirms the same general mechanism for the reactions in CXLs as has been described for other media, including *sc*CO_2.

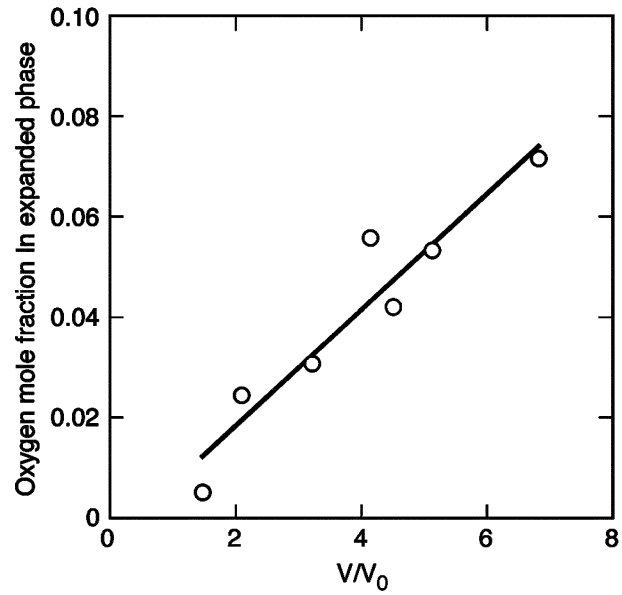

Fig. 12 Variation of O_2 concentration in CO_2-expanded CH_2Cl_2 phase with expansion ratio (T = 30 °C; total oxygen mole fraction in the system = 0.11).

The investigation showed that the combination of CO_2 and organic solvents facilitates control of the solubilities of two reaction partners, namely the transition metal catalyst and the preferred terminal oxidant, oxygen. The solubility of the catalyst decreases with further addition of CO_2. The catalyst can be made to precipitate by adding CO_2 in excess of the maximum homogeneous expansion limit, MHEL, which varies with the specific catalyst/solvent system, the catalyst concentration and the temperature. The oxygen solubility was measured for CH_2Cl_2-based CXLs and found to increase with CO_2 expansion. In general (2 examples now), the solubility of oxygen in CXLs exceeds that in the corresponding neat organic solvent, by 1 or 2 orders of magnitude, approximating that in liquid CO_2.

Acknowledgement

This research was supported by research grant CHE-9815321 from the National Science Foundation.

References

1 (*a*) G. B. Combes, F. Deghani, F. P. Lucien, A. K. Dillow and N. R. Foster, in *Reaction Engineering for Pollution Prevention*, ed. M. A. Abraham and R. P. Hesketh, Elsevier, Amsterdam, 2000, 173–181; (*b*) C. A. Thomas, R. J. Bonilla, Y. Huang and P. G. Jessop, *Can. J. Chem.*, 2001, **79**, 719–724; (*c*) P. G. Jessop, R. R. Stanley, R. A. Brown, C. A. Eckert, C. L. Liotta, T. T. Ngo and P. Pollet, *Green Chem.*, 2003, **5**, 123–128; (*d*) G. Musie, M. Wei, B. Subramaniam and D. H. Busch, *Coord. Chem. Rev.*, 2001, **219–221**, 789–820; (*e*) M. Wei, G. T. Musie, D. H. Busch and B. Subramaniam, *J. Am. Chem. Soc.*, 2002, **124**(11), 2513–2517; (*f*) Z. Hou, B. Han, L. Gao, T. Jiang, Z. Liu, Y. Chang, X. Zhang and J. He, *New J. Chem.*, 2002, **9**, 1246–1248; (*g*) M. F. Sellin, P. B. Webb and T. J. Cole-Hamilton, *Chem. Commun.*, 2001, 781–782.

2 H. Jin and B. Subramaniam, *Chem. Eng. Sci.*, 2003, **58**, 1897–1901.

3 (*a*) K. W. Hutchenson, in *Supercritical Fluid Technology in Materials Science and Engineering*, ed. Y-P Sun, Marcel Dekker, New York, 2002; (*b*) P. G. Jessop, T. Ikariya and R. Noyori, *Chem. Rev.*, 1999, **99**, 475–494; *Chemical Synthesis Using Supercritical Fluids*, ed. P. G. Jessop and W. Leitner, VCH-Wiley, Weinheim, 1999; (*c*) E. R. Birnbaum, R. M. Le Lacheur, M. Richard, A. C. Horton and W. Tumas, *J. Mol. Catal. A*, 1999, **139**, 11–24; (*d*) D. R. Pesiri, D. K. Morita, W. Glaze and W. Tumas, *Chem. Commun.*, 1998, **9**, 1015–1016; (*e*) G. R. Haas and J. W. Kolis, *Organometallics*, 1998, **17**, 4454–4460; (*f*) X.-W.

Wu, Y. Oshima and S. Koda, *Chem. Lett.*, 1997, 1045–1046; (*g*) E. Sahle-Demessie, M. A. Gonzalez, J. Enriquez and Q. Zhao, *Ind. Eng. Chem. Res.*, 2000, **39**, 4858–4864.

4 (*a*) P. T. Anastas and T. C. Williamson, in *Green Chemistry: Designing Chemistry for the Environment, ACS Symposium Series, No: 626*, ed. P. T. Anastas and T. C. Williamson, *Am. Chem. Soc*., Washington, D.C., 1996, 1–17; (*b*) P. T. Anastas and M. M. Kirchhoff, *Acc. Chem. Res.*, 2002, **35**, 686–694; (*c*) P. T. Anastas and J. B. Zimmerman, *Env. Sci. Technol.*, 2003, **37**, 94A–101A.

5 I. Kohara, H. Fujiyama, K. Iwai, S. Nishiyama and S. Tsuruya, *J. Mol. Catal. A: Chem.*, 2000, **153**(1–2), 93–101; I. G. Kolesnik, E. G. Zhizhina and K. I. Matveev, *J. Mol. Catal. A: Chem.*, 2000, **153**, 147–154; R. Pathak and G. N. Rao, *J. Mol. Catal. A: Chem.*, 1998, **130**(3), 215–220.

6 (*a*) Y. Deng and D. H. Busch, *Inorg. Chem.*, 1995, **34**, 6380–6386; (*b*) M. Yamada, K. Araki and S. Shiraishi, *J. Chem. Soc., Perkin Trans.*, 1990, 2687–2701; (*c*) B. B. Corden, R. S. Drago and R. P. Perito, *J. Am. Chem. Soc.*, 1985, **107**, 2903–2907; (*d*) R. S. Drago, J. Gaul, A. Zombeck and D. Straub, *J. Am. Chem. Soc.*, 1980, **102**, 1033–1038; (*e*) X.-Y. Wang, R. J. Motekaitis and A. E. Martell, *Inorg. Chem.*, 1984, **22**, 271–275.

7 G. Musie, M. Wei, B. Subramaniam and D. H. Busch, *Inorg. Chem.*, 2001, **40**, 3336–3341.

8 T. D. Smith and J. R. Pilbrow, *Coord. Chem. Rev.*, 1981, **39**, 295–283; R. D. Jones, D. A. Summerville and F. Basolo, *Chem. Rev.*, 1979, **79**, 139–179; G. McLendon and E. A. Martell, *Coord. Chem. Rev.*, 1976, **19**, 1–39.

9 *Solubility Data Series: Volume 7, Oxygen and Ozone*, ed. R. Battino, Pergamon Press, Oxford, New York, 1981.

10 J. H. Hildebrand, J. M. Prausnitz and R. L. Scott, *Regular and Related Solutions: The Solubility of Gases, Liquids, and Solids*, John Wiley, New York, 1970.

EDITORIAL

www.rsc.org/greenchem

Sustainable Chemical Engineering

This special issue of Green Chemistry represents an attempt to illustrate some of the activities and work of chemical engineers in the area of green and sustainable chemical engineering. Responding to the global drive towards multidisciplinarity in industry and academia, and particularly following a recent RSC report on "Benign and Sustainable Chemical Technologies"[1] the ambition of this issue is to encourage collaboration between green chemists and chemical engineers in the area to which the two communities bring complementary skills.

Most of the papers in this issue are in the area of green chemical engineering, but some go beyond to encompass the concept of sustainability and consider not only the environmental ("green") aspects but also the other two components of sustainable development: economic and social. This is the main difference between "green" and "sustainable" chemical engineering: the former concentrates mainly on the environment while the latter, in addition to environmental, takes into account economic and social criteria.

Sustainable development of the chemical industry is recognised as one of the key challenges for the industry.[2,3] It is now widely accepted that this can only be achieved by balancing all three dimensions of sustainability and the industry is already working actively towards this goal.[4] However, one of the challenges for the industry in trying to become more sustainable is to be able to assess whether it is moving towards or away from sustainability. In other words, the industry (and society) must be able to tell which processes, products and activities are sustainable and which are not. Some of the papers in this issue deal with this problem by demonstrating what tools can assist the industry in becoming more sustainable and how they can be used in the design of new or the improvement of existing products and processes.

Following their EU-based study on tools and technologies for a more sustainable chemical industry, Tsoka *et al*.[5] found out that potentially sustainable technologies favoured by the industry include highly selective catalysts, process intensification, supercritical separation and small-scale processing. The study also found that the industry believes that Computer-Aided Molecule Design (CAMD) as well as process design and simulation are among the tools that could help in the design of more sustainable products and processes. Hugo *et al*.[6] complement these findings by demonstrating how CAMD can be used for improved economic and environmental performance. Focussing on liquid–liquid extraction operations, they use Life Cycle Assessment (LCA) and multiobjective optimisation as tools for designing solvents that are both environmentally benign and cost effective.

Hellweg *et al*.[7] also use solvents as an example and in addition to LCA demonstrate the use of a further two tools for assessing the level of sustainability of chemicals: the first tool identifies potential environmental, health and safety hazards associated with the production process and the second helps determine the environmental persistence and exposure to chemicals in the environment. The differences between the three methods and the results are illustrated on 13 organic solvents. For example, one of the results obtained consistently by all three tools is that the use of chlorinated solvents is unsustainable.

Romero-Hernandez[8] uses a combination of process optimisation, LCA and risk assessment to assess the level of sustainability of a clean-up technology. Concentrating on the case study of organic pollution in waste water, he concludes that on a life cycle basis it does not make much sense to treat the water because the environmental impact of operating the water treatment plant is higher than that of the untreated water. However, from the social point of view, the treatment is necessary because of the adverse impact that the organic pollution in the waste water would have on human health.

These are just some examples of the many sustainability tools and methods that chemical engineers use in practice.[9] We hope that, in addition to the other papers published in this issue, they demonstrate that green chemists and chemical engineers have the skills and knowledge necessary for meeting the challenge of sustainable development by designing chemical products and processes that provide the required effects at a price the market can bear, while not threatening human health or the environment.[1]

Adisa Azapagic
Professor of Sustainable Engineering
School of Engineering
University of Surrey
Guildford, England

References

1 *Benign and Sustainable Chemical Technologies*, ed. C. Web and A. Palermo, Royal Society of Chemistry, London, 2003.
2 CEFIC, *Horizon 2015: Perspectives for the European Chemical Industry*, CEFIC, March 2004, http://www.cefic.org.
3 *Technology Vision 2020*, The US Chemical Industry, The American Chemistry Society, American Institute of Chemical Engineers, The Chemical Manufacturers Association, The Council for Chemical Research, and The Synthetic Organic Chemical Manufacturers Association, December 1996, Washington, DC, http://www.acs.org.
4 A. Azapagic, Sustainability: Lip Service or a Genuine Commitment?, *IChemE Trans. B*, 2004, **82**, B4, 267–268.
5 C. Tsoka, W. R. Johns, P. Linke and A. Kokossis, *Green Chem.*, 2004, **6**, DOI: 10.1039/b402799j, this issue.
6 A. Hugo, ´C. Ciumei, A. Buxton and E. W. Pistikopoulos, *Green Chem.*, 2004, **6**, DOI: 10.1039/b401868k, this issue.
7 S. Hellweg, U. Fischer, M. Scheringer and K. Hungerbühler, *Green Chem.*, 2004, **6**, DOI: 10.1039/b402807b, this issue.
8 O. Romero-Hernandez, *Green Chem.*, 2004, **6**, DOI: 10.1039/b401871k, this issue.
9 *Theory and Practice of Sustainable Development: Case Studies for Engineers and Scientists.*, ed. A. Azapagic, S. Perdan and R. Clift, John Wiley & Sons, Chichester, UK, 2004, pp. 437.

DOI:10.1039/b411953n

PAPER

www.rsc.org/greenchem

To treat or not to treat? Applying chemical engineering tools and a life cycle approach to assessing the level of sustainability of a clean-up technology†

Omar Romero-Hernandez
Dep. of Industrial Engineering, ITAM. Rio Hondo No. 1, Col. Tizapan San Angel, Mexico City 01000, Mexico. E-mail: oromero@itam.mx; Fax: +52 55 5490 4663; Tel: +52 55 56284000 x3682

Received 6th February 2004, Accepted 5th July 2004
First published as an Advance Article on the web 13th August 2004

A traditional approach used to evaluate clean-up technologies, in which only plant discharges are considered, is contrasted with a sustainability assessment. The sustainability of any technology can be assessed from three complementary points of view: economic, environmental and social. As such, this paper presents a comprehensive scheme that can be applied to any process, product or technology. In addition, the use of chemical engineering tools such as process design, process modelling and simulation represent a baseline for the sustainability assessment of technologies, as presented in a case study. The optimal granular activated carbon adsorption process design is used as a model system to demonstrate the advantages of sustainability approaches over traditional approaches. A mathematical model that describes the performance of the process at various design options was developed. This model includes cost equations that were used to estimate the total cost of each alternative under different plant designs and two waste scenarios (a benzene and a 1,2-dichloroethane discharge). Life Cycle Assessment tools were applied to generate an inventory of emissions and the impact assessment measured as Photochemical Ozone Creation (POC) and Global Warming Potential (GWP). The model examined trade-offs between pollutants discharged into the atmosphere and pollution associated with the adoption and operation of the technology. One of the main results from the technology assessment is that the environmental impact, measured in terms of GWP proved to be higher for the technology operation than for the untreated waste streams themselves, and therefore suggested that the streams should not be treated. However, the social impact evaluation (measured as risk assessment) conducted as part of this work proved that it was morally and legally mandatory to treat them due to the adverse effects on human health that they may represent. As such, a triple bottom line sustainability assessment was demonstrated to be one of the most important frameworks for decision making. The evaluation scheme presented in this work can also be applied to other areas such as the identification of the most sustainable process design and different green chemistry route alternatives.

1. Introduction

The rapid development of process industries has given rise to multiple environmental problems which, in some cases, have led to the development of cleaner technologies and waste minimisation techniques.[1] These initiatives tend to ameliorate pollution problems by using, or generating, lower amounts or less harmful pollutants. However, waste minimisation techniques and cleaner technologies have not been able to eliminate completely the discharge of pollutants into the environment, therefore, treatment of pollutants at the end-of-the-pipe is still a common practice among process industries. This situation leads to the need to identify the best option among several process routes, design options, process conditions and technologies. This is still an area of research for those involved in process design, green chemistry, and environmental policy makers. One alternative to deal with this situation is to perform a sustainability evaluation.

The sustainability of any process or technology requires the traditional evaluation scheme in which environmental constraints (discharge limits) were satisfied at minimum economic cost to be waved. Current sustainability assessments include considerations towards economic, environmental and social impacts.[2] However, deciding on the most adequate technology or process is not crystal clear since trade-offs among economic, environmental and social impacts usually appear. Furthermore, process performance differs depending on the type of environmental impact that is analysed and the boundaries defined for the assessment.[3]

The hypothesis behind this paper is that the environmental impact caused by a treatment process may, under certain conditions, be greater than the environmental impact generated by the wastewater emissions. Romero-Hernandez *et al*. described trade-offs between decreasing environmental impact due to wastewater emissions and increasing environmental impact associated with inputs to the wastewater treatment process, such as electricity, steam and raw materials.[3] This work is based on the use of Life Cycle Assessment (LCA) as a methodology to assess the environmental impacts of a product or process. Under this methodology, a consistent system boundary around the wastewater process is defined so that all wastes associated with the process (*i.e*., electricity, raw materials generation, steam and steel production), are included when the inventory of emissions is performed.[4] This approach has been successfully incorporated into process analysis and design.[5,6] Thus, an economic assessment (measured in terms of treatment costs), an environmental assessment (with the use of Life Cycle Assessment tools) and a social assessment (measured in terms of human risk assessment) have been conducted.

In order to explore the use of life cycle tools and chemical engineering for the assessment of technologies, the authors have studied a widely used end-of-the-pipe treatment technology: activated carbon adsorption. This process is considered as one of the most effective methods for controlling emissions of volatile organic compounds, VOCs, a class of pollutant that is often present in industrial wastewater streams.[7] Its great pollutant flexibility and its potential to eliminate organic contaminants from water, have

† Electronic supplementary information (ESI) available: granular activated carbon adsorption. Process design and modelling. See http://www.rsc.org/suppdata/gc/b4/b401871k/

DOI: 10.1039/b401871k

made carbon adsorption a yardstick by which other treatment technologies and industrial processes should be evaluated.[8]

The following sections describe the design considerations applied in the cost optimised carbon adsorption model, the use of LCA techniques to obtain an inventory of all the emissions associated with the process system, and its environmental and social impacts.

2. Technology: carbon adsorption

There are several process configurations associated with the design of an activated carbon adsorption process. This paper presents a cost optimised process model developed for a downflow fixed-bed pressured system. The system comprises two carbon absorption columns, pumps, eductors, pipes and tanks which are part of a clean-up technology. The purpose of this design is to treat discharges of volatile organic compounds (VOCs) such as benzene and 1,2-dichloroethane. The main adsorbent is granular activated carbon (GAC). This configuration has been acknowledged as the most common adsorption option for industrial water treatment applications, since it is convenient for the treatment of relatively small flowrates of wastewater, with moderate concentration of organics and achieves high degrees of removal.[7,9]

2.1 Process description

The carbon adsorption process designed for this work is illustrated in Fig. 1. Wastewater is pumped into the top of a first adsorber

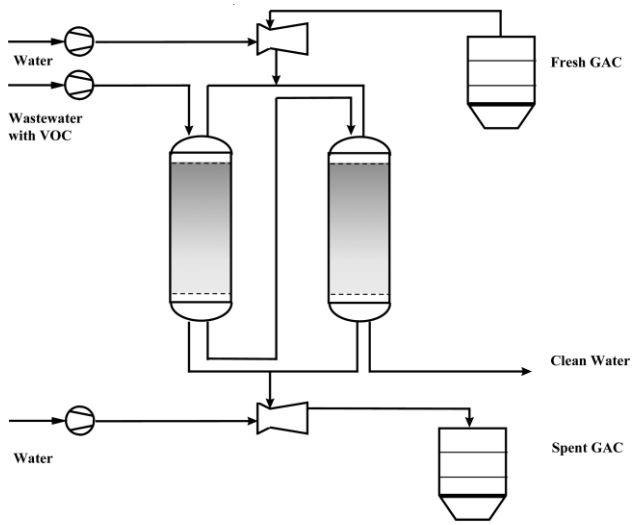

Fig. 1 Carbon adsorption process.

column, where organic compounds are removed as they pass through the column. Then, the stream is fed to the top of a second adsorber column and leaves from the bottom as a stream depleted of pollutant. When saturation in the first column occurs, the adsorber is disconnected from the process and the wastewater enters only into the second adsorber. The carbon in the first adsorber is removed through an hydraulic pumping system and sent to a spent carbon storage container for regeneration. Once the column has been replenished with virgin or regenerated carbon, it is connected as the second adsorber. The carbon replacement process is repeated once the second column is exhausted.

Adsorption columns, and thus the amount of GAC required for the process, are the most important considerations for process design. They both dictate the specifications for further equipment including pumps, eductors and storage tanks. This process model is based on the ideas presented by Crittenden *et al*. since their procedures have been applied successfully for the design of carbon adsorption columns.[10–12] The constant-pattern-homogeneous-surface-diffusion-model developed by Hand was used to predict liquid phase GAC usage rates for selected organics. The activated carbon adsorption calculations performed in this work assume two inlet flow scenarios:

1. A wastewater flow of 10 m^3 h^{-1} containing 1000 g m^{-3} of benzene and,

2. A wastewater flow of 10 m^3 h^{-1} containing 1000 g m^{-3} 1,2-dichloroethane (DCE).

3. Economic performance: cost optimised model

The mathematical model consists of 36 equations, 37 variables and 1 degree of freedom (*mass throughput*, which is the ratio of mass fed compared to the mass required to saturate the adsorber). It has been solved with the use of an optimisation tool. The general algebraic modelling system (GAMS) was employed to obtain the optimal cost design for the carbon adsorption process and the environmental impacts that may result from its operation. A complete description of the carbon adsorption process design and modelling is presented in the Electronic Supplementary Information.† Total costs of treatment are estimated as a capital and operating cost function. The equipment contributing to capital cost includes: two adsorber columns, the wastewater pump, two pump-eductor systems for carbon transportation, and two storage tanks for fresh and exhausted GAC. Conversely, operating costs are a function of the electricity consumed to run the process pumps, water required to transport the GAC and replacement of GAC employed for the process. Due to the relatively low volume of GAC employed, regeneration was considered to be performed off-site.

Costs for the main components of the GAC wastewater treatment process are presented in Table 1. The main equipment items are the feed pump, the pump-eductor systems, the adsorption column and the storage tanks.

Table 1 Cost of treatment for the carbon adsorption process

	Benzene	DCE
Total cost/£ yr^{-1}	**459 120**	**511 470**
Capital cost/£ yr^{-1}	**103 550**	**100 730**
Operating cost/£ yr^{-1}	**355 560**	**410 740**
Cost of adsorbers (£/yr)	**30 640**	**27 235**
Height/m	2.617	2.267
Diameter/m	1.614	1.614
Cost of storage tanks (£/yr)	**57 198**	**58 947**
Cost of feed pump and eductors/£ yr^{-1}	**6 825**	**6 646**
Cost of GAC/£ yr^{-1}	**352 580**	**407 500**
GAC/kg yr^{-1}	248 296	286 971
Load ratio kg_{VOC}/kg_{GAC}	0.328	0.284
Cost of electricity/£ yr^{-1}	**2,721**	**2,852**
Electricity/kWh yr^{-1}	54 420	57 040
Cost of water/£ yr^{-1}	**260**	**384**

Characteristics of the feed pump are affected by the flowrate, the nature of the liquid and the head required. In this model, the inlet flowrate is assumed to be constant during the process operation. Since benzene and DCE are present in the wastewater stream at low concentrations, the viscosity and density of the inlet stream were assumed to be those of pure water. Therefore, the power requirements for the feed pump are only dictated by the height of the adsorption columns. The design of pump-eductor systems is affected by the flow of water required to convert the GAC into slurry and by the operating time of this intermittent system. Nonetheless, both previously mentioned variables depend directly on the amount of GAC required for the wastewater treatment process.

The adsorption columns and the storage tanks are the equipment items that are most significantly affected by the process design. Both items are directly related to the amount of GAC required for the process. As expected, the adsorptive capacity of the carbon to attract organics is a very sensitive variable, since it determines the amount of GAC needed to achieve water purification and the height of the adsorption columns.

Although the amount of GAC required also influences the size and electricity requirements of pumps and eductors, its impact is relatively small compared to the columns and the storage tanks. In general, a higher adsorption column leads to a smaller number of GAC exchanges per year but it also leads to higher electricity requirements of the inlet pump.

The amount of GAC required for the process is the most cost significant component, and **represents more than 75% of total costs**. This amount is related to the Freundlich isotherm constants, and the inlet concentration for each organic compound in water. Sensitivity analyses were carried out in order to determine the relative influence of K, $1/n$, and C_{in}.

4. Emissions inventory

A life cycle approach (LCA) was applied to estimate the environmental burdens associated with the system. The emission of contaminants to the three environmental media was inventoried under an LCA approach, based on recommendations presented by Aelion, the US Environmental Agency and SETAC.[13–15] System boundaries include wastewater streams, inputs required for operating the clean-up technology and emissions related to carbon regeneration (Fig. 2). In order to be consistent with the cost model, the functional unit is defined as one year of continuous operation of the clean-up technology. Emissions produced through electricity generation, production-use-regeneration of granular activated carbon (GAC), and untreated pollutant, were all considered. Pollutant species involved within the system were: benzene or 1,2-dichloroethane which are removed from the wastewater stream (*Outputs*) and SO_2, hydrocarbons (HC), NO_2, N_2O, CO, CO_2, associated with *Inputs* generation.

4.1 Emissions related to electricity generation

The amount of electricity consumed by the feed pump and two pump-eductor systems is correlated to emission factors, *e.g.*, grams of pollutant per kWh. These data are calculated from the cost optimal process model previously described. The optimal size of equipment and its operating characteristics (power requirements) indicate the amount of electricity that is required in order to pump the water and operate the eductors. Emission factors used for this work can be consulted in BUWAL.[16]

4.2 Emissions related to GAC production, use and regeneration

Four stages have been identified in the life cycle assessment of GAC, as shown in Fig. 2. The first one describes those emissions associated with the production of raw materials. The second provides information of those pollutants discharged during the transformation of raw materials into GAC. The third is related to the use of GAC for the wastewater treatment process and the fourth deals with the carbon regeneration.

4.2.1 Raw materials. There are four basic raw materials considered for the production of GAC: water, coal, wood and coke. There are no emissions related to the production of H_2O and wood, being that they are natural species in the environment.

4.2.2 Production of GAC. A mixture of typical raw materials is assumed for the production of GAC.[7] It is comprised by 50% H_2O, 30% coal, 10% wood and 10% coke. Fig. 3 describes the

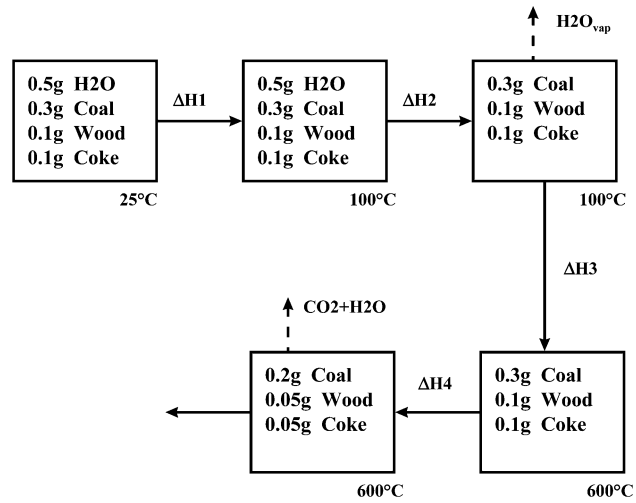

Fig. 3 Production of GAC at 30% conversion of raw materials.

stages considered for the production of GAC from 1 g of raw materials. The mixture is first burnt in order to evaporate the water, which inevitably burns off a portion of the organics, releasing CO_2 and H_2O. The use of external fuels for the combustion is not considered since coal, wood and coke are combustible. The final product is 0.3 g of GAC which is ready for use in the wastewater treatment process assumed.[7]

Mass balances were performed in order to estimate emissions associated with the production of GAC. The chemical formulas of the three organics are used to calculate emissions related to combustion. It assumes: a basic model to describe the structure of coal; cellulose as the only structural component of trees and; *Continental No. 1* as the type of coke used for the process. Stoichiometric equations describing the combustion of coal, wood and coke were applied in order to perform mass and energy balances associated with the production of GAC as presented by Bailey and Ollis[17] and the US National Research Council.[18]

$$2C_{100}H_{70}O_{10}N_2 + 226O_2 \rightarrow 200CO_2 + 70H_2O + 2N_2O \quad (1)$$

Molecular weight of coal: 1458 g mol^{-1}. Therefore, combustion of 1 g of coal leads to the following emissions: 2.744 g CO_2, 0.432 g H_20 and 0.0267 g of NO_2.

$$2C_{18}H_{30}O_{16} + 35O_2 \rightarrow 36CO_2 + 30H_2O \quad (2)$$

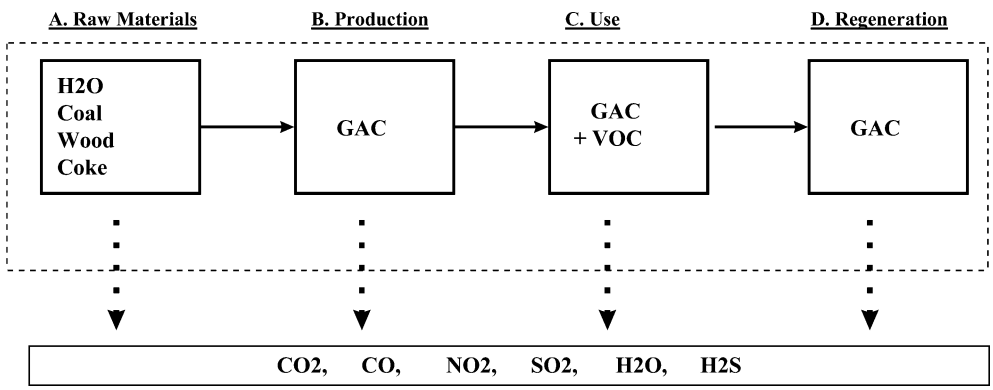

Fig. 2 Life cycle analysis of granular activated carbon (GAC).

Molecular weight of cellulose: 502 g mol^{-1}. Thus, combustion of 1 g of wood leads to the following emissions: 3.168 g CO_2 and 1.08 g H_20.

$$C_{288}H_{28}N_8S_1 + 297O_2 \rightarrow 288CO_2 + 14H_2O + 8NO_2 + SO_2 \quad (3)$$

Molecular weight of coke: 3572 g mol^{-1}. Therefore, combustion of 1 g of coke leads to the following emissions: 3.8 g CO_2, 0.076 g H_20, 0.18 g of NO_2 and 0.02 g of SO_2.

4.2.3 Use of GAC. The use of GAC is described by the utilities required to run the GAC adsorption process. In this analysis, electricity is highlighted as the only source of emission. The inputs required for the process are calculated from the process mathematical model.

4.2.4 Regeneration of GAC. Information provided by Hutchins is used to calculate the amount of electricity and fuel consumed during the carbon regeneration process.[19] Correlations correspond to thermal reactivation, which is the most common technique used to regenerate GAC.[20] This work assumes a thermal regeneration plant with a typical capacity of 7500 kg_{GAC} d^{-1}.[19]

Mass and energy balances performed for the life cycle analysis of GAC are based on 1 m^3 of GAC, therefore, proper unit transformation and conversion factors have been applied for consistency. Emissions related to steel manufacture were found to be negligible since they are at least five orders of magnitude lower than the rest.

Fig. 4 provides an indication of the type and amount of pollutants that may be discharged during the raw materials, production, use or regeneration stages in the GAC life cycle assessment. This figure suggests that carbon re-use may bring environmental benefits to the treatment process. The raw materials and the production stages create significantly more emissions of various pollutant species than those related to the use and regeneration of carbon. However, the inventory of emissions needs to be transformed into environmental impacts in order to gain insight into the environmental phenomena that may be caused by these emissions.

5. Environmental impacts

Two environmental impacts, photochemical ozone creation (POC) and global warming potential (GWP), were incorporated into the process model in order to assess the environmental performance of the wastewater treatment processes, according to a standard methodology.[21,22] POC, also known as photochemical smog, reflects the ability of chemical compounds to react with NO and eventually form ozone, O_3. POC values are determined relative to emissions of the reference substance, ethylene.[23] GWP estimates the relative contribution of each pollutant, compared to carbon dioxide, to heat up the atmosphere (greenhouse effect).[24] These two environmental indicators were chosen for several reasons. GWP is one of the most studied environmental phenomena and there is reasonable agreement among global organizations towards its implication. However, this is a global and long-term effects measure. In order to account for short term and local effects, POC was selected. Other measures such as Ozone Depletion and Critical Air/Water Volumes (CV) were not incorporated. There are no CFCs related to this process so there is no contribution to Ozone Depletion while CV are not internationally accepted as a health reference. Health effects can be better evaluated by a risk assessment methodology such as the one presented later in this paper.

The possible benefits derived from the re-use of GAC are also explored in this section for three rates of re-use: 30, 60 and 90%. However, it is important to note that breakthrough curves developed for this process assume that fresh carbon is used. This is due to the fact that breakthrough curves with regenerated carbon can only be reliably predicted by laboratory or pilot plant experiments. Thus, the adsorptive capacities of fresh and regenerated carbon are considered to be equal. The present model considers that in every regeneration at least 10% of the GAC is lost due to attrition and the exchange of GAC (fresh and re-used) for fresh carbon after one year. The price of new GAC is set at £1.42 per kg while the price for regenerated carbon is £1.12 per kg; both of them being typical market values (Faust and Aly,[7] Stenzel[8]). The environmental impacts of the system are described in the following sections.

POC impact evaluated for the GAC system is (slightly) lower for benzene than for DCE, as shown in of Fig. 5. However, the POC impact of the untreated benzene and DCE discharges, presented on the ordinate axes, shows that benzene causes a higher POC impact. Treatment of benzene requires lower electricity and activated carbon, and thus generates lower POC impact than the treatment of DCE. Since the carbon adsorption process removes 100% of the

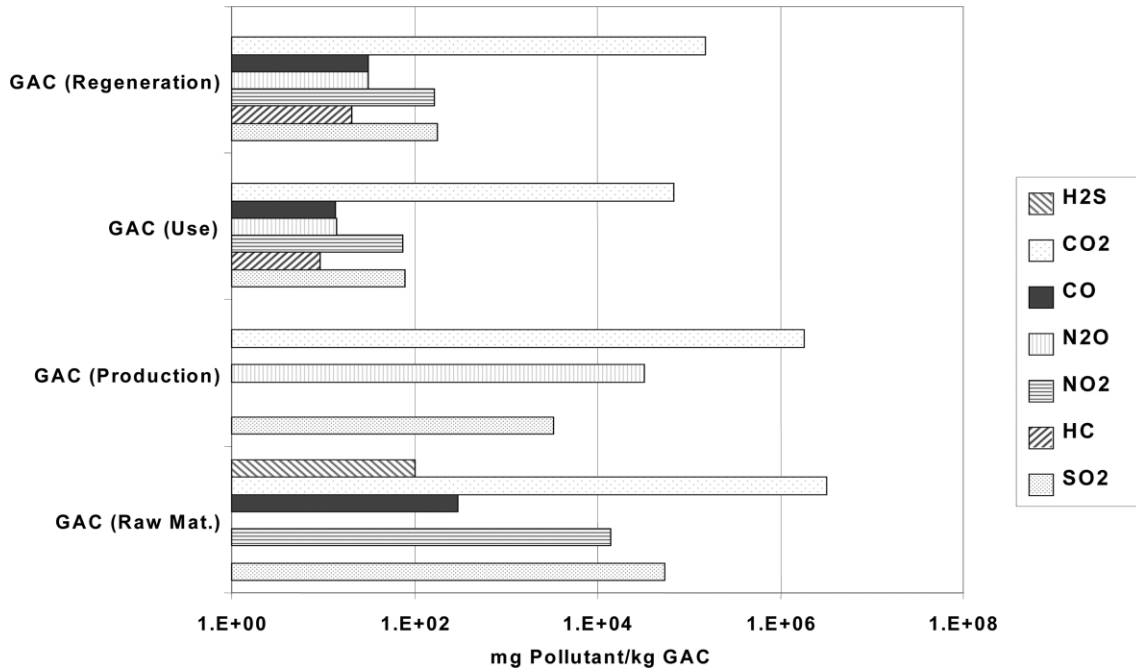

Fig. 4 Inventory of emissions derived from a life cycle assessment on the GAC.

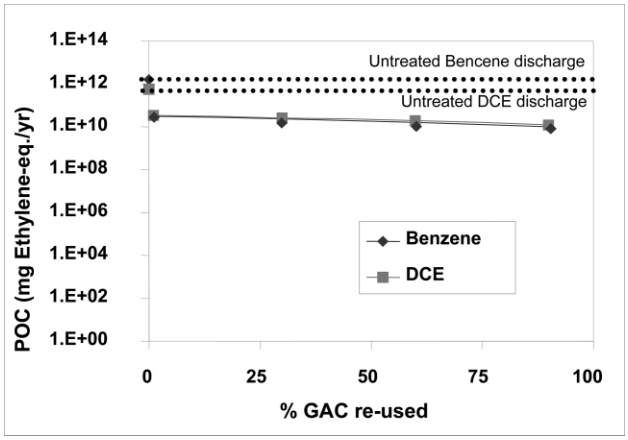

Fig. 5 POC impact of the carbon adsorption process, operating at various degrees of carbon re-use.

benzene and DCE, the POC impact presented in Fig. 5 is due only to *Inputs*. It should be noted that the POC impact associated with process inputs is significantly lower than the POC impact caused by an untreated wastewater discharge, even if more than 250 tonnes of carbon are consumed per year of operation. Viewed another way, setting up a carbon adsorption process to remove benzene provides considerable environmental benefits as shown in Fig. 5, where the environmental impact of the untreated benzene discharge, plotted on the ordinate axis, is significantly higher than the corresponding environmental impact, when the treatment technology is used. Fig. 5 shows also that higher rates of GAC re-use lead to lower POC impacts. As such, avoiding the acquisition of raw materials and the production of new GAC *via* carbon regeneration and re-use is found to be more environmentally friendly.

Fig. 6 shows the GWP impact of both organics. Note that the environmental untreated benzene and DCE impact discharges are shown on the ordinate axis. Values are equivalent for both organics

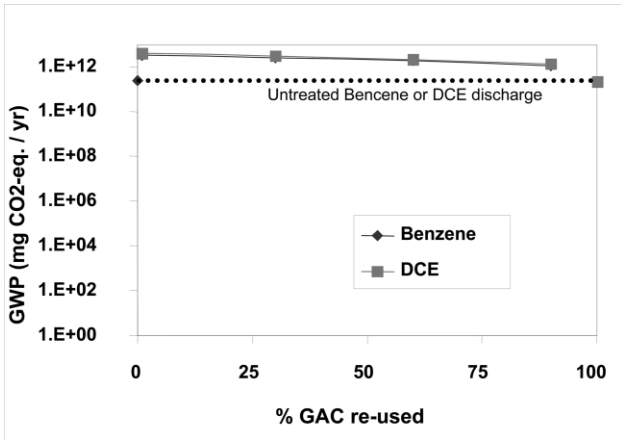

Fig. 6 POC impact of the carbon adsorption process, operating at various degrees of carbon re-use.

since the global warming index is the same for benzene and DCE. The environmental analysis, based on global warming impact, shows that the GAC process is not an effective option for the removal of benzene or DCE, if reduction of global warming is the goal. Setting up and operating a GAC treatment plant causes higher environmental impact than an untreated wastewater discharge! This is consistent for both the benzene and the DCE wastewater streams. Hence, treatment of benzene or DCE results in both higher environmental impact and unnecessary treatment costs.

6. Social implications

The economic and the environmental implications (measured in terms of GWP) of the GAC treatment plant discourage the acquisition of this technology. However, there is a third aspect in the sustainability assessment that changes the picture. The social impact, measured in terms of human and environmental risk, calculates the maximum load of pollutants that can be discharged without posing significant adverse effects to humans' health or the environment in the "surrounding area". This measurement is based on the fact that the environment has a capacity to assimilate substances either by breakdown or dilution, but if this capacity is exceeded, ecosystem and human health damage may occur.

A risk assessment was carried out in order to determine the negative effects that would occur if no treatment technology is adopted. The assessment comprised a mathematical fate model that describes almost all processes involved in the distribution and fate of a substance, including partitioning between the air, water and solid phases within compartments; degradation and advection between compartments; non-equilibrium between compartments; and mass transfer between compartments driven by non-equilibrium conditions. Furthermore, the risk assessment also included information related to toxicity data, safety factors and estimated human dose. The fugacity model and the risk assessment are not presented in this paper due to space limitations. However, a complete description of the fugacity model, which is based on the Mackay level III model can be consulted in the literature[25,26], while the risk assessment is fully available upon request.

Accordingly, the maximum safe discharge values at which no significant risk is posed, were identified. These values indicate that at least 99.8% of the benzene and 99.7% of the DCE must be removed from the waste stream, in order to avoid social consequences. In other words, a treatment technology must be adopted, disregarding the previous finding in which the environmental impact (GWP) was higher than the sole environmental impact of the waste streams. Note that the GAC technology removes 100% of the pollutant.

7. Conclusions

This paper has illustrated the use of life cycle and chemical engineering tools to assess the sustainability of a clean-up technology. The assessment included a mathematical model for process design, and considerations towards economic, environmental and social impacts of the technology.

A typical wastewater treatment technology, carbon adsorption (GAC), and two different chemical waste streams have been used as a motivating example. The mathematical model of the process and its consequent optimal design provided an understanding of the process operation and performance. Benzene and DCE compounds cause different effects on the carbon adsorption treatment process. Treatment costs are lower for the former while total POC and GWP environmental impact is slightly higher for the latter. These results were consistent even under the assumption of an ideal adsorption isotherm.

The mathematical cost optimised model provided economic and environmental information on one of the most common adsorption configurations for industrial wastewater treatment. However, there are several possible configurations that can be applied to the carbon adsorption process ranging from the type of operation (batch or continuous), the type of carbon (powered or granular), and the type and location of carbon regeneration (steam or thermal reactivation; in- or off-site). The optimal process configuration is case specific and depends on factors such as flowrate, type and concentration of pollutants, carbon re-use rate, and removal degrees. Hence, the best design option in terms of economics and environmental impact can only be identified by applying a life cycle analysis approach for each process alternative.

Findings have serious implications on the use of sustainability assessment as opposed to traditional feasibility studies. A traditional approach, applied to treatment technologies, would show that higher degrees of wastewater pollution abatement always lead to lower environmental impacts. Therefore, the degree of abatement

should be as high as possible, while costs should not be excessive. This approach only guarantees a reduction of emissions *within* the process. In contrast, a sustainability approach demonstrates that, under certain conditions, higher degrees of wastewater pollution abatement damage the environment, and probably worst, unnecessarily demand the implementation of treatment technologies. Moreover, this work shows that environmental solutions, such as treatment technologies, may produce a higher environmental impact than the one that can be caused by untreated discharges, as shown in the GWP assessment.

The social evaluation, measured in terms of risk, justified the adoption of a GAC technology. Even if the total GWP environmental impact was higher than an untreated discharge and the cost was around a half million pounds, the social evaluation demonstrated that adverse effects would occur and, therefore, the implementation of the designed technology was morally and legally mandatory. Therefore, in this case the streams should be treated.

The sustainability assessment presented in this work was mathematically robust, so it can also be applied to other areas such as process design and development, green chemistry and technology management. The same approach presented in this paper can be used to evaluate several treatment options such as: steam stripping, incineration, pervaporation and so on. Applying this approach to these technology options will lead to a sustainable comparison for technology selection. In this case, sustainability issues helped to provide a decision making basis, regarding the use of a GAC technology. Ultimately, this approach made the difference on whether "to treat or not to treat".

Acknowledgements

Financial support from Consejo Nacional de Ciencia y Tecnologia (CONACYT - MEXICO) through completion of this work is highly appreciated.
Comments and feedback from Prof. Andrew Livingston and Prof. Efstratios Pistikopoulos during the development of part of this work at the Department of Chemical Engineering, Imperial College of London, UK are highly appreciated

References

1 A. P. Rossiter, *Waste Minimisation through Process Design*, First edn., McGraw Hill, USA, 1995.
2 A. Azapagic, A. Emsley and I. Hamerton, *Polymers, the Environment and Sustainable Development*, First edn., Wiley, UK, 2003.
3 O. Romero-Hernandez, E. N. Pistikopoulos and A. G. Livingston, Waste Treatment and Optimal Degree of Pollution Abatement, *Environ. Eng.*, 1998, **17**(4), 270–277.
4 M. A. Curran, Using Life Cycle Analysis-Based Approaches to Evaluate Pollution Prevention, *Environ. Prog.*, 1995, **14**(4), 247–253.
5 E. Hochschorner and G. Finnveden, Evaluation of two Simplified Life Cycle Assessment Methods, *Int. J. Life Cycle Assess.*, 2003, **8**(3), 119–128.
6 E. N. Pistikopoulos, S. K. Stefanis and A. G. Livingston, A Methodology for Minimum Environmental Impact Analysis, *AIChE Symp. Ser.*, 1996, **90**(303), 150.
7 S. D. Faust and O. M. Aly, *Adsorption Process for Water Treatment*, Butterworths, USA, 1987.
8 M. H. Stenzel, Remove Organics by Activated Carbon Adsorption, *Chem. Eng. Prog.*, 1993, **89**(4), 36–43.
9 W. W. Eckenfelder, *Industrial Water Pollution Control*, Second edn., McGraw Hill, USA, 1989.
10 J. C. Crittenden, M. Asce and W. J. Weber, Predictive Model for Design of Fixed-Bed Adsorbers: Parameter Estimation and Model Development, *ASCE J. Environ. Eng.*, 1978, **104**(2), 185–197.
11 J. C. Crittenden, D. W. Hand, H. Arora and B. W. Lykins, Design Considerations for GAC Treatment of Organic Chemicals, *J. Am. Water Works Assoc.*, 1987, **79**(1), 74–82.
12 D. W. Hand, J. C. Crittenden, M. Asce and W. E. Thacker, Simplified Models for Design of Fixed-Bed Adsorption Systems, *ASCE J. Environ. Eng.*, 1984, **110**(2), 440–457.
13 V. Aelion, F. Castells and A. Veroutis, Life Cycle Inventory Analysis of Chemical Processes, *Environ. Prog.*, 1995, **14**(3), 193–200.
14 US Environmental Protection Agency, *Life Cycle Design Guidance Manual. Environmental Requirements and The Production System*, EPA/600/R-92/226, USA, 1993.
15 SETAC, *A Conceptual Framework for Life-Cycle Impact Assessment*, USA, 1993.
16 BUWAL [Swiss Federal Office of Environment, Forest and Landscape], *Ecobalance of Packing Materials State of 1990*, Environmental Series No. 132, Switzerland, 1991.
17 J. E. Bailey and D. F. Ollis, *Biochemical Engineering Fundamentals*, McGraw Hill, USA, 1986.
18 US National Research Council, *International Critical Tables of Numerical Data, Physics, Chemistry and Technology*, McGraw Hill, USA, 1972.
19 R. A. Hutchins, Thermal Regeneration Costs, *Chem. Eng. Prog.*, 1975, **71**(5), 80–86.
20 J. Q. Adams and R. M. Clark, Evaluating the Cost of Packed-Tower Aeration and GAC for Controlling Selected Organics, *J. Am. Water Works Assoc.*, 1991, **85**(1), 49–57.
21 A. Azapagic and R. Cliff, Life Cycle Assessment as a tool for improving process performance: a case study on boron products, *Int. J. Life Cycle Assess.*, 1999, **4**(3), 133–142.
22 US Environmental Protection Agency, *An International Workshop on Life Cycle Impact Assessment Sophistication*, EPA/600/R-00/023, USA, 2000.
23 R. G. Derwent and M. E. Jenkin, Hydrocarbons and the long-range transport of ozone and PAN across Europe, *Atmos. Environ.*, 1991, **25A**(8), 1661–1678.
24 D. A. Lashof and D. R. Ahuja, The Relative Contribution of Greenhouse Gas Emissions to Global Warming, *Nature*, 1990, **334**, 529–531.
25 D. Mackay, S. Patterson and W. Y. Shiu, Generic Models for Evaluating the Regional Fate of Chemicals, *Chemosphere*, 1992, **24**(6), 695–717.
26 D. Mackay, W. Y. Shiu and K. Ching Ma, *The Illustrated Handbook of Physical-Chemical Properties*, vol. 1, Lewis Pub., USA, 1992.

PAPER

www.rsc.org/greenchem

Towards sustainability and green chemical engineering: tools and technology requirements

C. Tsoka,[a] W. R. Johns,[b] P. Linke[a] and A. Kokossis*[a]

[a] *Centre for Process & Informations Systems Engineering, University of Surrey, Guildford, Surrey, UK GU2 7XH. E-mail: a.kokossis@surrey.ac.uk*

[b] *Chemcept Limited, Crayside, Whitchurch Road, Crays Pond, Reading, UK RG8 7QA*

Received 23rd February 2004, Accepted 29th June 2004
First published as an Advance Article on the web 16th August 2004

We report on a consultation with a panel of senior technical managers within the European process industries. The outcome of the consultation is that, with known and foreseeable technology, the European industry could remain profitable, and reduce pollution by over 20% within 10 years. This paper reports the tools and technologies that are perceived to be important in achieving low pollution levels economically. Alongside established tools such as process simulation, the study gives priority to less established tools including Computer-Aided Molecular Design (CAMD) and process synthesis. The study places a high priority on a range of established and emerging technologies. These include highly selective catalysts, fuel cells, process intensification, supercritical separation and reaction, solar cells, bulk chemicals from renewables, novel chemicals, design for recycle and processes that are economic on smaller scales.

1 Introduction

The chemical process industries are currently the most successful sector of manufacturing industry within Europe. The European Union has identified a sustainable process industry as a major priority. To that end, the EC supported a consultation study with senior industrialists and academics to identify priorities in enhancing the sustainability of the process industries. The study embraced the economic, social and environmental aspects of sustainability. This paper focuses on two aspects of the study, namely the priority tools and technologies for reducing pollution.

The study employed a "Delphi" consultation.[1] We describe the consultation in Section 2. The tools considered, and their rankings, are described in Section 3, and the technologies in Section 4.

It is concluded that, given the political will, the European chemical industry is capable of reducing pollution by over 20% in the next 10 years. Tools that need to be more widely used include Computer-Aided Molecular Design (CAMD) and process synthesis. Technologies that need to be more widely used include highly selective catalysts, fuel cells, process intensification, supercritical separation and reaction, solar cells, bulk chemicals from renewables, novel chemicals, design for recycle and processes that are economic on smaller scales.

2 Delphi methodology

The consultation was undertaken on a European-wide basis with advice taken from experts from Finland, France, Germany, Holland, Hungary, Spain, Sweden and the UK. We also consulted a limited number of US experts in the field. Their input helped in the formulation and analysis of the questionnaires. However, their views were not included in the statistical analysis of results. The consultation was organized as follows:

(1) Telephone and personal interviews were conducted with about 20 experts to elicit their views on the priorities and actions that could be taken to enhance the sustainability of the European chemical process industries. Most respondents were senior industrialists. However, the panel was augmented by relevant academics and with individuals working to improve technology transfer and industrial/academic collaboration.

(2) The interviews were analysed and a set of topics identified. These topics were organized under the headings "Incentives", "Tools", "Technologies", "Communication and Technology Transfer" and "International Competition". A questionnaire was developed to explore views on the topics. Approximately 60 questions were sent to panel members by e-mail or *via* the World Wide Web. The panellists for the questionnaire provided about a 50% overlap with people consulted by telephone. Questions on incentives were formulated requesting views on the effectiveness of each incentive. Other questions were formulated as illustrated in Table 1. Thus, each question could be answered with a tick, with the option of respondents entering additional remarks. The results of this first questionnaire were analysed to determine the majority views on each topic. Where there were clear divisions of opinion, members holding the opinion were asked to support their positions. For example, panel members stating that a technology was "not needed" were asked to support that view against the view that "more R & D is needed". Similarly, arguments from panellists supporting the view "already adequately known" were sought. These arguments were analysed and consolidated. Thus, if several panellists gave arguments supporting the view "not needed", the arguments were compared and the common themes abstracted. The consolidated arguments were returned to the panellists for review. Where indicated by the review, the first consolidated argument was revised and passed for re-review until an agreed consolidation was produced. (In 90% of cases, the consolidation was simple and non-controversial. In the few cases that re-review was needed, the review process clarified the points made.) The objective was to provide a single concise argument to support each position. Where a number of panellists gave the same argument in different words, a single set of words was used to summarize the arguments. Where quite distinct arguments were put forward to support the same position, the arguments were listed separately. The consolidated arguments were sent back to relevant panellists for confirmation, or amendment.

Table 1 Example question: would additional work or information on the following technologies benefit sustainability?

Technologies	Not needed	Already adequately known	More information needed	Needs more R & D
Design for product recycle				

(3) A second questionnaire was prepared. It omitted questions on which there had been complete agreement. It added a few further questions prompted by feedback from the first questionnaire. For each topic from the first questionnaire, the percentage responding to each option was given. Additionally, the consolidated "for" and

DOI: 10.1039/b402799j

"against" arguments were given. The objective of the second questionnaire was to give panellists an opportunity to revise their opinions in the light of the new arguments. As for the first questionnaire, panellists were given the opportunity to raise new points that occurred to them as a result of the first round feedback. The results were analysed, and a consolidated response prepared. Unanimity of view was neither sought, nor expected. Nevertheless, a near-consensus was achieved for many topics.

4) A third questionnaire was prepared. It did not give a further opportunity to revise views. However, it gave the opportunity to report whether the panellists thought that the consultation had been fair and representative. In addition, it introduced a very limited number of additional questions which had been raised in response to the second questionnaire. The feedback was that, with minor caveats, the results were fair and representative of the views of those knowledgeable both of the chemical industry and of the steps needed to progress sustainability.

The consultation was performed over a nine month period. A response level of between 80% and 100% was achieved at each round of consultation ensuring a consistent process.

3 Tools to support sustainability

The panel considered 19 tools that might be of value in enhancing the sustainability of the chemical process industry. Fig. 1 shows the ten tools that more than 10% of the panel considered worthy of more R & D. A further nine tools received little or no support for further R & D. We give here just R & D rankings because we believe that these identify the topics in which substantial progress can be expected. Note that the list excludes tools that are already widely used and will also be employed to develop the next generation of clean processes. For example, process simulation[2] is employed in assessing virtually all new processes and operating improvements. Process optimization[3] is rated relatively low for additional research because it is already well established. Given the opportunity, it is never desirable to design or operate a process in a sub-optimal manner. Hazard and Operability (HAZOP)[4] is an example of an important non-computer-based tool that is routinely employed. The top four tools shown in Fig. 1 can certainly make an impact on sustainability and deserve additional R & D, and support for technology transfer to industry.

It should be emphasized that the list is by no means exhaustive. For example, approximately 300 software tools are routinely used to evaluate the performance and impact of actual or proposed chemical processes. For a selection of tools, we give a brief description of the tools and a discussion of their relevance to pollution minimization below. A fuller list can be seen at the site maintained by Process and Information Systems Engineering (PRISE) at the University of Surrey.

Computer-aided molecular design

Harper *et al.*[5] and Marcoulaki and Kokossis[6] give recent developments in CAMD. The primary goal of the chemical process industries is to sell effects; it only incidentally sells chemicals. The desired effect may be solvent action, detergent action, refrigeration *etc.* CAMD provides tools to design molecules with desired effects and, at the same time, to eliminate undesired side effects. For example, it can design a chemical that has a desired solvent action, but avoids ozone depletion and certain toxic properties. The tool is needed because of the vast numbers of possible chemical species that could exist. For example, the number of possible different chemical species that could be synthesized from 20 carbon atoms and 42 hydrogen atoms exceeds the number of chemicals known to mankind (including natural and synthetic chemicals). CAMD builds on tools to predict the chemical, physical and environmental properties of chemicals from their chemical formulae. It seeks to determine a formula that provides a favorable combination of commercial and environmental properties. Clean chemicals are central to a clean chemical industry.

Further work in the area should provide better ways to predict some of the important environmental impacts of molecules. Additional research should also provide improved methods to solve the optimization problem of "inventing" molecules with the best combination of economic and environmental characteristics.

Integrated process and product design

In developing a sustainable industry, we are concerned with the total environmental impact of the process to manufacture the product and of the product itself. The objective of integrated process and product design is to minimize the total environmental impact by designing both the product and the process as an integrated whole. The principle of the approach is readily accepted. However, the approach lacks a formal methodology and needs support from computer tools. Specifically, a tool that combines CAMD and process synthesis would be desirable. Recent developments in this direction appear promising.[7,8]

The technology is at the very early stages of development. There have been very limited applications. Furthermore, there is not yet a formal methodology for the approach. There are no integrated computer tools and no formal non-computer methods similar to HAZOP (for safety), or environmental critical assessment. It is

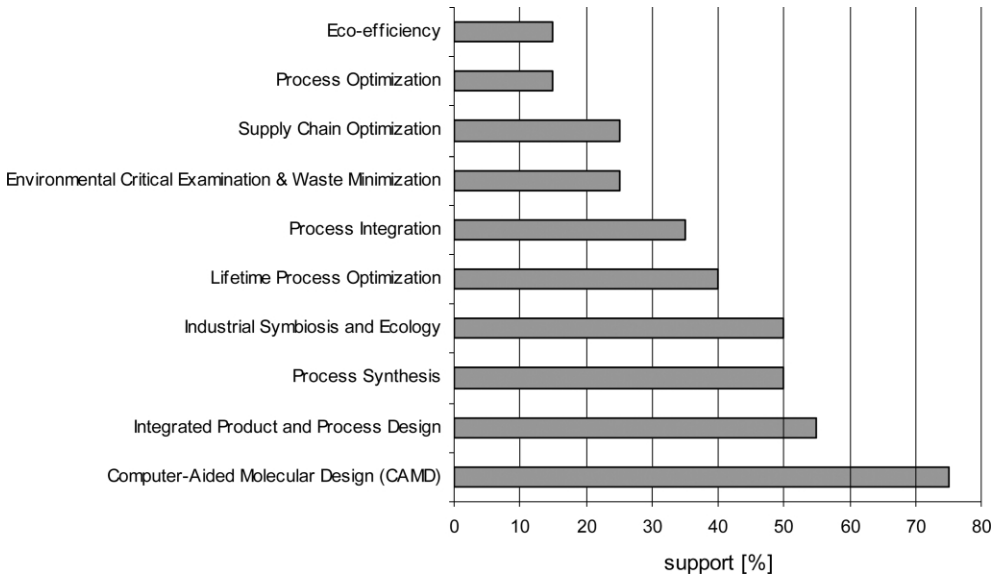

Fig. 1 Tools to support sustainability.

probable that more work is needed on supporting tools such as CAMD and process synthesis before substantial progress will be made.

Process synthesis

Process synthesis has been known for over thirty years, and successful, environmentally significant applications have been reported. However, it is only recently that generally available tools are being developed. The history and current status of the technique is described by Johns,[9] and some recent developments are given by Linke and Kokossis.[10] Process synthesis extends optimization to include discrete variables, such as number and sequence of operating units, choice of extracting agents and selection of recycle streams. The optimization is computationally difficult. There are three competing approaches (AI, superstructure and implicit enumeration), and none is yet sufficiently mature for routine application. The major goal is to identify promising process structures, reactants and extractants. Once the process topology has been identified, conventional simulation and optimization can be employed to fine-tune the design. The software addresses the problem that, even for apparently simple processes, there are hundreds of millions of variants that could be made to work. It is not practicable for the human designer to look at more than a dozen or so in any detail.

It is common experience that real-value optima are flat. Thus, there is a value from conventional optimization, but it is small compared to the radical design improvements that can result from a process synthesis study. There are examples where effluents have been eliminated entirely, and major cost savings have resulted from eliminating equipment items. Commercial activity in process synthesis is in its infancy, and still needs to be backed by a vigorous R & D activity.

Industrial ecology and symbiosis

Industrial ecology is a system-oriented approach that seeks a balance between industrial systems and natural ecological systems. Industrial symbiosis is the methodology that is employed within the general framework of industrial ecology; it includes the environmental cost in the production and consumption processes. It stimulates industrial clusters or "eco-industrial" parks, in order to maximize the use of co-located operations, which can reuse the wastes of one process as "raw materials" for another.

The areas currently being analysed are the chains of products and materials, the human influence on biochemical cycles, and issues related to production. Issues related to production include product and process design, environmental management systems, environmental supply chain management, and eco-industrial parks. A successful example of industrial symbiosis exists in Denmark, in the eco-industrial park. However, much work needs to be done before generally applicable tools become available. The topic is perceived to be important also from the symbiosis of industry and community whereby wastes from both sources are minimized. More details on industrial ecology can be found in Ehrenfeld.[11]

Opponents of industrial ecology believe that the potential is overrated because:

(1) The possibilities for use of residues in other industries are limited and depend on spatial proximity (*e.g.* in eco-industrial parks). There are also serious disadvantages. Production facilities become linked so that supplies of unrelated products must be made in proportion. Where the demand for one declines and the other increases, production problems result. Either process "A" has to be kept in production to consume the by-product of process "B", or production of process "B" has to be curtailed. Thus, in practice, it is only applicable for manufacture that forms a very small part of the total production of each product.

(2) It is also complex to design, operate and manage. There are insurmountable problems in organizing and maintaining synchronized production facilities.

(3) It is thought of in terms of "by-product synergy" or "waste to product opportunities". In that narrow sense, there is limited scope. However, the broader problem of identifying and re-using significant waste streams across industry sectors is important.

Lifetime process optimization

Conventional optimization does not take into account the wear and tear on a process resulting from load changes, or operation under extreme conditions. An alternative method that enables an effective compromise to be struck between instantaneous profit and long plant life by including constraints on wear and tear into the problem formulation would be advantageous. The incentive to employ such a tool is clear; however, the impact may be limited compared to the tools discussed above.

Process integration

Process integration is the best-established technical approach for improving sustainability. The most frequently applied process integration technique is Pinch technology which allows the calculation of targets for energy and waste minimization.[12] Related methods have been extensively employed to reduce energy consumption. Significant reductions (> 40%) have been achieved in numerous cases. Pinch technology is now an established area that is taught in undergraduate and postgraduate courses. It has delivered, and will continue to deliver, major economic and environmental benefits to industry. It is one of the few tools to have a track record of simultaneously reducing cost and reducing energy use. As it is generalized beyond energy reduction, it becomes more closely integrated within the broader area of process synthesis.

Environmental critical examination and waste minimization

These are both panel, or team-based, exercises. Both have been applied successfully during the last ten years. They employ formal step-by-step methods of identifying wastes or pollutants and determining how they can be reduced. The waste minimization methodology is described in the IChemE "Waste Minimization Guide"[13] which was initially developed from US Environmental Protection Agency Guidelines. Environmental Critical Examination[14] is an environmental analogue of Hazard and Operability (HAZOP) analysis. Although having different origins, much of the methodology is common to both.

Process optimization

Process optimization builds on process simulation to optimize process design and operation. By restricting the optimization to controllable variables such as pressure, temperature and flow rate, existing plant operations can be optimized. These optimizations can be undertaken off-line, or can be incorporated into on-line optimizing control. By extending the optimization to include design variables such as unit sizes and shapes, design optimization can be achieved. Optimization can maximize profitability or minimize release of pollutants. It can also achieve a desired optimal balance between profit and pollution. Supply chain optimization takes a broader (but less detailed) view to model the whole supply chain including production and distribution.

Eco-efficiency

Eco-efficiency is described by Saling.[15] It is a method to facilitate the rapid assessment of the life-cycle environmental impact of new processes, or proposed process modifications. It is designed to focus on those elements critical to environmental performance and hence assist the designer to select the best compromise between profitability and pollution. There are many competing methods for analysing life-cycle impacts and this tool is just an example of those available. As such, the support it received can be viewed as a general reflection of support for this range of tools.

4 Technologies to support sustainability

The tools and methods described above result in efficient ways of deploying known technologies. However, the results achieved depend on the technologies that the designer has already considered using. It is expected that the next generation of "clean" processes will include enhanced technologies to deliver improved performance. Some of these technologies will be new; some will be developments of well-known technologies that currently have limited application. Fig. 2 gives a list of technologies ranked in order of research priority.

Fig. 2 includes only technologies that are currently not used extensively. Many already extensively-used technologies will continue to play an important role, including methods for energy and material recovery. Brief reasons why some of the technologies listed in Fig. 2 may be important for sustainable processes are given as follows.

It should be emphasized that the list is not an exhaustive list, it covers only those technologies noted by more than one person in the preliminary discussions from which the questionnaires were drawn up. An exhaustive consideration of all the technologies that may be relevant in providing better sustainability was beyond the scope of the project.

Highly-selective catalysts

Such catalysts make better use of raw materials and produce less by-products and waste. In principle they improve both profitability and environmental performance.

Process intensification

There are a series of technologies that enable equipment sizes to be radically reduced. These include, amongst others, spinning disc reactors, reactive distillation, and high specific surface heat exchange. The state of the art in process intensification technologies is discussed in Moulijn and Stankievicz.[16] Such technologies enable plant sizes to be correspondingly reduced. The very low inventories have environmental benefits and there are also claimed cost benefits. An important incidental benefit is that the processes may be economic on a smaller scale. (See discussion below on small-scale processes.)

Fuel cells

Fuel cells offer the prospect of more efficient conversion of chemical energy to electrical (and hence mechanical) energy. The comparison is with traditional heat engines. It is over 100 years since fuel cells were proposed. For most of that time applications have been very limited. However, recent developments (for example, better understanding of the physico-chemical processes which allow computer modelling and optimization) make fuel-cells a more attractive proposition.

Compact units that convert chemical energy directly to electrical energy at high thermodynamic efficiency and with no moving parts provide the promise of wider application. However, the panel felt that the main application was for transport use and for local electricity production (for example, replacing diesel generators). Specific chemical industry applications are likely to be limited.

Bulk chemicals from renewables

Vegetable raw materials are already employed for products at the scale of many thousands of tonnes per annum. The objective is to use raw materials that can be replaced indefinitely by natural processes. It is only when we have achieved this goal that the chemical process industries can become truly sustainable. Currently, only a trivial proportion of chemical production comes from renewable resources. Thus, the chemical industry can make no claim to be sustainable. Any significant change will require long-term commitment. Some panellists held the alternative view that the priority for renewable raw materials is lower in the chemical industry than in many other industries. Thus, only 8% of total world hydrocarbon production goes to chemical manufacture. There is a broader problem of which the chemical industry is only a small part.

Supercritical separation and reaction

Solvents become more effective under supercritical conditions (for example supercritical carbon dioxide). The greater efficiency can obviate the necessity to use aggressive materials. There may also be energy benefits because latent heat effects are minimized.

Novel chemicals

The objective is to develop new replacement chemicals with lower environmental impact in their production or use. The laboratory and technical scale research required to commercialize novel chemicals complements computer-based methods such as CAMD that suggest chemicals with improved properties.

Solar cells

Solar cells provide the prospect of inexhaustible energy without depleting mineral resources, or generating pollution. Currently efficiencies are extremely low, so that manufacture and installation is costly and has a significant environmental impact. Work on solar

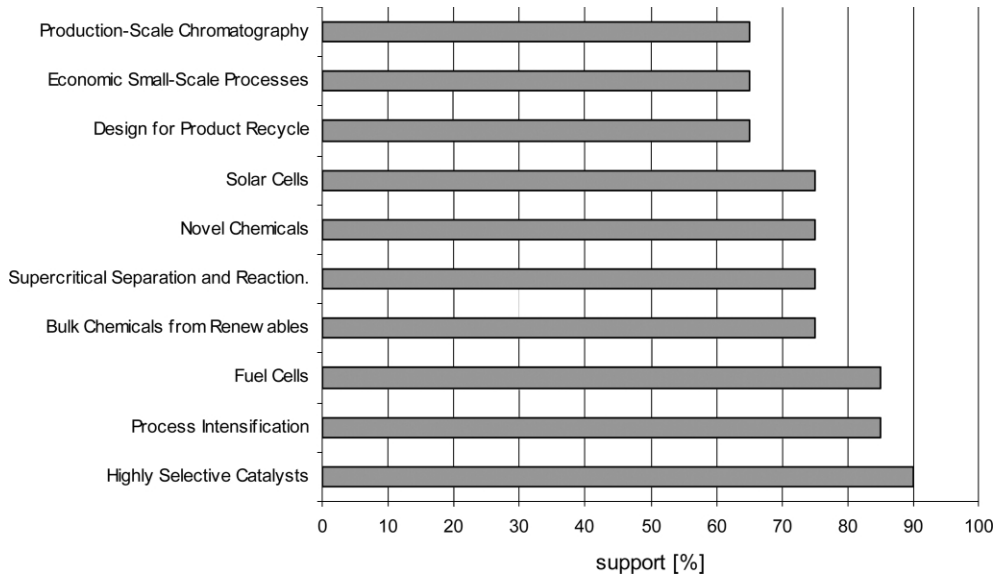

Fig. 2 Technologies for sustainable processes.

cells is justified because of their broad application. However, solar energy has a relatively low impact on the sustainability of the chemical industry; it is just an alternative source of electrical energy.

Design for recycle

Products should be designed so that they can be recycled. Thus, the recyclability of the product should be considered from the earliest stages of conceptual design through to the detailed design of both the manufacturing process and the processes needed to effect recycling at the end of its useful life. This recycle design could include new reprocessing facilities, or the product could be designed to make use of existing facilities. In either case, product recycling is an integral part of the design. The principles are generally well known. However, the problem is to make an economic case, which has to be done on a case-by-case basis. Far higher priority should be placed on waste reduction than re-cycling.

Economic small-scale processes

The chemical industry is well aware of economies of scale. The rationale for such economies is that as you double the linear dimension of the plant, you quadruple the surface area and multiply the throughput (vessel volumes, flow-rates) by eight. The capital cost is roughly proportional to the surface area. Thus, doubling the linear dimension roughly halves the capital cost per unit throughput. There are further benefits in that heat losses and material leakages are roughly proportional to surface area. Thus the energy and material efficiency also improves with equipment size. Better energy and material efficiencies provide environmental benefits. The inverse of this finding is that the processes become more expensive and less efficient when built on a small scale. Large-scale plants do, however, have the disadvantage that raw materials and products may need to be transported over large distances, with corresponding costs and environmental impacts. There are benefits to developing technologies that are efficient on a small scale.

Production-scale chromatography

The technology is energy-efficient and highly selective. It can be used at near ambient conditions. In this respect, it contrasts with traditional widely used technologies such as distillation. However, following separation by chromatography, there remains a significant cost in removing the desired product from the carrier. Foreseeable developments in chromatography should enable both economic larger-scale applications and more cost-effective ways of removing desired products from the carrier. The flexibility of chromatography may also find applications in economic small-scale production.

Microbiological processes

Many microbiological processes are highly selective, and thus avoid by-products. They also take place under near-ambient conditions. However, a major disadvantage is that the desired product is frequently only present as a fraction of a percent. Thus, the manufacture of a few grams of product might require the processing of tonnes of contaminated and slightly warm water. Waste treatment and energy recovery for this depleted nutrient solution is difficult. The environmental benefits are thus very case specific. More extensive use of microbiological process in the pharmaceutical industry is foreseen. However, for general application, biotechnological processes are rarely clean or environmentally friendly. Most such processes utilise raw materials in a very inefficient way and produce substantial quantities of polluting wastes. For example, wastes are characterized by high Biological Oxygen Demand (BOD). Thus, biotechnology is seen as holding an important niche, rather than having potential wide-scale application in the chemical industry. Indeed, for bulk chemicals and some pharmaceuticals, there are often pollution and cost benefits in switching from microbiological processes to more traditional chemical processes.

Carbon dioxide capture and re-injection

The principle is to inject carbon dioxide into underground reservoirs for indefinite storage. The rationale is that, if methane has been safely stored underground for geological times, the same geological reservoir can be used to store carbon dioxide. In this way, we can continue to use natural gas (and other mineral fuels) with no net effect on the environment until they are all depleted. Indeed, carbon dioxide is a less effective global warmer than methane, so we may actually be benefiting the environment.

The major concern is that the large uncertainties may only be resolved on a geological timescale. The uncertainties cannot be resolved by conventional research. Considering the cost-balance between re-injection and methods of reducing carbon dioxide production at source, it was felt that the probability of successful application by the chemical industry is small.

Wind power

The wind provides an inexhaustible supply of renewable energy. It appears that, with increasing scale, wind power is becoming more economic. However, from the chemical industry viewpoint, wind power is just another source of bought-in electricity.

5 Scope for improvement with known methods

Industry-based members of the panel noted that European industry had spent large sums of money in anticipatory research. They had expected the EU to move faster in encouraging more sustainable technologies. As such, there is already the capability to reduce pollution levels significantly if the incentives are provided. A separate study was made of the effectiveness of incentives. This study showed that the consensus belief is that pollution levels could be considerably reduced without destroying international competitiveness. For example, we received the following response to the question, "what reduction in pollution could be delivered over 10 years with appropriate fiscal incentives". With the proviso that the incentives had to be neutral (thus not increase the total tax burden on industry), the following response was obtained:

Mean estimation of reduction: 22.0%, standard deviation of response 11.5%.

If we restrict the question to industrial respondents, the response was:

Mean estimation of reduction: 24.0%, standard deviation of response 13.0%

Thus, industrialists who were aware of the anticipatory R & D already undertaken were more confident of reductions than academics. (However, the statistical significance of the difference is clearly very low.)

Details of a much broader study are given in a forthcoming publication.

6 Discussion and conclusions

The Delphi method has provided an effective means of consulting a geographically dispersed panel. The consultation has provided a broad consensus that substantial reductions in pollution are possible. However, these reductions can only be achieved by establishing a fiscal environment in which taxes reflect environmental impacts. With, or without, such incentives, some reduction will be delivered.

The radical advances needed to deliver the improvements will come from deployment of new tools and introduction of novel technology. Specifically, two computer-based tools will need to be more widely deployed. The tools are computer-aided molecular design and process synthesis. In the longer run, such tools are likely to be integrated to provide effective means for the integrated design of products and processes. These computer-based tools will be used

alongside more traditional means of designing products and processes. Computers alone cannot include all the operability and safety characteristics that must be considered before any new process or product is brought on line.

The most important improved technologies required specifically by the chemical industry seem to be highly selective catalysts, process intensification, supercritical separation and reaction and novel chemicals. In recent years, catalyst development has advanced from a black art to a science. The advances have built on improved understanding of the chemical and physical behaviour of molecules at surfaces. Process intensification builds on well-known phenomena, such as enhanced contact and separation under high gravity. It also benefits from improved fabrication methods on a small scale. Supercritical separation and reaction is achieved from a better understanding of near-critical conditions. "Novel chemicals" may be "invented" using CAMD. However, the important advances are in the ability to predict physico-chemical properties from molecular structure. Such advances facilitate both computer-based methods and methods based on human insight. All the novel technologies depend on laboratory chemistry and small-scale prototype processes to verify the benefits and practicability.

Acknowledgements

The authors acknowledge the support of the European Commission for this research, under contract number G1MA-CT-2002-00016.

References

1 *The Delphi method: techniques and applications*, ed. H. A. Linsto, Addison–Wesley Pub. Co., Reading, MA, USA, 1975.
2 W. L. Luyben, *Process Modelling Simulation and Control for Chemical Engineers*, London, Mc Graw-Hill, New York, 2nd edn., 1990.
3 U. M. Diwekar, *Introduction to Applied Optimization and Modeling*, Kluwer Academic Publishers, Netherlands, 2003.
4 T. A. Kletz, *HAZOP and HAZAN: Identifying and Assessing Process Industry Hazards*, IChemE, Rugby, 4th edn., 1999.
5 P. M. Harper, R. Gani, P. Kolar and T. Ishikawa, Computer-aided molecular design with combined molecular modeling and group contribution, *Fluid Phase Equilib.*, 1999, **158–160**, 337–347.
6 E. C. Marcoulaki and A. C. Kokossis, On the development of novel chemicals using a systematic synthesis approach. Part I. Optimisation framework, *Chem. Eng. Sci.*, 2000, **55**(13), 2529.
7 P. Linke and A. C. Kokossis, Simultaneous synthesis and design of novel chemicals and chemical process flowsheets, *Comput. Aided Chem. Eng.*, 2002, **10**, 115–120.
8 A. I. Papadopoulos and P. Linke, *An Efficient Decomposition-based Approach For The Integrated Design of Solvents and Processes*, paper 426t, AIChE Annual Meeting, San Francisco, CA, 2003.
9 W. R. Johns, Process Synthesis: Poised for a wider role, *Chem. Eng. Prog.*, 2001, **97**(4), 59–64.
10 P. Linke and A. C. Kokossis, Attainable designs for reaction and separation processes from a superstructure-based approach, *AIChE J.*, 2003, **49**(6), 1451–1470.
11 J. R. Ehrenfeld, Industrial ecology: A framework for product and process design, *J. Cleaner Prod.*, 1997, **5**(1–2), 87–95.
12 R. Smith, *Chemical Process Design*, McGraw-Hill, New York, 1995.
13 B. D. Crittenden and S. T. Kolaczowski, *Waste Minimization Guide*-Institution of Chemical Engineers, Rugby, UK, 1992.
14 W. R. Johns, G. M. Smith, K. Cherrill and E. P. Whitley, *Pollution Control for Processes Involving Uranium*, report IC3235-1, Intera Information Technologies Ltd., Henley-on-Thames, UK, 1993.
15 P. Saling, A. Kicherer, B. Dittrich- Krämer, R. Wittlinger, W. Zombik, I. Schmidt, W. Schrott and S. Schmidt, Eco-efficiency analysis by BASF—The method, *Int. J. Life Cycle Assess.*, 2002, **4**, 203–218.
16 *Re-Engineering the chemical processing plant*, ed. J. A. Moulijn and A. Stankievicz, Marcel Dekker, The Netherlands, 2003.

PAPER

Environmental impact minimization through material substitution: a multi-objective optimization approach

André Hugo, Céline Ciumei, Andrew Buxton and Efstratios N. Pistikopoulos*
Centre for Process Systems Engineering, Department of Chemical Engineering, Imperial College London, London, UK SW7 2BY. E-mail: e.pistikopoulos@imperial.ac.uk; Fax: +44-20-75946606; Tel: +44-20-75946620

Received 6th February 2004, Accepted 24th June 2004
First published as an Advance Article on the web 13th August 2004

In this paper, we present a process design methodology for identifying opportunities where step-change improvements in *both* process economics *and* environmental impact can be achieved. In particular, the use of computer aided molecular design techniques is proposed as a method for identifying alternative processing materials that can lead to improved designs. Fundamental to the overall approach is the formulation of environmental performance objectives to drive the process design decisions. For this task, a recently developed method of damage modelling for life cycle impact assessment is used to derive an explicit environmental performance metric. Trying to give consideration to not only the traditional financial objectives, but also the multiple environmental concerns, inevitably results in the process design task being formulated as a multi-criteria decision-making process. Using multi-objective optimization techniques, a set of alternative trade-off designs is established that reflect the conflict between the economic and environmental concerns. Accepting that this inherent conflict exists, whereby one objective can not be improved without sacrificing another, the next task is to modify the process through the use of alternative materials in search of superior designs. Focussing specifically on liquid–liquid extraction operations, extensions to our previously developed methodology for designing solvents that are both environmentally benign and cost effective are presented as part of the overall methodology.

1 Introduction

Progressively, the chemical processing and manufacturing industry has been faced with escalating waste treatment costs and stricter regulatory compliance limits. The result is that the traditional end-of-pipe abatement approaches to waste management have started losing their attractiveness. Instead, manufacturers are increasingly interested in adopting waste minimization, waste reduction and pollution prevention strategies *at source* during the very early conceptual stages of chemical process selection, design and optimization.

In their extensive review of over 180 citations related to the area of environmentally conscious process design, Cano-Ruiz and McRae[1] bring together a variety of approaches that consider avoiding environmental damage as a part of the process design objectives. Undoubtedly, the most important conclusion from their review is that adopting a strategy that considers the environment as a design objective and not merely as a constraint on operations can lead to the discovery of novel processing alternatives that achieve both improved economic *and* environmental performance.

However, formulating the process design problem such that environmental concerns are treated as design objectives instead of constraints, requires (a) quantifying suitable environmental performance measures, and (b) balancing the environmental criteria against the traditional cost incentives. Especially, the selection of appropriate performance indicators has proven to pose a significant obstacle in developing a design strategy driven by an environmental objective. Efforts have, therefore, focussed on developing indices that can be used within a quantitative process design framework.[2,3] In this respect, Life Cycle Assessment (LCA) has also proven to facilitate the environmental impact assessment of a process design.[4] It allows the environmental performance of a product, process or service to be quantified from "cradle-to-grave", *i.e.* from natural resource extraction to final use and disposal.[5]

Once the suitable impact assessment techniques have been applied, the resulting environmental performance measures can be traded-off against the economic objectives—as well as against each other—to generate and evaluate alternatives. A number of design methodologies have incorporated multiple criteria decision-making (MCDM) techniques as part of the process selection task. Multi-objective optimization, being one particular MCDM approach, tries to identify the set of non-inferior alternative solutions before they are explicitly evaluated.[6] As such, the feasible alternatives are not explicitly known in advance and it is acknowledged that an infinite number of solutions potentially exist. A representative selection of process design and synthesis methodologies that employ the principles of multi-objective optimization to account for *environmental* considerations is reviewed in Table 1. In all the methodologies particular attention is given to the use of advanced Environmental Impact Assessment (EIA) methods to construct the

Table 1 Examples of environmental and economic trade-offs in process design

Authors	Problem type	Method of EIA	Objectives	Solution technique
Fu *et al.*[7]	Simulation and optimization	PEI[3] 6 indicators	Profit and indicators	Constraint method and interactive NLP
Hoffmann and Hungerbühler[8]	Simulation and screening	Material intensity per service unit (MIPS)	Profit and IMPS	Explicit alternative evaluation
Alexander *et al.*[10]	Simulation and optimization	LCA[45] 2 indicators	Rate of return and indicators	Multi-stage goal programming
Azapagic and Clift[11]	Optimization (moLP)	LCA[45] 7 indicators	Operating cost and indicators	Constraint method
Dantus and High[9]	Stochastic programming	EII[46]	Profit and indicator	Simulated annealing and compromise programming
Lakshmanan and Biegler[12]	Reactor synthesis (moMINLP)	Waste stream compositions	Profit and waste load	Constraint method
Stefanis *et al.*[13]	Optimization (moNLP)	LCA[45] 6 indicators	Operating cost and indicators	Constraint method

DOI: 10.1039/b401868k

environmental objectives. For example, the WAR algorithm[3] is used to arrive at six Potential Environmental Impact (PEI) indicators which enter together with a profit objective function into the multi-objective formulation.[7] Not all the examples listed in Table 1, however, *strictly* apply the principles of multi-objective optimization. Some aim at explicitly evaluating and screening a pre-determined set of possible technological alternatives in terms of multiple objectives.[8] Hybrid methods that rely upon the interaction between an external optimizer and process simulation packages are also popular.[9,10] The remaining examples that adopt a more rigorous mathematical programming based approach can be classified according to the type of solution method used. In the examples that do not require the articulation of the decision maker's preferences in advance, the ε-constraint method is the most commonly chosen solution approach and is used to solve problems of multi-objective linear programming (moLP),[11] multi-objective mixed integer nonlinear programming (moMINLP),[12] and multi-objective nonlinear programming (moNLP).[13]

The use of multi-objective optimization techniques allows the conflict between the emerging environmental concerns and the conventional business incentives to be explored for a given design. Accepting that this inherent compromise exists, the goal is still to try and identify opportunities of so-called "*win–win*" scenarios where step-change improvements in all the performance criteria are simultaneously achieved. While such improvements can be achieved by finding alternative process topologies and technologies, molecular design offers the advantage of actually avoiding the creation of damaging substances by identifying substitute materials that are both more environmentally benign and cost-effective.

Material design has long been recognised as a key process engineering objective with a variety of techniques reported in the literature. These methods have been applied to the design of a wide range of materials, including solvents, extractants, refrigerants, CFC substitutes, polymers and drugs. Various solution techniques have been used, some of which include automated and interactive enumeration,[14] single and multi-stage screening and ranking,[15,16] multi-stage optimization,[17,18] stochastic optimization,[19] mixed integer linear programming (MILP),[20,21] local mixed integer nonlinear programming (MINLP),[22] mixed integer dynamic optimization (MIDO)[23] and global MINLP optimization.[24]

With this diverse array of solution strategies, numerous objective functions have also been employed. However, the most common application of material substitution by far has been the design of materials with desired processing properties. Only in a limited number of studies have environmental objectives explicitly been used as part of the material design task.[24,22,25] While these approaches include environmental considerations, it was argued that in order to fully exploit the potential that material design techniques have to offer to the environmentally conscious process design problem, it is not sufficient merely to design materials which are themselves environmentally benign.[18] In addition, the *plant-wide* environmental performance of the selected material must also be taken into account. Only at a systems level where the entire process and its life cycle is considered can the selection of alternative materials achieve consistent, cost optimal and environmental benign results. Consequently, within the Methodology for Environmental Impact Minimization (MEIM) of Pistikopoulos and co-workers,[18] a multi-stage optimization procedure for the identification of alternative solvents was formulated for a separation process of interest.[17]

This procedure demonstrated that material substitutes could be identified that are economically and environmentally promising, both within themselves *and* on a global, plant-wide basis. However, as processing, economic and environmental demands become ever more stringent, the identification of appropriate single materials becomes ever more difficult. Material blends however, provide access to a wider range and combination of properties than single materials can offer. Furthermore, their compositions may be tuned to meet demanding operational constraints. Accordingly, MEIM was extended and applied to the design of solvent blends for non-reactive, multi-component absorption processes.[17]

In this paper, we present an extension of the previously developed Methodology for Environmental Impact Minimization, focussing on the multi-objective comparison of different process/material design alternatives. First, an overview of the methodology is presented, showing how a recently developed environmental damage modelling approach to LCA can be used to formulate environmental design criteria. In this section, a generic multi-objective optimization algorithm for detecting Pareto optimality is also presented. Next, the key features of the procedure for the design of solvents for non-reactive, multi-component liquid extraction processes is summarised. Instead of presenting an exhaustive discussion of the solvent design procedure, only the most recent developments and contributions compared to previous work are highlighted. In particular, the introduction of extended mixture property verification is described. In this new feature, full mixture property prediction techniques are employed to verify compliance with task level mixture property bounds. New verification level azeotropy and phase stability tests are also introduced. At the task level, the implementation of improved molecular structural feasibility constraints and the development of new mass transfer feasibility constraints based on liquid equilibrium considerations are also briefly discussed. The paper concludes with a demonstration of the procedure to an illustrative example problem where it is shown how the plant-wide integration of alternative materials can offer step-change reductions in *both* process economics *and* life cycle environmental damage.

2 Motivating example

Consider a design specification for the industrial production of 150 tons per day of crude acrylic acid (95% pure on a weight basis) from propylene, air and steam. As shown in Fig. 1, preliminary design tasks have established that a feasible manufacturing route involves a reactor, followed by a cooler, an absorption column (using demineralised water as absorbent), a solvent extraction column and a distillation column for solvent recovery and product purification. Efficient operation of the reactor requires rapid cooling of the outlet stream in order to avoid further oxidation reactions. A cooler combined with quenching in an absorption column perform this task. The absorption also separates the acrylic and acetic acid from the light vapour components. The vapour stream leaving the absorption tower is, therefore, rich in nitrogen, carbon dioxide, steam and unreacted oxygen and propylene and is considered to be the main gaseous emission leaving the process.

The liquid stream leaving the absorber is a dilute aqueous acid stream which is sent to a liquid–liquid extractor where it is contacted with a suitable organic solvent to preferentially separate the acid and water fractions. To facilitate the recovery of the solvent in the extract, it is desirable to have a low boiling solvent, *i.e.* one that has a boiling point lower than that of the desired organic components. Di-isopropyl ether (DIPE) is the existing (base case) solvent used for this separation task. The aqueous raffinate stream leaving the extractor is emitted into the environment and contains trace amounts of acrylic acid, acetic acid and DIPE. Critical to the operation of the liquid–liquid extractor and the environmental damage caused by the process is the choice of organic solvent. To improve the economic and environmental performance of the process, the solvent has to have high capacity and selectivity combined with low toxicity. Such improvements can only be achieved by substituting the solvent. Alternatives should, however, also be verified at a process-wide level in terms of both economics and life cycle environmental impact. The need for a multi-objective systems analysis becomes even more apparent when one realises that the energy demand of the downstream regeneration column is also affected by the chosen solvent. And since the energy input to the distillation column carries off-site emissions with it, the

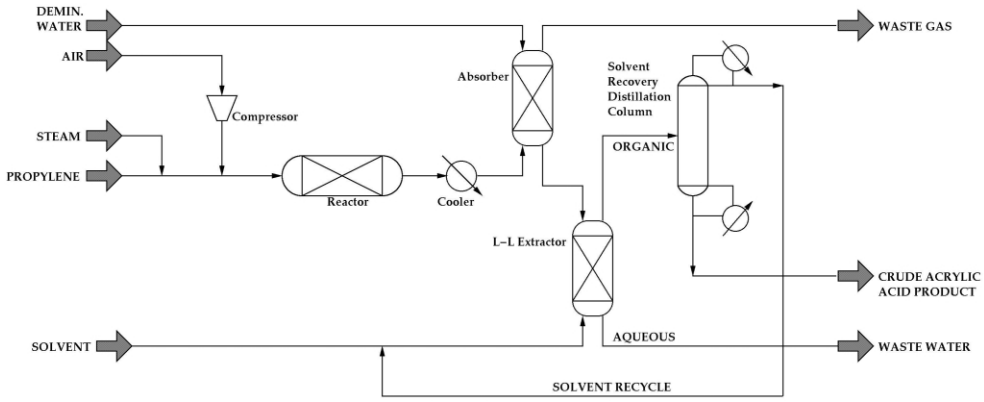

Fig. 1 Acrylic acid production flow diagram.

selection of an appropriate solvent is critical to the life cycle environmental performance of the design.

3 Methodology for environmental impact minimization

3.1 Problem formulation

The environmentally conscious process design problem addressed in this paper can be formulated as follows:

Given:

• the demand for a chemical product and a potential manufacturing process model

• a set of alternative processing options related to separation technologies, purification sequences, raw material feedstock and mass separating agents

• capital and operating cost data

• life cycle assessment related information, such as emissions inventories and characterisation factors

then the objective is to:

explicitly formulate objectives that represent both the economic and environmental performance of the process and to determine the optimum design giving simultaneous consideration to the multiple objectives.

The purpose of this process design problem is, therefore, to determine the process flowsheet, equipment specifications and operating conditions that achieve both the optimum economic and environmental performance. The choice of the economic performance criterion is a standard feature of almost all process design tasks. However, the key part of the environmentally conscious process design problem is the formulation of the *environmental* objectives. This requires the use of life cycle assessment and appropriate environmental impact assessment methodologies.

3.2 Impact assessment: Eco-Indicator 99

Although a number of impact assessment methods exist for use during life cycle assessment, very few account for the temporal and spatial behaviour of pollutants. One of the more recently developed methods for life cycle analysis is the so-called Eco-Indicator 99.[26] Unlike most other approaches that try to model the impacts, the Eco-Indicator 99 method attempts to model the potential damages. It is, therefore, classified as a damage-oriented approach which aims to assess the adverse effects on a European scale according to three main damage categories: Human Health, Ecosystem Quality and Resources.

More specifically, four steps are followed to arrive at the single Eco-Indicator value for a particular process. The first step takes the emissions inventories and feedstock requirements and analyses the fate of the emissions and the extraction of the resources. Step two, the Exposure and Effect Analysis step, determines how much of a substance released into the environment is actually taken in by living life forms, such as plants, animals and humans. The effect that resource extraction has on future generations is also analysed at this stage. The result is the classification of the impacts according to 12 indicators—some of which are common to most impact assessment methods, such as climate change, ozone layer depletion, acidification and eutrophication, and ecotoxicity. The third step, Damage Analysis, quantifies the impact of each category by using a damage factor. The 12 indicators are then aggregated to form the three main damage categories: Damage to Human Health, Damage to Ecosystem Quality, and Damage to Mineral and Fossil Resources. Finally, the three main categories are put on a common dimensionless basis through normalisation and then by assigning scores/weighting factors of relative importance to each category a single aggregated Eco-Indicator 99 value can be calculated. Since assigning relative importance to the different impact categories is a subjective exercise, the Eco-Indicator 99 methodology provides three different "perspectives" based upon the principles of Cultural Theory.

The Eco-Indicator 99 methodology offers a number of advantages over other methods, the most important advantage being the systematic way that it approaches the subjective procedure of scoring the relative importance of the different impact categories. It offers the advantage of arriving at a single value that is representative of all the different environmental concerns. Of equal merit though, is the advantage that the calculation procedure can be "interrupted" at any stage according to the particular needs of the impact assessment. For example, if it is desired to represent the potential damage caused by a process without any normalisation then the calculations are merely terminated before the normalisation step.

Next, a general mathematical framework will be developed for including the Eco-Indicator 99 within process systems decision-making models.

Set definition. Following the structure of life cycle assessment, the first step is to define in accordance with the Goal and Scope Definition appropriate sets of:

• environmental burdens (emissions), $b \in \mathcal{B}$,

• damage indicators, $e \in \mathcal{E}$,

• normalisation categories, $n \in \mathcal{N}$, and

• life cycle stages, $p \in \mathcal{P}$.

Starting with the set of environmental burdens, a list of all the various emissions and resources that will be considered in the study must be identified. This set is typically of high dimensionality, containing many hazardous chemical compounds and scarce resources. For example:

$$b \in \mathcal{B} := \{CO_2, SO_2, VOC, \text{crude oil}, \ldots\} \quad (1)$$

Next, for the set of damage indicators, 10 of the 12 indicators, as defined by the detailed Eco-Indicator 99 methodology, are most relevant to process design and are used to represent the impact of each life cycle stage. This set of indicators are represented by:

$$e \in \mathscr{E} := \{hh_{ca}, hh_{ro}, hh_{ri}, hh_{cc}, hh_{ir}, hh_{od}, ec_{tx}, ec_{ae}, rd_{mn}, rd_{ff}\} \quad (2)$$

where hh_{ca} = human health damages due to carcinogenic emissions; hh_{ro} = human health respiratory damages due to organic emissions; hh_{ri} = human health respiratory damages due to inorganic emissions; hh_{cc} = human health damages due to climate change; hh_{ir} = human health damages due to ionisation radiation; hh_{od} = human health damages due to ozone depletion; ec_{tx} = ecosystem quality damages due to ecotoxic emissions; ec_{ae} = ecosystem quality damages due to acidification and eutrophication; rd_{mn} = resource depletion of mineral reserves; and rd_{ff} = resource depletion of fossil fuel reserves.

During Step 3 each impact indicator is categorised under a specific damage category heading from the set of normalised categories:

$$n \in \mathcal{N} := \{n_{hh}, n_{ec}, n_{rd}\} \quad (3)$$

where n_{hh}, n_{ec}, and n_{rd} correspond to the Human Health, Ecosystem Quality and Resource Depletion categories respectively. Categorisation of impacts, e, into normalised categories, n, is effectively performed using a multi-dimensional set, L_{en}.

Finally, it is necessary to define a set of $p \in \mathcal{P}$ life cycle stages that will be considered in the study—such as raw material acquisition, transportation, primary product manufacturing, packaging, product use *etc*. Both the foreground and background processes are included in this set.

Impact assessment. The main independent variable in the model is the reference flows of each life cycle stage, M_p, which links it to the foreground system. For example, a study conducted for a refinery (*i.e.* the foreground system) would have the Amount of Crude Oil received as the reference flow for the Extraction life cycle stage. Within an optimization model, these reference flows will be free variables. The dependent variable calculated from the reference flows is then the damage indicator, D_{ep}—the value of indicator e resulting from the operation of life cycle stage p. The calculation is as follows:

$$D_{ep} = \sum_b \upsilon_{be}\omega_{bp}M_p \quad \forall e \in E, p \in P \quad (4)$$

Classification and characterisation of burdens into impacts is achieved by the parameter υ_{be}, representing the damage factor of substance b contributing to impact indicator e. For example, the υ_{be} entry for b = CO_2 and e = hh_{cc} is 2.10×10^{-7} DALY/kg CO_2. The emissions inventory per unit reference flow of life cycle stage p is captured in the parameter ω_{bp}. Taking as an example the ω_{bp} entry for b = CO_2 and the life cycle stage k = Propylene Production, the value is 1.2 kg CO_2/kg propylene.[42]

Normalisation and weighting. The final step involves the normalisation and weighting of the impacts in terms of the three main categories to arrive at the single Eco-Indicator 99 score for the entire life cycle. This requires the use of two parameter vectors, namely normalisation factors, η_n, and weighting factors, ϑ_n. The values of these parameters depend on the particular chosen "perspective". For example, with the Average Hierarchist perspective, human health (n = n_{hh}) and ecosystem quality (n_{ec}) are considered equally important and receive a 40% weighting each. The damage due to resource depletion (n_{rd}) is considered less significant and consequently only contributes 20% towards the Eco-Indicator 99 score. Given these parameters, normalisation and aggregation are simply:

$$H_n = \eta_n \sum_{e \in L_{en}} \sum_p D_{ep,} \quad \forall n \in N \quad (5)$$

$$Eco-Indicator\ 99 = \sum_n \vartheta_n H_n \quad (6)$$

where H_n represents the normalised values.

3.3 Multi-objective optimization model

With the Eco-Indicator 99 methodology allowing the quantification of an overall environmental objective function based upon LCA considerations, the multi-objective environmentally conscious process design problem can be formulated as:

$$\min_{x,y} U\begin{Bmatrix} f_1(x) = \text{Total Annualised Cost} \\ f_2(x) = \text{Eco-Indicator 99} \end{Bmatrix}$$

s.t.

$$x \in S \begin{Bmatrix} \text{PROCESS MODELS} \\ \text{MASS AND ENERGY BALANCES} \\ \text{DESIGN AND EQUIPMENT SPECIFICATIONS} \\ \text{EMISSIONS REGULARTORY LIMITS} \\ \text{LIFE CYCLE EMISSIONS INVENTORIES AND BALANCES} \\ \text{ENVIRONMENTAL IMPACT ASSESSMENT} \end{Bmatrix} \quad (7)$$

where U is the (unknown) utility function relating the comprise between the multiple objectives, $f_1(x)$, $f_2(x)$, subject to the various continuous and discrete decision variables x belonging to the steady state feasible region S of equality and inequality constraints. The solution to this problem is a set of efficient or Pareto optimal solutions (also referred to as non-inferior and non-dominant) representing alternative process designs, each achieving a unique combination of environmental and economic performance. The definition of efficiency can be stated as:[27]

Definition 3.1 *A decision vector $\bar{x} \in S$ is efficient iff there does not exist another $x \in S$ such that $f_i(x) \leq f_i(\bar{x})$ for all i = 1, …, k and $f_j(x) < f_j(\bar{x})$ for at least one objective j. Otherwise, $\bar{x}$ is inefficient.*

A criterion vector $\bar{z} \in Z$ is efficient iff there does not exist another criterion vector $z \in Z$ such that $z_i \leq \bar{z}_i$ for all i = 1, …, k and $z_j < \bar{z}_j$ for at least one index j; or equivalently, $\bar{z}$ is efficient if its corresponding decision vector is efficient. Otherwise, $\bar{z}$ is inefficient.

In other words, a solution is efficient (Pareto optimal) if it is not possible to find another feasible solution so as to improve one objective without worsening at least one of the others. This set of efficient solutions is obtained by firstly reformulating the multi-objective optimization problem as a parametric programming problem:

$$\begin{aligned} &\min_x f_1(x) \\ \text{st}: \ &f_2(x) \leq \theta_2 \\ &\vdots \\ &f_k(x) \leq \theta_k \\ &x \in S \\ &\theta_2 \in \left[\theta_2^L, \theta_2^U\right], \ldots, \theta_k \in \left[\theta_k^L, \theta_k^U\right] \end{aligned} \quad (8)$$

where

$$\begin{aligned} \theta_j^L &= \min_x f_j(x) \\ \text{st}: \ &x \in S \\ &1 \leq j \leq k \end{aligned} \quad (9)$$

while at each solution the value of each objective function i is recorded

$$\theta_{ij} = f_i(\bar{x}) \ 1 \leq i \leq k \quad (10)$$

such that the upper bound on each objective function is given by its greatest value over all the solutions:

$$\theta_i^U = \max_j \left(\theta_{ij}\right) \quad 1 \leq i \leq k \quad (11)$$

In principle, the reformulated problem can then be solved using recently developed algorithms for parametric optimization.[28] However, since the expansion of the system boundary—as required by the environmentally conscious process design problem—often results in a large number of variables and constraints which typically exhibit highly non-linear behaviour, an enumeration

based approach is required instead. This is achieved by discretising the parameter space into $NQ^{(k-1)}$ sufficiently small intervals and applying the ε-constraint method at each parameter interval realisation:

$$\begin{aligned} &\min_x f_1(x) \\ \text{st}: \; &f_2(x) \le \theta_2 \\ &\vdots \\ &f_k(x) \le \theta_k \\ &x \in S \\ &\theta_2 \in \left[\theta_2^1, \ldots, \theta_2^q, \ldots, \theta_2^{NQ}\right], \ldots, \theta_k \in \left[\theta_k^1, \ldots \theta_k^q, \ldots, \theta_k^{NQ}\right] \end{aligned} \quad (12)$$

where

$$\theta_k^1 = \theta_k^L, \quad \theta_k^q = \theta_k^L + q \times \frac{\theta_k^U - \theta_k^L}{NQ}, \quad \theta_k^{NQ} = \theta_k^U \quad (13)$$

However, it is important to note that the ε-constraint method can neither guarantee feasibility nor efficiency and both conditions need to be verified once the complete set of solutions has been obtained.[6] An additional post-processing step for detecting efficiency based on the concepts of dominance, therefore, has to be included as part of the overall multi-objective optimization algorithm.

The major advantage of the particular approach developed and employed here is that it does not require the *a priori* articulation of preferences by the decision-maker. Instead, the aim is to generate the full set of trade-off solutions and not to present only a single alternative. From the *set* of alternatives, the decision-maker can then further investigate interesting trade-offs and ultimately select a particular solution that best satisfies his/her willingness to compromise.

While the set of trade-off solutions provide invaluable insight into the inherent conflicts that exist within the process design, it is often still desired to improve both cost and environmental objectives simultaneously. One way of achieving such step-change improvements is through the use of computer aided molecular design techniques whereby substitute materials are identified that potentially avoid the creation of damaging substances in the first place.

4 Optimal solvent/blend design for minimum environmental impact

The optimal solvent/blend design problem addressed here is stated as follows: *given* a manufacturing scheme with specified reaction routes and a set of separation alternatives, the *objective* is to identify the set of feasible solvent molecules and/or blends which simultaneously offer optimal separation and environmental performance at reduced cost. A three step procedure is applied, involving: (i) the identification of agent based operations within the process of interest (such as gas absorption, liquid extraction), specification of performance constraints for each separation task and property constraints for the desired solvents, (ii) at the separation *task* level, the determination of a list of candidate solvents/blends which satisfy the performance and property constraints and (iii) at the *verification* level, the selection of optimal candidates based on global plant-wide process, property, environmental and economic constraints.

At both task and verification levels, any of a number of process performance, property, environmental or economic objective functions may be used. Environmental and economic assessment are always included at the verification level, however, at the task level the objective may depend on the process topology. Separation systems which are embedded within a process may have no effluent stream which is emitted directly to the environment, so that an environmental objective is inappropriate. In such cases, process performance, property or economic objectives may be used instead.

The mathematical sets employed in the solvent design procedure are:

$i \in I$	all molecules
$s \in S \; (\subset I)$	solvent molecules
$ns \in NS \; (\subset I)$	non-solvent molecules
$j \in J$	chemical structural groups
ii	alias for i
nj	alias for j

5 Solvent identification formulation—separation task level

5.1 Overview

For non-reactive, multi-component absorption and liquid extraction processes, the task level solvent identification problem is defined as follows. Given, (i) a multicomponent stream of fixed flowrate and composition, (ii) an absorption/liquid extraction task with known operating conditions, (iii) a set of structural groups (*e.g.* $-CH_3$, –CHO…) and their associated group contribution parameters and (iv) the type of agent molecules required (acyclic, monocyclic, bicyclic, aromatic or a combination), then the objective is to design a feasible solvent or a mixture of molecules featuring optimal separation performance at minimum environmental impact.

The model consists of a number of equation sets, which are summarised below. In general, the following assumptions are made in the analysis: isobaric operation, pure and regenerable solvents, no reactions, negligible enthalpies of solution and homogeneous mixtures and no minimum composition approach between streams. In addition, the inherent inaccuracies of the many property prediction techniques and thermodynamic models employed are accepted. As mentioned earlier, instead of presenting an exhaustive discussion of the procedure, only the recent developments and contributions compared to previous work[17] are summarised.

5.2 Structural and chemical feasibility constraints

For structural feasibility, the octet rule is used to ensure that each solvent molecule has zero valency.[29] For acyclic molecules, an additional bonding rule is used to ensure that no two adjacent groups are linked by more than one bond. For cyclic and aromatic molecules, a newly developed, generalised form of this bonding rule is used.[30]

For chemical feasibility, an additional set of rules is required. In general, these rules limit the numbers and combinations of functional groups which may appear in a solvent molecule, based on knowledge of chemistry. They may be empirical rules derived on a case by case basis depending on the solvent design task.[17] Alternatively, more general rules may be employed. Recently, it was shown how the general chemical feasibility rules of Gani and co-workers[15] can be cast as linear integer constraints which can be included in the task level solvent blend design formulation.[30]

5.3 Pure component and mixture property equations

Many properties may be used in the design of absorption and liquid extraction solvents. Table 2 summarises the properties and prediction methods used in the current formulation. A combination of correlations and group contribution (GC) techniques from various sources are employed. As shown in Table 2, reformulated UNIFAC equations are used to estimate activity coefficients. Since the procedure facilitates the design of both single solvents as well as blends, mixture properties are estimated using linear mixing rules. These estimates may provide composition restrictions for the solvent blends, so that any inaccuracy may affect the optimal solutions obtained. To account for this, a new set of mixture property based tests are included in solvent verification.

Table 2 Properties and prediction methods

Pure component properties	Prediction method	Source
Vapour pressure P_i^{vap}	Correlation	Cox-Antoine relationship[38]
Normal boiling point T_i^b	GC	Joback[47]
Critical properties T_i^{cr}, P_i^{cr} and V_i^{cr}	GC	Joback,[47] Horvath[48]
Saturated liquid molar volume V_i^{sat}	Correlation	Hankinson correlation[38]
Compressed liquid molar volume V_i	Correlation	Thomson correlation[38]
Vapour heat capacity $C_{p,i}^{gas}$	GC	Joback and Stephanopoulos[49]
Liquid heat capacity $C_{p,i}^{liq}$	GC, Correlation	Horvath[48]
Acentric factor ω_i	Correlation	Horvath[48]
Heat of vaporisation $\Delta H_{i,\,298}^{vap}$	Correlation	Chen equation[48]
Heat of vaporisation $\Delta H_i^{vap}(T)$	Correlation	Watson relation[38]
Lethal concentration $LC50_i$	GC	Martin and Young[34]
Solubility parameters δ_i^D, δ_i^P, δ_i^H	GC	Buxton *et al.*[17]
Mixture properties	**Prediction method**	**Source**
Activity coefficient γ_i	GC	Reformulated UNIFAC, Buxton *et al.*[17]
Infinite dilution activity coefficient γ_i^∞	GC	Reformulated UNIFAC, Buxton *et al.*[17]

5.4 Mixture property operational feasibility constraints

For both absorption and liquid extraction processes, feasibility of solvent regeneration requires the avoidance of azeotropes and, to a certain extent, unstable liquid mixtures. Furthermore, complete mutual solubility (phase stability) between the different solvent components is required to ensure the feasibility of the separation task itself. In liquid extraction, phase stability is doubly important since the solvents must exhibit high mutual solubility with the desired solutes, while they must also form unstable mixtures with the other raffinate components.

Azeotropy. In the current formulation, two azeotropy tests are performed. At the task level, the following constraint is applied to preclude binary azeotropes between solvent components, and between each pair of solvent and desired solute components:

$$(P_i^{vap} - \gamma_{ii,i}^{\infty} P_{ii}^{vap})(P_{ii}^{vap} - \gamma_{i,ii}^{\infty} P_i^{vap}) < 0 \quad \forall i \neq ii, ii \in I \quad (14)$$

where P_i^{vap} is the pure component vapour pressure of component i and $\gamma_{ii,i}^{\infty}$ is the activity coefficient of component ii at infinite dilution in component i. This constraint applies to isothermal systems. Later, in solvent verification, it is shown how a newly developed azeotropy constraint for isobaric systems is applied.

Phase stability. The following binary phase stability condition provides a local test of phase stability at a given composition:[31]

$$\left[\frac{\partial \ln \gamma_i}{\partial X_i^l}\right]_{T,P} - \frac{1}{X_i^l} > 0 \quad (15)$$

where γ_i is the activity coefficient of component i and X_i^l is the mole fraction of component i in the (binary) liquid.

At the task level, this constraint is applied (at intervals) across the entire composition range to ensure complete (binary) miscibility amongst solvent components, and to ensure high mutual solubility between solvent and desired solute component pairs. In liquid extraction solvent design it is also applied to ensure low mutual solubility between individual solvent components and all other raffinate components. Application of this constraint in solvent verification is described in Section 6. Clearly, the greater the number of intervals, the greater the chance of capturing any phase instability.

Note that these binary azeotropy and phase stability constraints constitute preliminary screening measures only which are not designed to eliminate all undesirable multicomponent mixtures. Methods for capturing multi-component azeotropy and phase instability are available in the literature[32] and could be incorporated at the verification level.

5.5 Process model equations

For both absorption and liquid extraction processes, a single mass/heat transfer module[33] is used to provide an aggregated model of the processing task (absorber or liquid extraction contactor). Key to the formulation of these models are the driving force constraints, which describe the phase equilibrium limitation to mass transfer between adjacent streams. Details of these equations, including the derivation of new mass transfer driving force constraints for liquid–liquid systems are provided elsewhere.[30]

The process models also include the task level objective functions. The set of objective functions may include environmental impact metrics and process performance objectives.

Environmental impact metrics. Detailed environmental impact assessment criteria based on life cycle considerations, such as the Eco-Indicator 99, cannot be used at the solvent design level since the solvent molecule structures are unknown and the separation unit is investigated in isolation. However, more simplistic distance-to-target type of metrics such as Critical Air Mass (CTAM) and Critical Water Mass (CTWM) can be quantified as a function of lethal concentration LC50 (mol l^{-1}) by ingestion or inhalation:

$$CTAM\ (CTWM) = \sum_i \frac{F_i^o}{LC50_i} \quad (16)$$

where F_i^o is the effluent flow of component i (mol s^{-1}), and $LC50_i$ is the lethal concentration of component i from group contributions.[34]

Process performance objectives. Typical process performance objectives in solvent design include solvent loss, capacity and selectivity. For liquid extraction, these quantities may be defined as follows (similar definitions apply for gas absorption):

$$\text{Solvent loss (mol\%)} = 100 X_s^R, \quad \forall s \in S \quad (17)$$

$$\text{Solvent capacity} = \frac{X_{ns}^E}{X_{ns}^R}, \quad \forall ns \in NS \quad (18)$$

$$\text{Solvent selectivity} = \frac{X_{ns}^E / X_{ns'}^E}{X_{ns}^{R^o} / X_{ns'}^{R^o}}, \quad \forall ns \in NS \quad (19)$$

where X_s^R is the mole fraction of solvent s in the treated raffinate, X_{ns}^E and X_{ns}^R are the mole fractions of non-solvent ns in the contaminated extract and treated raffinate respectively, and $X^{Ro}{}_{ns}$ is the mole fraction of non-solvent ns in the untreated raffinate.

In multi-component separations using solvent blends, solvent loss, selectivity or capacity objectives may need to be cast in terms of several solvent components simultaneously. For solvent loss, this is achieved by setting the arithmetic or geometric mean of

solvent losses as the objective. For multi-component liquid extraction using solvent blends, the following selectivity objective is proposed:

$$\text{Maximize} \left(\frac{\prod_{nse} m_{nse}^{R^o}}{\prod_{nsr} m_{nsr}^{R^o}} \right) \quad (20)$$

where *nse* are the target non-solvent components to be selectively extracted, *nsr* are the (non-target) components to be left in the raffinate and $m^{Ro}{}_i$ represents the distribution coefficient of component *i* between extract and raffinate. Similarly, a multi-component liquid extraction capacity objective may be defined as:

$$\text{Maximize} \left(\frac{\prod_{nse} X_{nse}^{E}}{\prod_{nse} X_{nse}^{R}} \right) \quad (21)$$

where X_{nse}^{E} and X_{nse}^{R} represent the mole fraction of component *nse* in the extract and raffinate phases respectively.

Coextraction and recovery objectives may also be employed. For liquid extraction, these quantities are defined as follows:

$$\text{Coextraction (mol\%)} = 100 X_{nsr}^{E}, \ \forall nsr \in NSR \quad (22)$$

$$\text{Component recovery (\%)} = 100 \frac{X_{nse}^{E} E}{X_{nse}^{R^o} R^o}, \ \forall nse \in NSE \quad (23)$$

where X_{nsr}^{E} is the mole fraction of non-target component *nsr* in the extract, X_{nse}^{E} and $X^{Ro}{}_{nse}$ are the mole fractions of target component *nse* in the extract and untreated raffinate respectively and *E* and R^o are the extract and untreated raffinate flows.

Each of the above expressions may be used in an operational feasibility constraint if it is not selected as part of the objective function set.

5.6 Solution procedure

The task level model described above is solved in a mixed integer optimization setting. The optimization variables are *x*, the set of continuous process variables and n_{ij}, the set of integer variables representing the numbers and types of groups that constitute each solvent molecule.

A step-wise decomposition based algorithm is employed, based on the general principles of the Generalised Benders Decomposition.[35] In this algorithm, the non-linear programming (NLP) *primal* problem is decomposed in to several steps which are solved in series in order to simplify and initialise the final NLP problem as well as possible. Full details of this algorithm are available elsewhere.[17,30]

6 Solvent verification—process level

6.1 Overview

At the verification level, promising candidate solvents identified at the task level are tested to: (i) ensure the validity of the generated single solvents and/or blends, (ii) screen out candidates which are suboptimal or even infeasible due to equilibrium non-convexities or inaccurate property prediction, (iii) determine if the solvents are able to prevent pollution on a process wide level, and (iv) accurately estimate the operating cost of the process, as in many cases, candidates with excellent environmental performance might be prohibitively expensive.

For simplicity in previous work, short cut verification exercises were performed focussing on the technology of solvent regeneration and without property verification. Recently however, solvent verification has been extended to include mixture property validation. Using full mixture property prediction techniques, candidate solvents/blends are tested for validity according to the mixture property bounds imposed at the task level. They are also tested for azeotropy and phase stability under the conditions of regeneration. Details of the full verification formulation and short cut models are presented elsewhere.[17,30] However, the newly developed mixture property validation procedure is summarised below.

6.2 Property bound verification

As discussed in section 5.3, all bounded properties should be checked using full mixing rules as part of solvent verification. In the motivating example it is necessary to impose bounds only on solvent boiling temperatures and densities. For brevity, the following discussion is confined to these properties.

Boiling temperature bounds. To facilitate regeneration, low boiling solvents are required in the motivating example. However, in the search for low boiling solvents it is insufficient to bound only the mixture bubble point or the pure component boiling points. If only the bubble point is bounded, there is the possibility that the blend component boiling points will straddle this bound. If the pure component boiling points only are bounded, there is the possibility that within the solvent mixture, the individual components will exhibit effective boiling points above these bounds (due to non-ideal behaviour).

As a compromise, the pure component boiling points are bounded at the task level, and at the verification level the *effective boiling points* of all components within the contaminated extract (the feed stream to regeneration) are checked to ensure the validity of this bound.

The effective boiling point is here defined as the temperature at which the *effective vapour pressure* exerted by a component in the mixture is equal to the prevailing pressure. Rather than estimating the effective boiling temperature of each component in the mixture, it is sufficient to check the effective vapour pressure of each component. For low boiling solvents, the following constraint is applied:

$$\gamma_s^E P_s^{\text{vap}}(T_{s,up}^b) \geq P_{\text{oper}}^{\text{regen}} \quad (24)$$

where the operating pressure of the regeneration column ($P_{\text{oper}}^{\text{regen}}$) is set as a minimum limit, and the product of γ_s^E (the activity coefficient of solvent *s* in the extract *E*) and P_s^{vap} (the pure component vapour pressure of solvent *s*) represents the effective vapour pressure of solvent *s* in the extract *E*, evaluated at the boiling temperature upper bound $T_{s,up}^b$.

The boiling temperature bounds are intended to facilitate regeneration by imposing a minimum allowed boiling temperature approach between solvents and solutes. Rather than checking that this has been maintained, is it sufficient to check that relative volatility is high enough for an acceptable separation.

For low boiling solvents, the worst case is that the effective boiling temperature of the least volatile solvent component (the light key) is at the boiling point upper bound. Thus, for low boiling solvents, a lower bound is imposed on αLK_s, HK_{ns} ($T_{s,up}^b$), the relative volatility at this temperature between the light key solvent component LK_s and the heavy key solute component HK_{ns}:

$$\alpha_{LK_s, HK_{ns}}\left(T_{s,up}^b\right) = \frac{\gamma_{s,LK}^E P_{s,LK}^{\text{vap}}\left(T_{s,up}^b\right)}{\gamma_{ns,HK}^E P_{ns,HK}^{\text{vap}}\left(T_{s,up}^b\right)} \geq 1.5 \quad (25)$$

While this constraint does not guarantee that the minimum boiling temperature approach is obeyed, it does guarantee that there is sufficient relative volatility for the regeneration separation.

Density bounds. At the task level, correlations for computing saturated[36] and compressed[37] pure component liquid molar volumes are employed. Using a set of mixing rules,[38] saturated and compressed *mixture* volumes can also be estimated using these techniques. Since the rules are designed to predict the density of an entire mixture, rather than the partial molar volumes of the components within it, they are employed to predict the density of

the uncontaminated extract solvent mixture only. This density is then compared with the same density bound applied to the pure components. This does not guarantee that the partial molar volumes of the individual components in the mixture obey the bound, but this cannot be investigated because of the particular form of the mixture property prediction technique.

Azeotropy test. At the verification level, it is more appropriate to model solvent/blend regeneration columns as isobaric, rather than isothermal.[17] Since the task level azeotropy constraint (eqn. 14) applies to isothermal systems, a new azeotropy constraint for isobaric systems is required in verification.

For a binary isobaric system, an azeotrope exists if the mixture bubble point T^b_{mix} passes through a maximum or a minimum somewhere on the composition scale. The gradient of the mixture bubble point line must then be of a different sign at each end of the scale, so that the constraint can be written as follows:

$$\left[\frac{\mathrm{d}T^b_{\mathrm{mix}}}{\mathrm{d}X^l_i}\right]_{P,X_{i=0}} \left[\frac{\mathrm{d}T^b_{\mathrm{mix}}}{\mathrm{d}X^l_i}\right]_{P,X_{i=1}} > 0 \qquad (26)$$

where X^l_i is the mole fraction of component i in the mixture and P is the (constant) system pressure. Expressions for these mixture bubble point derivatives are presented elsewhere.[17]

Phase stability test. At the verification level, phase instability within the regeneration column and its condensor or reboiler may disrupt the column operation, affecting the compositions of boil-up and reflux and causing certain components to be held up preferentially on the column trays. To avoid these effects, phase instability should be avoided throughout. However in distillation column design, a procedure originally developed for homogeneous separations has been applied to determine the number of theoretical plates in a heterogeneous column, assuming that phase splitting occurs only in the decantor (*i.e.* the reboiler or condensor).[39]

On this basis, it is assumed that if phase splitting in the reboiler and condensor is avoided, any that may occur within the column does not affect the column operation. Thus, at the verification level, the phase stability constraint need only be applied to the mixtures present in the regeneration column condensor and reboiler. eqn. (15) is again used to perform the tests, at intervals across the composition ranges.

7 Application

7.1 Problem description

The motivating example, presented earlier, for the production of 150 tons per day of crude acrylic acid will now be used to illustrate the features of the methodology. In the first part of the methodology, a fixed process topology is considered, *i.e.* no structural alternatives in terms of the connectivity between unit operations are included in the design problem formulation. Problem 15, therefore, reduces in this example to a multi-objective non-linear programming (moNLP) problem, modelled in the GAMS[40] and solved using CONOPT2.[41] Later, in Section 7.5, it will be shown how both the environmental impact and economic performance of the process can be improved through *discrete* process design changes using solvent substitution.

7.2 Life cycle assessment

The boundaries of the acrylic acid plant (the foreground system) are expanded to include up-stream/input processes within the background system. The life cycle analysis can, therefore, be classified as a "cradle-to-gate" assessment. Downstream processes, such as secondary processing, product-use and disposal, are not included since the problem formulation is for a fixed production rate. The scope of the life cycle study is further simplified by only considering some and not all of the input processes belonging to the background system. The following processes associated with the production of acrylic acid are considered: Propylene Production, Steam Generation, Thermal Energy Generation, Electricity Generation. Emissions inventories for the chosen background processes are taken from standard literature sources.[42–44]† The mass and energy balance results as defined by the process models provide the emissions inventory for the foreground system (the acrylic acid plant). The expanded system boundary included by the life cycle goal and scope definition is presented in Fig. 2.

7.3 Base case results

First, each objective function is individually optimized. Next, using the solutions of the scalar objective function problems, the

† Since the time of conducting the study, the chosen emissions inventory data sources have been superseded by more recent initiatives such as the ecoinvent, http://www.ecoinvent.ch.

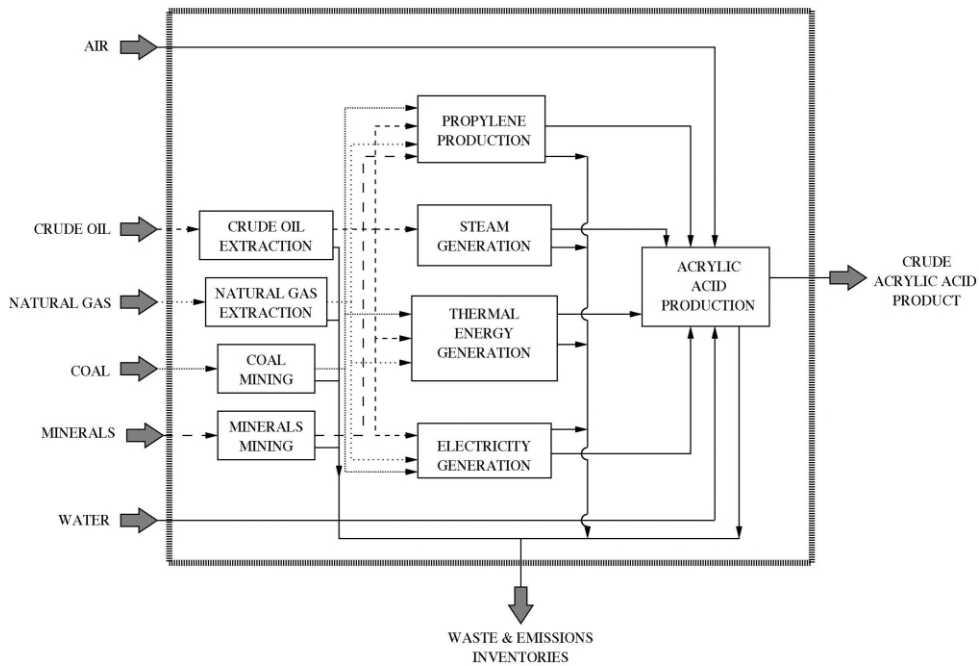

Fig. 2 Expanded acrylic acid production boundary.

parametric programming problem is formulated with the environmental objective entering as an inequality constraint. Discretisation of the parameter range over which f_2 exists into 300 (NQ = 300) equally separated points, allows the application of ε-constraint method. Next, removing the infeasible solutions and applying the principle of dominance, the efficient solutions are separated from the inefficient ones, resulting in a set of 284 uniquely Pareto optimal designs as presented in Fig. 3. As this efficient set of solutions highlight, a conflict exists between a design achieving minimum cost and a design which achieves minimum environmental impact. It shows that no improvement in environmental performance (*i.e.* reduction in environmental impact) can be achieved unless the economic performance is sacrificed and more capital is invested. The only way to improve *both* the economic *and* environmental performance of the design is to structurally modify the process topology through equipment or material substitutions. Analysis of the environmental impact assessment results shows that the liquid–liquid extraction and distillation column recovery unit contribute significantly towards the overall life cycle environmental performance due to the waste water stream and thermal energy requirement of the product purification column. Substitution of the base case solvent used in the liquid–liquid extractor, therefore, offers an ideal opportunity for potentially achieving step-change improvements in both its economic and environmental performance.

7.4 Single solvent identification—separation task level

The design task is now to identify a solvent substitute for the liquid extraction separation task using the proposed procedure. The specifications for this solvent identification problem are listed in Table 3. It is worth noting the operational constraint on coextraction imposed, owing to the large amount of water in the feed stream (originating from the quenching/absorption stage). Also, while the procedure is fully capable of identifying both single solvents as well as solvent blends, for brevity and clarity of presentation the example presented here is restricted to the generation of only single pure solvents. To facilitate downstream solvent regeneration, the boiling point of the solvent is bounded to 15 K below the lowest boiling point of the non-solvent molecules, *i.e.* acetic acid ($T^b_{\text{acrylic acid}}$ = 413.8 K and $T^b_{\text{acetic acid}}$ = 391.1 K), thereby ensuring that only low boiling solvents are designed.

The set of 16 candidate UNIFAC structural groups employed are:

$j \in J := \{CH_3, CH_2, CH, C, OH, H_2O, COOH, COCH_3, COCH_2, CHO, CH_3COO, CH_3O, CH_2O, COO, CH_2CH, OCH\}$

The total number of groups allowed to make up the solvent molecules are limited to between 3 and 15. In addition, appropriate chemical feasibility constraints are included to (i) preclude certain combinations of groups being present in solvent molecules, (ii) limit the occurrences of certain groups with certain others and (iii) provide upper and lower bounds on the number of functional and secondary groups which may appear within the generated solvent molecules.

Applying the algorithm to the illustrative example with the objective being the minimization of the overall toxicity of the treated raffinate stream ("AQUEOUS – WASTE WATER" on Fig. 1)—computed as the total CriTical Water Mass (CTWM)—a total of 43 unique structurally feasible solvents are generated. 21 of these 43 are excluded owing to the existence of an azeotrope and another 9 are excluded owing to the failure to achieve the desired level of extraction. Analysis of the remaining 13 solvents is presented in Table 4. It is interesting to note that the two most promising solvents, diethyl ether and methyl isopropyl ether, are structurally very similar to the base case solvent, di-isopropyl ether ($(CH_3)_4CH$ OCH). For comparative purposes, n-propyl acetate (NPA), which is structurally different from the base case solvent, but still promising at the identification level, will now be taken to the process level to illustrate how verification of its true performance at a plant-wide level within the life cycle multi-objective optimization framework can be performed.

7.5 Verification—step-change improvements through solvent substitution

Substituting the base case solvent with one of the potential candidates, NPA, and resolving the multi-objective NLP design problem results in a set of efficient solutions as shown in Fig. 4. Comparatively, the substitute solvent outperforms the base case one by improving *both* the process economics *and* life cycle environmental performance of the design. Changing the solvent used in the liquid–liquid extractor from DIPE to NPA can potentially result in an optimal plant-wide design requiring 14.8%

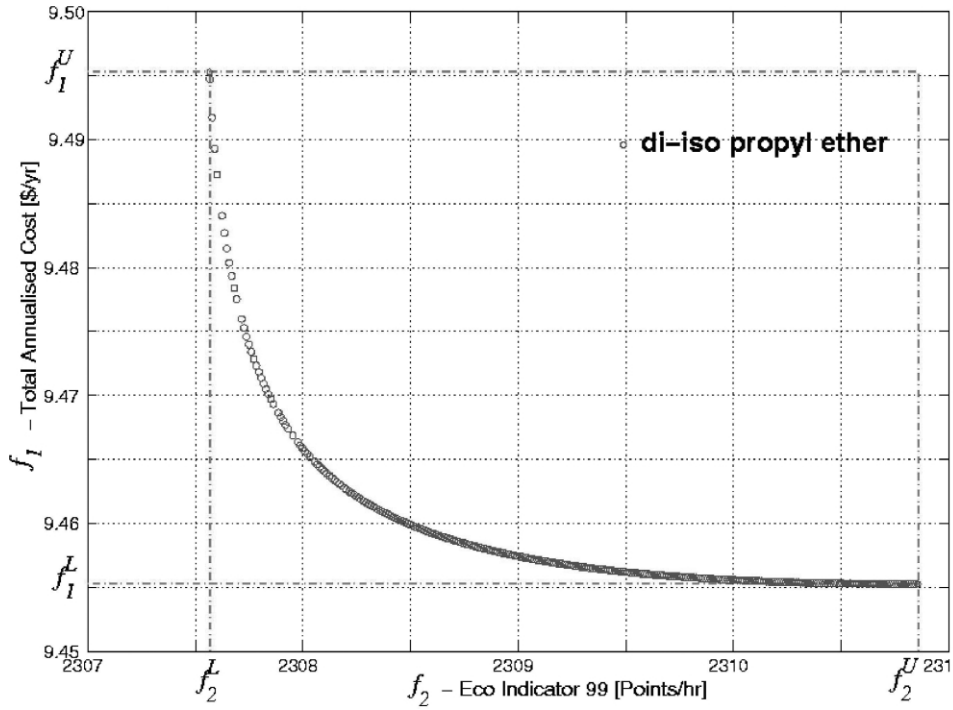

Fig. 3 Base case (DIPE) efficient set of solutions.

Table 3 Solvent identification problem specifications

Solvent specifications	Feed conditions
$s \in S := \{s_1\}$	P = 2.5 bar
3 ≤ number of groups ≤ 15	T = 313 K
300 K ≤ T_s^b ≤ 375 K	94.7076 kmol h^{-1} water
Solvent flowrate ≤ 71 kmol h^{-1}	0.248 kmol h^{-1} acetic acid
Coextraction ≤ 5 mol%	5.046 kmol h^{-1} acrylic acid
Acid recovery ≥ 96%	

less in total annual cost while simultaneously achieving a 9.27% reduction in environmental impact. As such, the results illustrate how a structural modification in the process topology through material substitution can shift the Pareto set of alternative designs to achieve step-change improvements.

It is interesting to highlight that when considering the liquid–liquid extractor in isolation, the NPA design has a worse performance than the DIPE design in terms of both performance criteria. Not only does the higher solvent make-up of the NPA design result in a more expensive extractor design, but also the environmental burden resulting directly from the operation of the NPA liquid–liquid extractor, *i.e.* the aqueous waste water stream, is greater than that of the DIPE design. However, within the expanded systems boundary, the weaknesses in the NPA design are counter balanced by the plant-wide improvements gained from the solvent integration, making it superior over the DIPE design. Overall reductions in the use of cooling water, demineralised water, steam and electrical power are achieved by the optimal design for the substitute, while the capital requirements of the reactor, absorber and distillation column are also lowered. It is these plant-wide interactions of the substitute solvent that allows it to achieve improvements in *both* the process economics *and* life cycle environmental impact, despite its relatively poor unit specific performance.

8 Concluding remarks

A systematic procedure for addressing the environmentally conscious process design problem has been presented in this paper. The approach extends the previously developed Methodology for Environmental Impact Minimization (MEIM) for process design[13] and solvent selection.[17] The first step in the methodology is the inclusion of environmental objectives within the process design task using a recently developed method of damage modelling for

Table 4 Single solvent identification results

Solvent groups	Selected structure	Selectivity: Acetic acid	Selectivity: Acrylic acid	Co-extraction	Total acid recovery	Solvent loss	Extract flow/ kmol h^{-1}	Objective function CTWM/ tn water h^{-1}
$(CH_3)_2CH_2CH_2O$	**Diethyl ether**	**26.50**	**19.11**	**5**	**100**	**0.874**	**71**	**61.81**
$(CH_3)_3OCH$	**Methyl isopropyl ether**	**51.65**	**31.82**	**3.637**	**96.277**	**0.339**	**71**	**74.04**
$(CH_3)_2CH_2CH_2COO$	**Ethyl propionate**	**34.96**	**909.81**	**5**	**100**	**0.113**	**71**	**121.17**
$CH_3(CH_2)_2CH_3COO$	***n*-Propyl acetate**	**26.70**	**862.73**	**5**	**100**	**0.172**	**71**	**185.39**
$(CH_3)_2CHCH_3OCH_2O$	1,2-Dimethoxypropane	7.47	7.54	5	100	2.771	71	242.58
$(CH_3)_2(CH_2O)_2$	Diethyl peroxide	7.92	7.94	5	100	6.129	71	264.63
$CH_3(CH_2)_2CH_3OCH_2O$	1,2-Ethoxy-2-methoxy ethane	7.48	7.54	5	100	2.788	71	324.30
$CH_3CH_2CHCOCH_2$	1-Penten-3-one	13.25	12.64	5	100	2.807	71	772.68
$(CH_3)_2CH_2COO$	Methyl propionate	25.97	14.82	5	100	2.418	71	952.98
$CH_3CH_2CH_2CHCOO$	Ethyl acrylate	17.68	18.19	5	100	2.448	71	5.92×10^3
CH_3CHCH_2CHCHO	2-Methyl-but-3-enal	26.58	33.43	5	100	1.165	71	5.73×10^4
$(CH_2)_2CH_2CHCHO$	4-Pentenal	26.56	33.38	5	100	1.169	71	7.63×10^4
CH_2CH_2CHCHO	3-Butenal	19.49	31.04	5	100	4.688	71	1.138×10^5

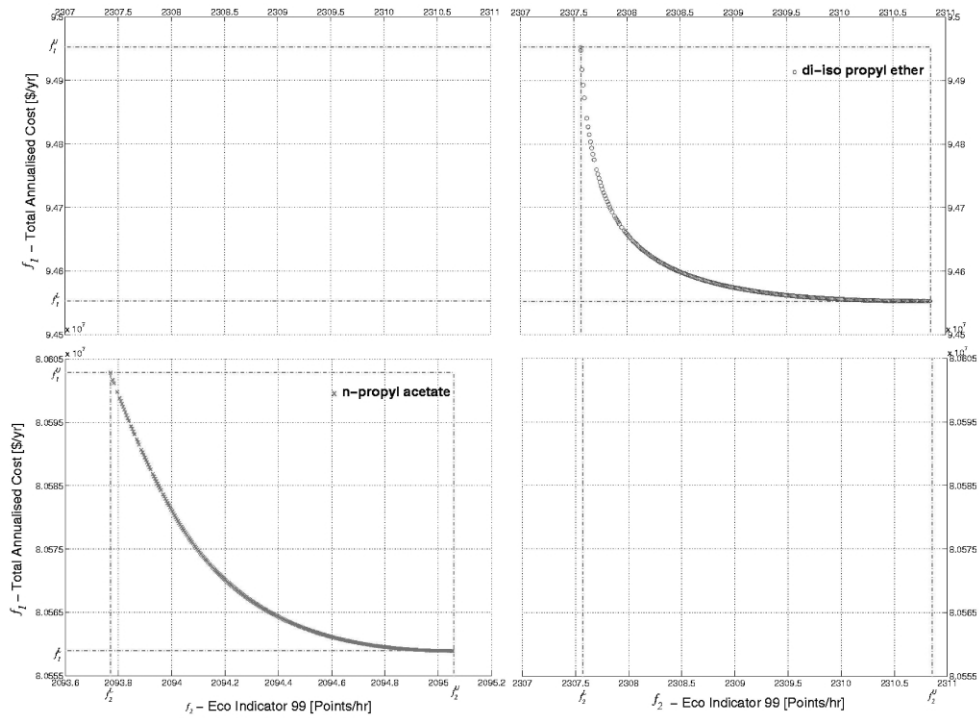

Fig. 4 Shifting the Pareto curve through solvent substitution.

life cycle impact assessment. This enables the trade-off between the environmental and economic concerns to be established. Once this inherent compromise has been identified, the next task is then to modify the process through the use of alternative solvents that offer potential improvements in terms of the *multiple* objectives.

Extensions to the previously developed methodology presented in this paper include the explicit formulation of new environmental performance criteria, and a multi-objective optimization algorithm based upon a domination set strategy for detecting pareto optimality. In addition, the previously developed solvent design procedure is enhanced here with new mixture property prediction and plant-wide verification level tests.

Application to an illustrative example has shown how the full plant-wide integration of alternative materials can offer improved performance in *both* economics *and* environmental impact. As such, it has been highlighted how step-change improvements can be achieved in the set of trade-off solutions.

Acknowledgements

The authors would like to acknowledge the support of BP p.l.c., the Association of Commonwealth Universities and the British Council for funding aspects of the research presented in this paper.

References

1 J. Cano-Ruiz and G. McRae, *Annu. Rev. Energy Environ.*, 1998, **23**, 499–536.
2 A. Azapagic and S. Perdan, *Trans. IChemE Part B*, 2000, **78**, 243–261.
3 H. Cabezas, J. Bare and S. Mallick, *Comput. Chem. Eng.*, 1997, **21**, S305–S310.
4 A. Azapagic, *Chem. Eng. J.*, 1999, **73**, 1–21.
5 J. Fava and R. Denison, *Society for Environmental Toxicology and Chemistry, A technical framework for life cycle assessment*, SETAC, Vermont, 1990.
6 R. E. Steuer, *Multiple criteria optimization: theory, computation and application*, John Wiley and Sons, New York, 1986.
7 Y. Fu, U. Diwekar, D. Young and H. Cabezas, in *Process design tools for the environment*, ed. S. Sikdar and M. El-Halwagi, Taylor and Francis, New York, 2001, pp. 295–319.
8 V. Hoffmann and K. Hungerbühler, *Ind. Eng. Chem. Res.*, 2001, **40**, 4513–4524.
9 M. Dantus and K. High, *Comput. Chem. Eng.*, 1999, **23**, 1493–1508.
10 B. Alexander, G. Burton, J. Petrie and J. Romagnoli, *Comput. Chem. Eng.*, 2000, **24**, 1195–1200.
11 A. Azapagic and R. Clift, *Comput. Chem. Eng.*, 1999, **23**, 1509–1526.
12 A. Lakshmanan and L. Biegler, *AIChE Symp. Ser.*, 1994, **90**, 139–151.
13 S. Stefanis, A. Livingston and E. Pistikopoulos, *Comput. Chem. Eng.*, 1995, **19**, S39–S44.
14 G. Stephanopoulos and D. Townsend, *Chem. Eng. Res. Des.*, 1986, **64**, 160.
15 L. Constantinou, K. Bagherpour, R. Gani, J. Klein and D. Wu, *Comput. Chem. Eng.*, 1996, **20**, 685–703.
16 P. Harper and R. Gani, *Comput. Chem. Eng.*, 2000, **24**, 667–683.
17 A. Buxton, A. Livingston and E. Pistikopoulos, *AIChE J.*, 1999, **45**, 817–843.
18 E. Pistikopoulos and S. Stefanis, *Comput. Chem. Eng.*, 1998, **22**, 717–733.
19 E. Marcoulaki and A. Kokossis, *Chem. Eng. Sci.*, 2000, **55**, 2529–2546.
20 B. Ahmad and P. Barton, *Comput. Chem. Eng.*, 1999, **23**, 1365–1381.
21 C. Maranas, *AIChE J.*, 1997, **43**, 1250–1264.
22 A. Duvedi and L. Achenie, *Chem. Eng. Sci.*, 1997, **51**, 3727–3739.
23 A. Giovanoglou, J. Barlatier, C. Adjiman, E. Pistikopoulos and J. Cordiner, *AIChE J.*, 2003, **49**, 3095–3109.
24 M. Sinha, L. Achenie and G. Ostrovsky, *Comput. Chem. Eng.*, 1999, **23**, 1381–1394.
25 K. Joback, *AIChE Symp. Ser.*, 1994, **90**, 98–103.
26 Pŕe Consultants, *The Eco-indicator 99, A damage oriented method for life cycle impact assessment. Methodology Report and Manual for Designers*, second edn., Amersfoort, The Netherlands, 2000.
27 K. Miettinen, *Nonlinear Multiobjective Optimization*, Kluwer Academic Publishers, The Netherlands, 1999.
28 V. Dua and E. Pistikopoulos, *Ann. Operations Res.*, 2000, **99**, 123–139.
29 O. Odele and S. Macchietto, *Fluid Phase Equilib.*, 1993, **82**, 47–54.
30 A. Buxton, Solvent blend and reaction route design for environmental impact minimization, PhD dissertation, Imperial College of Science, Technology and Medicine, London, 2002. http://personal-pages.ps.ic.a-c.uk/~umeca69/buxton_thesis.ps.
31 J. Smith, H. V. Ness and M. Abbott, *Introduction to chemical engineering thermodynamics*, McGraw-Hill, London, 5th edn., 1996.
32 S. Harding, C. Maranas, C. McDonald and C. Floudas, *Ind. Eng. Chem. Res.*, 1997, **36**, 160–178.
33 K. Papalexandri and E. Pistikopoulos, *AIChE J.*, 1996, **42**, 1010–1032.
34 T. Martin and D. Young, *Chem. Res. Toxicol.*, 2001, **14**, 1378–1385.
35 A. Geoffrion, *J. Optimization Theory Applications*, 1974, **10**, 237–260.
36 R. Hankinson and G. Thomas, *AIChE J.*, 1979, **25**, 653–663.
37 G. Thomson, K. Brobst and R. Hankinson, *AIChE J.*, 1982, **28**, 671–676.
38 R. Reid, J. Prausnitz and B. Poling, *The properties of gases and liquids*, McGraw-Hill, New York, 1987.
39 H. Pham, P. Ryan and M. Doherty, *AIChE J.*, 1989, **35**, 1585–1591.
40 A. Brooke, D. Kendrick, A. Meeraus and R. Raman, *GAMS: A user's guide*, GAMS Development Corporations, Washington, 1998.
41 A. Drud, *CONOPT Solver Manual*, ARKI Consulting and Development, Bagsvaerd, Denmark, 1996.
42 APME, *Ecoprofiles of the European plastics industry, Report 14, Polymethyl methacrylate (PMMA)*, APME, Brussels, 1997.
43 BUWAL 132, *Schriftenreihe Umwelt*, 1990, BUWAL 3003, Stand.
44 BUWAL 250, *Schriftenreihe Umwelt*, 1996, 1st edn., Bern.
45 R. Heijungs, J. Guinee, G. Huppes, H. Udo de Huyes and A. Wegener Sleeswijk, *Environmental life cycle assessment of products: background and guide*, MultiCopy, Leiden, The Netherlands, 1992.
46 G. Davies, L. Kincaid and M. Swanson, Chemical hazard evaluation for management strategies: a method for ranking and scoring chemicals by potential human health, *Technical Report EPA/600/R-94/177*, US EPA, Cincinnati, OH, 1994.
47 K. Joback, *Unified approach to physical property estimation using multivariate statistical techniques*, MSc Thesis, MIT, Cambridge, MA, 1984.
48 A. Horvath, *Molecular design*, Elsevier, Amsterdam, 1992.
49 K. Joback and G. Stephanopoulos, *Proc. FOCAPD, CACHE Corporation, Austin, TX*, 1989, **11**, 631–636.

PAPER

www.rsc.org/greenchem

Environmental assessment of chemicals: methods and application to a case study of organic solvents

Stefanie Hellweg,* Ulrich Fischer, Martin Scheringer and Konrad Hungerbühler
Swiss Federal Institute of Technology Zurich, Institute for Chemical- and Bioengineering, Safety and Environmental Technology Group, ETH Hönggerberg, HCI G129, CH-8093 Zurich, Switzerland. E-mail: stefanie.hellweg@chem.ethz.ch; Fax: +41-1-632 11 89

Received 23rd February 2004, Accepted 9th June 2004
First published as an Advance Article on the web 13th August 2004

Suitable environmental assessment tools are needed for the development of sustainable chemical products and processes. In this paper, three methods for the environmental assessment of chemicals with different focus, fields of application, and data requirements are presented. The first method aims to identify potential environmental, health and safety hazards in the early phases of chemical process design. The second approach is to calculate screening indicators for unwanted environmental exposure to chemicals in terms of persistence and spatial range. The third approach is to perform a full life-cycle assessment. The differences between the methods are discussed, first, on a theoretical basis and then within a case study of 13 solvents. The results of all three methods indicate that the use of chlorinated solvents should be avoided, while solvents such as methanol, isopropanol, toluene and xylene are less problematic. Moreover, there are results that are unique to each method: in addition to the chlorinated solvents, nitrobenzene has a potential for long-lasting and widespread exposure; concerning environmental, health and safety aspects, care should be taken with respect to formaldehyde, benzene, and acetic acid; according to the life-cycle assessment, energy use makes up for a large fraction of the impact for solvents such as aniline. In the case study, the three methods provide consistent results both in the overall environmental assessment of the chemicals and with regard to single aspects such as degradability or toxicity. Since not all aspects are considered in all methods, the methods also provide complementary results.

Introduction

As a result of legislation and increasing public awareness, more and more attention is being paid to environmental considerations in chemical product development and process design (*e.g.*[1,2]). The need for more sustainable products and processes has triggered the (further) development of a large number of environmental assessment tools over the past decades. Some examples of such tools are substance flow analysis[3,4] product risk assessment,[5] life-cycle assessment,[6] a variety of screening indicators[1,2,7–10] and eco-audit.[11] These tools differ in focus, data requirements and applicability to various decision-making processes. Because of the inherent differences, the application of different tools may produce different results and may lead to different conclusions. Such diversity in results is often meaningful as different methods highlight different problem areas and consider different system boundaries. However, it is not always obvious which tool is most adequate for a specific situation. The application of an inappropriate assessment tool may lead to less than optimal or erroneous decisions. It is therefore important to clarify the different characteristics of these tools and the particular environmental problems that they address.

In the present study, we compare the characteristics of three selected environmental assessment tools. The goal of this work is to facilitate the appropriate choice and application of these tools. The three methods we have chosen may be applied in the development of chemical products; namely, one screening tool for assessing environmental, health, and safety hazards (EHS), one tool for product assessment using persistence and spatial range (PSR) as indicators, and life-cycle assessment (LCA). First, we analyze and compare the inherent characteristics of all three methods. Second, the application of these approaches is illustrated in a case study on solvents. Finally, we discuss the results and draw conclusions based on the conclusions each method provides for decision-making.

Methods

Assessment of environmental, health and safety (EHS) hazards in early phases of chemical process design

The EHS (Environmental, Health and Safety) assessment method is a screening method that identifies possible hazards of chemical substances in early phases of chemical process design.[7] The EHS method heavily relies on the availability of data on physical and chemical properties, toxicity, environmental and safety aspects of the substances to be assessed. These data are automatically collected from various databases (*e.g.*,[12,13]) by the EHS tool[14] with the help of an interface between the tool and the databases. Results obtained from property estimation methods such as quantitative structure–activity-relationships (QSARs) are also considered for data input.

In the EHS method, substances are assessed in eleven effect categories: mobility, fire/explosion, reaction/decomposition, acute toxicity, chronic toxicity, irritation, air mediated effects, water mediated effects, solid waste, accumulation and degradation. Depending on the substance information available, different measures or properties can be used to calculate an index value for each of these effect categories. The index is called the Effective Dangerous Property (EDP). The index for Mobility, for instance, can be calculated by using the vapour pressure or boiling point or melting point *etc*. The indexes for Acute and Chronic toxicity contain fate factors (accounting for degradation, for example) and toxicity information. The method for the calculation of EDP values for the different effect categories is presented in Koller *et al*.[7]

Persistence and Spatial Range (PSR) as indicators for the exposure potential of chemicals

For many chemicals, information on their toxicity and eco-toxicity is scarce. This impedes the risk assessment of the substances and

DOI: 10.1039/b402807b

calls for assessment methods that do not require complete information on a chemical: emission estimates, environmental fate data, and toxicity data. One possible approach is to concentrate on the exposure potential of a chemical without consideration of actual release amounts and toxicity. Persistence and spatial range[15] or characteristic travel distance[16] are indicators used to describe the exposure potential of chemicals. These indicators describe the duration and the spatial extent of environmental exposure to a chemical released at a certain point. Because they are independent of the actual release amounts, these indicators do not represent a *risk*, but refer to the chemical-specific *hazard*, *i.e.* an unwanted property that can be considered inherent to the chemical.[17,18] Persistence and spatial range are derived from multi-compartment models that calculate the transport, environmental partitioning, and degradation of a chemical.[19,20] Such models assume a generic environment consisting of air, ocean water and/or freshwater, freshwater sediment and soil, and in some cases vegetation. As chemical-specific input parameters, they require degradation rate constants for the compartments considered and partitioning coefficients such as Henry's law constant and octanol–water partition coefficient. With these data, the residence time of the chemical in the model system (persistence) and the spatial concentration distribution are calculated. The spatial range is determined as the 95% interquantile distance of this concentration distribution, *i.e.* the distance that contains 95% of the area under the spatial concentration curve; it is used as a measure that quantifies a chemical's potential for long-range transport.

The degradation data used in the models should represent biotic and abiotic transformation. Often, these data are incomplete or uncertain and have to be estimated from the chemical structure of a substance. The transport mechanisms in the ChemRange model[19] represent large-scale atmospheric circulation and ocean currents. For volatile compounds such as solvents, transport occurs in the air and the residence time in air directly determines the potential for long-range transport.

The estimation of persistence and spatial range with the ChemRange model provides information on the extent to which a chemical use pattern might contribute to long-lasting and widespread exposure, which is an aspect that is often disregarded in risk and safety assessments. This aspect is relevant because long-lasting and widespread exposure of chemicals displaces a burden to remote regions and into the future, which is not in accordance with equity considerations.

Life-cycle assessment (LCA): assessing potential environmental impacts during the whole life cycle

Life-cycle assessment (LCA) is used to study the environmental impacts throughout a product's life, from raw material acquisition through production, to use and disposal (*i.e.* from cradle to grave).[6] LCA is used to compare different products and to identify environmental improvement potentials along the life-cycle of a product.

LCA consists of four phases:[6] In the *Goal and Scope Definition* (1), the purpose of the study, the functional unit, and the boundary conditions are discussed. The functional unit provides the reference by which all resource inputs and emission outputs are normalized. The *Life-Cycle Inventory* (LCI) phase (2) comprises the gathering of emission and resource use data. In the *Life-Cycle Impact Assessment* (LCIA) phase (3), resource consumption and potential environmental impacts of these emissions are quantified (*e.g.*, global warming or toxic impacts). Finally, in the *Interpretation* phase (4), conclusions are drawn.

Although LCA is an adequate tool for analyzing the environmental impacts during the life cycle of chemicals, it should be noted that LCA has traditionally put much emphasis on energy and transport systems, rather than on chemicals. Accordingly, inventory data (phase 2 above) of chemicals, especially fine and specialty chemicals, are often difficult to obtain. As a consequence, recent research has focused on the development of generic tools, with which emission and resource-use data may be estimated for a range of chemical products and end-of-pipe processes.[21–24] In the impact assessment, there are also several drawbacks with respect to chemicals: for instance, the impacts of many chemicals are not assessed or are poorly modeled in standard LCIA methods, in particular with respect to the toxicity-related impact categories.

Comparison of the three methods and their application in chemical product and process development

The three methods presented above have been designed for use in various decision-making processes (Table 1). As a consequence, they employ different modeling approaches and require different input data. Table 1 displays some characteristics of the three methods.

The EHS method is broadest in scope when compared to the other two methods, *i.e.* it takes health and safety aspects into account in addition to environmental impacts. At the same time, this method uses the simplest assessment approach and is therefore classified as a screening method. PSR and LCA only assess environmental exposure and impacts, but the assessment includes more information on environmental and technical processes: The PSR approach allows for an assessment of environmental exposure after a potential release of a chemical. A relatively detailed environmental fate modeling is conducted to this end. LCA considers not only the production of chemicals but also the preceding processes, the use and disposal phase, and transportation.

Table 1 Characteristics and fields of application of the methods EHS, PSR, and LCA in the context of assessing chemical products and processes. See text for further explanations

	EHS	PSR	LCA
Typical decisions and goals	Identifying possible environmental, health and safety hazards in early stages of chemical process design; comparison of different chemical process alternatives	Comparison of chemicals with respect to persistence and spatial range; identification of potential contributions to long-lasting and wide-spread exposure after possible release.	Identification of environmental shortcomings and improvement potentials throughout the life cycle of a product or service; comparison of products/activities within the same function
Type of method	Screening method for chemical substance assessment	Generic multi-compartment fate and transport model	Inventory analysis combined with environmental impact assessment
Time of application	Early chemical process development stage	Different stages of chemical product and process development; screening of existing chemicals	All stages of chemical product and process development except for very early stages; assessment of existing chemicals and processes
Data requirements	Substance properties concerning environmental, health and safety aspects	Selected substance properties related to environmental behavior	Amounts of all emissions and resource uses during the life-cycle of the chemical product as well as environmental fate and effect data

Potential environmental impacts due to resource use and emissions from all of these processes are aggregated into impact scores.

All three approaches can be used in the development of chemical products and/or processes. However, the time of application and input for decision-making differ from one method to another. In the early stages of product development, various chemical products offering the same service may be under consideration. In such a case, the PSR approach can be most adequately employed to identify the chemical with the least chemical-inherent exposure potential, as this method estimates the environmental fate of the different compounds with a relatively small amount of data needed. EHS comes into play once the chemical compound to be produced has been selected and different synthesis routes and process alternatives for the routes are to be evaluated. The method delivers a comprehensive screening of the chemicals involved in the different synthesis routes and process alternatives, and accounts for the different process operating conditions. The identified hazards then need to be investigated further with more elaborated methods. Process safety, in particular, must be evaluated with in-depth methods.[25] LCA may additionally be used to identify the synthesis route and formulation with the least environmental impact, or can be used to compare a new chemical with existing products available on the market.[26] If, in this later stage of the chemical process development, more and/or improved data on the chemical properties (most importantly environmental degradation half-lives) are available, the PSR approach can be re-applied to reduce the uncertainties of the results for persistence and spatial range.

Exact data that characterize the use phase of a chemical product only become available after finalizing the product and process development and after making the chemical available on the market. Therefore, a complete LCA based on exact and complete inventory data can only be performed at such a stage. Such LCAs could be used in the comparison of chemicals with the same function or in the optimization of the technologies used.

Results and discussion: case study of solvents

The application of the three methods presented above is illustrated in the following by using a case study of organic solvents. Organic solvents are important industrial chemicals that are used in many industries in large quantities. In Western Europe, about 3.3 million tonnes of solvents are used every year.[27] Solvents provide a number of different services. For instance, they are used in the chemical industry as reaction media for chemical synthesis, raw materials for products, and cleaning agents for chemical equipment. In this study, we investigate the solvents acetic acid, acetone, aniline, benzene, dichloromethane, formaldehyde, isopropanol, methanol, methylchloride, nitrobenzene, tetrachloroethylene (perchloroethylene), toluene, and xylene. These solvents represent different compound classes, such as alcohols, aldehydes, aliphatic carboxylic acids, aromatic hydrocarbons, chlorinated hydrocarbons, ether, and ketones. Some of them, such as methanol, toluene, and isopropanol, are among the most commonly used solvents, quantitatively, in the pharmaceutical and specialty chemical industry in Switzerland.[28] Others were selected according to other criteria, such as environmental persistence (*e.g.* tetrachloroethylene). The total market share of these solvents was 45% in Switzerland in 2002, on a mass basis. Fig. 1 shows the composition of solvent use in Switzerland and the prices of the solvents considered in this work.

We illustrate the application of the assessment tools to one common decision: the determination of which solvent to choose in a chemical synthesis step, from an environmental point of view. This example was constructed on a theoretical basis to compare the methods within the same decision-making process. It should be noted that the assessment tools are often applied to widely varied decision-making processes and that in some cases only one of these tools is adequate.

Application of the method Environmental, Health and Safety (EHS) Hazards to the case study

In contrast to the other two methods employed in this study, the EHS method considers three different areas of potential hazard resulting from chemical substances: the environment, workplace health, and chemical process safety. Fig. 2 shows the results obtained for the 13 solvents investigated and all 11 effect categories considered in the three areas.

One possibility for interpreting the results of Fig. 2 is to compare the different chemicals on the basis of the overall height of the bars, which is equivalent to an equal weighting of the effect categories. With this approach, formaldehyde, methylchloride, dichloromethane, tetrachloroethylene and benzene are identified as the most problematic solvents. Another approach is to determine the number of effect categories with an index value above 0.5 for each substance. For formaldehyde this approach leads to high index values in 6 critical effect categories, for methylchloride and benzene in 5 categories, and for tetrachloroethylene in 4 categories. Because dichloromethane is classified in a group of substances with 3 critical effect categories, we conclude that both approaches provide similar ranking for the same substances.

Fig. 3 shows the results obtained for the effect categories related to environmental hazards (the categories Accumulation and Solid Waste are not of importance for the solvents investigated). Based on the height of the bars in Fig. 3, the substances tetrachloroethylene, nitrobenzene, aniline, benzene and methylchloride are identified as the most critical solvents. These results are slightly different from the ones obtained on the basis of all eleven effect categories (see Fig. 2). The substances identified as most critical with regard to environmental hazards show high indexes in both Air Mediated Effects and Degradation. No substance shows a critically high index for the effect category Water Mediated Effects. We must take into account here that the results for this effect category include both fate and effect assessment data. Formaldehyde, for example, is a toxic substance, but the Fate Factor is rather low due to rapid degradation in the aquatic environment.

Finally, Fig. 4 shows the results for the effect categories related to workplace health. Again, formaldehyde shows the highest overall bar with high indexes in both chronic toxicity and irritation. For the other solvents, the results are somewhat different from those obtained for all eleven effect categories. Acetic acid shows a high Irritation index due to the fact that it is an acid. The solvents methylchloride and tetrachloroethylene both show high chronic toxicity indexes and are, therefore, again identified as critical substances. These results may help to determine protective measures if the substances are used despite not being inherently safe.

Determination of the Persistence and Spatial Range (PSR) of the solvents

With the octanol–water partition coefficient, the Henry's law constant, and half-lives in soil, water and air as chemical-specific inputs, the spatial ranges and persistences of 13 of the solvents are calculated with the ChemRange model (data given in Table 2).

In Fig. 5, the spatial range in air, R_a, and the overall persistence, $\tau_{ov,s}$, of the 13 solvents are shown. In these model calculations, the chemicals are released to the soil (index "s" in $\tau_{ov,s}$) so that they have to evaporate before long-range transport can occur. The spatial range is given in % of the circumference of the earth and the persistence in days (logarithmic scale). The solid line represents the spatial range as a function of the residence time in air after release to air, τ_a. This function can be calculated analytically.[29] For chemicals lying on this line, the overall persistence is dominated by their half-life in air, independent of the release pathway. Chemicals to the left of the line have $\tau_{ov,s} < \tau_a$; these are chemicals with shorter half-lives in soil and water than in air (only a few chemicals have this combination of half-lives). Chemicals to the right of the line have $\tau_{ov,s} > \tau_a$ and, accordingly, half-lives in water and soil

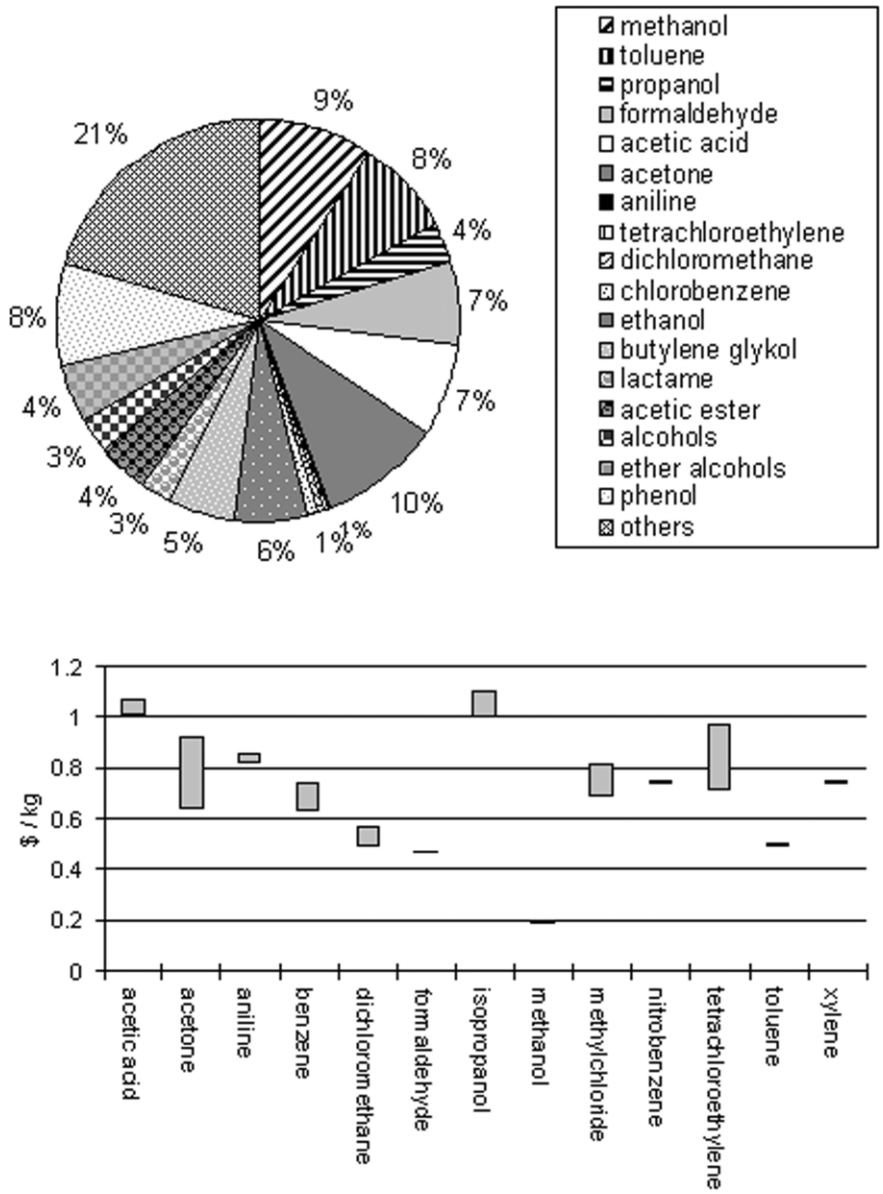

Fig. 1 Composition of the total use of solvents in Switzerland (440,000 t in 2002, above), estimated from the Swiss solvent trade balance,[43] and prices in US$ per kg solvent (below, prices refer to April 2004[44]). The amounts of benzene and xylene are not shown because they are very small (less than 200 t per year). Data on the use of nitrobenzene and methylchloride were not available.

greater than in air (this is the more common combination of half-lives).

Nitrobenzene and all chlorinated solvents have a high persistence of around or greater than 100 days, as well as high spatial ranges greater than 55%. Acetone, methanol, acetic acid and benzene have a lower persistence of around 10 days but still relatively high spatial ranges around 20% because their half-lives in air are relatively high. For acetone and benzene, environmental long-range transport has been reported (,[18] footnote 1 on p. 161). The last five solvents also have a persistence of around 10 days but spatial ranges below 10% (toluene, xylene, isopropanol), or even below 5% (aniline, formaldehyde). The results indicate that the chlorinated solvents and nitrobenzene, if released in significant quantities, can cause long-lasting and widespread exposure. The chemicals of the second group do not pose a persistence problem but can be transported over rather long distances. The third group of solvents has no potential for widespread and long-lasting exposure, but these compounds have, of course, to be assessed with respect to occupational health and local environmental safety (*e.g.* see Fig. 3 for the EHS occupational health assessment of formaldehyde). Here, an additional clarification is necessary. If "short-range" chemicals such as xylene are released from many adjacent sources, a larger exposure pattern occurs. However, this exposure pattern can be "decomposed" into many single "patches" that can be influenced by local emission reductions. Therefore, such widespread exposure is different from exposure caused by long-range transport from a single source.

Application of Life-Cycle Assessment (LCA)

The goal of this LCA is to identify environmental key problem areas of solvent use in the chemical industry and to provide information for solvent choice. The functional unit is defined as the production, use, and disposal of 1 kg of solvent.

Data about solvent production was taken from Althaus *et al.*[30] All process steps, from resource extraction to the final process steps and transport, were considered, with the exception of transportation of the final product to the place of use. With respect to disposal, we present data for solvent incineration, as this is the most common type of disposal in Switzerland.[28] Credit was granted for the energy produced. This credit is based on the assumption that electricity and heat produced during solvent incineration prevent environmental impacts for the production of the same amounts of energy with power plants. Here, we used the reference systems 'electricity,

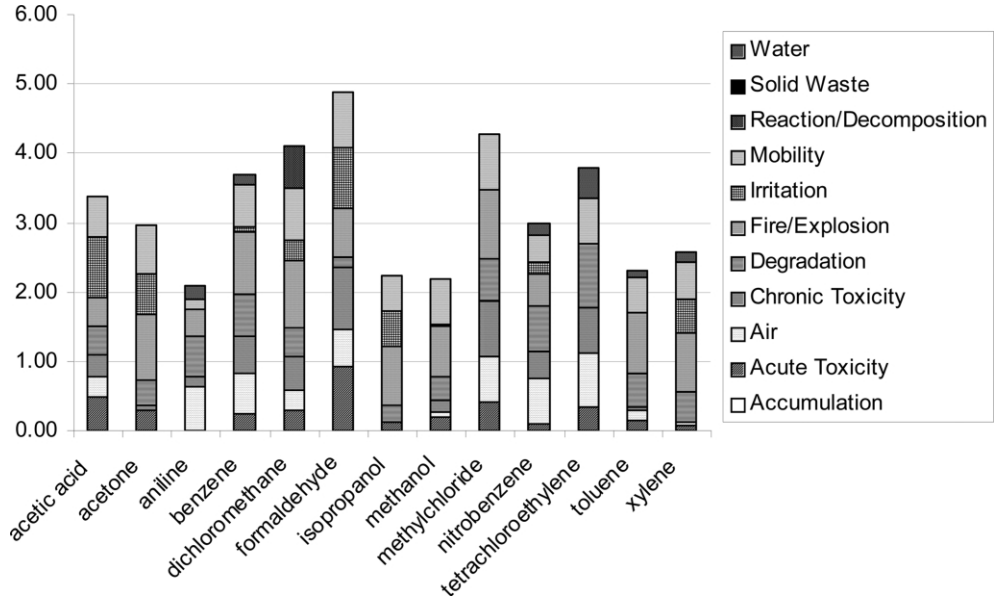

Fig. 2 Effective Dangerous Properties (environmental, health and safety hazards) of solvents according to the EHS method. The unit is cumulative index.

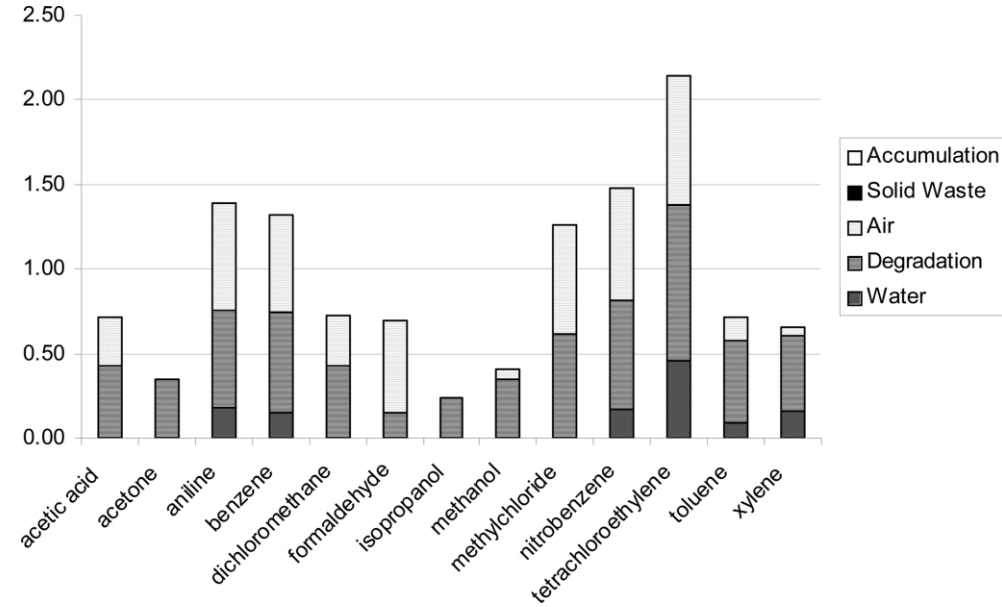

Fig. 3 Effective Dangerous Properties (only environmental hazards) of solvents according to the EHS method. The unit is cumulative index.

medium voltage, at grid CH' and 'heat, heavy fuel oil, at industrial furnace 1 MW, CH'.[31] The inventory data on solvent incineration were calculated according to Seyler-Jahn.[23]

Table 3 shows a selection of inventory data from the production of solvents (for the complete inventory table see Althaus *et al.*[30]). The data are partially interdependent, as some solvents are used in the production of others. For instance, methanol is used in the production of formaldehyde (1.13 kg kg^{-1}) and acetic acid (0.5 kg kg^{-1}); benzene is used to synthesize nitrobenzene (0.66 kg kg^{-1}); and nitrobenzene is used to produce aniline (1.33 kg kg^{-1}).[30] The production of all solvents requires fossil resources such as natural gas and oil (used as feedstock and fuel), as shown in Table 3. The production and use of fossil fuels results in emissions of CO_2 and NO_x. Additionally, halogenated hydrocarbons are emitted in the production of chlorinated solvents. The emissions of solvents other than halogenated hydrocarbons are shown in the last line of Table 3.

When solvents are used in a chemical synthesis step, a small fraction of the solvent is released into air. The masses emitted depend mostly on the effectiveness of emission abatement installations, while substance properties play a minor role.[21] Solvent emissions to air are between 0.0001 g and 1 g per kg of solvent when the solvents are used in a chemical process step including reaction and work up (batch-production).[21] This is a relatively small amount compared to the cumulated solvent emissions from the production of some solvents (last two lines of Table 3).

In the LCIA, we applied the method Eco-indicator 99[32] (Fig. 6) and crosschecked the results with the methods Swiss Ecopoints[33] and cumulative energy demand (CED).[34] Additionally, we display selected results using the toxicity impact categories of the CML baseline method.[35] The overall results according to the Eco-indicator 99 method (hierarchist perspective weighting) are presented in Fig. 6.

Resource consumption contributes significantly to the total environmental impact potential according to Eco-indicator 99 (Fig. 6), while it is far less weighted in terms of the Swiss Ecopoints (data not shown). The scores for resource consumption are highest for aniline, toluene, acetone, benzene, and xylene. Fossil resources are most important, as they are used as energy source and feedstock.

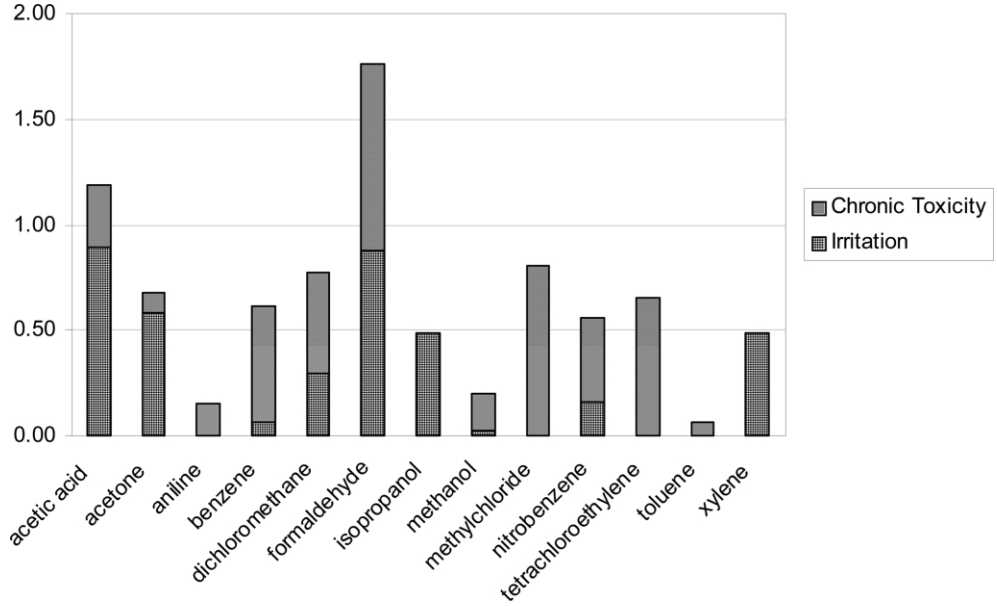

Fig. 4 Effective Dangerous Properties (only health hazards) of solvents according to the EHS method. The unit is cumulative index.

Table 2 First-order degradation rate constants and partition coefficients of the 13 solvents used in the PSR method. K_{aw}: dimensionless Henry's law constant. K_{ow}: octanol–water partition coefficient. Data are from Howard *et al.*,[40] Howard and Meylan,[41] and Mackay *et al.*[42]

Compound	k_{soil}/d^{-1}	k_{water}/d^{-1}	k_{air}/d^{-1}	K_{ow}	K_{aw}
Formaldehyde	0.262	0.262	6.07	2.239	1.38×10^{-5}
Aniline	0.154	0.154	5.545	7.943	7.76×10^{-5}
Acetic acid	0.231	0.231	0.026	0.676	4.09×10^{-6}
Methanol	0.3001	0.3001	0.0739	0.17	1.86×10^{-4}
Isopropanol	0.26199	0.26199	0.7874	1.122	3.31×10^{-4}
Methyl chloride	0.0495	0.04951	0.00357	8.128	0.36
Dichloromethane	0.0495	0.04951	0.01148	17.78	0.133
Benzene	7.75×10^{-2}	7.75×10^{-2}	1.05×10^{-1}	135	0.222
Toluene	7.39×10^{-2}	7.39×10^{-2}	0.516	5.37×10^{2}	0.2429
Acetone	2.62×10^{-1}	2.62×10^{-1}	1.89×10^{-2}	0.5754	1.50×10^{-3}
Tetrachloroethylene	2.81×10^{-3}	2.81×10^{-3}	1.37×10^{-2}	2.51×10^{3}	0.6093
p-Xylene	0.0495	0.0495	1.253	1.41×10^{3}	0.308
Nitrobenzene	0.01348	0.01348	0.00545	7.08×10^{1}	9.81×10^{-4}

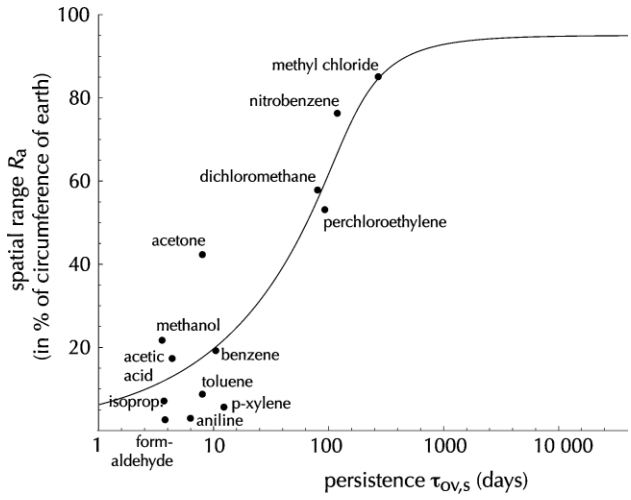

Fig. 5 Spatial range in air, R_a, *vs.* overall persistence, $\tau_{ov,s}$, of the 13 solvents, calculated with the ChemRange model (PSR method). The chemicals are released to the soil and the spatial range is determined for the spatial concentration curve in the air compartment.

The use of radioactive resources, namely uranium, is only relevant concerning certain solvents (*e.g.* dichloromethane) that require a large amount of electricity during production.

Human health also provides important contributions to the impact scores according to the LCIA methods applied; particularly concerning dichloromethane, aniline, methylchloride, and tetrachloroethylene. With Eco-indicator 99 (hierarchist), respiratory effects are most relevant, primarily because of SO_x, NO_x, and particle emissions from fuel production and use, followed by climate change and carcinogenic effects. Additionally, emissions of halogenated hydrocarbons and, to a much lesser extent, emissions of non-chlorinated solvents to air are relevant according to the Swiss Ecopoints (results not shown).

The incineration of waste solvents in special waste solvent incinerators generally leads to a net environmental benefit if credit is given for energy production (Fig. 6, right columns of each pair). Chlorinated solvents are an exception, as they demand large amounts of sodium hydroxide for eliminating chlorine from the flue gas.

The LCIA results of direct solvent emissions due to the use of solvents in a chemical process are displayed in Table 4. These impacts are three to four orders of magnitude lower than the impacts due to solvent production and incineration (Fig. 6). However, risk assessment studies[36] indicate that in other applications outside the chemical industry, the use phase of solvents may be of importance.

The LCIA results may be seen in relation to the amounts of solvents used in Switzerland to identify overall improvement potentials and practical implications of the results. In Fig. 7, we weighted the results from the impact assessment (aggregated results of Fig. 6) with the respective amounts of solvents (Fig. 1). Chlorinated solvents contribute to the total impact of all solvents considered here with a fraction of only 6%. This is due to the fact

Table 3 Selected inventory data for the production of 1 kg solvent,[30] used in the LCA

	Acetic acid	Acetone	Aniline	Benzene	Dichloro-methane	Formal-dehyde	Isopro-panol	Methanol	Methyl-chloride	Nitroben-zene	Tetra-chloroe-thylene	Toluene	Xylene
Use of natural gas/m^{-3}, standard cubic meter	0.61	1.06	1.13	0.98	0.54	1.06	0.75	0.93	0.84	0.77	0.36	1.13	1.09
Use of oil/kg	0.41	0.52	0.76	0.67	0.09	0.02	0.64	0.01	0.08	0.55	0.18	0.64	0.56
CO_2 emissions/kg	1.37	1.96	2.59	1.40	2.31	0.94	1.59	0.61	2.41	1.63	2.02	1.51	1.30
NO_x emissions/kg	0.003	0.009	0.013	0.006	0.014	0.002	0.005	0.001	0.013	0.009	0.009	0.006	0.005
Emissions of halogen-ated hydrocarbons/g	0.00	0.00	0.00	0.00	3.40	0.00	0.00	0.00	0.78	0.00	2.40	0.00	0.00
Solvent emissions to air/g[a]	5.29	0.00	3.12	0.00	0.00	0.66	0.01	0.54	0.00	0.33	0.00	0.00	0.00

[a] Only accounting for emissions of the solvents investigated here without emissions of halogenated hydrocarbons.

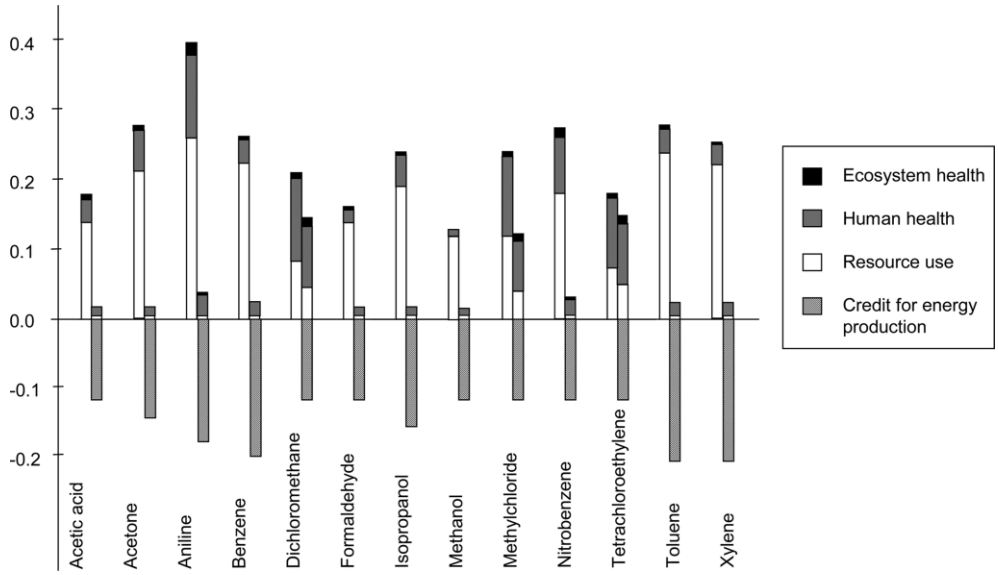

Fig. 6 LCIA results of the production (left bars of each pair) and thermal disposal (right bars) of solvents (Eco-indicator 99, hierarchist perspective, in points). The functional unit is 1 kg of solvent used in Europe. Results for other LCIA methods are not shown for reasons of brevity, but are discussed in the text.

Table 4 Impacts from solvent emissions during the use phase (use of solvent in a generic chemical process step[21]) according to the LCIA methods Eco-indicator 99 (hierarchist, the unit is points)[32] and CML-baseline[35] (human toxicity and terrestrial ecotoxicity, the unit is 1,4-dichlorobenzene equivalents) in the worst-case emission scenario (1 g solvent emission per kg solvent,[21] see text). N.a. stands for 'characterization factor not available'

	Acetic acid	Acetone	Aniline	Benzene	Dichloro-methane	Formal-dehyde	Isopro-panol	Methanol	Methyl-chloride	Nitroben-zene	PER	Toluene	*p*-Xylene
Eco-indicator 99	5.5×10^{-6}	5.3×10^{-6}	3.3×10^{-5a}	7.7×10^{-5}	6.6×10^{-5}	5.5×10^{-5}	3.3×10^{-5a}	7.3×10^{-6}	5.5×10^{-4b}	5.5×10^{-5}	1.4×10^{-5}	3.5×10^{-5}	5.7×10^{-5}
Human toxicity	n.a.	n.a.	n.a.	1.9	1.9×10^{-3}	8.3×10^{-4}	n.a.	n.a.	n.a.	n.a.	5.5×10^{-3}	3.3×10^{-4}	4.3×10^{-5}
Terrestrial ecotoxicity	n.a.	n.a.	n.a.	1.6×10^{-8}	4.3×10^{-9}	9.4×10^{-4}	n.a.	n.a.	n.a.	n.a.	8.1×10^{-6}	1.6×10^{-8}	5.4×10^{-10}

[a] Sum factor for non-methane volatile organic compounds (NMVOC) used as specific data were lacking. [b] The large impact factor can be explained by the ozone depletion through methylchloride. All other solvents contribute only to carcinogenic and respiratory effects and, in the case of dichloromethane, global warming.

that the use of these solvents has already been reduced considerably in the past (*e.g.* tetrachloroethylene[36]). Therefore, the environmental benefit of further reduction is limited in countries such as Switzerland. The most significant improvements might be achieved by reducing the use of solvents such as acetone.

Discussion

The three methods discussed here share some common features and use similar substance property input data. All methods consider the fate of chemicals in the environment. PSR concentrates solely on this aspect and identifies chemicals with high lifetimes and mobility. Both EHS and LCA, by contrast, additionally take toxic effects into account. Moreover, LCA includes environmental impacts from production and disposal. In the following, we briefly discuss whether, for common aspects in the case study, consistent results were obtained from the three methods.

The results for the degradability index in EHS are relatively consistent with the persistence results from PSR. Tetrachloroethylene, nitrobenzene, methylchloride, as well as benzene have high persistence in both methods; formaldehyde, isopropanol and methanol are indicated as rather short-lived. Some differences occur, however, for dichloromethane, aniline, xylene and acetone. These differences are caused by differences in evaluating the chemicals' persistence: in PSR, a chemical's fraction that is present in an environmental compartment defines the weight of the half-life

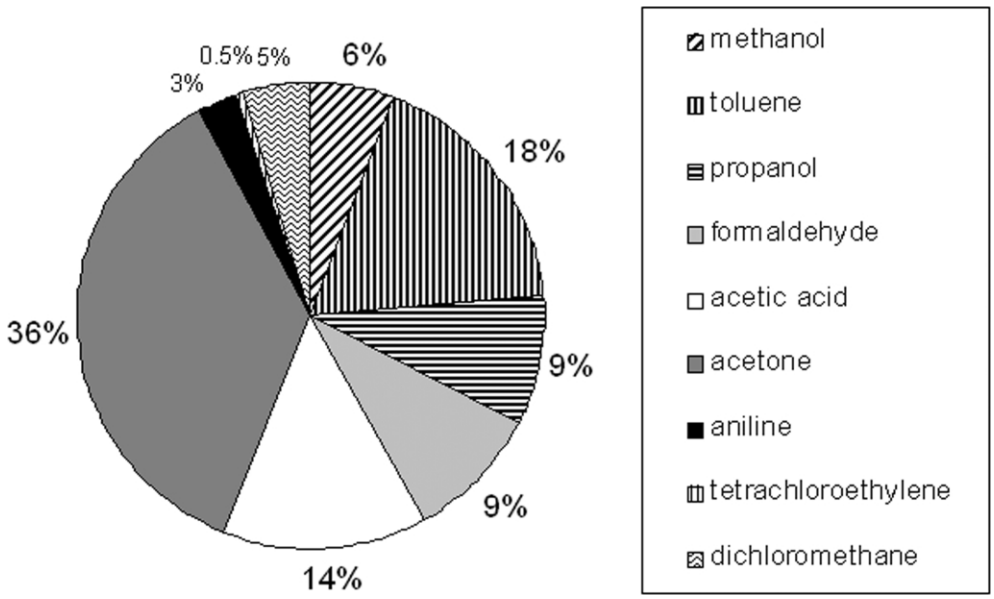

Fig. 7 Total impact of the solvents considered in this paper in Switzerland in 2002 (LCIA method: Eco-indicator 99, hierarchist perspective).

for this compartment. Since dichloromethane is primarily found in the air, the long air half-life strongly influences the overall persistence. By contrast, in EHS a shorter half-life in soil is also considered so that the score for the Degradation category is lower. In a few cases, differences in results are caused by different chemical properties used as input data, as EHS retrieves the data from various databases in an automated manner, while for PSR selected data were entered manually. A thorough evaluation of the data on chemical properties can be very demanding, as reported by Pontollilo and Eganhouse.[37] Therefore, a consistent and comprehensive database for chemical properties would be highly desirable. Furthermore, additional extensive measurements of chemical properties are clearly a research need in the context of Green Chemistry.

Concerning the combined assessment of fate and effect by EHS (Fig. 2) and LCA (Table 4), methylchloride, benzene, tetrachloroethylene, dichloromethane, and formaldehyde are most relevant. However, the ranking of these five substances varies between the two methods as well as among different LCIA methods (Table 4). This is due to the different ways of weighting and combining fate and effect data.[38]

The results of all three assessment methods indicate that chlorinated solvents are – for different reasons – environmentally problematic chemicals. The environmental relevance can be explained by the high persistence of these substances (Fig. 5) and by their considerable chronic toxicity (Fig. 4). According to the LCA results, the environmental relevance is also due to the use of large amounts of sodium hydroxide needed in flue gas cleaning when these solvents are treated thermally after use. Therefore, chlorinated solvents are environmentally problematic even if efficient end-of-pipe treatments minimize emissions.

The amounts of solvents used in Switzerland (Fig. 1) indicate that the use of chlorinated solvents is now avoided to a large extent (less than 2% of solvent consumption). Therefore, the additional overall benefit of further reduction is limited (see also Fig. 7). Solvents that are of minor to medium environmental importance according to all three assessment methods (methanol, isopropanol, toluene and xylene) make up about 50% of the used mass of all solvents considered in this work. Due to the fact that these solvents have a relatively low impact potential, their impact can only be reduced further, to any significant proportion, if they are entirely eliminated or substituted by water. The avoidance or substitution of other solvents, such as acetone, which was found to be relevant by the LCA (Fig. 7) and PSR (spatial range, Fig. 5) results, might be the most promising strategy to reduce environmental impacts from solvents. This could be achieved by substituting acetone with more 'benign' solvents. However, it may be difficult to reduce the use of acetone without simultaneously reducing the use of phenol, because these two chemicals are produced in a joint process.

An aspect made evident by the LCA results is the high energy demand in the production of some of the solvents. Energy consumption leads to particularly high impacts for the production of aniline, benzene, toluene, xylene, and acetone (>70 MJ equivalents per kg solvent, data not shown), followed by nitrobenzene and isopropanol (>60 MJ equivalents). Because of the importance of energy use, the production and disposal phases appear to be most relevant in the complete life cycle of solvents used in the chemical industry, while the use phase of solvents in chemical synthesis steps is generally of minor relevance. Therefore, LCA enables a ranking for environmental relevance of solvents even in chemical plants where emissions of solvents are reduced to very small amounts.

In addition to the environmental hazards and impacts discussed above, the EHS method encompasses safety and occupational health hazards. Concerning these effects, care should be taken with respect to the use of formaldehyde, benzene, acetic acid and chlorinated solvents. The use of these solvents should either be avoided or protective measures should be implemented.

The three methods can contribute in different ways to choices concerning solvent use in the chemical industry. Health and safety aspects addressed by EHS should be included in the decision-making process early on and with high priority. As a screening tool, EHS can be applied to numerous alternative process designs with reasonable effort.

LCA provides important additional information on the entire solvent life cycle. For instance, it assesses the amounts of energy and materials used in addition to the impacts from emissions. It may thus facilitate overall process optimization in a chemical plant or it may aid in the selection of a solvent through considering the environmental impacts over the entire life cycle. This could lead to significant environmental improvement even if releases from solvent use in the chemical plant have already been minimized.

PSR addresses the potential for unwanted exposure that exceeds the direct vicinity of the place where a solvent is used. Such exposure might occur in cases in which solvents are released from diffuse sources without the possibility of end-of-pipe treatment or in the case of accidental releases. Transport over long distances and high persistence are not of direct importance to technical performance and cost, health and safety, and process efficiency but should, according to the polluter-pays-principle, also be taken into account

in a comprehensive assessment of the impacts (possibly) caused by a chemical plant.

In practice, environmental criteria as assessed by the three methods presented in this study are usually considered to be secondary to other criteria. For instance, in an inquiry of the chemical industry concerning waste solvent management,[28] (1) regulations, (2) logistical aspects, (3) costs, (4) and technical constraints were all rated as more important than environmental aspects. Financial costs (Fig. 1) and environmental assessment results (Figs. 2–7) do not necessarily provide the same incentives. For instance, some of the environmentally problematic substances, such as dichloromethane, are rather cheap (Fig. 1), while isopropanol is quite expensive. From an environmental point of view, such discrepancies are problematic. It would be desirable for environmental assessments to receive greater significance in decision-making.

In order to optimize their leverage, environmental assessment tools should be applied early in product and process development, as the degrees of freedom are higher and the costs of potential changes lower.[1,26] Such application in early phases of product and process development is possible with PSR and EHS, while the use of complex tools such as LCA is limited due to data constraints. This could change if more estimation procedures for inventory data (such as[21]) and inventory databases including data about substrates, auxiliary materials, and energy (such as[39]) were available. However, it remains necessary to determine whether decisions made on the basis of such uncertain or incomplete data correlate well with the decisions that would have been made at a later stage, when more information is available.

In the current case study, results from the three methods are consistent with respect to the overall environmental assessment of the chemicals and with respect to specific aspects, such as degradability or toxicity. Since each method does not consider all of the same aspects, the methods yield some complementary results that are unique to each method.

Acknowledgements

We would like to thank Shailesh Shah for his support in generating the EHS results and Christian Capello for cross-checking the LCA results and compiling the statistics on solvent use. We are also indebted to Georg Geisler for his comments on a previous draft of the manuscript and to Scott Loren for language corrections.

References

1 E. Heinzle and K. Hungerbühler, Integrated Process Development: the Key to Future Production of Chemicals, *Chimia*, 1997, **51**, 176–183.
2 J. A. Cano-Ruiz and G. J. McRae, Environmentally Conscious Chemical Process Design, *Annu. Rev. Energy Environ.*, 1998, **23**, 499–536.
3 P. Baccini and H. Bader, Regionaler Stoffhaushalt, *Spektrum*, 1996.
4 P. Brunner and H. Rechberger, *Practical Handbook of Material Flow Analysis*, Lewis Publishers, Boca Raton, FL, 2004.
5 C. VanLeeuwen and C. Hermens, *Risk Assessment of Chemicals: An Introduction*, Kluwer Academic Publishers, Dordrecht, The Netherlands, 1995.
6 Anonymous, ISO 14040-43, B-Brüssel: European Committee for Standardization (CEN), 1997–99.
7 G. Koller, U. Fischer and K. Hungerbühler, Assessing Safety, Health and Environmental Impact during Early Process Development, *Ind. Eng. Chem. Res.*, 2000, **39**, 960–972.
8 E. Heinzle, D. Weirich, D. Brogli, V. H. Hoffmann, G. Koller, M. A. Verduyn and K. Hungerbühler, Ecological and Economic Objective Functions for Screening in Integrated Development of Fine Chemical Processes. 1. Flexible and Expandable Framework Using Indices, *Ind. Eng. Chem. Res.*, 1998, **37**(8), 3395–3407.
9 V. H. Hoffmann, K. Hungerbühler and G. J. McRae, Multiobjective Screening and Evaluation of Chemical Process Technologies, *Ind. Eng. Chem. Res.*, 2001, **40**, 4513–4524.
10 M. Eissen and J. Metzger, Environmental Performance Metrics for Daily Use in Synthetic Chemistry, *Chem. Eur. J.*, 2002, **8**, 3580–3585.
11 Anonymous, ISO 14010, B-Brüssel: European Committee for Standardization (CEN), 1996.
12 IGS, http://www.aac.ch/acc/igs_hp2.shtml/, Nationale Alarmzentrale, 1997.
13 IUCLID, http://www.technidata.de/coremedia/generator/Sites/TD__de/UIT/Produkte_26Services/IUCLID/index.html, 1998.
14 G. Koller, *Identification and Assessment of Relevant Environmental, Health and Safety Aspects During Early Phases of Process Development*, Dissertation ETH No. 13607, http://e-collection.ethbib.ethz.ch/cgi-bin/show.pl?type = diss&nr = 13607, Zurich, 2000.
15 M. Scheringer, Persistence and Spatial Range as Endpoints of an Exposure-Based Assessment of Organic Chemicals, *Environ. Sci. Technol.*, 1996, **30**(5), 1652–1659.
16 D. Bennett, T. McKone, M. Matthies and W. Kastenberg, General Formulation of Characteristic Travel Distance for Semivolatile Organic Chemicals in a Multi-Media Environment, *Environ. Sci. Technol.*, 1998, **32**, 4023–4030.
17 M. Scheringer, K. Hungerbühler and M. Matthies, The Spatial Scale of Organic Chemicals in Multimedia Fate Modeling: Recent Developments and Significance for Chemicals Assessment, *Environ. Sci. Pollut. Res.*, 2001, **8**, 150–155.
18 M. Scheringer, *Persistence and Spatial Range of Environmental Chemicals*, Wiley-VCH, Weinheim, 2002.
19 M. Scheringer, H. Held and M. Stroebe, *Chemrange 2.1 – A Multimedia Transport Model for Calculating Persistence and Spatial Range of Organic Chemicals*, http://ltcmail.ethz.ch/hungerb/research/product/chemrange.html, Zürich, 2002.
20 A. Beyer and M. Matthies, *Criteria for Atmospheric Long-Range Transport and Persistence of Pesticides and Industrial Chemicals*, UBA Berichte Nr. 7/02, E. Schmidt Verlag, Berlin, 2002.
21 G. Geisler, T. Hofstetter and K. Hungerbühler, Production of Fine and Speciality Chemicals: Procedure for the Estimation of LCIs, *Int. J. LCA*, 2003, **9**(2), 101–113.
22 S. Seyler, S. Hellweg, M. Monteil and K. Hungerbühler, Life Cycle Inventory for Use of Waste Solvent as Fuel Substitute in the Cement Industry: A Multi-Input Allocation Model, *Int. J. LCA*, 2004, in press.
23 C. Seyler-Jahn, *Ein inputabhängiges Oekoinventar-Modell für die thermische Verwertung von Abfall-Lösungsmittel in der chemisch-pharmaeutischen Industrie*, Dissertation, ETH, Zurich, 2003.
24 S. Hellweg, T. B. Hofstetter and K. Hungerbühler, Modeling Waste Incineration for Life Cycle Inventory Analysis in Switzerland, *Environ. Model. Assess.*, 2002, **6**(4), 219–235.
25 S. Shah, U. Fischer and K. Hungerbühler, A Hierarchical Approach for the Evaluation of Chemical Process Aspects from the Perspective of Inherent Safety, *Trans. IChemE*, 2003, **81**, 430–443.
26 G. Geisler, *Life Cycle Assessment in the Development of Plant Protection Products: Methodological Improvements and Case Study*, Dissertation, ETH, Zurich, 2003.
27 D. Stoye, Solvents – Economic Aspects, in *Ullmann's Encyclopedia of Industrial Chemistry*, Wiley-VCH, Weinheim, 2002.
28 C. Capello, *Abfall-Lösungsmittelverwertung in der chemischen Industrie, Phase 2. Jahresbericht zu Handen des Bundesamtes für Energie*, Projekt-Nr. 100065, Zürich, ETH, 2003.
29 H. Held, Robustness of Spatial Ranges of Environmental Chemicals against Model Dimension, *Stochastic Environ. Res. Risk Assess.*, 2003, **17**, 20–41.
30 H. Althaus, R. Hischier, M. Ossés, A. Primas, S. Hellweg, N. Jungbluth and M. Chudacoff, *Life Cycle Inventories of Chemicals. Final Report ecoinvent No. 8*, Swiss Centre for Life Cycle Inventories, Dübendorf, 2003.
31 *Sachbilanzen von Energiesystemen: Grundlagen für den ökologischen Vergleich von Energiesystemen und den Einbezug von Energiesystemen in Oekobilanzen für die Schweiz. Final Report ecoinvent No. 6*, ed. R. Dones, C. Bauer, B. Burger, M. Faist, R. Frischkrecht, T. Heck, N. Jungbluth and A. Röder, Swiss Centre for Life Cycle Inventories, Dübendorf, 2003.
32 M. Goedkoop, R. Spriensma, R. Müller-Wenk, P. Hofstetter, T. Köllner, T. Mettier, A. Braunschweig, R. Frischknecht, D. van de Meent, M. Rikken, T. Breure, R. Heijungs, E. Lindeijer and H. Sas, *The Eco-indicator 99: A Damage Oriented Method for Life Cycle Impact Assessment. Methodology Report*, Pré Consultants, Amersfoort, 1999.
33 SAEFL, *Bewertung in Ökobilanzen mit der Methode der ökologischen Knappheit*, Ökofaktoren 1997, SRU-297, Bern: Swiss Agency for the Environment, Forests and Landscape, 1998.

34 VDI, *Cumulative Energy Demand – Terms, Definitions, Methods of Calculation*, in VDI-Richtlinien 4600, Verein Deutscher Ingenieure, Düsseldorf, 1997.
35 M. A. J. Huijbregts, *Priority Assessment of Toxic Substances in the Frame of LCA*, University of Amsterdam, Amsterdam, The Netherlands, 1999, http://www.leidenuniv.nl/interfac/cml/lca2/.
36 J. Von Grothe, C. Hürlimann, M. Scheringer and K. Hungerbühler, Reduction of Occupational Exposure to Perchloroethylene and Trichloroethylene in Metal Degreasing over the Last 30 Years: Influences of Technology Innovation and Legislation, *J. Exposure Anal. Environ. Epidemiol.*, 2003, **13**, 325–340.
37 J. Pontolillo and R. Eganhouse, *The Search for Reliable S_w and K_{ow} Data for Hydrophobic Organic Compounds: DDT and DDE as a Case Study*, Water-Resources Investigations Report 01-4201, US Geological Survey, Reston, VA, 2001.
38 D. W. Pennington, J. Potting, G. Finnveden, E. Lindeijer, O. Jolliet, T. Rydberg and G. Rebitzer, Life-Cycle Assessment (Part II): Current Impact Assessment Practice, *Environ. Int.*, 2004, in press.
39 ecoinvent Centre, ecoinvent data v1.01. Final reports ecoinvent 2000 No. 1-15., Swiss Centre for Life Cycle Inventories, Dübendorf, 2003.
40 *Handbook of Environmental Degradation Rates*, ed. P. Howard, R. Boethling, W. Jarvis, W. Meylan and E. Michalenko, Lewis Publishers, Chelsea, MI, 1991.
41 P. Howard and W. Meylan, *Handbook of Physical Properties of Organic Chemicals*, CRC Press/Lewis Publishers, Boca Raton, FL, 1997.
42 D. Mackay, W. Shiu and K. Ma, *Illustrated Handbook of Physical-Chemical Properties and Environmental Fate for Organic Chemicals*, Vol. I: Monoaromatic Hydrocarbons, Chlorobenzenes and PCBs; Vol. III: Volatile Organic Chemicals; Vol. IV: Oxygen, Nitrogen and Sulfur Containing Compounds, CD-ROM, Chapman & Hall/CRCnetBase, Boca Raton, FL, 2000.
43 Eidgenössische Oberzolldirektion, Statistik nach Waren und Ländern, Bern, 2003.
44 CMR, Prices & People, *Chem. Mark. Rep.*, 2004, **265**, , 16), pp. 24–27.

PAPER

www.rsc.org/greenchem

Investigation of accelerated carbonation for the stabilisation of MSW incinerator ashes and the sequestration of CO_2

M. Fernández Bertos,[a] X. Li,[b] S. J. R. Simons,[a] C. D. Hills[b] and P. J. Carey[b]

[a] *Centre for CO_2 Technology, University College London, Torrington Place, London, UK WC1E 7JE*

[b] *Centre for Contaminated Land Remediation, University of Greenwich, Chatham Maritime, Kent, UK ME4 4TB*

Received 6th February 2004, Accepted 22nd July 2004
First published as an Advance Article on the web 18th August 2004

Accelerated carbonation has been used for the treatment of contaminated soils and hazardous wastes, giving reaction products that can cause rapid hardening and the production of granulated or monolithic materials. This technology provides a route to sustainable waste management and it generates a viable remedy to the problems of a decreasing number of landfill sites in the UK, global warming (due to greenhouse gas emissions) and the depletion of natural aggregate resources, such as sand and gravel. The application of accelerated carbonation (termed Accelerated Carbonation Technology or ACT) to sequester CO_2 in fresh ashes from municipal solid waste (MSW) incinerator/combined heat and power plants is presented. The purpose of this paper is to evaluate the influence of fundamental parameters affecting the diffusivity and reactivity of CO_2 (*i.e.* particle size, the reaction time and the water content) on the extent and quality of carbonation. In addition, the major physical and chemical changes in air pollution control (APC) residues and bottom ashes (BA) after carbonation are evaluated, as are the optimum reaction conditions, and the physical and chemical changes induced by accelerated carbonation are presented and discussed.

Introduction

The likelihood of significant environmental and social damage will increase significantly if concentrations of CO_2 in the atmosphere exceed about 550 ppm. To stabilise CO_2 concentrations at or below this level over the next 100 years would require global emissions reduction (relative to the current trend) of 50 to 60% by 2050 and 70–90% by 2100.[1] The Royal Commission of Environmental Pollution in the UK has recommended that there should be a 60% reduction in CO_2 emissions compared with current levels by 2050. The UK government has stated in its recent Energy White Paper (February 2003) that it is committed to this target.[2]

There is considerable discussion at scientific and industrial levels about how best to limit CO_2, particularly at large scale. One possibility is to capture and then store the CO_2 in geological structures, saline aquifers, depleted oil and gas wells or in materials. As an example of the latter, we have investigated an innovative technology, known as Accelerated Carbonation Technology (ACT), that has the major advantage of permanently binding CO_2 whilst at the same time upgrading waste material. The approach adopted utilises the ability of fresh, non-hydrated waste and other materials to react with CO_2 gas in quantities that are significant in terms of the weight% of material treated.

Atmospheric carbonation is a natural phenomenon affecting commonly used cementitious materials. It can have detrimental effects on, for example, structural concrete, or can act positively in the immobilisation of heavy metal-contaminated soils and other residues.[3–8] In a patented application, carbonation has been used intentionally[9,10] to overcome the inhibiting effects of complex waste materials on the hydraulic and pozzolanic reactions responsible for effective stabilisation/solidification. In this application, the carbonation reaction products can cause rapid hardening and result in the production of distinct materials with improved physical and chemical containment characteristics.[6,11–15] Therefore, this process has certain advantages for the treatment of waste residues and has great potential to engineer the properties of certain wastes, so that they can be reused as, for example, artificial construction aggregates.

Accelerated carbonation

Hydraulic calcium silicates become rapidly activated by CO_2, resulting in a high consumption of the gas. Some waste materials processed in the laboratory have consumed more than 50% CO_2 w/w, which indicates the great potential for the sequestration of CO_2 emissions.[16]

During accelerated carbonation the mixture is carbonated under a gaseous, CO_2 rich environment, which promotes rapid stiffening (in minutes) of the non-hydrated product into an engineering medium

The theoretical maximum CO_2 uptake capacity upon carbonation can be calculated as a function of the chemical composition of the original material using the Stenoir formula[17] given in eqn. 1:

$$CO_2\ (\%) = 0.785(CaO - 0.7SO_3) + 1.09Na_2O + 0.93K_2O \quad (1)$$

The degree of carbonation is strongly dependent upon calcium content, though the presence of certain components might influence the effective diffusivity and reactivity of the CO_2. There are many waste materials with potential for accelerated carbonation (see Fernández Bertos *et al.*[18] for a summary of these wastes and ref. 19 for the extent of carbonation against the calcium oxide composition of the initial waste).

The overall stoichiometry of the carbonation reaction of the silicate phases is shown in eqn. 2. At first, carbonation is accompanied by hydration and is followed, after some delay, by secondary carbonation:[20]

$$3CaO{\cdot}SiO_2 + y\,H_2O + (3\text{-}x)CO_2 \longrightarrow xCaO{\cdot}SiO_2{\cdot}yH_2O + (3\text{-}x)\,CaCO_3$$
$$+ z\,CO_2 \longrightarrow (x\text{-}z)CaO{\cdot}SiO_2{\cdot}yH_2O + z\,CaCO_3 \quad (2)$$

Material selection for accelerated carbonation

A review of waste streams suitable for economic treatment by accelerated carbonation has been undertaken in terms of the impact on current waste management practices and in meeting the challenges set by recent legislation.[21] Utilising the European Waste

DOI: 10.1039/b401872a

Catalogue,[22] more than 100 UK thermal residues were examined for their potential for carbonation.

The total amount of wastes produced per year, the land disposal options, the amount reused and recycled were examined in order to maximise the potential benefits of accelerated carbonation. One major waste stream identified was Municipal Solid Waste Incinerator (MSWI) residues. MSWI residues (ashes) are rich in calcium oxide and silica and have particle dimensions suitable for use as aggregate materials and properties that appear to favour treatment by accelerated carbonation.

MSW incinerator ashes

It is estimated that 29.3 M tonnes of MSW were produced in England and Wales in 1999/2000.[23] The amount produced has increased annually by 3–4% from 1996–2000, the most common methods for disposal being: landfilling (82%), recycling or composting (11%) and thermal treatment (7%).

In an incinerator the unprocessed MSW is burnt at 700–1000 °C, resulting in a solid residue which generally accounts for 30–35 wt% of the burnt waste and 10% of the initial volume. The combustion of MSW in incinerators results in two solid waste streams: bottom ashes (BA) and air pollution control residues (APC). The composition of these ashes depends on the waste input, which may vary with location, the season and whether there are any local recycling schemes in operation.

Bottom Ash (BA): represents 80% of the incinerator residue produced and is classified as a non-hazardous waste, according to the European Waste Catalogue. BA consists mainly of aluminosilicate phases and certain amounts of metallic components (~8%), including Cr, Ni, Cu, Zn, Ba, Pb, Cd, As, Ti, Mn and Hg.

Air Pollution Control Residues (APC): are a mixture of fly ash (FA), carbon and lime and are the result of a treatment process to clean the gases before they are released to atmosphere. APC residues are classified as hazardous waste due to the high lime content, high concentrations of heavy metals, soluble salts and chlorinated compounds. MSWI APC residues consist of very fine particles, which are mostly < 300 μm in size.

Carbonation of MSW incinerator ashes

The alarming decrease in primary aggregate resources has led to recent legislation to encourage the development of alternative sources.[24] Municipal Solid Waste Incinerator (MSWI) ashes (in particular, bottom ashes) can be used as a substitute for fine aggregates for construction purposes or can be used as a stone in asphalt. However, before bottom ash can be used, a stabilisation step involving natural weathering over a three to six month period is required. As a result, the pH, redox potential, leaching behaviour and acid neutralisation capacity of the ashes are modified.

An alternative to natural weathering is to apply an accelerated carbonation step[15] to accelerate a major part of the natural weathering process, thereby obtaining a stable solid with improved engineering properties more rapidly.

Studies on the influence of carbonation and the relative importance of certain variables in the stabilisation of heavy metals have been reported.[25,26] However, in contrast to these, the present work aims to find the fundamental parameters that control the extent of carbonation of MSW incinerator APC residues. Once the kinetics of accelerated carbonation are known, it will be possible to model the process for application in continuous, large scale processing of MSW ashes to produce artificial aggregates.

At this stage the work is mostly focused on achieving maximum CO_2 uptake in a short period of time. The process conditions that make ACT feasible and distinct from other forms of carbonation are:

- Slight positive pressure of 3 bars
- Reaction time below 12 h
- CO_2 concentration is kept constant at 100%
- The relative humidity is kept constant at 65%. There is a strict control of the water in the system.
- No additives are used to improve the stabilisation of contaminants (unlike other authors[3,4,27]).

Materials and methods

BA and APC residues from different incinerators across the UK were supplied by Ballast Phoenix Ltd., Onyx and the Environmental Agency (EA). These ashes were stored for 2 to 3 months before being used for the carbonation experiments, which caused some early weathering of the material. They were:

- APC from the Tyseley incinerator in Birmingham
- APC from the Edmonton incinerator
- APC from the SCHELP incinerator
- APC1, APC2 and APC3 provided by the EA
- BA from the Castle Bromwich incinerator
- BA from the Cleveland incinerator
- BA1, BA2 and BA3 provided by the EA

The ashes were received damp and were oven dried at 105 °C to constant weight prior to investigation. They were characterised for their moisture content, bulk density, particle size distribution and mineral phases using XRD, whilst their morphology was studied using an electron microscope.

The particle size distribution of the APC and BA prior to carbonation is given in Fig. 1 and Fig. 2, respectively. Table 1 shows the mean particle size for the BA and the APC.

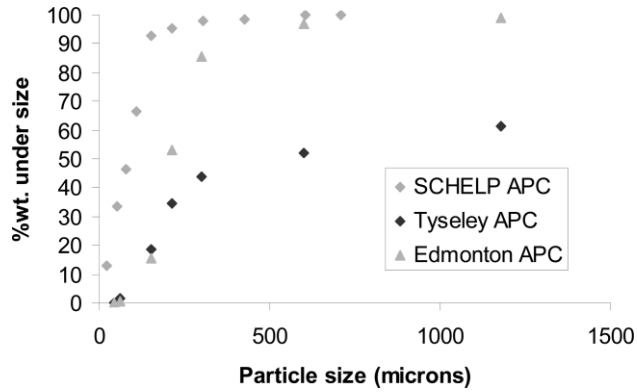

Fig. 1 Particle size distribution of APC residues.

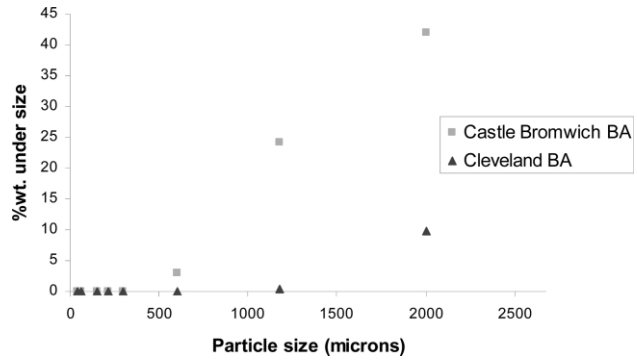

Fig. 2 Particle size distribution of BA.

The bulk density was measured by means of a water picnometer. The density and moisture contents for BA and APC are shown in Table 2. The high moisture contents recorded for bottom ash are due to quenching during the cooling process.

Methods

To ascertain ash susceptibility to carbonation and to determine the optimum range of particle size, water content and reaction time, the ashes were carbonated in the stainless steel chambers (see (1) in Fig. 3) exposing the ash to a 100% CO_2 atmosphere at 65% relative

Table 1 Mean particle size of BA and APC

Ash	Mean particle size/μm
Tyseley APC	918.07
Edmonton APC	156.32
SCHELP APC	66.12
Castle Bromwich BA	1582.02
Cleveland BA	2094.77

Table 2 Bulk density and moisture content of BA and APC

Ash	Moisture content (%)	Density/kg m^{-3}
Tyseley APC	2.5	422.68
Edmonton APC	1.2	682.8
SCHELP APC	2.9	562.8
Castle Bromwich BA	16.8	1030.6
Cleveland BA	21.9	1248.4

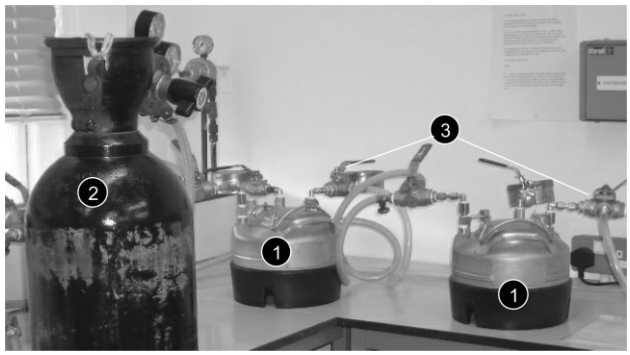

Fig. 3 Carbonation chambers.

humidity and a pressure of 3 bar. The CO_2 was continuously fed from a gas cylinder (see (2) in Fig. 3). Each chamber was equipped with an analogue pressure gage to monitor the chamber pressure (see (3) in Fig. 3). Humidity was maintained in the chambers using a small bath containing a solution of NaCl. Before exposing the ashes to CO_2, they were mixed thoroughly with water in 100 ml beakers at selected water-to-solid (w/s) ratio and then placed in 9 ml cylindrical plastic dishes of 25 mm internal diameter. For each set of experiments, control samples were prepared in the same manner and then sealed and stored under ambient laboratory conditions for the same time period.

Before starting the reaction the chambers were flashed with CO_2 three times to ensure that all the air was expelled. The extent of the carbonation was assessed by measuring the gain in dry weight (105 °C, to constant weight) before and after carbonation. The value obtained was then compared to the weight gain experienced by the control sample, the difference indicating how much carbon dioxide had reacted with the ash.

Reaction time. The ashes were mixed with water at a ratio of 0.2, which is known to be optimum for carbonation of cement-solidified wastes.[28–30] The samples were exposed to CO_2 for different time intervals from 20 min to 24 hours, and the extent of reaction was evaluated for each set of experiments.

Size fraction. Four different size fractions were prepared for each ash by sieving two of the APC residues and the BA. The BA had to be ground prior to sieving using a pestle and mortar. Table 3, shows the different fractions in which they were separated. Then, once mixed with the water at w/s = 0.2, they were left to carbonate for the time determined in the previous experiment. The comparison between the particle size, distribution before and after the reaction for APC was also established.

Water-to-solid ratio. For the optimum water content, samples of BA and APC residues of the selected size fraction (x < 710 μm and x < 212 μm respectively) were carbonated in the same chamber, during the same time interval, at different water–solid ratios ranging between 0 and 0.6.

Table 3 Selected size fractions of APC and BA to determine the optimum size fraction

Tyseley APC	Edmonton APC	Cleveland and Castle Bromwich BA
x < 75 μm	x < 125 μm	x < 500 μm
75 μm < x < 125 μm	125 μm < x < 212 μm	500 μm < x < 710 μm
125 μm < x < 212 μm	212 μm < x < 500 μm	710 μm < x < 2800 μm
x > 212 μm	x > 500 μm	x > 2800 μm

The influence of CO_2 diffusion on the carbonation reaction rate was studied by comparing carbonation under static and dynamic conditions. These experiments were carried out with the aid of an eudiometer, see Fig. 4, which measures the CO_2 consumed at

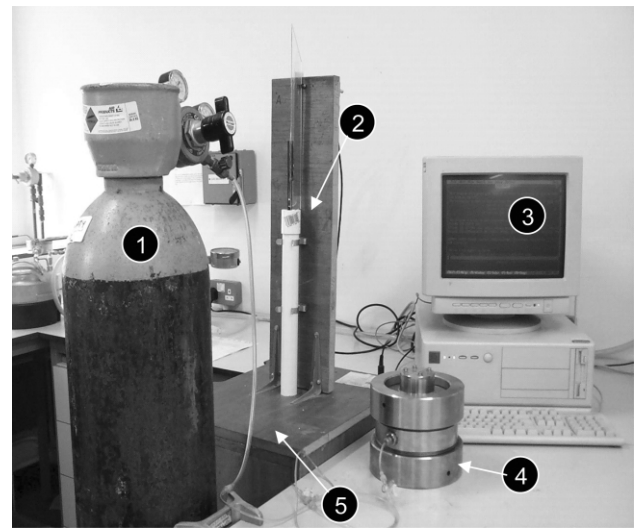

Fig. 4 Eudiometer.

different reaction times. The gasbag, which is submerged in water, is filled with CO_2 from the cylinder (see (1) in Fig. 4) before reaction. 10 g of dry ash was mixed with water at a w/s ratio of 0.2 and placed in the reactor (see (4) in Fig. 4). During the reaction, the consumption of CO_2 results in a decrease in volume of the gasbag, and a consequent change in the water level. The change of water level (see (5) in Fig. 4) is detected (see (2) in Fig. 4) and recorded by the computer (see (3) in Fig. 4). The reaction curve, calculated from the recorded change of the water level through the reaction, gave the rate and amount of CO_2 consumed by the ash. The dynamic conditions were attained by shaking the vessel throughout the reaction.

The mineralogy and microstructure of carbonated and non-carbonated ashes were analysed by X-Ray Diffraction (XRD) and Scanning Electron Microscopy (SEM) respectively. The carbonate content was obtained by using Differential Thermogravimetrical Analysis (DTA).

The pH of the ashes was examined according to BS 1377 part 3:1990.[31] Leaching was carried out with a liquid–solid ratio of 10 l kg^{-1} and 2 l kg^{-1} using deionised water (BS EN12457: 2002[32]). The eluate was filtered with a 0.45 μm filter paper after 24 hours of end-over-end shaking. Chloride and sulfate content in leachates were measured by Ion-Chromatography (DIONEX) and the concentration of the major elements Al, Ca, K, Na and minor elements As, Ba, Cd, Cr, Cu, Fe, Pb, Ni, Zn in leachates were analysed by ICP-OES after acidification with 10% nitric acid to pH < 2. All analyses were carried out in triplicate.

Results and discussion

Reaction time

The CO_2 uptake with time for Edmonton APC residue and Cleveland BA are given in Figs. 5 and 6, respectively.

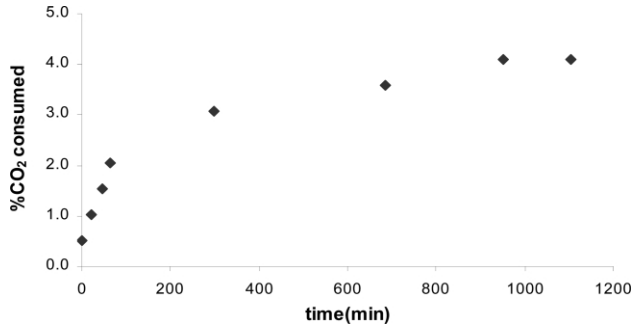

Fig. 5 CO_2 consumed with time by Edmonton APC.

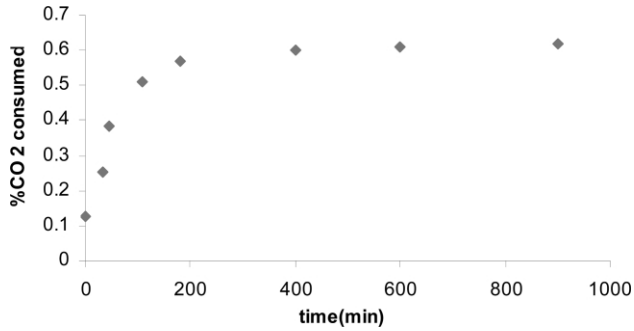

Fig. 6 CO_2 consumed with time by Cleveland BA.

Initially there is a steep rise in the consumption of the gas, which then slows down until the sample is saturated. A compromise is required between the reaction time and the extent of reaction. When carbonating the ash for 24 hours, 75% of the reaction takes place in the first 150 min. Therefore, 2.5 hours has been selected as the optimum reaction time. For both APC and BA, the velocity of consumption of CO_2 after 2.5 h is rather slow.

As seen on the graphs, the consumption of CO_2 is higher for APC than for BA. This is mainly due to the higher content of lime in APC, although some of the physical characteristics also play an important role. APC particles are of much smaller size and therefore the surface area and microporosity of this ash are higher than that of BA, factors that favour carbonation.

Particle size

Figs. 7 to 10 show the weight gain recorded during carbonation for the different size fractions of the four MSW ashes. As might be

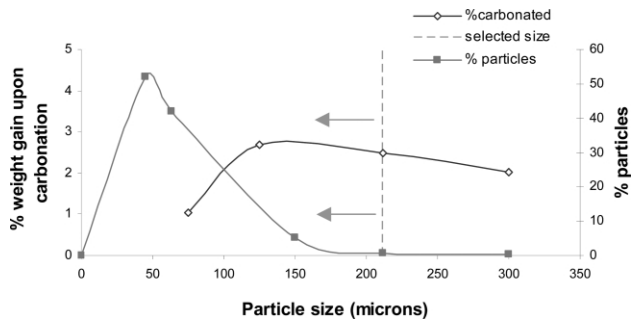

Fig. 7 Carbonation as a function of particle size for Tysley APC.

expected, the reaction is greater for the smaller and more homogeneous particle sizes,[16] due to their higher surface area. Based on this and considering the size distribution of the particles,

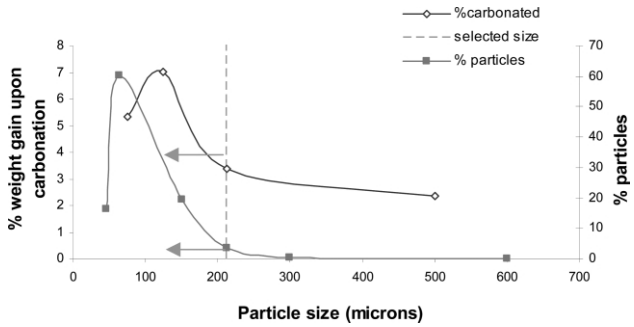

Fig. 8 Carbonation as a function of particle size for Edmonton APC.

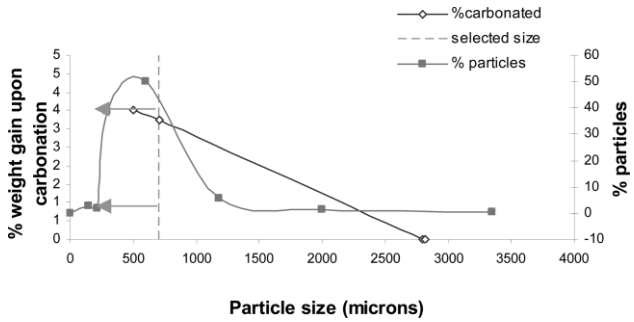

Fig. 9 Carbonation as a function of particle size for Castle Bromwich BA.

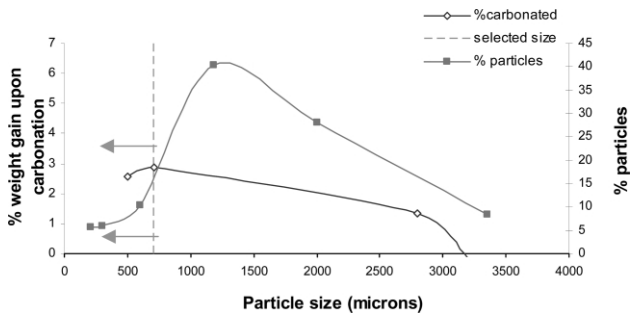

Fig. 10 Carbonation as a function of particle size for Cleveland BA.

specific particle sizes have been selected for BA and APC as optimal size fractions for carbonation; 710 μm for BA and 212 μm for APC.

Water-to-solid ratio

The influence of the water content on the carbonation reaction was also studied. The carbonation was carried out with the selected size fraction over a period of 2.5 hours. The gain in weight of the dry ash was determined for w/s ratios 0 to 0.6 for the four ashes (Fig. 11).

These experiments indicate that the w/s ratio should be 0.3–0.4 for BA and 0.2–0.3 for APC. Fig. 11 also shows how the behaviour of both BA and APC is rather similar. The great difference in weight gain between Edmonton and Tysley APC is explained by the fact that the latter was an older ash that had probably already undergone natural carbonation to a considerable extent.

It is known that water is necessary for the carbonation reaction to proceed, but too much water hinders the diffusion of CO_2 into the pores of a solid. Pore water hydrates and solvates the CO_2 and dissolves the Ca^{2+} ions from the solid phase to react and form calcium carbonate. At low w/s ratios, the material's gas permeability is increased, and the CO_2 effectively diffuses into the solid. Some authors have found the optimum ratio between w/s 0.06 and 0.20,[28–30] although others have successfully carbonated with values up to 0.35.[11]

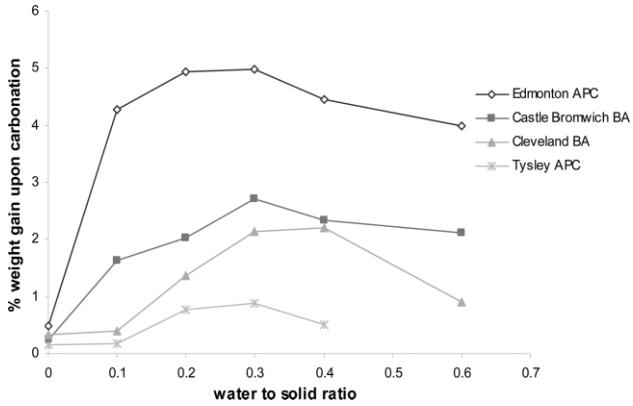

Fig. 11 Carbonation as a function of water content for the four MSW ashes.

Static and dynamic carbonation

During carbonation the diffusion of CO_2 into the ash particles is the rate-controlling step. The rate of CO_2-uptake with time from the eudiometer is shown in Fig. 12. The reaction velocity with shaking

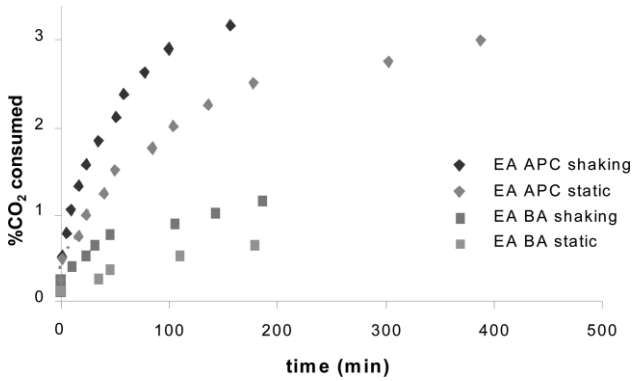

Fig. 12 Consumption of CO_2 in APC and BA from the EA for dynamic and static conditions.

is about two to three times greater than that under static conditions, clearly indicating that the carbonation process is a diffusion-controlled reaction. This infers that grinding the ash to fine particle sizes to increase the surface area exposed to reaction will be beneficial.

Property changes of carbonated MSW incinerator ash

Carbonate content. The increase of carbonate content in carbonated ashes was determined by DTA. Fig. 13 shows the

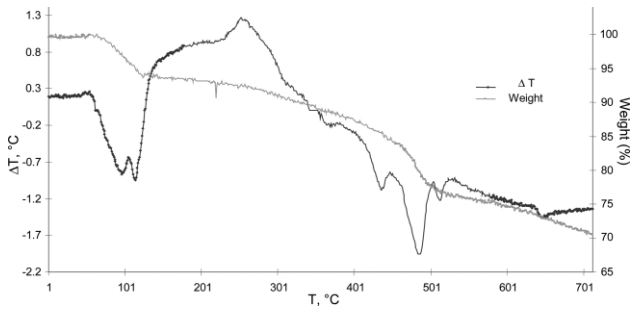

Fig. 13 DTA of SCHELP APC residue.

weight loss and ΔT curve obtained with the DTA for carbonated APC residue from the SELCHP incinerator. The weight loss curve indicates that in carbonated ash, the loss of pore and combined water occurred under 200 °C and the decomposition of the carbonate reaction products occurred above 450 °C. The combustion of organics is characterised by a positive peak in the ΔT curve between 300 and 420 °C.

Table 4 shows the difference in carbonate content between the ashes before and after 24 h carbonation at 100% CO_2 and 65% RH.

Table 4 Carbonate content and weight gain for BA and APC

Kind of ash	% $CaCO_3$ before	% $CaCO_3$ after	$CaCO_3$ gain (%)	Weight gain (%)
BA	3.46	4.74	1.34	3.19
APC	11.84	16.01	4.96	7.31

These values are also compared with the gain in weight of the samples after carbonation. The gain in weight is greater than can be explained by the observed increase in carbonate content, suggesting that other reaction products are being generated.

The gain in calcite is expressed with respect to the initial mass and is calculated as follows:

$$\%\ CaCO_3\ \text{gain} = \frac{(\%\ CaCO_3\ \text{after} - \%\ CaCO_3\ \text{before})}{(1 - \%\ CaCO_3\ \text{after})} \quad (3)$$

Particle size distribution. Particle size is a fundamental parameter, if carbonated ashes are to be used as aggregates. The comparison between the particle size distributions before and after carbonation for SELCHP APC residue is given in Fig. 14, which

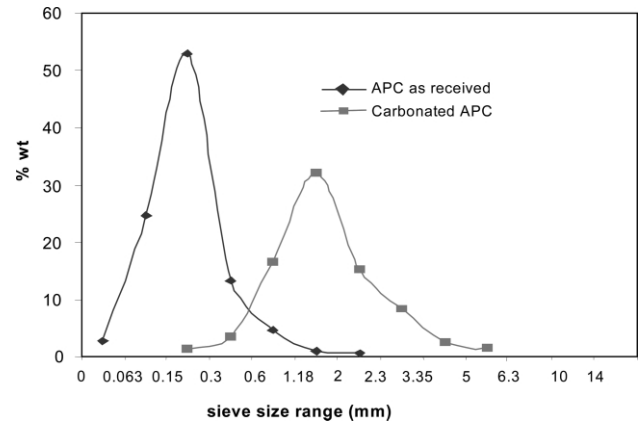

Fig. 14 Particle size distribution for APC from the EA before and after accelerated carbonation.

shows an increase in particle size due to particle agglomeration during carbonation. The size distributions of BA however, showed no difference after carbonation and are explained by a lower extent of carbonation in comparison to the APC.

Pore structure. The change in porosity, tortuosity and total pore area has been measured by means of a mercury porosimeter (see Table 5). After carbonation there is a decrease in porosity, tortuosity and total pore area due to the precipitation of carbonation products in the pore space.

Table 5 Change in porosity, tortuosity and pore area before and after accelerated carbonation

Ash	Porosity (%)	Tortuosity	Total pore area/$m^2\ g^{-1}$
Non-carbonated	73.05	6.2	4.39
Carbonated APC	62.37	2.6	0.14

Mineralogy changes. Table 6 shows the major mineral compounds identified by XRD in BA and APC residues, before and after carbonation, in order of decreasing relative concentration.

The main alterations in the mineralogy of BA and APC residues resulting from carbonation at the optimal conditions identified can

Table 6 Major compounds found in BA and APC before and after carbonation

Ash	Raw		Carbonated	
APC	Anhydrite	$CaSO_4$	Anhydrite	$CaSO_4$
	Halite	NaCl	Quartz	SiO_2
	Sylvite	KCl	Calcite	$CaCO_3$
	Quartz	SiO_2	Sylvite	KCl
	Gehlenite	$Ca_2Al_2SiO_7$	Halite	NaCl
	Calcite	$CaCO_3$	Gehlenite	$Ca_2Al_2SiO_7$
	Portlandite	$Ca(OH)_2$	Gibbsite	$Al(OH)_3$
	Thenardite	$NaSO_4$	Hematite	Fe_2O_3
	Na,K feldespar	$(AlSi_3O_8)Na$, K	Anhydrite	$CaSO_4$
	Sygenite	$K_2Ca(SO_4)_2H_2O$	Gehlenite	$Ca_2Al_2SiO_7$
	Cementic phases	CAS_2, AS	Iron oxides and hydroxides	
	Complex oxides of metals (Pb, Cu, Ba, As, Zn)		Calcium silicate complexes with metals	
BA	Quartz	SiO_2	Quartz	SiO_2
	Calcite	$CaCO_3$	Calcite	$CaCO_3$
	Dicalcium silicate	C_2S	Gypsum	$CaSO_4$ $2H_2O$
	Hematite	Fe_2O_3	Gehlenite	$Ca_2Al_2SiO_7$
	Gehlenite	$Ca_2Al_2SiO_7$	Gibbsite	$Al(OH)_3$
	Olivine	$(Mg, Fe)_2SiO_4$	Calcium silicate complexes with metals	
	Wollastonite	$CaSiO_3$		
	Feldespar group	$(Al, Si)_4O_8(Ca,Na,K)$		
	Metal oxides and hydroxides (Pb, Zn, Cu, Cr, Ni, Mn, Fe, Mg)			

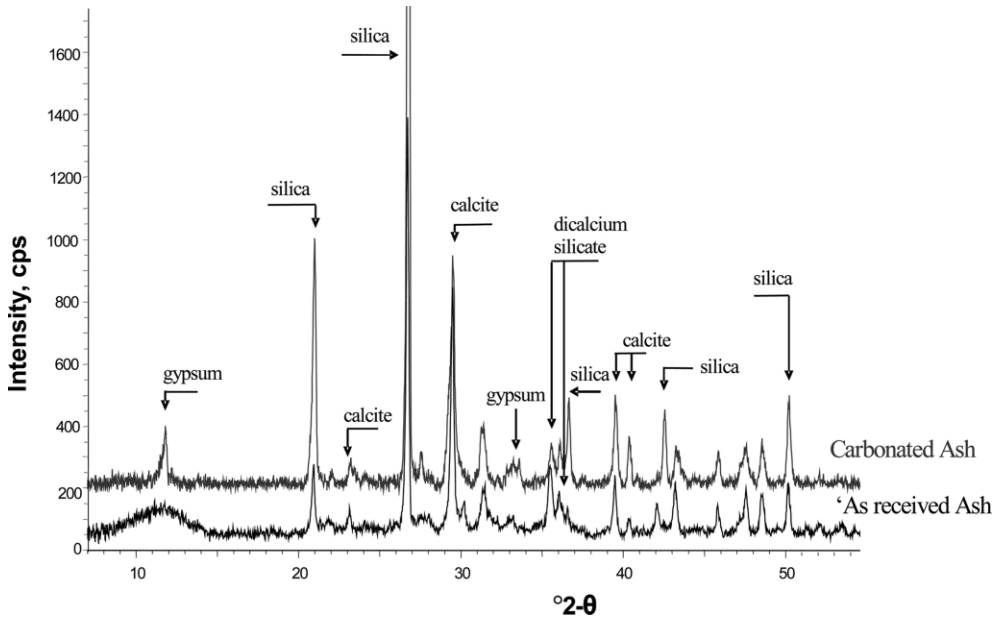

Fig. 15 XRD Diffractogram of Castle Bromwich BA.

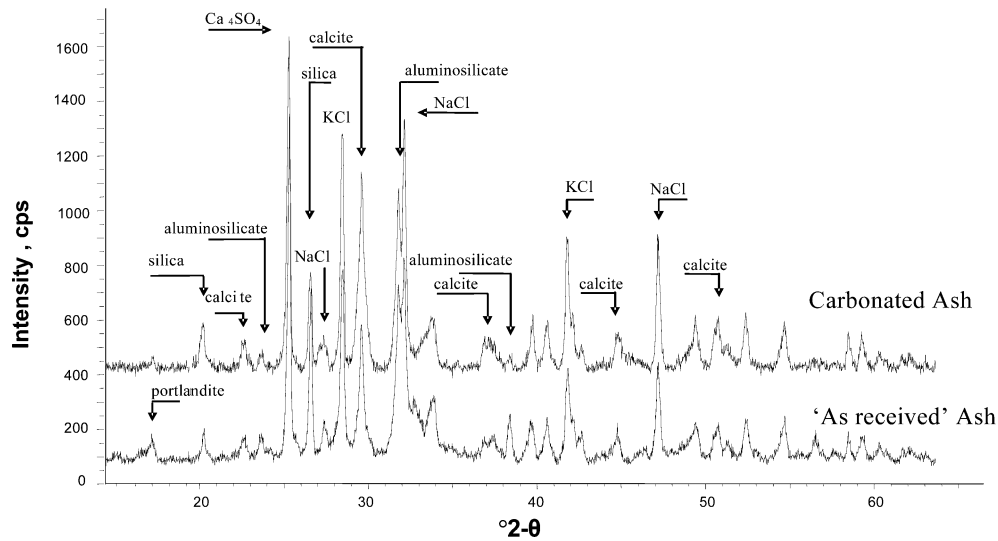

Fig. 16 XRD Diffractogram of Edmonton APC residue.

be examined by X-Ray Diffraction. Figs. 15 and 16 show the XRD diffractograms for before and after carbonation, for Castle Bromwich BA and Edmonton APC residues, respectively.

The intensity of peaks corresponding to calcite and silica are higher in carbonated samples for both MSW ashes. Both ashes have very noisy signals due to their heterogeneity and complex mineralogy. The presence of calcite in the initial samples is due to partial, earlier weathering of the ash.

The breakdown of $2CaO{\cdot}SiO_2$ and the formation of calcite and gypsum can be observed for BA. There was an increase in the degree of crystallinity in the diffractograms resulting from carbonation. In the non-carbonated sample of APC there was some evidence of hydration by the existence of minor peaks for portlandite $Ca(OH)_2$, which were absent in the carbonated sample.

Microstructure changes. Examination of the ashes with a JEOL 5110 LV SEM, using both secondary electron and back-scattered imaging, revealed distinct differences in the morphology between carbonated and non-carbonated samples. Fig. 17 (a) and (b) illustrate this by showing fracture surfaces of APC residue from SELCHP before and after carbonation, respectively. The appearance of the non-carbonated APC is granular and individual grains are clearly visible. The carbonated sample reveals a less porous solid where crystalline reaction products are clearly evident.

Fig. 18 (a) and (b) show the images of BA from SELCHP incinerator before and after carbonation, respectively. The difference is less evident than for the APC residue, as the extent of carbonation is lower for BA. Despite this, precipitated solids can be seen filling the pores of the ash.

Fig. 19 shows a backscattered image (BSI) of a polished section of the carbonated APC. The picture shows a metal rich core (bright), a rim depleted in calcium (light grey colour), and carbonate filling the porous region (dark grey colour).

pH change. The effect of carbonation on pH is of great importance as it influences metal mobility. Fig. 20 shows the change of pH due to carbonation. For the three BA and APC1 provided by the EA, the pH before carbonation is around 12 whereas after carbonation, the pH of APC falls below 8 and for BA drops to 9.

Anions and heavy metal leaching. The leaching properties of ashes are important if they are to be either reused or landfilled. The chloride and sulfate contents in leachate (L/S = 10 l kg^{-1}) have been studied for five of the ashes provided by the EA and the results obtained are shown in Fig. 21.

With the exception of the chloride in leachate from the APC residues, the chloride in BA and the sulfate in all ashes are lower than the landfill limit.[22] After carbonation, the chloride and sulfate content for the carbonated APC decreased significantly. There was, however, no great difference between leachable chloride levels for the BA. The sulfate content in BA leachate was increased, after carbonation, though it remained below the landfill limit.

Regarding the analysis of metal contaminants, special attention must be given to lead and zinc whose concentrations exceeded the

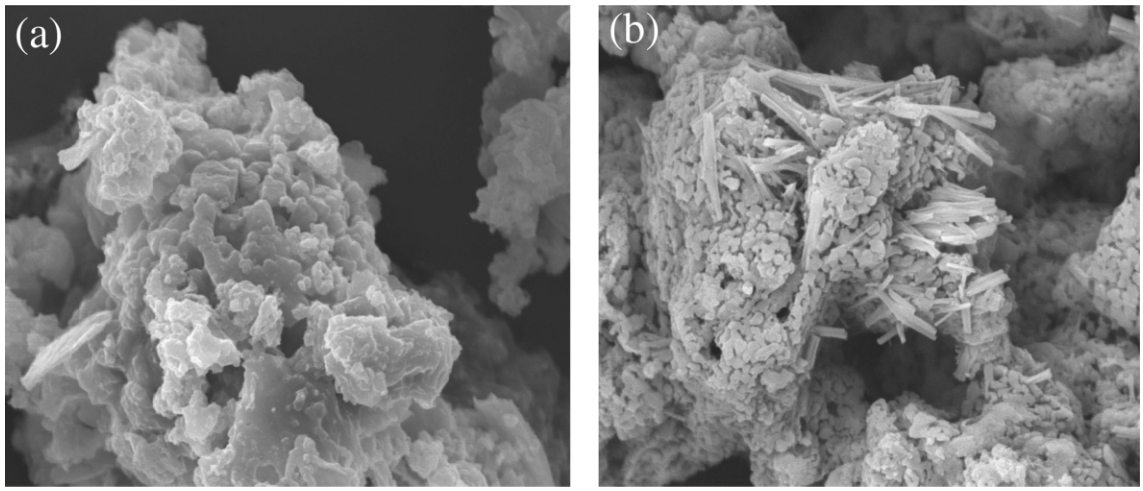

Fig. 17 SEM pictures of carbonated and non-carbonated APC residues (a) non-carbonated APC residue (b) carbonated FA.

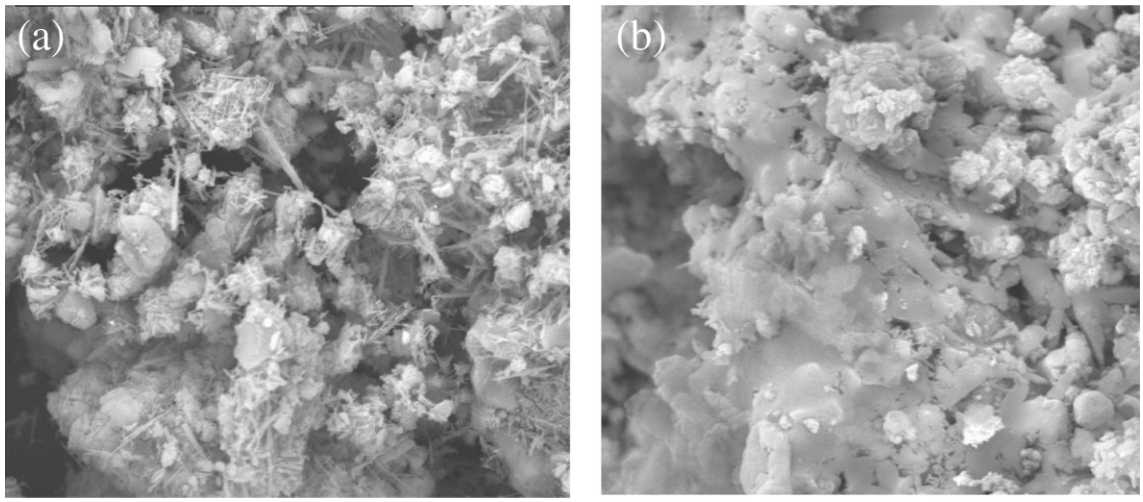

Fig. 18 SEM pictures of carbonated and non carbonated BA (a) non carbonated BA (b) carbonated BA.

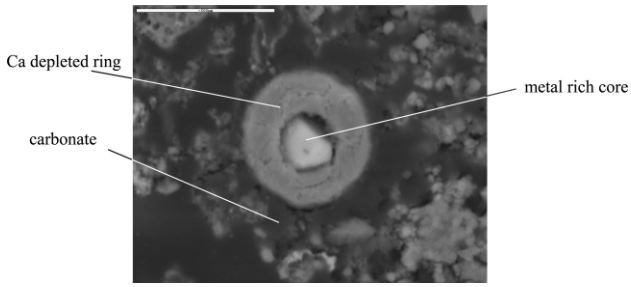

Fig. 19 BSI carbonated ash.

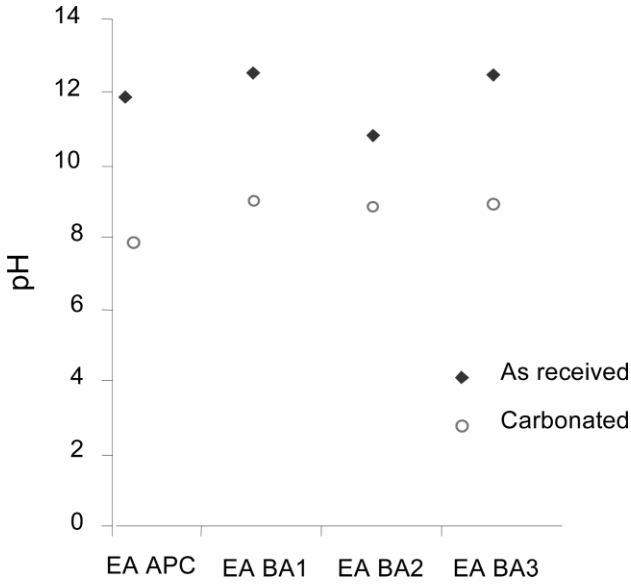

Fig. 20 pH change after carbonation for APC and BA.

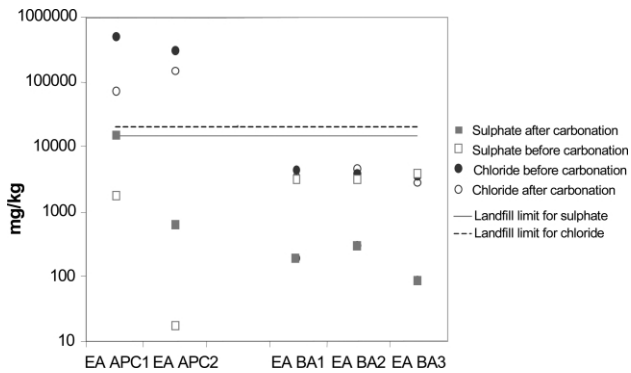

Fig. 21 Content of sulfate and chloride in the ashes before and after carbonation.

value for hazardous wastes. Figs. 22 and 23 show the leachable levels of lead and zinc, respectively, for the ashes provided by the EA.

The concentration of Pb in almost all of the leachates was 50–1000 mg kg^{-1}, which was much higher than the landfill acceptance value (50 mg kg^{-1} for hazardous wastes, 10 mg kg^{-1} for non-hazardous wastes) especially for the APC residues. However, after carbonation Pb leaching was reduced by two to three orders of magnitude and was < 1 mg kg^{-1} in some ashes.

In the un-carbonated ash, zinc leached from BA was lower than 50 mg kg^{-1}, whereas after carbonation, it dropped to < 1 mg kg^{-1}, within the acceptance value for inert wastes. The leaching of zinc from APC residues also decreased significantly upon carbonation. Generally, following carbonation the reduction in metals release meant that the ash could be classified as non-hazardous waste.

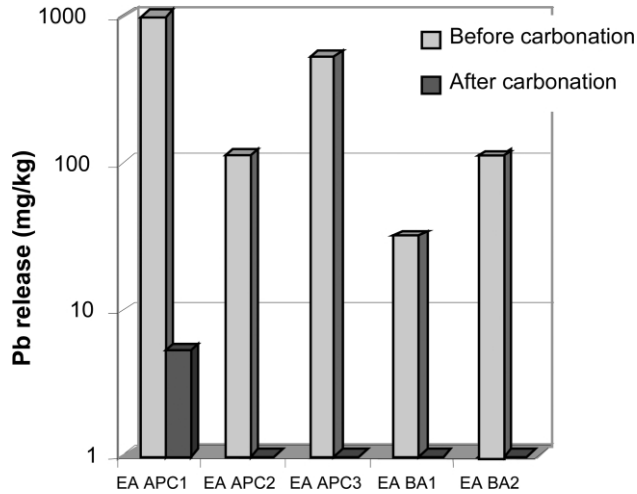

Fig. 22 Lead release before and after carbonation for different BA and APC residues.

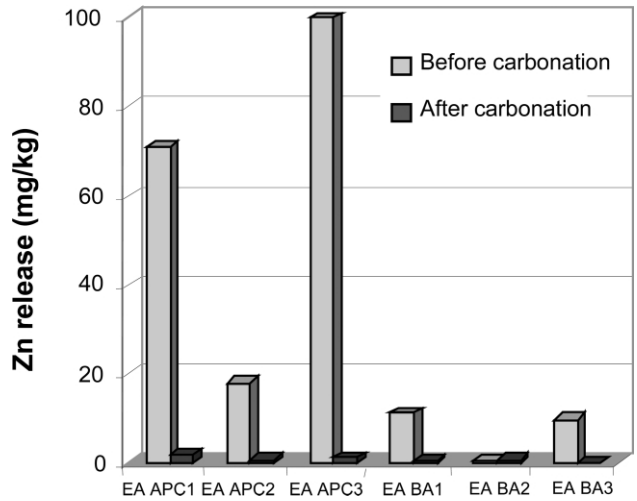

Fig. 23 Zinc release before and after carbonation for different BA and APC residues.

Conclusions

Waste materials presented for carbonation have great potential to not only sequester CO_2, particularly when they exist in high volumes, but also to be re-used as, for example, construction aggregates.

The use of incineration for MSW disposal continues to grow as UK landfill space decreases. Thus, in the future there will be increasingly large volumes of combustion wastes to be managed. Due to their composition, MSWI ashes can be made to react with CO_2 to form materials with improved properties. Accelerated carbonation imparts chemical and mineralogical changes on the ashes, which reduce their environmental impact through cementation by carbonate precipitation. This preliminary study shows the potential of using accelerated carbonation for the treatment of bottom and fly ashes.

As a first approach to the accelerated carbonation of incinerator ashes, three fundamental parameters controlling the carbonation reaction have been studied, namely the reaction time, ash water content and particle size. The following optimum values were obtained:

• The reaction time to get an optimum extent of carbonation for BA and APC residues is 2.5 h. After that time the reaction is effectively slowed down.

• The carbonation is better for smaller particle size. Considering the particle size distribution of MSW ashes, the fraction below 710 μm for BA and below 212 μm for FA have been selected as the optimum for carbonation.

• The optimum water–solid ratio for the selected size fraction is 0.3–0.4 for BA and 0.2–0.3 for APC residues.

The ACT process rate of reaction is controlled by the diffusion of the gas to the solid. Experiments in dynamic conditions have shown that the velocity of reaction is significantly higher than in static conditions.

Accelerated carbonation imparts considerable physical and chemical changes in MSW ashes:

• The amount of $CaCO_3$ in the ashes after ACT treatment is increased. The increase is higher in APC residues than in BA, mainly due to their higher initial concentration of $Ca(OH)_2$.

• The particles of APC residues after carbonation become coarser due to agglomeration. This effect is beneficial if they are to be used for aggregate manufacturing.

• The carbonated product is a solid of lower porosity, lower tortuosity and lower pore area with calcite infilling the pore space.

• The formation of calcium-metal salts and metal silicate complexes has been confirmed using XRD analysis.

• The pH drops to nearly neutral after carbonation.

• The leaching of lead and zinc is markedly reduced upon carbonation for both APC and BA.

• The leaching of sulfate is increased by carbonation, but it is still below the relevant landfill limits. Carbonation does not affect the leaching of chlorides in BA, whilst it decreases chloride leaching for APC; though the final value is still over the limit.

The information obtained in this study will set the basis for further work that is currently being developed to determine the kinetics of carbonation of BA and APC residues. Once the reactions can be modelled, it will be possible to optimise the parameters required for the design of continuous large scale accelerated carbonation of MSW ashes using stack gas emissions of CO_2 to produce artificial aggregates.

Acknowledgements

The authors acknowledge La Caixa, The British Council and Millennium Chemicals for the financial support of M. Fernández Bertos. The work reported here was partly supported by the Biffaward Scheme (Grant no. B/1797a).

References

1 DTI, *Review of the feasibility of carbon dioxide capture and storage in the UK*, Cleaner Fossil Fuels Programme, The Stationery Office, Norwich, UK, 2003.
2 DTI, *Energy White Paper: Our energy future—creating a low carbon economy*, The Stationery Office, Norwich, UK, 2003.
3 S. Valls and E. Vazquez, Accelerated carbonation of sewage sludge-cement-sand mortars and its environmental impact, *Cem. Concr. Res.*, 2001, **31**, 1271–1276.
4 M. A. Venhuis and E. J. Reardon, Vacuum Method for Carbonation of Cementitious Wasteforms, *Environ. Sci. Technol.*, 2001, **35**, 4120–4125.
5 A. Macias, A. Kindness and F. P. Glasser, Impact of carbon dioxide on the immobilisation potential of cemented wastes: chromium, *Cem. Concr. Res.*, 1997, **27**(2), 215–225.
6 J. Walton, S. Bin-Shafique, N. Gutierrez, R. Smith and A. Tarquin, Role of Carbonation in Transient Leaching of Cementitious Wasteforms, *Environ. Sci. Technol.*, 1997, **31**, 2345–2349.
7 M. Bin-Shafique, J. Walton, N. Gutierrez, R. Smith and A. Tarquin, Influence of Carbonation on Leaching of Cementitious Wasteforms, *J. Environ. Eng.*, 1998, 463.
8 H. Ecke, Carbonation for Fixation of Metals in Municipal Solid Waste Incineration (MSWI) Fly Ash, Department of Environmental Engineering, Division of Waste Science & Technology, Luleå University of Technology, Sweden, 2001.
9 US5,997,629, C. Hills, Hazardous waste treatment. Imperial College of Science, Technology and Medicine, London, UK, 7-12-1999.
10 WO 01/34294 A1, C. D. Hills and C. L. MacLeod, Silicate/Aluminate materials, GB, 17-5-2001.
11 M. Yousuf, A. Mollah, T. R. Hess, Y.-N. Tsai and D. L. Cocke, An FTIR and XPS investigation of the effects of carbonation on the solidification/stabilization of cement based systems-Portland type V with Zn, *Cem. Concr. Res.*, 1993, **23**, 773–784.
12 C. D. Hills and C. L. MacLeod, Recycling CO_2 in contaminated land, *Sustain' Built Environment Matters*, 2000, **1**(2), 34–35.
13 L. C. Lange, C. D. Hills and A. B. Poole, The effect of accelerated carbonation on the properties of cement-solidified waste forms, *Waste Management*, 1996, **16**(2), 757–763.
14 C. D. Hills, R. E. H. Sweeney and N. R. Buenfeld, Microstructural study of carbonated cement-solidified synthetic heavy metal waste, *Waste Management*, 1999, **19**, 325–331.
15 A. Polettini and R. Pomi, *The influence of accelerated ageing on leaching behaviour of incinerator bottom ash*, 615, Fifth International Conference on the Environmental and Technical Implications of Construction with Alternative Materials WASCON, San Sebastian, Spain, June 2003.
16 D. C. Johnson, C. L. MacLeod, P. J. Carey and C. D. Hills, Solidification of stainless steel slag by accelerated carbonation, *Environ. Technol.*, in press.
17 H. H. Steinour, Some effects of carbon dioxide on mortars and concrete-discussion, *J. Am. Concr. Inst.*, 1959, **30**, 905–907.
18 M. Fernández Bertos, S. Simons, C. D. Hills and P. J. Carey, A Review of Accelerated Carbonation Technology in the Treatment of Cement-based Materials and Sequestration of CO_2, *J. Hazard. Mater.*, in press.
19 M. Fernández Bertos, S. Simons, C. D. Hills and P. J. Carey, *Sequestration of carbon dioxide in artificial aggregates*, 5th International Conference on the Environmental and Technical Implications of Construction with Alternative Materials WASCON, San Sebastian, Spain, June 2003.
20 L. C. Lange, C. D. Hills and A. B. Poole, The influence of mix parameters and binder choice on the carbonation of cement solidified wastes, *Waste Management*, 1996, **16**(2), 749–756.
21 A. Scuzzarella, X. Li, M. Fernández Bertos, S. R. J. Simons, C. D. Hills and P. J. Carey, Review of Thermal Process Wastes with Carbonation Potential, *Internal Report for Biffaward Gr. No. B/1797a*, 2004.
22 Environmental Protection Agency, European Waste Catalogue and Hazardous Waste List, 2002, http://www.environment-agency.gov.uk/commondata/105385/ewc.pdf.
23 Environment Agency, Solid Residues from Municipal Waste Incinerators in England and Wales. England and Wales http://www.environment-agency.gov.uk.
24 Her Majesty's Stationery Office, Finance Act 200, Aggregate Levy, 2001.
25 H. Ecke, N. Menad and A. Lagerkvist, Carbonation of municipal solid waste incineration fly ash and the impact on metal mobility, *J. Environ. Eng.*, 2003, **129**(2), 435–440.
26 H. Ecke, Sequestration of metals in carbonated municipal solid waste incineration (MSWI) fly ash, *Waste Management*, 2003, **23**, 631–640.
27 T. Van Greven, J. Moors, V. Dutre and C. Vandecasteele, Effect of CO_2 on leaching from a cement-stabilised MSWI fly ash, *Cem. Concr. Res.*, 2004, in press.
28 S. Asavapisit, G. Fowler and C. Cheeseman, Solution chemistry during cement hydration in the presence of metal hydroxide wastes, *Cem. Concr. Res.*, 1997, **27**(2), 1249–1260.
29 W. A. Klemm and R. L. Berger, Accelerated curing of cementitious systems by CO_2, *Cem. Concr. Res.*, 1972, **2**, 567–576.
30 M. A. Sorochkin, A. F. Shchrov and I. A. Safonov, Study of the possibility of using carbon dioxide for accelerating the hardening of products made from Portland cement, *J. Appl. Chem.*, 1975, **48**(2), 1211–1217.
31 BS 1377: 1990, *Methods of test for soils for civil engineering purposes*, BSI.
32 BS EN 12457: 2002, *Characterisation of Waste-Leaching-Compliance Test for Granular Waste Materials and Sludges*, BSI.